AD 286 316

U. S. ARMY
TRANSPORTATION RESEARCH COMMAND
FORT EUSTIS, VIRGINIA

TCREC TECHNICAL REPORT 62-50

SUPPLEMENTARY LIFT FOR AIR CUSHIONED VEHICLES

(DATA ANALYSIS)

Volume II of III

Task 9R99-01-005-03

Contract DA44-177-TC-708

June 1962

prepared by:

GRUMMAN AIRCRAFT ENGINEERING CORPORATION
Bethpage, New York

DISCLAIMER NOTICE

When Government drawings, specifications, or other data are used for any purpose other than in connection with a definitely related Government procurement operation, the United States Government thereby incurs no responsibility nor any obligation whatsoever; and the fact that the Government may have formulated, furnished, or in any way supplied the said drawings, specifications, or other data is not to be regarded by implication or otherwise as in any manner licensing the holder or any other person or corporation, or conveying any rights or permission, to manufacture, use, or sell any patented invention that may in any way be related thereto.

ASTIA AVAILABILITY NOTICE

Qualified requesters may obtain copies of this report from

Armed Services Technical Information Agency
Arlington Hall Station
Arlington 12, Virginia

This report has been released to the Office of Technical Services, U. S. Department of Commerce, Washington 25, D. C., for sale to the general public.

The information contained herein will not be used for advertising purposes.

The findings and recommendations contained in this report are those of the contractor and do not necessarily reflect the views of the Chief of Transportation or the Department of the Army.

HEADQUARTERS
U. S. ARMY TRANSPORTATION RESEARCH COMMAND
Fort Eustis, Virginia

The principle of increasing the efficiency of Air Cushion Vehicles (ACV) by making use of the aerodynamic lift available at forward speeds has been investigated in this instance for vehicles oriented to the command and reconnaissance mission and to the off-road logistics mission. The study points up the considerable benefits of utilizing this concept; however, it also illustrates the limitation of the concept, i.e., relatively high speeds are required to gain a significant advantage. The basic wind-tunnel data contained in Volume I and the data analysis contained in Volume II are sufficiently comprehensive to enable a designer to make a preliminary design study of an ACV that would satisfy mission requirements other than those considered in Volume III.

Based on the results of this investigation, it is concluded that any ACV designed for mission requirements which include a significant portion of high-speed operation should be configured to take advantage of aerodynamic off-loading.

FOR THE COMMANDER:

Kenneth B Abel
KENNETH B. ABEL
Captain, TC
Adjutant

W D. Hinshaw
WILLIAM D. HINSHAW
Project Engineer
Ground Effect Research Group

Task 9R99-01-005-03

Contract DA 44-177-TC-708

TCREC TECHNICAL REPORT 62-50

June 1962

SUPPLEMENTARY LIFT FOR AIR CUSHIONED VEHICLES
VOLUME II OF III. DATA ANALYSIS

by

N. Kirschbaum
J. Helgesen
Research Department
Grumman Aircraft Engineering Corporation

Approved by: William Aubin
William Aubin
Head, Special Projects

Approved by: for Richard H. Fleming
Charles E. Mack, Jr.
Director of Research

for

U.S. Army Transportation Research Command
Fort Eustis, Virginia

PREFACE

This report is an account of the results obtained during a wind tunnel study of supplemental lift for air cushioned vehicles. The study was conducted under contract DA 44-177-TC-708 for the U.S. Army Transportation Research Command (USATRECOM), Mr. William Hinshaw of USATRECOM served as the Army's technical representative. Responsibility for conducting the study was assigned to the Special Projects Section of the Research Department, Grumman Aircraft Engineering Corporation. Mr. William Aubin is Section Head and Dr. Charles E. Mack, Jr. is Director of Research.

The results of this study are presented in three volumes. Volume I* presents the basic wind tunnel data. This volume (Volume II) presents the data in parametric form as a function of air mass flow coefficient. In this form the data allow evaluation of the effect of vehicle jet nozzle configuration changes on aerodynamic off-loading (supplemental lift). Volume III utilizes the results of this investigation in a performance study of vehicles for the command reconnaissance and logistics missions of the U.S. Army.

The authors gratefully acknowledge the efforts of the Aero-Test Operations Group, in particular Mr. Richard Ledesma, in conducting the wind tunnel tests, Mr. Geoffrey Gardner and Mrs. Freda Cellana for data reduction, Mr. Jack Graham and Mr. George Clark for editorial and reproduction matters, and Mrs. Milly Sudwischer and Miss Arleen Messina for typing.

*Available on loan basis from USATRECOM

TABLE OF CONTENTS

LIST OF ILLUSTRATIONS

LIST OF SYMBOLS

AR	aspect ratio, $\frac{\text{width}}{\text{length}}$
C	cushion chord (base plus jet), ft
C_D	drag coefficient, $\frac{\text{drag}}{qS}$
C_j	peripheral jet length, ft
C_L	lift coefficient, $\frac{\text{lift}}{qS}$
C_ℓ	rolling moment coefficient, $\frac{\text{rolling moment}}{CqS}$
C_m	pitching moment coefficient, $\frac{\text{pitching moment}}{CqS}$ (moment reference center at 48.8 percent cushion chord)
C_μ	blowing coefficient, $\frac{\dot{m}V_{j_o}}{qS}$
D	drag, lbs
h	height above terrain (ground board), measured to base at moment reference center, in., ft.
$\dot{m}$	mass flow, slugs/sec
P_T	total pressure, psf
q	free stream dynamic pressure, psf
q_{j_o}	jet total pressure above ambient, psf
S	cushion base area (basic configuration, base plus jet) ft^2

S_j	peripheral jet area, ft^2
SHP	shaft horsepower
t_e	thickness of jet, in., ft.
V	free stream velocity, ft/sec
V_{j_o}	velocity of jet at nozzle when expanded to atmospheric pressure, ft/sec
V_j	average jet velocity, ft/sec
$\dot{w}$	weight flow, decimal equivalent of maximum weight flow, lbs/sec
α	angle of attack
Δ	increment
η_D	inlet and ducting efficiency
η_F	fan efficiency
η_I	intake efficiency (inlet q recovery)
η_P	propulsive efficiency
ϕ	angle of roll
θ_j	angle of jet (measured from horizontal)
ρ	free stream density of air

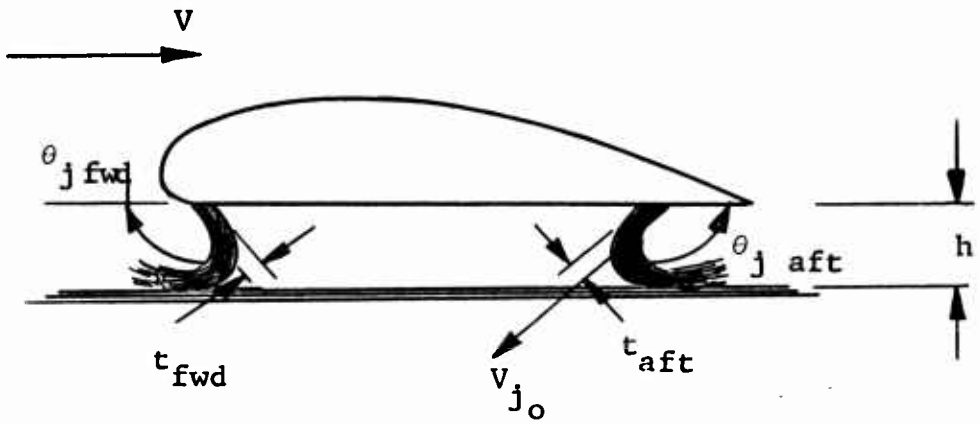

Sign Convention

pitch	-	positive nose up
roll	-	positive right wing down
lift	-	positive up
drag	-	positive aft

SUMMARY

The wind tunnel study of supplemental lift for air cushioned vehicles utilized a three-dimensional, half-span reflection-plane, airfoil-shaped GEM model and covered speeds from 0 to 100 miles per hour.

The first series of tests evaluated the effects of various leading and trailing edge jet configurations on the performance of the model at zero degree angle of attack. The data are presented in parametric form as a function of air mass flow coefficient. The results of this study indicate that the propulsive requirements for the lift system decrease with increasing speed or, for constant power the operating height can be increased.

The second series of tests evaluated the stability characteristics of the cruise configurations at cruise speed (100 miles per hour). The results of these tests indicate that all cruise configurations tested could be made longitudinally stable by locating the moment reference center (cg) at the 37 percent air cushion base chord. For the Jet Flap configurations, the required nose down trim loads increased with increasing mass flow. With the Tip Jet Only Configuration, there was an adverse rolling moment with roll angle. (This was the only configuration tested in roll.)

INTRODUCTION

The advantages inherent in applying aerodynamic lift to air cushioned vehicles are manifold. The performance of air cushioned vehicles is compromised at higher speeds by the momentum, or ram, drag caused by the air taken aboard. This is particularly evident where large mass flows of air are involved, such as they are for high base loadings and/or high traversal heights. Ram drag for these configurations severely inhibits maximum speed or leads to large increases in required power above that needed for hover. It thus affects the practicability of air cushion vehicles by reducing the speeds, payloads and/or range. Reduction of ram drag can be achieved by decreasing the vehicle weight that has to be supported on the air cushion. This can be achieved practically by aerodynamic off-loading of the air cushion, which is most effective where it is most needed — at high speeds. With respect to configurations with integrated powerplant systems, where the total power is divided as needed between the air cushion and the propulsive systems, aerodynamic off-loading of the air cushion not only reduces the ram drag (and over-all drag) by decreasing the mass-flow required to maintain the air cushion, but also increases the gross thrust available for forward propulsion by reducing the power required by the air cushion system. For configurations with independent power plants for the air cushion and propulsive systems, aerodynamic off-loading should reduce total power expenditure and fuel consumption by allowing a reduction of power (or number of engines operating) in the air cushion system.

The investigation reported herein was conducted to explore the performance benefits and stability problems associated with aerodynamic off-loading of air cushioned vehicles. The wind tunnel program consisted of a series of tests conducted in the Grumman Aircraft Engineering Corporation's 7-by 10-foot low speed wind tunnel on a semispan, reflection-plane model. The jet configuration was consistently varied to represent a family of aerodynamically off-loaded air cushion vehicles, in order to duplicate configurations and conditions requisite for cruise, and transition to and from cruise, that were specified by Ref. 1.

The model was rectangular in planform and of aspect ratio 0.833. It had a 16-percent thick, highly cambered, flat-bottomed airfoil section. The air cushion base was of aspect ratio 1.00 and was formed by a rectangularly shaped peripheral jet which could be varied in both thickness and deflection at the leading and trailing edges. The air cushion was instrumented to record jet total pressures and base pressure distribution. The model was mounted vertically from the tunnel floor but on top of a 10-inch tunnel boundary layer diverter. The air for the air cushion entered the model spanwise through the tunnel floor allowing a smooth airfoil upper surface. The model was pitched about an axis passing through the 48.8 percent air cushion chord with respect to a vertical ground board to investigate longitudinal stability. The vertical ground board could be moved horizontally with respect to the model to vary the height-to-chord ratio, and could be pitched about an axis lying in the plane of symmetry of the model (at the junction with the boundary layer diverter) to vary roll angle. The tunnel velocity was varied from 33 to 150 feet per second and the air weight flow to the model was varied from 0 to approximately 10 pounds per second.

Volume I of this report discusses the test program and test apparatus and includes the corrected aerodynamic data, in coefficient form, obtained in the wind tunnel. Volume III presents an analysis of air cushioned vehicles for the command reconnaissance and logistics missions outlined in Ref. 1, utilizing the results of this investigation. This portion of the report includes the data reduced to parametric form and discusses the application and use of the data so presented. The lift coefficient C_L and V/V_{j_o} are presented as a function of C_μ. The drag and pitching moment (about 48.8 percent chord) data obtained were small and of the same magnitude as the tares due to the air supply system; consequently they are not considered sufficiently reliable to be presented here. These data can be obtained however, by consulting Volume I.

DISCUSSION

WIND TUNNEL MODEL

The wind tunnel tests employed a half-span, reflection-plane model that utilized low pressure, high mass flow air obtained through the airfoil cross-section at the configuration centerline (tunnel floor). Photographs illustrating the model installation in the wind tunnel are presented in Figs. 1 and 2. Fig. 3 illustrates air delivery to the model (photo actually taken outside of the tunnel) and the base configuration. The chord of the model is a constant 4.8 feet and the model semispan is 2.0 feet (rectangular planform of 0.833 aspect ratio). A detailed drawing of the model is presented in Fig. 4. The semispan can be increased to 2.5 and 3.0 feet by the addition of spanwise segment panels which increase the aspect ratio to 1.04 and 1.25, respectively. The 3.0-foot semispan, aspect ratio 1.25 configuration was utilized in the investigation of aspect ratio effect. The airfoil section is a modified Clark Y profile. The ordinates of the Clark Y profile were increased to yield a 16 percent thick airfoil section, the bottom flattened between the 8 and 30 percent chord, the leading edge radius increased and faired-in tangentially to the flat bottom at the 8-percent chord, and the trailing edge reflexed 1-inch starting at the 89-percent chord.

Both the leading and trailing edge jet thickness and jet angle were varied by replacing whole leading and trailing edge nozzle block sections (Fig. 5). The basic jet thickness and deflection angle is 0.94 inch and 90-degrees. Leading edge and trailing edge nozzle blocks provide four other jet thicknesses (1.18, 1.41, 0.71, and 0.47 inches) and two other jet deflection angles (120 degrees and 60 degrees). When these nozzle blocks were utilized, the wing-chord-to-ground-effect-base chord varied (in relation to the basic configuration) with jet deflection angle, but not with jet thickness. Although the ground effect base area varied because of this procedure (-2.3, +2.7 percent), it should be appreciated that practical air cushion vehicles utilizing variable deflection nozzles will suffer a similar change in ground effect base area with

jet nozzle variations (Ref. 2) for given external dimensions. In addition, three trailing edge nozzle block assemblies were constructed for the tip jet plus jet flap tests. These nozzle blocks of 30-,45-, and 60-degree deflection have no structural overlap. Their use increases the ground effect base chord (and area) by 4.1 percent, in relation to the basic configuration.

The ratio of wing-chord-to-ground-effect-base chord is 1.26 and wing-chord-to-ground-effect-system chord (including jet) was 1.20 when both the leading and trailing edge jets are vertical. The spanwise overlap is confined to the thickness of the tip jet nozzle (held constant at 0.94 inch, 90-degree deflection throughout the test program). The spanwise overlap ratio is, therefore, 1.04 with respect to the ground effect base chord and 1.0 with respect to the ground effect system chord. These structural overlaps yielded a ground effect base area of 8 square feet (semispan) with an aspect ratio of approximately 1.0 for the basic jet configuration and 0.833-aspect ratio wing. The ground effect base is promulgated as a square, or very nearly so, because of the desire to achieve equivalent stability with height about both the lateral and longitudinal axes during hover. Further details of the model are discussed in Volume I.

The model was tested at heights of 7.5, 5.0, and 2.5 inches above the ground board, which resulted in thickness to height t_e/h values of 0.125, 0.25, and 0.375 for the 0.94-inch thick jet, and height-size ratios $hC_j/4S$ of 0.156, 0.104, and 0.052 for the basic jet configuration. The height-size ratios are increased 2.3 percent for the 120-degree jet configurations and decreased 2.7 percent for the 60-degree jet configurations. These values represent full scale heights of 4.00, 2.67,and 1.33 feet for the command reconnaissance vehicle. Tests at 2.5-inches height also represent the specified full scale height of 2.00 feet for the larger logistics vehicle. These ratios of test-to-full-scale height fixed the size of the respective vehicles (above) to 30.7-and 46.1-foot wing chords, and 25.6-and 38.4-foot wing spans.

Four rows of 8 static pressure taps were constructed into the base of the model (Fig. 6). These taps, located at the 20-, 40-, 60-, and 80-percent semispan were utilized to obtain ground effect base pressure distribution throughout the tests (recorded photographically). The static pressure taps in Fig. 6 are numbered to correspond to the numbers on the manometer board photograph shown in Fig. 7.

The basic wing aerodynamic data for the two aspect ratios (0.833 and 1.25) in and out of ground effect are given in Figs. 8 and 9. The nozzles were taped shut during these tests to present a smooth under surface. It should be noted that these data are based on cushion area and not wing planform area. The corresponding coefficients based on wing planform area are 0.83 of that presented.

TEST PROGRAM

The wind tunnel tests were conducted to explore the performance benefits and stability problems associated with aerodynamic off-loading of air cushioned vehicles. This was accomplished through a systematic variation of jet nozzle angle and thickness and differential mass flows (between leading and trailing edge jet nozzles) up to and including the cruise speeds set forth in Ref. 1. The test summary is presented in the appendix. Parametric configuration changes are listed in this schedule.

Two series of wind tunnel tests were conducted. The first series of tests evaluated the performance aspects of various leading and trailing edge jet nozzle configurations at zero degree angle of attack. During these tests, force, moment, air mass flow, static air mass flow distribution, tip jet total pressure, and air cushion pressure data were gathered. Jet air horsepower can be calculated using these data. The second series of tests evaluated the stability of these configurations at cruise speed. Force, moment, air mass flow, and air cushion pressure data were gathered during these tests.

The first four experiments gave basic performance data at hover and at three forward speeds (each at three air mass flows). These tests can also be considered applicable to a "simple" airfoil shaped air cushion vehicle in which

the leading and trailing edge nozzle angles are fixed and symmetrical about the 50-percent air cushion base chord. The parameter varied in these four experiments were:

1. Effect of height with basic jet configuration of 0.94 inch-thick nozzles, 90-degree jet angles, and equally distributed air flow.

2. Effect of jet thickness with basic jet angle of 90 degrees at the two specified (scale) heights of 7.5 and 2.5 inches, and equally distributed air flow.

3. Effect of jet angle with basic jet thickness of 0.94 inches at the two specified (scale) heights of 7.5 and 2.5 inches, and equally distributed air flow.

4. Effect of differential leading edge to trailing edge air mass flow with basic jet angle of 90 degrees at the two specified (scale) heights of 7.5 and 2.5 inches.

The next four experiments were designed to obtain data to appraise acceleration and deceleration of the vehicles to and from cruise speed. These four tests are similar to those performed in Ref. 3 but with subsonic peripheral jets, a three-dimensional planform, and scale heights representing the specified heights of the selected full scale vehicles. Jet thickness distribution (leading and trailing edge jets) and jet angle, as indicated in the appendix, were the basic configuration variations during these tests. The tests were performed at three values of total air mass flow for each speed in the ranges given below.

CONFIGURATION	VELOCITY (FT/SEC.)							
Initial Hover	33	49	65	82	98			
Midacceleration to Cruise		49	65	82	98	114		
Near Cruise Speed Acceleration			65	82	98	114	131	
Cruise Speed						114	131	147

These tests were conducted at heights of 5.0 and 2.5 inches instead of 7.5 and 2.5 inches. Preliminary evaluation of the data from earlier tests indicated that the objectives of Ref. 1 could not be met at 7.5-inches height with the blowing equipment in this test installation. It should be noted also that the height-size ratio associated with 7.5 inches ($hC_j/4S=.156$) is well outside that considered practical for air cushioned vehicles. Since it appeared that the 5.0-inches height could lead to satisfactory results, it was decided to proceed with further tests at this height.

The speed ranges for the different configurations were overlapped so that there would be a great probability of blanketing the areas where minimum power expenditure is realized. In addition to lowering the maximum test height to 5.0 inches, the speed ranges were shunted toward the smaller command reconnaisance vehicle, specified to cruise at 100 miles per hour, when preliminary evaluation of the initial test data revealed that aerodynamic offloading at the lower speeds specified for the logistics vehicle would be very small.

The "initial hover" configuration had the largest mass flows jetting from the leading edge. The "cruise" configuration had the leading edge jets blocked off and flow issued only from the tip and trailing edge jets. Since the cruise free stream dynamic pressure is greater than the cushion pressure, it was anticipated that the vehicle could operate effectively as a ram wing. The configurations between the "initial hover" configuration

and the "cruise" configuration had leading and trailing edge jet thickness (and therefore air mass flow distribution) between the above two extremes. It was anticipated that this variation of jet thicknesses and air mass flows although quite arbitrary would alleviate some of the pitching moment problems encountered in Ref. 3 and extend the results of Ref. 4 to forward speeds.

These tests were:

5. Effect of differential air mass flow in acceleration with leading and trailing edge jets angled aft (120 degrees at the leading edge and 60 degrees at the trailing edge) at 5.0-and 2.5-inches height.

6. Effect of differential air mass flow in deceleration with leading and trailing edge jets angled forward (60 degrees at the leading edge and 120 degrees at the trailing edge at 5.0-and 2.5-inches height).

The next four experiments were designed to evaluate more fully aerodynamic off-loading during cruise. The effects of tip jet plus jet flap action and aerodynamic aspect ratio on aerodynamic off-loading were investigated. The tip jet plus jet flap tests employed special nozzles and supplemented the cruise configuration data obtained in the previous tests which used the standard trailing edge jet nozzles with sharp trailing edge overhangs beyond the jets. One configuration, employing the tip jet only, was also tested to investigate the possibility of increasing the effective aerodynamic aspect ratio by a side air wall endplating effect.

These tests were:

7. Effect of tip jet plus jet flap with deflection angles of 30, 45,and 60 degrees at 5.0-and 2.5-inches height.

8. Effect of tip jets only on aerodynamic efficiency at 5.0-and 2.5-inches height.

9. Effect of increasing the aspect ratio from 0.83 to 1.25 on tests 7 and 8.

The second series of tests was performed to evaluate stability. Six repeat tests of previous configurations were also run to ascertain the repeatability of data. One of these repeat investigations was also re-run with a jet flap (of similar jet angle) in place of the conventional trailing edge to evaluate the loads and moments caused by the trailing edge overhang in the conventional configurations. Pressure distribution data under the conventional leading edge and trailing edge overhang were also obtained during the initial repeat run. In addition, 4 drag polars were obtained with the unblown wing at 2 heights and 2 aspect ratios, so that comparisons could be made with respect to air cushion ram wings.

These tests were:

10. Drag polar tests from -4-to +10-degrees angle of attack at 7.5-and 2.5-inches height and at aspect ratios of 0.83 and 1.25.

11. Repeat performance tests. Repeat of set-ups 1, 3, 11, 15, 27, and 35.

12. Repeat performance test of set-up 11, but with similar angled jet flap replacing the conventional trailing edge nozzle.

13. Pitch stability tests of tip jet only at 7.5, 5.0,and 2.5 inches.

14. Roll stability tests of tip jet only at 5.0 inches.

15. Pitch stability tests with tip jet plus jet flaps of 60-degrees and 30-degrees deflection at heights of 7.5, 5.0,and 2.5 inches.

16. Pitch stability tests of maximum differential mass flow configuration at 7.5, 5.0, and 2.5 inches.

PERFORMANCE

The data suitable for performance evaluation are presented in graphical form in Figs. 10 through 60. Lift coefficient C_L and free stream to jet velocity ratio V/V_{j_o} are presented as a function of C_μ. A summary of the data presented and model parameters tested is included in the appendix. In addition, data from the repeat tests are presented in figures subscripted a to the tests they repeat (Figs. 10a, 12a, 20a, 24a, 36a, and 44a). The parameters enable air horsepower (shaft horsepower with the inclusion of pertinent efficiencies) to be obtained for various weights and sizes of air cushioned vehicles as a function of velocity. In the range of mass flow, jet velocity, and forward velocity tested and within the accuracy of the data measuring system, both C_L and V/V_{j_o} are a function of C_μ only and not of the magnitude of the individual factors effecting C_μ $(\dot{m}, V, V_{j_o})$. The parameter V_{j_o}, used in calculating C_μ, was measured at four places along the tip jet. Since both forward velocity and leading and trailing edge jet configurations affected the velocity distribution along the tip jet, the value of V_{j_o} that was used was the average of the highest pair of jet velocities.

The data presented in Figs. 10 through 60 are illustrated below.

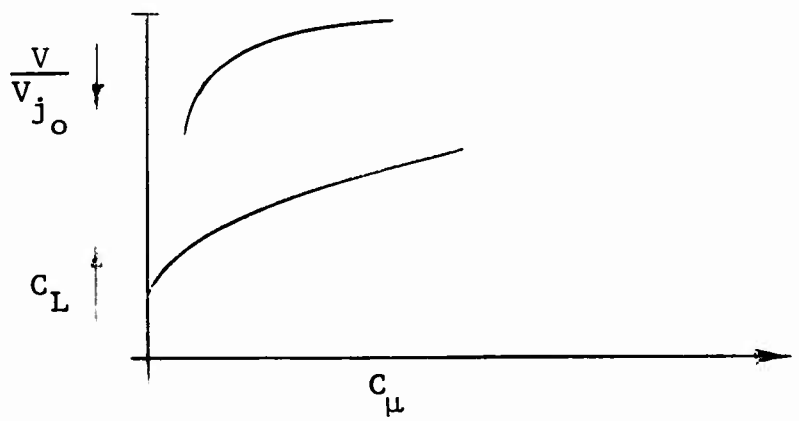

In general, for the configurations considered and the velocity range tested, the total power required by a given configuration is dominated by the power required for the air-cushion lift system and the power required to overcome ram drag. This is discussed in detail in the section entitled DATA UTILIZATION. At any given velocity, the air horsepower required for the lift system is proportional to $(C_\mu) \times \left(\frac{1}{V/V_{j_o}}\right)$ and the air horsepower required for ram drag is proportional to $(C_\mu) \times (V/V_{j_o})$ (actually proportional to $\dot{m}$ but C_μ contains V_{j_o} in the numerator). Since C_μ itself is proportional to $V_{j_o}^2$, it can be stated, as a generality, that the air horsepower required for the lift system is proportional to $(C_\mu)3/2$ and the air horsepower required for ram drag is proportional to $(C_\mu)1/2$. Naturally, since vehicle geometric parameters and operating height affect the relationship between C_μ and V/V_{j_o}, both these parameters must be used in the relations derived in the section on DATA UTILIZATION when actually evaluating power requirements. For a "first try", however, configurations can be compared on the basis of minimum C_μ for a required C_L. The required C_L is a function of base loading and velocity. A full quantitative assessment, however, requires that loads due to trimming out pitching moments, ram drag, etc. be evaluated. In this respect, air cushioned vehicles designed for aerodynamic lift should also benefit from low parasite drag.

Drag and pitching moment (measured about the 48.8-percent ground effect base chord) were also measured during the test program. However, these values were quite small and of the same magnitude as the tares due to the air supply system. As a consequence, these data are not considered sufficiently accurate to be presented here. They are included, however, in the Wind Tunnel Data Report (Volume I). In general as speed increased, the drag

coefficient approached that of the configuration without blowing, being slightly less for the acceleration and cruise configurations and slightly greater for the deceleration configurations. Comments with regard to drag and pitching moment will be made during the discussion of data. Prior to the stability tests, an attempt was made to improve the accuracy of the drag and pitching moment data by improving the air supply ducting system.

The coefficients presented at high C_μ's are quite high due to the derivation of these coefficients. In general, high C_μ's corresponds to low forward speeds. The parameter $L/\dot{m}V_{j_o}$ for zero forward speed is also tabulated on Figs. 10 through 60, in order to allow comparison with the data obtained at forward speeds. $(L/\dot{m}V_{j_o})$ at zero forward speed is analogous to (C_L/C_μ) at forward speed. In addition, Figs. 62 through 68 present lift/air horsepower as a function of wing loading at zero forward speed for the configurations tested during the first four experiments.

One series of tests (set-up 61) was conducted to evaluate the effect of the trailing edge overhang on the performance (C_L) of the model at a height of 2.5 inches. The configuration employed during these tests was identical to that of set-up 11, with the exception that the conventional trailing edge was replaced by the jet flap type trailing edge (no overhang). A comparison of the data of Fig. 61 with that of Fig. 20 indicates that there is an approximately 10-percent loss in lift due to the overhanging trailing edge (intermediate C_μ range). This loss in lift decreases as C_μ decreases.

During the tests of set-up 57 (repeat performance test of set-up 11), the leading and trailing edge nozzle blocks were instrumented to record static pressures at one spanwise location (approximately midspan). Static pressures were obtained ahead of the leading edge jet at 10 locations spaced 1 inch apart and behind the trailing

edge jet at 10 locations spaced 0.62-inch apart (Figs. 69 through 72). Pressure data were recorded at zero tunnel speed for maximum and intermediate mass flows and at 105-ft/sec for zero, intermediate, and maximum mass flows. For the trailing edge, the suction pressures were additive; i.e., the pressure at 105 ft/sec and maximum mass flow was approximately equal to the sum of the pressures at 105 ft/sec with zero mass flow and 0 ft/sec with maximum mass flow. This did not hold for the leading edge.

The performance tests were conducted to assess the relative merits of various leading and trailing edge jet configurations with the model at zero degree angle of attack. The first four experiments were designed to obtain basic performance data at hover and at three forward speeds (each at three air mass flows). These tests could also be considered applicable to "simple" airfoil shaped air cushion vehicles, in which the leading and trailing edge jets are angularly fixed and angularly symmetrical about the 48.8-percent air cushion base chord. The parameters varied in these four experiments were:

1) Effect of height with the basic jet configuration of 0.94-inch thick nozzles, 90-degree jet angle, and equally distributed air flow. Tests were conducted at 7.5-, 5.0-, and 2.5-inches clearance height (h/C = 0.156, 0.104, and 0.052, respectively) and the results may be compared in Figs. 10 (set-up 1), 11 (2), and 12 (3). For a required C_L of 1.25 (corresponding to a base loading of 15 lbs/ft^2 at 100 ft/sec), the C_μ's required at 7.5-inches height are approximately 1.77 times that required at 2.5-inches height. This would correspond to an increase in required air horsepower for the lift system by a factor of 2.35 and an increase in air horsepower required for ram drag by a factor of 1.35, over that required at 2.5 inches. These differences decrease with increasing speed. The results for the hover condition are presented in Fig. 62. The effect of height follows the expected course; the smaller the ground height, the less required horsepower. For 7.5-inches height, the horsepower required is approximately 2.35 times that required at 2.5-inches height.

2) Effect of jet thickness with the basic jet angle of 90 degrees at the two specified (scale) heights of 7.5 and 2.5 inches and equally distributed air flow. Tests were conducted with leading and trailing edge jet thicknesses of 0.94, 1.41, and 0.47 inches. The results for 7.5-inches height are given in Figs. 10 (set-up 1), 13 (4), 15 (6); and for 2.5-inches height are given in Figs. 12 (3), 14 (5), and 16 (7). The graphs clearly indicate the expected results of better performance with a thick jet at low speeds (high C_μ's). At higher speeds, however, the differences in performance decrease and other factors such as the size of the associated fans, inlets, and ducting, compromises in volume utilization and overall configurations, etc., must be considered. The results for the 7.5-inches height hover condition are given in Fig. 63 and for 2.5-inches height hover condition are given in Fig. 64. Again, as in the translation case, the thin jets are clearly inferior with respect to hover performance. However, at 2.5-inches height the nominal jet thickness (0.94 inch) is equally as good as the thickest jet, (1.41 inches).

3) Effect of jet angle with the basic jet thicknesses of 0.94 inch at the two specified (scale) heights of 7.5 and 2.5 inches and equally distributed air flow. Tests were conducted with 90-, 120-, and 60-degree jet deflection angles. The results for 7.5-inches height are given in Figs. 10 (set-up 1), 17 (8), 19 (10), and for 2.5-inches height are given in Figs. 12 (3), 18 (9), and 20 (11). The "classical" effect of increased performance with increasing jet deflection angle can be illustrated by comparing these graphs. It should be noted that these differences in performance decrease with increasing speed (decreasing C_μ). The results for the 7.5-inches height hover condition are given in Fig. 65 and for the 2.5-inches height hover condition are given in Fig. 66. Again, as in the translation case, the 60-degree jet deflection configuration is clearly inferior with respect to hover performance.

4) Effect of differential leading edge to trailing edge air flow with the basic jet angle of 90 degrees at the

two specified scale heights of 7.5 and 2.5 inches. These tests were conducted at leading edge to trailing edge nozzle ratios of 1.00, 1.67, 3.00, 0.67, and 0.33 with total nozzle area held constant. The results for 7.5-inches height are given in Figs. 10 (set-up 1), 21 (12), 23 (14), 25 (16), 27 (18); and for 2.5-inches height are given in Figs. 12 (3), 22 (13), 24 (15), 26 (17), 28 (19). At lower speeds, the increase in power required by the lifting system when utilizing nozzles of different jet thickness (same jet angle) are appreciable. At the higher speeds (100 mph), this increase in lifting power is not as large, but the better configuration (with respect to lifting power) is one with equal jet thickness distribution. This is illustrated in Fig. 73. There may, however, be some drag benefits due to the thicker trailing edge nozzles. The results for the 7.5-inches height hover condition are given in Fig. 67 and for the 2.5-inches height hover condition are given in Fig. 68. The most efficient configuration at both heights is the one with the equal jet thickness distribution. The configuration with the thickest leading edge jet and thinnest trailing edge jet were least efficient at both heights.

General observations of these tests indicated that at high C_μ's (corresponding to high mass flow, low tunnel speed) small negative drag values, that is, small thrust values, were always obtained. (Drag data is presented in Volume I). As speed increased (low C_μ) the drag values tended toward that obtained for the basic wing (no blowing). At any given air mass flow and for all the jet configurations tested in the preceding series, the cushion pressure decreased with increasing tunnel speed. The cushion pressures at the leading edge decreased at a faster rate than the rest of the cushion pressures. This is illustrated in Figs. 74 through 77 for maximum mass flows and tunnel speeds between zero and the maximum. At low and medium mass flows and high tunnel speeds the cushion pressures toward the leading edge were largely suction pressures and the cushion pressures toward the trailing edge were only slightly positive. The cushion pressure adjacent to the tip jet (80 percent semispan) was generally less positive than the rest of the pressures.

The distribution of air mass flow with differential jet nozzle thickness was generally satisfactory, as illustrated in Figs. 78 and 79. However, the slope of the pitching moment curve with differential mass flow did not show any recognizable or expected trend to locate the center of pressure toward the nozzle with the greater mass flow. The increased mass flow due to the thicker nozzles, although it increased the thrust of the jet, diminished the adjacent cushion pressure due to the decreased jet velocities from the thickened nozzles. This effectively cancelled the contribution of the greater jet thrust to the pitching moment. This was substantiated by integrating the jet and cushion forces over the cushion base. This situation would probably not arise if the jets were supplied from a common plenum, for then the jet velocities would be equal.

In Figs. 62 through 68, lift/shaft horsepower is presented as a function of base loading (ground effect base) for the hover condition for those configurations tested during the first four experiments. The data are presented in the form illustrated below.

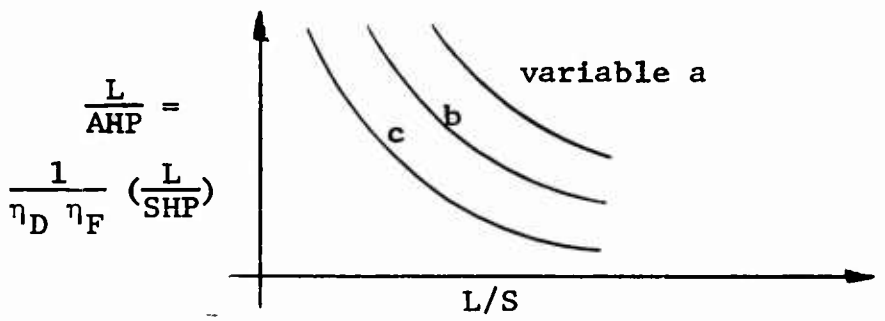

Shaft horsepower can be evaluated directly, after inclusion of estimated fan and ducting efficiences. In addition, the data are presented so that the effect of each variable in the experiment is readily discernible.

The next four experiments were designed to obtain data to appraise acceleration and deceleration of the vehicles to and from cruise speed. These four tests were similar to those performed in Ref. 3, but with subsonic peripheral jets, a three-dimensional planform, and scale heights representative of the specified heights of selected

full scale vehicles. Jet configurations were chosen to reflect possible nozzle arrangements for acceleration and deceleration and were tested in an overlapping speed range. The ranges for the different configurations were overlapped so that there would be greater probability of blanketing the areas where the minimum power expenditure is realized. The tests were performed at three values of total air mass flow for each speed in the ranges given below. Each configuration was tested in acceleration (leading and trailing edge jets angled aft) and deceleration (leading and trailing edge jets angled forward).

CONFIGURATION	VELOCITY (FT/SEC)							
Initial Hover	33	49	65	82	98			
Midacceleration to Cruise		49	65	82	98	114		
Near-Cruise-Speed Acceleration			65	82	98	114	131	
Cruise Speed						114	131	147

These tests were conducted at heights of 5.0 and 2.5 inches instead of 7.5 and 2.5 inches. Preliminary evaluation of the data from the earlier tests indicated that the design objectives of Ref. 1 could not be obtained with the blowing equipment in this installation. It should be noted also that the height-size ratio associated with 7.5 inches is well above that considered practical for air cushioned vehicles. Since it appeared that the 5.0-inches height (set-up 2) could lead to satisfactory results, at least with respect to attaining the C_L's required for practical base loading, it was decided to substitute this height for 7.5 inches in the following series of tests.

In addition to lowering the maximum test height to 5.0 inches, the speed ranges were shunted toward the smaller command reconnaissance vehicle, specified to cruise at 100 miles per hour when preliminary evaluation of the

initial test data indicated that aerodynamic off-loading at the speeds specified for the logistics vehicle was very small.

The initial hover configuration had the largest jet nozzle thickness (1.41 inches) and smallest jet nozzle thickness (0.47) inches at the leading and trailing edges, respectively. The cruise configuration had the leading edge jets blocked off and flow issued only from the tip and trailing edge jets, both of which were 0.94-inch thick. Since the cruise free-stream dynamic pressure would be greater than the cushion pressure, it was anticipated that the vehicle could operate effectively as a ram wing. The jet configuration between the initial hover configuration and the cruise configuration had varying leading- and trailing-edge jet thicknesses between the two extremes. The midacceleration configuration nozzles were 0.94-and 0.94-inch thick, respectively, and the near-cruise-speed configuration nozzles were 0.47-and 1.41-inches thick, respectively. It was anticipated that this variation of jet thickness and associated air mass flows, although quite arbitrary, would alleviate some of the pitching moment problems encountered in Ref. 3 and extend the results of Ref. 4 to forward speeds.

These tests were:

5) Effect of differential air mass flows in acceleration with leading-and trailing-edge jets angled aft (120-degrees at the leading edge and 60-degrees at the trailing edge) at 5.0-and 2.5-inches height. The nozzle thickness variation of 3.0, 1.0, 0.33, and with leading edge nozzle blocked, produced the air mass flow variation shown in Figs. 80 and 81. The results are given for 5.0-inches height in Figs. 29 (set-up 20), 31 (22), 35 (26), and 32 (23) for 2.5-inches height in Figs. 30 (21), 33 (24), 36 (27), and 34 (25).

6) Effect of differential air mass flows in deceleration with leading-and trailing-edge jets angled forward 60-degrees at the leading edge and 120-degrees at the trailing edge (5.0-and 2.5-inches height). The nozzle thickness variation of 3.0, 1.0, 0.33 and with leading

edge nozzle blocked, produced the air mass flow variation shown in Figs. 82 and 83. The results are given for the 5.0-inches height in Figs. 37 (set-up 28), 39 (30), 43 (34), 40 (31); and for 2.5-inches height in Figs. 38 (29), 41 (32), 44 (35), and 42 (33).

In general the "acceleration" configurations yielded negative drag, or thrust, while the "deceleration" configurations yielded positive drag. This was as expected; however, the values obtained were small and were the same magnitude as the tares due to the air supply system. The C_μ's required for a given C_L were higher for the deceleration configurations than for the acceleration configurations, with the exception of the configurations with the leading edge blocked. In this case, the forward-directed aft jet required less C_μ for a given C_L than the aft-directed aft jet configuration due to higher cushion pressures (Fig. 84 through 87). An indication as to optimum jet configuration, for both the acceleration and deceleration tests, can be obtained by superimposing the C_L vs C_μ curves upon each other. This is illustrated in Figs. 88 and 89. Since C_L varies with velocity for a given base loading, this superposition indicates optimum configuration variations with velocity. A more detailed analysis, however, requires consideration of ram drag with each configuration and the complexity associated with variable geometry peripheral nozzles. Typical comparative cushion pressure distributions are shown in Figs. 90 through 93.

The next four experiments were designed to evaluate more fully aerodynamic off-loading during cruise. The effect of tip jet plus jet flap action and aerodynamic aspect ratio on aerodynamic off-loading were investigated. The tip jet plus jet flap tests employed special trailing edge nozzles and supplemented the cruise configuration data obtained in the previous tests, which used the standard trailing edge jet nozzles with sharp trailing edge overhangs beyond the jets. One configuration, employing tip jets only was also tested to investigate the

possibility of increasing the effective aerodynamic aspect ratio by a side air wall endplating effect. The leading and trailing edge jet nozzles were taped shut during these tests.

These tests were:

7) Effect of tip jet plus jet flap with deflection angles of 60, 45, and 30 degrees (5.0-and 2.5-inches height). The results are given for the 5.0-inches height in Figs. 49 (set-up 40), 47 (38), 45 (36), and for 2.5-inches height in Figs. 50 (41), 48 (39), and 46 (37). In comparison with the standard, or overhanging trailing edge, the tip jet plus jet flap trailing edge nozzles (60-degree deflection) increased lift slightly, increased the thrust obtained, and decreased the positive pitching moment (due to the elimination of suction forces on the overhanging trailing edge), for a given C_μ. This can be seen by comparing Figs. 49 and 50 with Figs. 32 and 34. As expected, the tip jet plus 60-degree jet flap provided more lift and less thrust than the tip jet plus 30-degree jet flap; the tip jet plus 45-degree jet flap falling in between the above results.

8) Effect of tip jet only at 5.0-and 2.5-inches height. The results are given in Figs. 51 (set-up 42), and 52 (43). It was initially hypothesized that the air side wall would endplate the wing and increase the effective aspect ratio of the wing, thereby increasing the lift and aerodynamic off-loading. This was not the case, however. The air side wall jet, rather than curve out, away from the wing, curled in and under forming a vortex between the bottom surface of the test section and the ground board. The vortex, so formed, created large suction pressures on the bottom of the wing, extending from 100-to 60-percent semispan, and decreased lift. This effect was more pronounced at the 2.5-inches height than at the 5.0-inches height. Figs. 94 and 95 illustrate this phenomena by showing the base pressure distribution at 2.5-inches height and two velocities. The tip jet plus 60 degree jet flap trailing edge, under similar conditions of mass flow and ground height, Figs. 96 and

97, receives full positive pressures on the base of the model and a review of Figs. 49 and 50 indicates a greater lift for an equivalent C_μ.

9) Effect of increased aspect ratio on tip jet plus jet flap and tip jet only configurations. Tests 7 and 8 were repeated with an aspect ratio 1.25 wing. The increase in aspect ratio was obtained by adding a 1-foot span extension to the previous test section. This new test section suffered from a very large reduction in flow velocity in the added section due to the absence of a flow diverter vane assembly in the added section. However, although this probably diminished the attainable cushion pressure, the increased aspect ratio test sections exhibited increased C_L for equivalent C_μ. (C_L for the aspect ratio 1.25 wing is based on the larger base area associated with this wing). The results are shown for the 5.0-inches height in Figs. 53 (set-up 44), 55 (46), 57 (48), and 59 (50); and for the 2.5-inches height in Figs. 54 (45), 56 (47), 58 (49), and 60 (51).

STABILITY

Stability tests were performed in the longitudinal mode for the cruise configurations tested previously. The pitch angle was formed by rotating the model about an axis passing through the 48.8 percent air cushion chord. The height of the axis of rotation remained fixed in relation to the ground plane. This produced variable height to chord ratios for the leading and trailing edges. Fig. 98 presents h/C values with respect to the reference air cushion chord for ground effect parameter evaluation and 99 presents h/C values with respect to the wing chord for aerodynamic parameter evaluation. Limited stability tests were also performed in the lateral mode for the tip jet only configuration. The roll angle was formed by rotating the ground board in relation to the model about an axis lying in the plane of the centerline (root) chord which was, in effect, the junction of the ground board with the turntable.

The air ducting system that supplied air to the model was modified for these tests. Previous testing had shown unexpectedly large tare values which invalidated the

drag and moment data obtained during the performance series of tests. The previous fully flexible system was replaced with the rigid-flexible coupling system, as discussed in Volume I. This system reduced the tare values and gave better return readings.

The majority of the stability tests were performed at a tunnel speed of 100 miles per hour and at one value of air mass flow. The tests performed were:

1) Effect of angle of attack on tip jet only at 7.5-, 5.0-and 2.5-inches height. The angle of attack range for the 7.5-inches height was -4 to +8 degrees; for 5.0-inches height, -4 to +4 degrees; and for 2.5-inches height, -4 to 4 degrees. The results are given in Figs. 100 and 101. Fig. 100 demonstrates the effect of mass flow on the stability at 7.5-inches height. This configuration is slightly unstable about the reference moment center but has a sharp unstable break occuring at 4-degrees angle of attack for all mass flow ratios. This unstable break is evident at 5.0-inches height also, Fig. 101, which demonstrates the effect of height on stability. The data at 2.5-inches height showed no unstable break, although it was limited to less than 4-degrees angle of attack by ground clearance. A nose-up trim is evident at all conditions. The nose-up trim, as well as lift, increases with increasing mass flow or decreasing height. With respect to decreasing height, the configuration should be height stable if the angle of attack could be maintained at a constant value; however, a porpoising effect in translation is quite probable if the increased nose-up trim manifests itself in a positive pitch with decreasing height.

2) Effect of roll angle on tip jet only at 5.0-inches height and 0 degree angle of attack. The angle of roll was varied from -4 to +4 degrees. The results are given in Fig. 102. The values of the rolling moment coefficient C_{ℓ}, and lift coefficient C_L, have been adjusted to take into account the half span nature of the tests (which indicated a value of rolling moment coefficient at 0 degrees roll angle, Volume I). It is seen that the Tip Jet Only configuration, tested at 5.0-inches height and 0 degree angle of attack, has an unstable "Dihedral Effect"

with roll angle. As the right wing (the half-span tested) rotates down a positive rolling moment occurs which indicates that the right wing wants to further rotate down. This adverse effect is due to the Bernoulli effect between the wing bottom surface and the ground, which in effect forms a venturi. The contraction ratio of this venturi increases with decreasing ground height, causing larger suction loads on the bottom surface of the wing. This is clearly evident in the lift coefficient relationship of the half span panel presented in Volume I. Figs. 108 to 112 illustrate the suction loads on the cushion area of the right wing panel with roll angle. It is seen that the vortex formed by the tip jet, and trapped between the wing bottom surface and the ground (page 21) acts in opposition to the Bernoulli effect, but that it is not powerful enough to overcome this adverse rolling moment with roll angle. This adverse effect should be present at all the foreseen height ratios at which this type of air cushion vehicle will operate.

3) Effect of angle of attack on tip jet plus jet flaps at 7.5-, 5.0-, and 2.5-inches height. The jet flap angles tested were 60 and 30 degrees. The angle of attack range for the 7.5-inches height was -4 to +8 degrees; for 5.0-inches height, -4 to +4 degrees; and for 2.5-inches height, -4 to +4 degrees. The results are given in Fig. 103 (tip jet plus 60-degree jet flap) and 104 (tip jet plus 30-degree jet flap) for three mass flow ratios at 7.5-inches height. Figs. 105 and 106 illustrate the effect of height for the 60-degree and 30-degree jet flaps, respectively. Figs. 103 and 104 indicate that both configurations are unstable about the reference moment center with a mild pitch-up and stable recovery after 4-degrees angle of attack. Both the 60-degree and 30-degree jet flaps exhibit equivalent instability and both exhibit nose-down trim at small angles of attack. With the reference moment center moved forward 12 percent reference chord for neutral stability, (the CG now at 36.8 percent reference chord), the nose-down trim for the tip jet plus 60-degree jet flap configuration is larger than that for the tip jet plus 30-degree jet flap configuration at all angles of attack. This is as expected, as is the increase of the out-of-trim pitching moments with increased mass flows.

For the tip jet plus 60-degree jet flap, a decrease in height indicates a decrease in the instability (Fig. 105). A decrease in height also increases the lift and causes small changes in the trim loads, the direction of change depending on angle of attack. Fig. 106 indicates that the tip jet plus 30-degree jet flap has similar effects with height. In general, for both configurations, increased height progressively increased the instability; with the stability at 2.5-inches height being neutral. At any angle of attack a decrease in height causes a pitch-up as well as increased lift. This can be cancelled by moving the reference moment center 12 percent reference chord forward.

4) Effect of angle-of-attack on near cruise speed acceleration configuration (leading edge nozzle 0.47-inch thick and 120-degree deflection, trailing edge nozzle 1.41-inches thick and 60-degree deflection) at 7.5-, 5.0-, and 2.5-inches height. The angle of attack ranges were identical to those listed above. The results are given in Fig. 107. The stability of the configuration about the reference moment center is slightly unstable for the 7.5- and 5.0-inches height. An unstable break in these curves occurs at 4-degrees angle of attack. The stability at 2.5-inches height is neutral although a strong nose-up trim is evident. The configuration becomes progressively more unstable with increased height. Again, as in the previous tip jet plus jet flap configurations, at any angle of attack a decrease in height causes a pitch-up as well as increased lift. This effect can be alleviated by moving the reference moment center forward 12 percent.

It should be noted that the effects of the inlet on the stability of the model are here absent. However, at high cruise speeds the effects of the inlets on aerodynamically off loaded air cushioned vehicles are reduced. (At least with respect to flying ducts and other heavily loaded inlets where inlet induced stability problems have manifested themselves.) The air cushion mass flow requirements (and air horsepower) for efficient cruise configurations are only a small fraction of that required for hover. In addition, inlets can be so located on vehicles where their effects on stability are alleviated.

DATA UTILIZATION

This section presents a method of evaluating the power requirements of air cushioned vehicles utilizing aerodynamic lift during cruise and the data generated during this investigation. The shaft horsepower required during translation can be expressed in the following four terms.

$$SHP_{req'd.} = SHP_{aero.\ drag} + SHP_{air\ cush.} + SHP_{ram\ drag} - SHP_{dyn.\ head}$$

The horsepower required terms for the air cushion and dynamic head recovery can be expressed as fan horsepower. Thus,

$$SHP_{req'd.} = SHP_{aero.\ drag} + SHP_{ram\ drag} + SHP_{fan}$$

These terms, expanded in coefficient form, are:

$$SHP_{\substack{aero.\\drag}} = D\left(\frac{V}{550}\right)\left(\frac{1}{\eta_P}\right) = C_D\left(\frac{qSV}{550}\right)\left(\frac{1}{\eta_P}\right) \qquad (1)$$

$$SHP_{\substack{ram\\drag}} = (\dot{m}V)\frac{V}{550}\frac{1}{\eta_P} = \frac{C_\mu qS}{V_{j_o}}\left(\frac{V^2}{550}\right)\frac{1}{\eta_P}$$

$$SHP_{\substack{ram\\drag}} = C_\mu\left(\frac{qSV}{550}\right)\left(\frac{V}{V_{j_o}}\right)\left(\frac{1}{\eta_P}\right) \qquad (2)$$

The fan horsepower can be written as

$$SHP_{fan} = S_j V_j \frac{\Delta P_T}{550} \frac{1}{\eta_F} = \frac{\dot{m}}{\rho} \frac{\Delta P_T}{550} \frac{1}{\eta_F}$$

$$= \frac{C_\mu qS}{V_{j_o}} \frac{1}{\rho} \frac{\Delta P_T}{550} \frac{1}{\eta_F}$$

However,

$$\Delta P_T(\text{fan}) = q_{j_o} - \eta_I q + \Delta P_T(\text{inlet and ducting}),$$

where ΔP_T(inlet and ducting) equals the total pressure drop in the inlet and ducting and $(\eta_I q)$ equals the recovered free stream dynamic head. Consequently,

$$\Delta P_T(\text{fan}) = \left[\frac{q_{j_o}}{\eta_D} - \eta_I q \right] = q \left[\frac{q_{j_o}}{q} \frac{1}{\eta_D} - \eta_I \right]$$

Therefore, we write

$$SHP_{fan} = \frac{C_\mu qS}{V_{j_o}} \frac{1}{\rho} \frac{q}{550} \left[\frac{q_{j_o}}{q} \frac{1}{\eta_D} - \eta_I \right] \frac{1}{\eta_F}$$

$$= C_\mu qS \left(\frac{V}{V_{j_o}}\right) \frac{V}{550} \frac{1}{2} \left[\left(\frac{V_{j_o}}{V}\right)^2 \frac{1}{\eta_D} - \eta_I \right] \frac{1}{\eta_F}$$

$$= C_\mu \left(\frac{qSV}{550}\right) \frac{1}{2} \left(\frac{V}{V_{j_o}}\right) \left[\left(\frac{V_{j_o}}{V}\right)^2 \frac{1}{\eta_D} \frac{1}{\eta_F} - \frac{\eta_I}{\eta_F} \right]$$

$$SHP_{fan} = C_\mu \left(\frac{qSV}{550}\right) \frac{1}{2} \left[\left(\frac{1}{V/V_{j_o}}\right) \frac{1}{\eta_D} \frac{1}{\eta_F} - \left(\frac{V}{V_{j_o}}\right) \frac{\eta_I}{\eta_F}\right] \quad (3)$$

Combining equations (1), (2) and (3) we find

$$SHP_{req'd.} = C_D \left(\frac{qSV}{550}\right) \frac{1}{\eta_P} + C_\mu \left(\frac{qSV}{550}\right) \left(\frac{V}{V_{j_o}}\right) \frac{1}{\eta_P}$$

$$+ C_\mu \left(\frac{qSV}{550}\right) \frac{1}{2} \left[\left(\frac{1}{V/V_{j_o}}\right) \frac{1}{\eta_D} \frac{1}{\eta_F} - \left(\frac{V}{V_{j_o}}\right) \frac{\eta_I}{\eta_F}\right]$$

$$SHP_{req'd.} = \frac{qSV}{550}\left\{\frac{C_D}{\eta_P} + \frac{C_\mu}{\eta_P}\left(\frac{V}{V_{j_o}}\right) + \frac{C_\mu}{2}\left[\frac{1}{V/V_{j_o}} \frac{1}{\eta_D} \frac{1}{\eta_F} - \frac{V}{V_{j_o}} \frac{\eta_I}{\eta_F}\right]\right\} \quad (4)$$

C_μ and V/V_{j_o} can be obtained from Figs. 10-61 for any required lift coefficient C_L (C_L is a function of base loading and velocity). These data, along with pertinent efficiencies for fan, ducting, propulsive system, and inlet recovery, provide the required data for calculation of the required shaft horsepower (with the exception of C_D).

The values of drag obtained during the performance tests were small and of the same magnitude as the tares due to the air supply system. This was discussed in the section on performance. At low speed, (corresponding to high C_μ) drag did depend on the configuration tested. The acceleration configurations had small values of negative drag (or thrust) while the deceleration configurations had small values of positive drag. For the configurations with symmetrical jet angles, the drag was slightly negative. At high speeds (corresponding to low C_μ) the drag coefficient

approached that of the basic wing (no blowing), see Figs. 8 and 9. It should be noted, however, that this drag is representative for the configurations tested and does not include drag increments for such obvious provisions as air intakes, nacelles, cockpit appendages, fins, rudders, etc., and Reynolds number variation (test - full size).

In addition, the shaft horsepower required during hover can be estimated by use of Figs. 62 through 68 for design base loadings. These figures allow direct evaluation of lift/shaft horsepower for experimentally obtained values of lift/air horsepower and base loading (for the configurations tested) at zero speed when suitable fan and ducting efficiencies are added. The lift was obtained directly during each static test. The air horsepower was obtained by multiplying the mass flow by the jet velocity squared.

$$AHP = \frac{\dot{m}}{\rho} \tfrac{1}{2}\rho \, V_{j_o}^{\,2} \, \frac{1}{550}$$

$$AHP = \frac{1}{1100} \dot{m} \, V_{j_o}^{\,2}$$

The mass flow was measured at the intake and V_{j_o} was obtained at the tip jet. The value of V_{j_o} that was used in obtaining these air horsepower values was the average of the highest pair (of four) jet velocities.

REFERENCES

1. TRECOM Request for Quotation #TC-44-177-61 (neg-6), 26 September, 1960.

2. Stanton-Jones, R., Some Design Problems of Hovercraft. Presented at IAS 29th Annual Meeting, New York, New York, Paper No 61-45, January 23-25, 1961.

3. Poisson-Quinton, Ph., Two-Dimensional Studies of a Ground Effect Platform. Presented at Symposium on Ground Effect Phenomena, Princeton University, Princeton, N. J., October 21-23, 1959.

4. Sweeney, T.E., The Effect of Planform on the Static Characteristics of Peripheral Jet Wings, Contract DA 44-177-TC-524.

APPENDIX

SUMMARY OF MODEL PARAMETERS TESTED AND DATA PRESENTED

Set-up No:	h (inches)	t_{Fwd} (inches)	t_{Aft} (inches)	$\theta_{j_{Fwd}}$ (degrees)	$\theta_{j_{Aft}}$ (degrees)	Notes
1	7.5	.94	.94	90	90	Test Parameter 1 - Ef-
2	5.0	"	"	"	"	fect of height h at
3	2.5	"	"	"	"	$\alpha, \Phi = 0.$
4	7.5	1.41	1.41	90	90	Test Parameter 2 - Ef-
5	2.5	"	"	"	"	fect of jet thickness t_e
6	7.5	.47	.47	"	"	t, at 2 values of
7	2.5	"	"	"	"	h; $\alpha, \Phi = 0.$
8	7.5	.94	.94	120	120	Test Parameter 3 - Ef-
9	2.5	"	"	"	"	fect of jet angle θ_j,
10	7.5	"	"	60	60	at 2 values of
11	2.5	"	"	"	"	h; $\alpha, \Phi = 0.$
12	7.5	1.18	.71	90	90	Test Parameter 4 - Ef-
13	2.5	"	"	"	"	fect of differential
14	7.5	1.41	.47	"	"	mass flows, $\dot{m}_F/\dot{m}_A$, at
15	2.5	"	"	"	"	2 values of h; $\alpha, \Phi = 0$
16	7.5	.71	1.18	"	"	
17	2.5	"	"	"	"	
18	7.5	.47	1.41	"	"	
19	2.5	"	"	"	"	
20	5.0	1.41	.47	120	60	Low speed acceleration
21	2.5	"	"	"	"	
22	5.0	.94	.94	120	60	Mid acceleration-to-
24	2.5	"	"	"	"	cruise speed
26	5.0	.47	1.41	120	60	Near cruise speed
27	2.5	"	"	"	"	acceleration
23	5.0	-	.94	-	60	Acceleration to cruise
25	2.5	-	"	-	"	speed
28	5.0	1.41	.47	60	120	Low speed deceleration
29	2.5	"	"	"	"	
30	5.0	.94	.94	60	120	Mid deceleration-from-
32	2.5	"	"	"	"	cruise speed
34	5.0	.47	1.41	60	120	High speed deceleration
35	2.5	"	"	"	"	
31	5.0	-	.94	-	120	Deceleration from
33	2.5	-	"	-	"	cruise speed
36	5.0	-	.94	-	30 JF	Test of tip jet plus 30-degrees
37	2.5	-	"	-	"	jet flap
38	5.0	-	.94	-	45 JF	Test of tip jet plus 45-degrees
39	2.5	-	"	-	"	jet flap
40	5.0	-	.94	-	60 JF	Test of tip jet plus 60-degrees
41	2.5	-	"	-	"	jet flap
42	5.0	-	-	-	-	Test of tip jets to eval-
43	2.5	-	-	-	-	uate endplating effect.
44	5.0	-	.94	-	30JF	Repeat of set-ups 36,
45	2.5	-	"	-	"	37 at AR 1.25
46	5.0	-	.94	-	45JF	Repeat of set-ups 38,
47	2.5	-	"	-	"	39 at AR 1.25
48	5.0	-	.94	-	60JF	Repeat of set-ups 40,
49	2.5	-	"	-	"	41 at AR 1.25
50	5.0	-	-	-	-	Repeat of set-ups 42,
51	2.5	-	-	-	-	43 at AR 1.25

SUMMARY OF MODEL PARAMETERS TESTED AND DATA PRESENTED (Cont.)

Set-up No.	h (inches)	t_{Fwd} (inches)	t_{Aft} (inches)	$\theta_{j_{Fwd}}$ (degrees)	$\theta_{j_{Aft}}$ (degrees)	Notes
52	7.5	-	-	-	-	AR 1.25 } Basic Aero-dynamic Data
53	5.0	-	-	-	-	AR 1.25 } α = -2 to +6
54	5.0	-	-	-	-	AR .833 } Nozzles taped
55	7.5	-	-	-	-	AR .833 }
56	7.5	.94	.94	90	90	Repeat of Set-up 1
56a	2.5	.94	.94	90	90	Repeat of Set-up 3
57	2.5	.94	.94	60	60	Repeat of Set-up 11
58	2.5	1.41	.47	90	90	Repeat of Set-up 15
59	2.5	.47	1.41	120	60	Repeat of Set-up 27
60	2.5	.47	1.41	60	120	Repeat of Set-up 35
61	2.5	.94	.94	60	60 JF	Repeat of Set-up 11 but with jet flap T.E. to check effects of overhang.
62	2.5	-	-	-	-	Tip jets only; $-4 \leq \alpha \leq 4$; $-4 \leq \Phi \leq 4$ V_o = 147 ft/sec
63	5.0	-	-	-	-	Same as Set-up 62 ; change in height
64	7.5	-	-	-	-	
65	7.5	-	.94	-	60 JF	$-4 \leq \alpha \leq 4$; jet flap T.E.
67	7.5	-	.94	-	30 JF	" "
68	5.0	-	.94	-	30 JF	" "
70	5.0	-	.94	-	60 JF	" "
71	2.5	-	.94	-	60 JF	" "
73	2.5	-	.94	-	30 JF	" "
74	2.5	.47	1.41	120	60	$-4 \leq \alpha \leq 4$; standard T.E.
75	5.0	.47	1.41	120	60	" "
76	7.5	.47	1.41	120	60	" "

Note: All tests with AR .83 wing unless otherwise indicated.

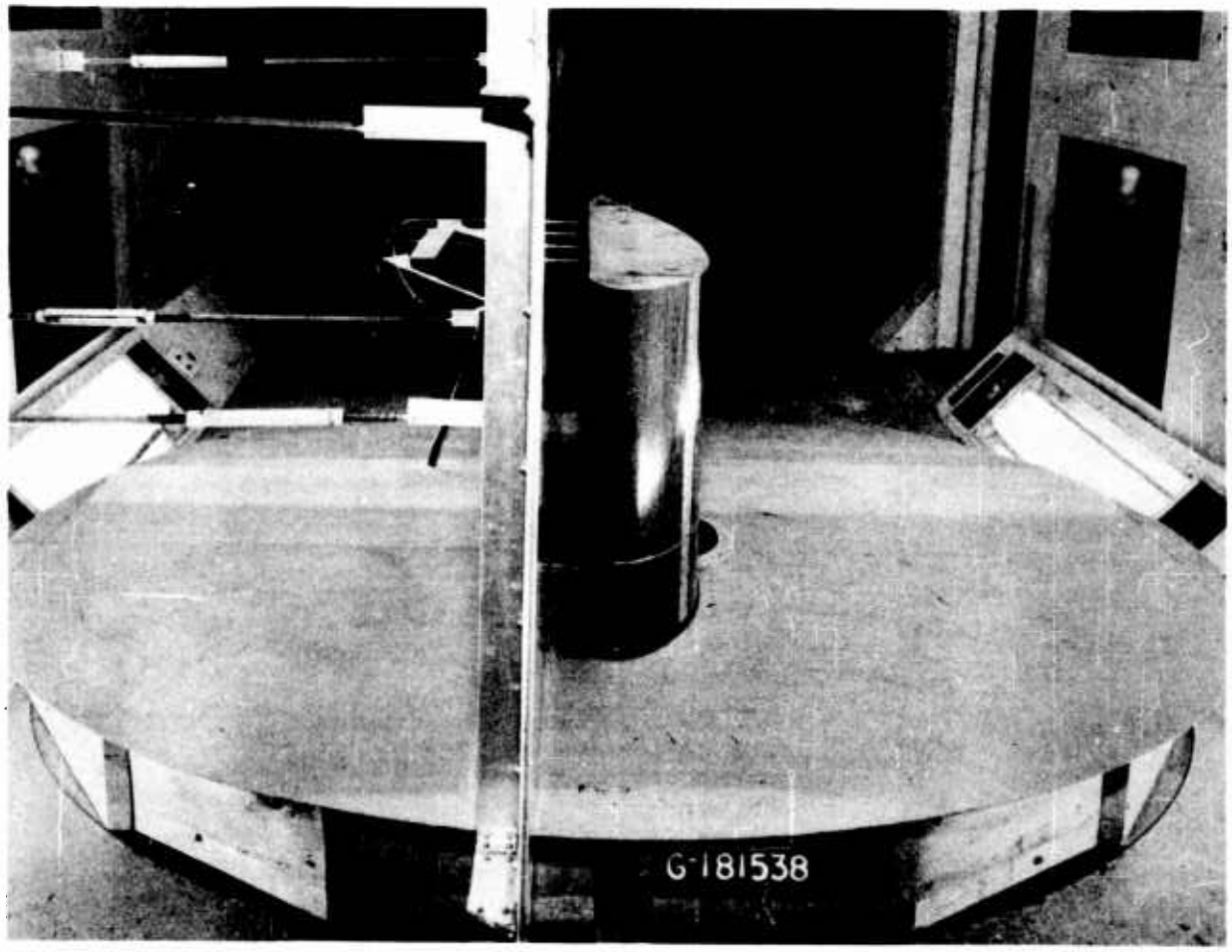

Fig. 1 Wind Tunnel Model — Front View

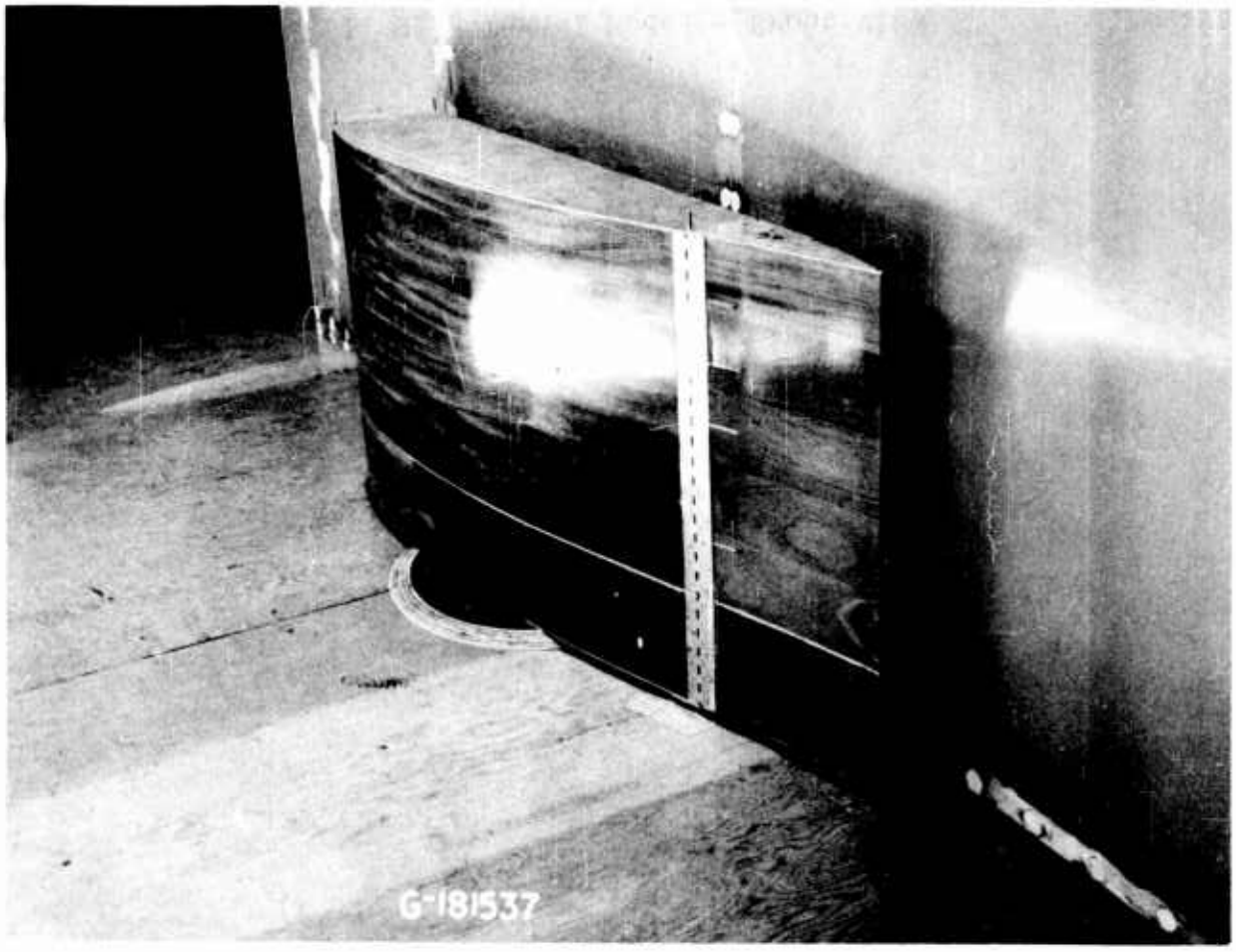

Fig. 2 Wind Tunnel Model — Rear View

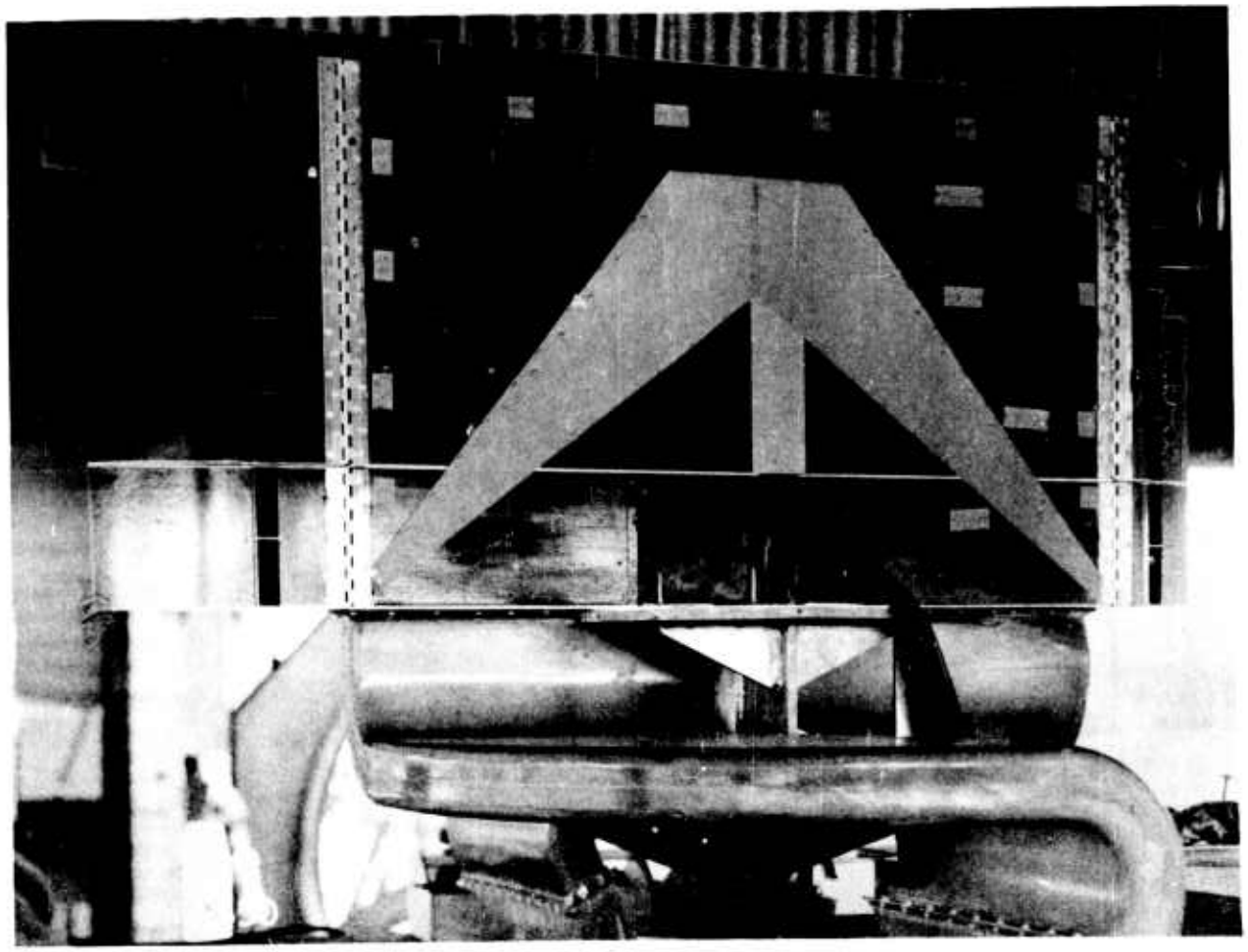

Fig. 3 Base Configuration and Air Delivery System

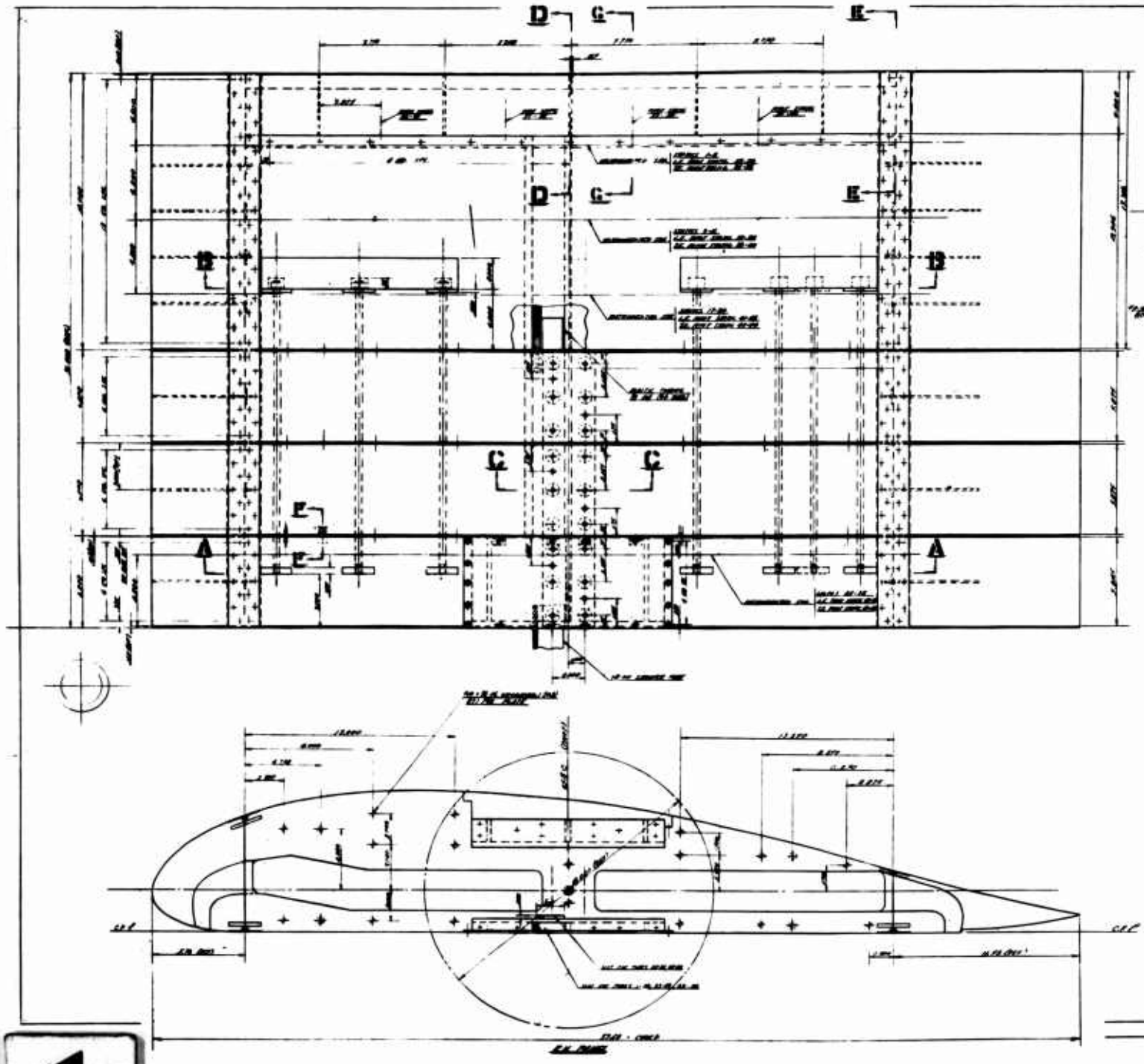

Fig. 4 Detailed Drawing

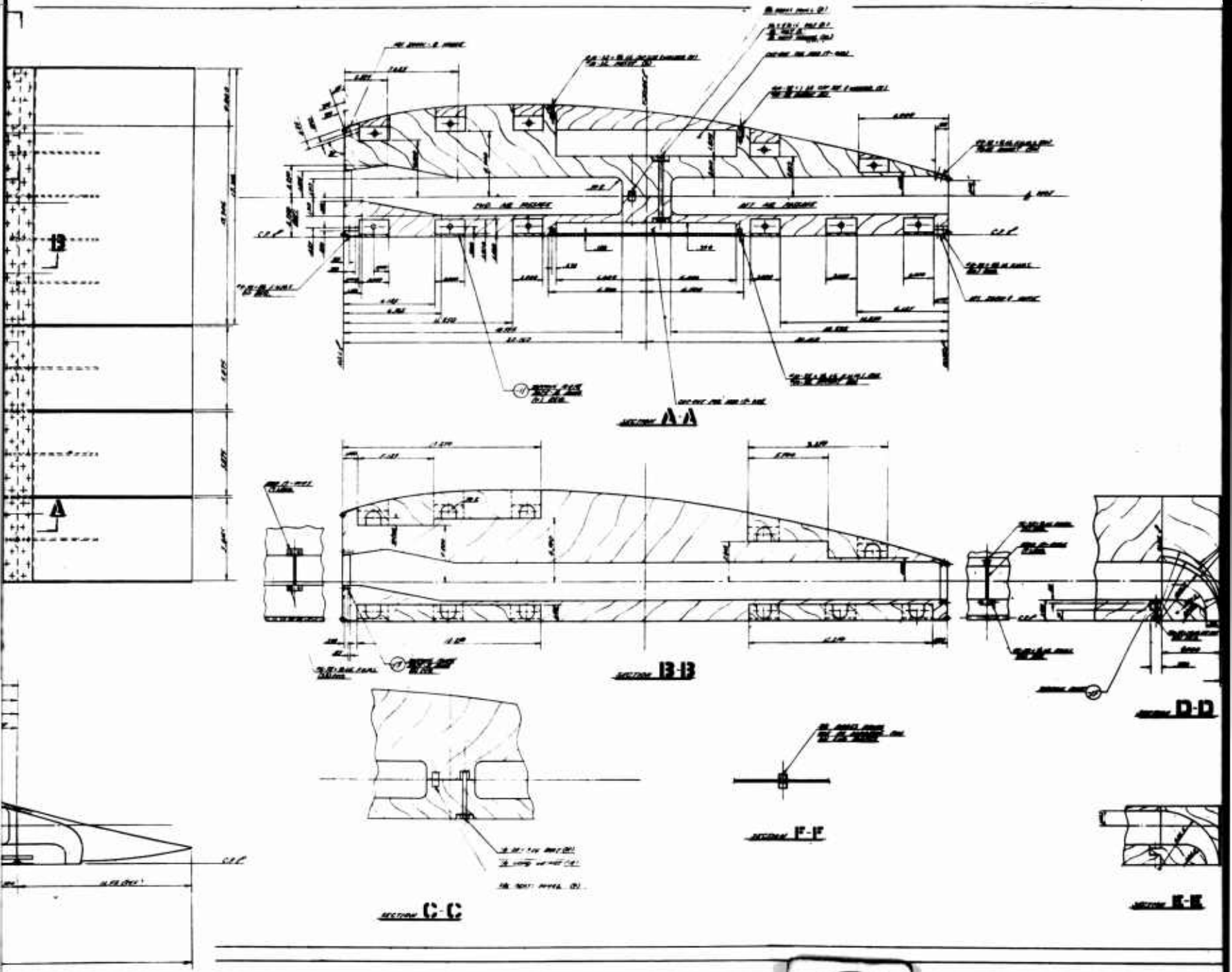

g. 4 Detailed Drawing of Model (Sheet 1 of 2)

2

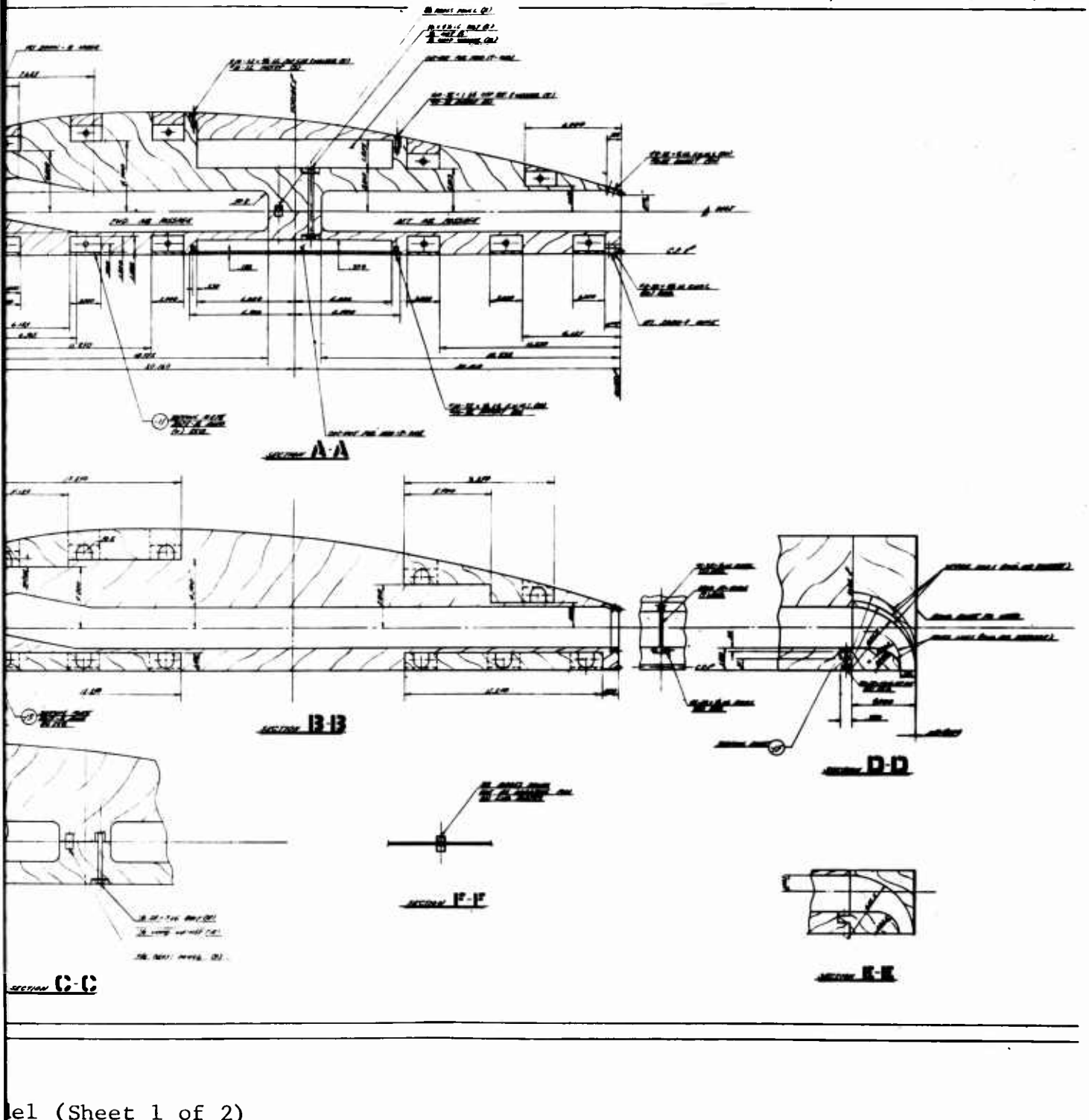

el (Sheet 1 of 2)

3

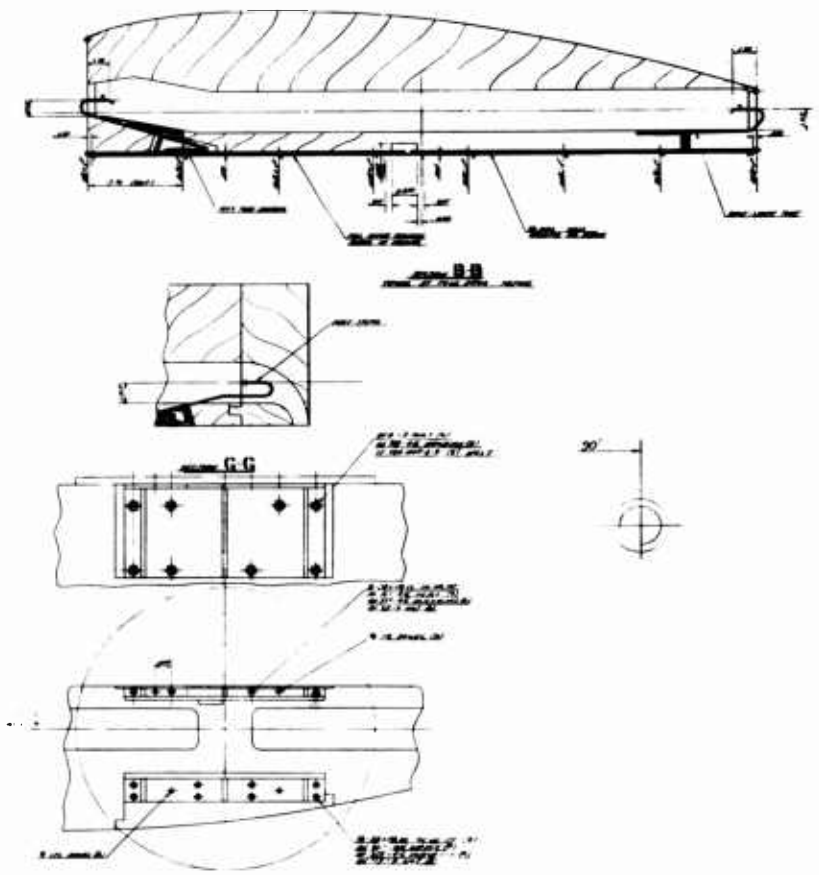

Fig. 4 Detailed Drawing of Model (Sheet 2 of 2)

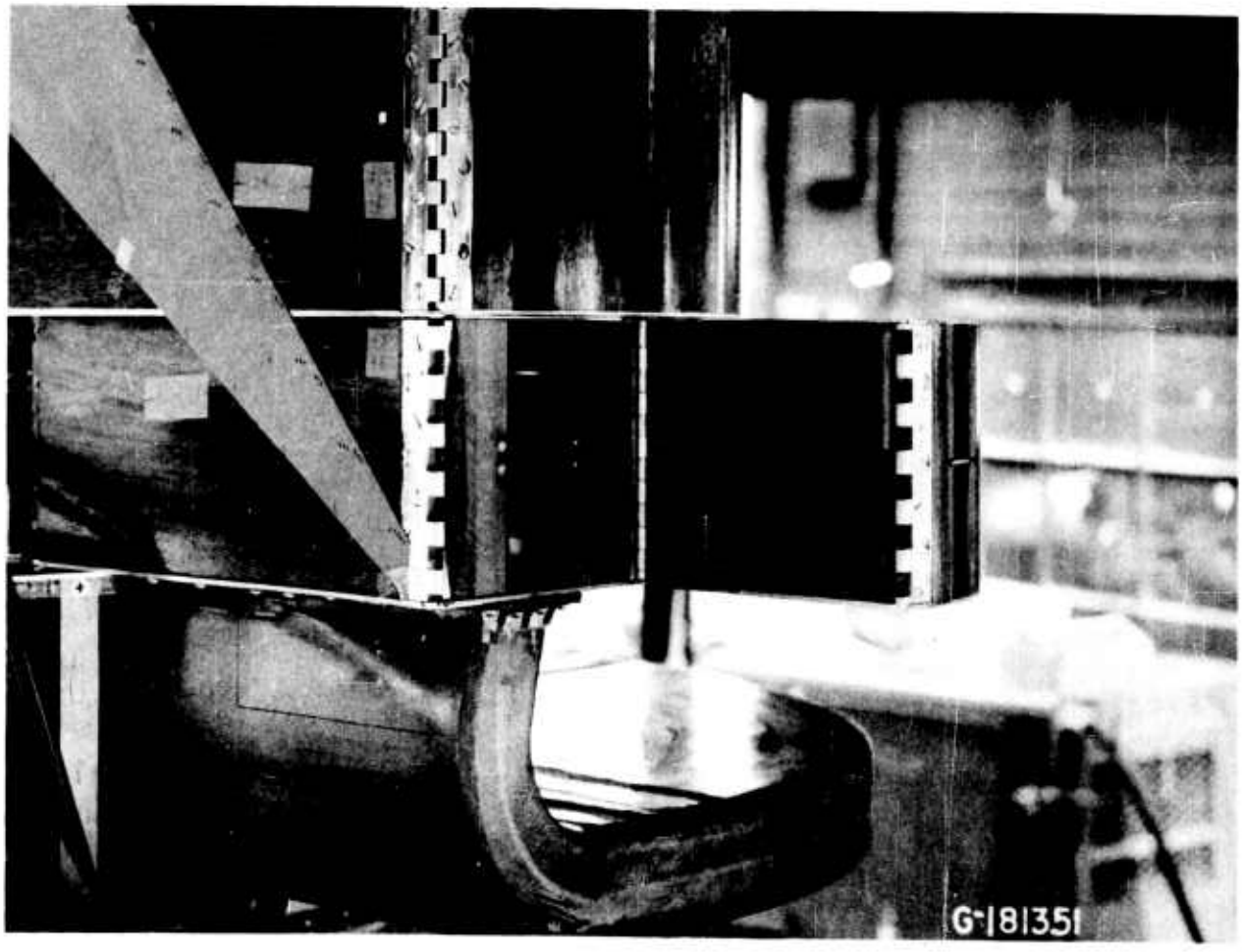

Fig. 5 Wind Tunnel Model — Replaceable Nozzle Blocks

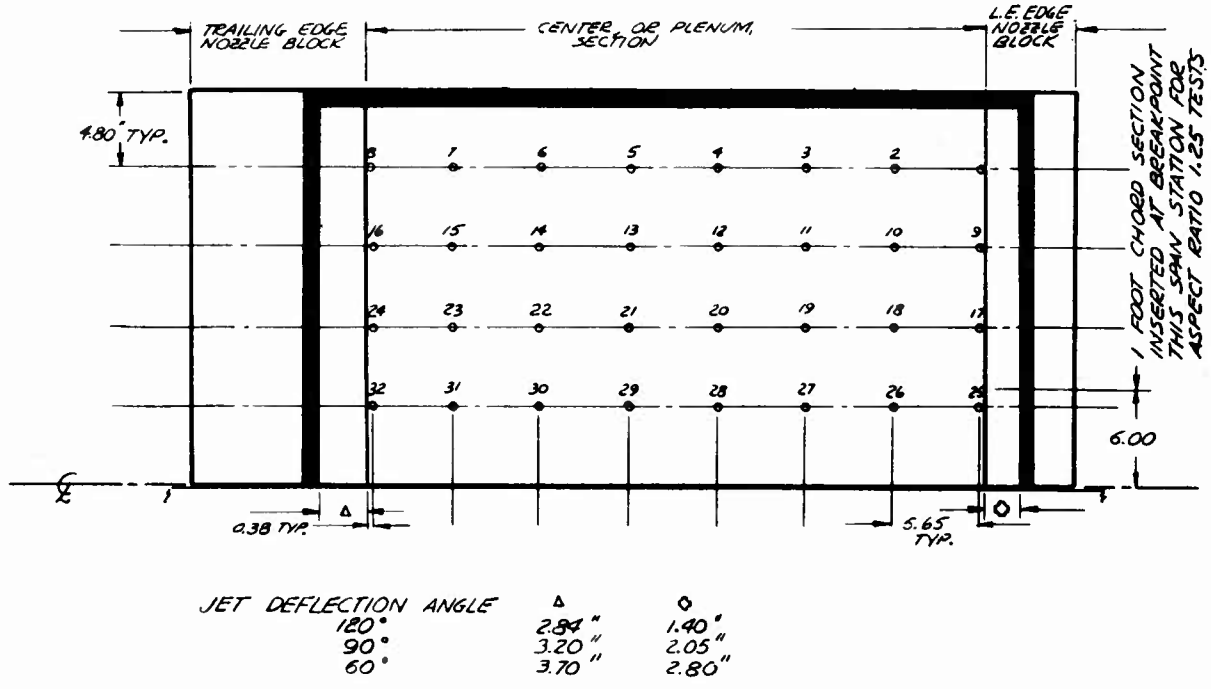

Fig. 6 Base Pressure Tap Locations

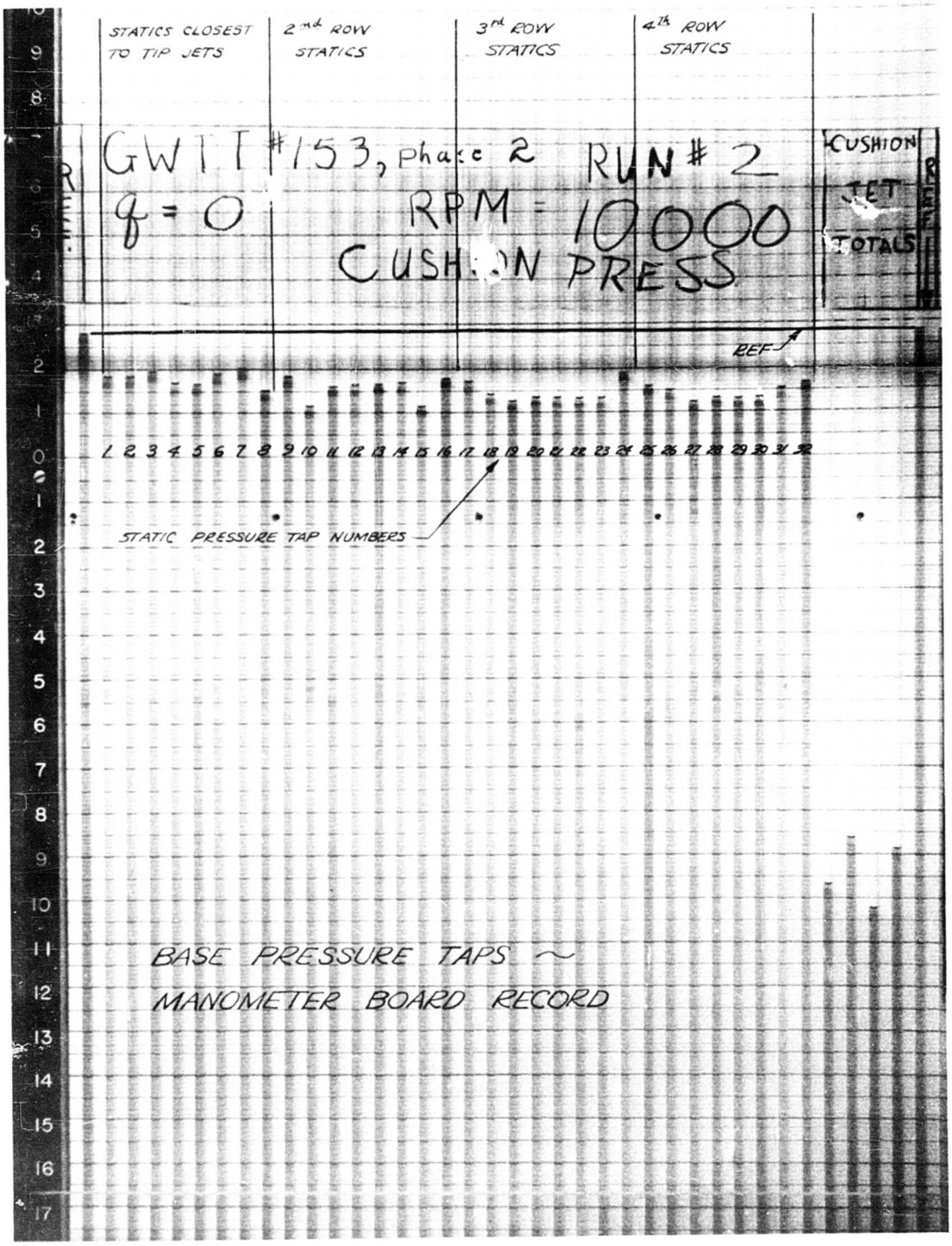

Fig. 7 Base Pressure Taps – Manometer Board Record

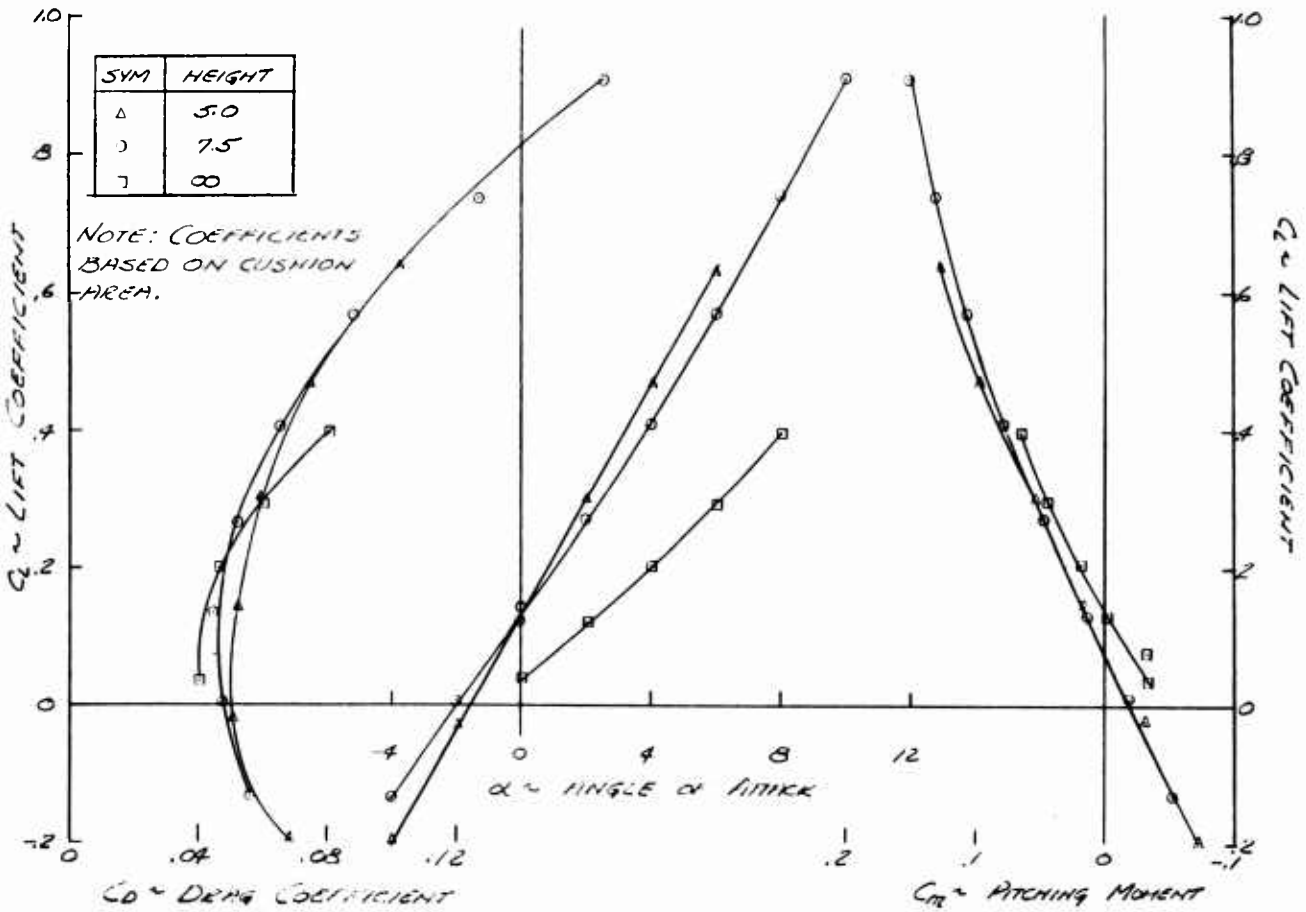

Fig. 8 Basic Aerodynamic Data - AR = .83

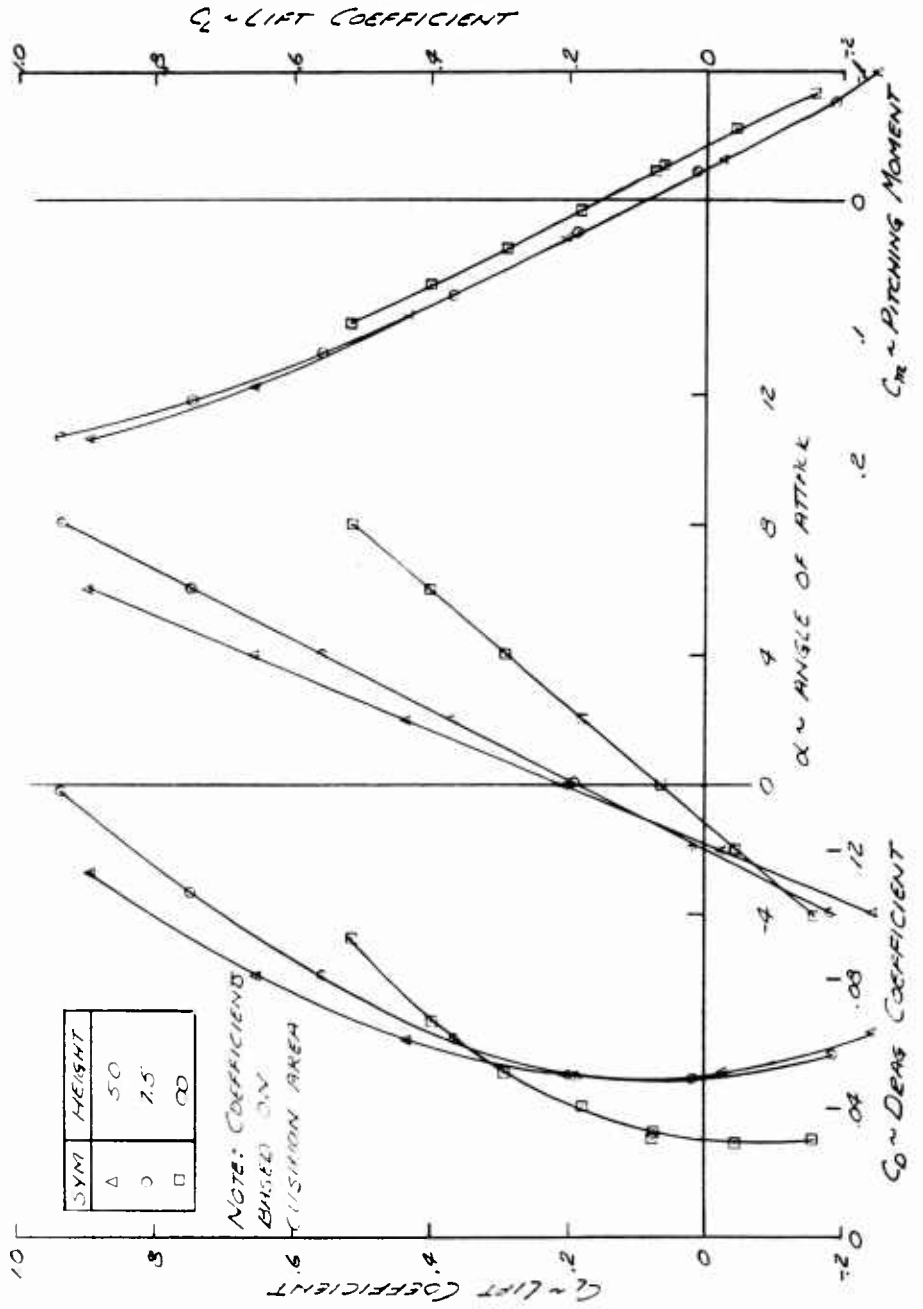

Fig. 9 Basic Aerodynamic Data - AR = 1.25

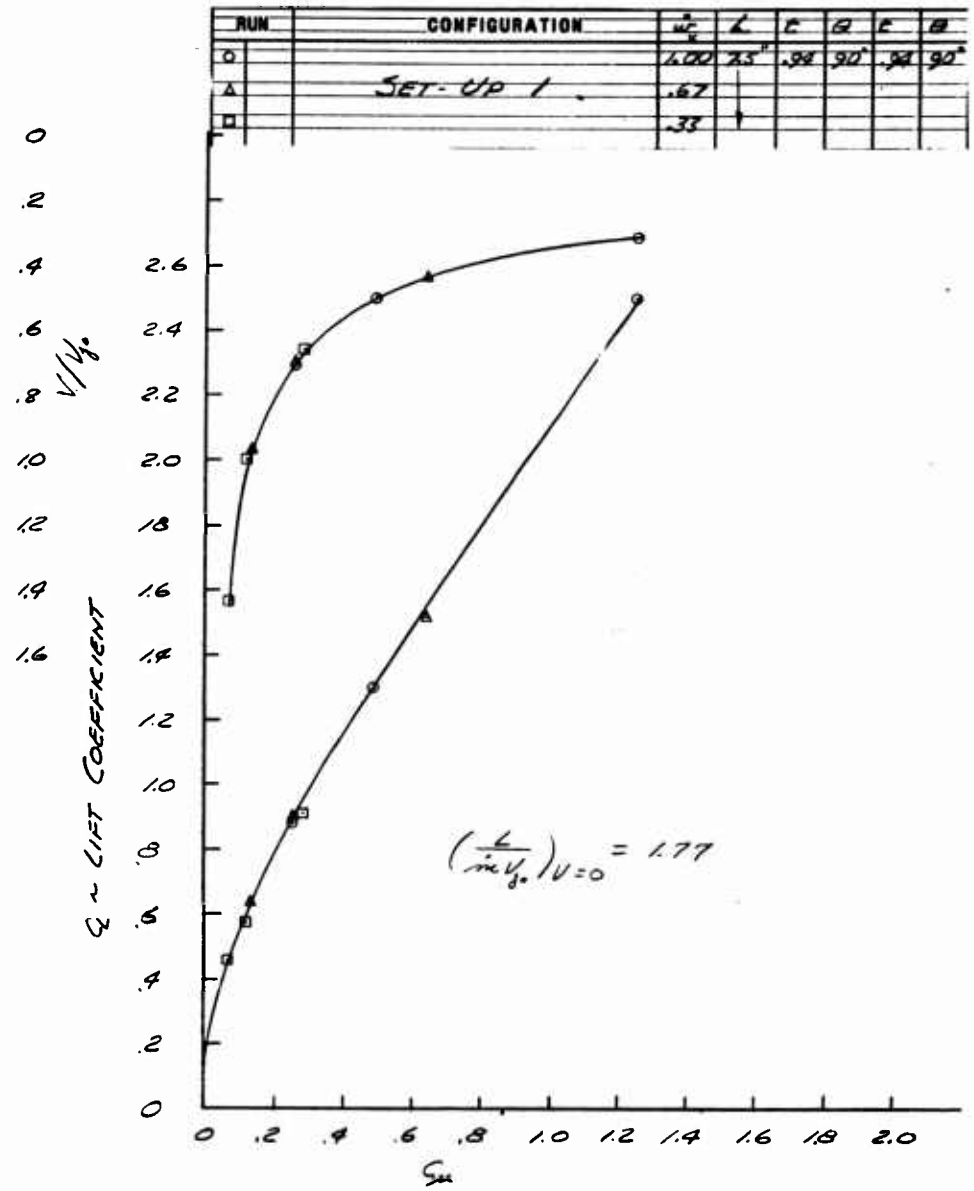

Fig. 10 C_L and V/V_{j_o} vs C_μ

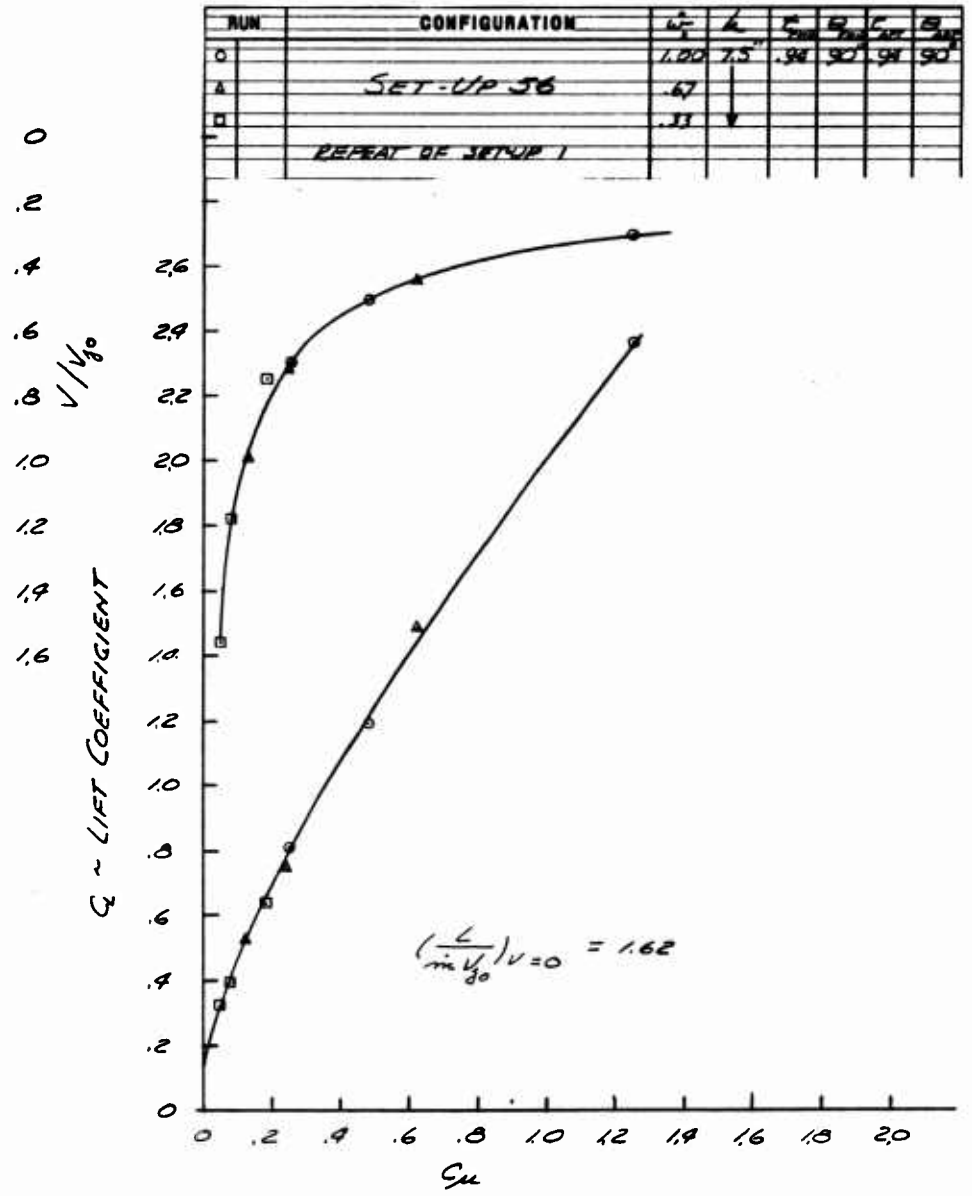

Fig. 10a C_L and V/V_{j_o} vs C_μ

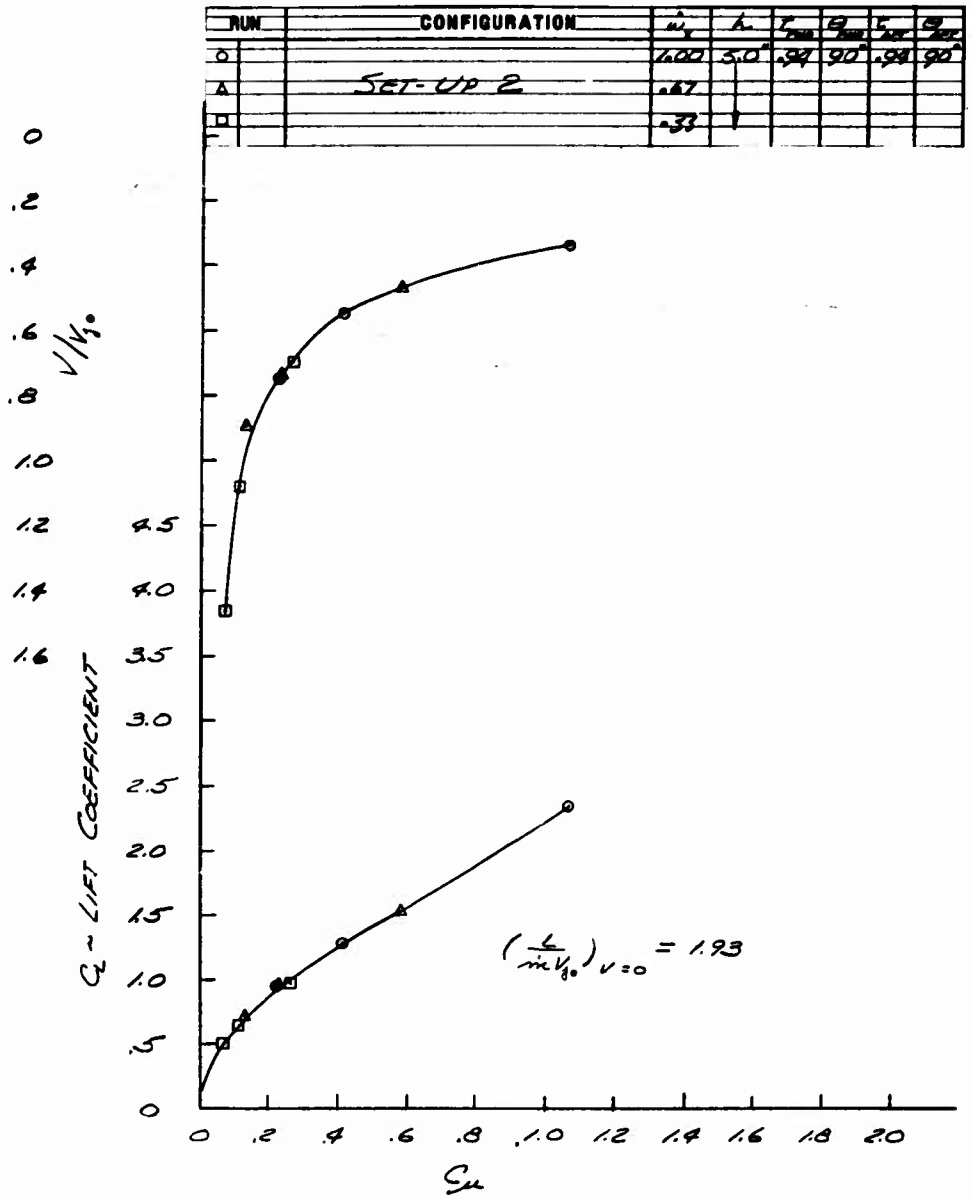

Fig. 11 C_L and V/V_{j_o} vs C_μ

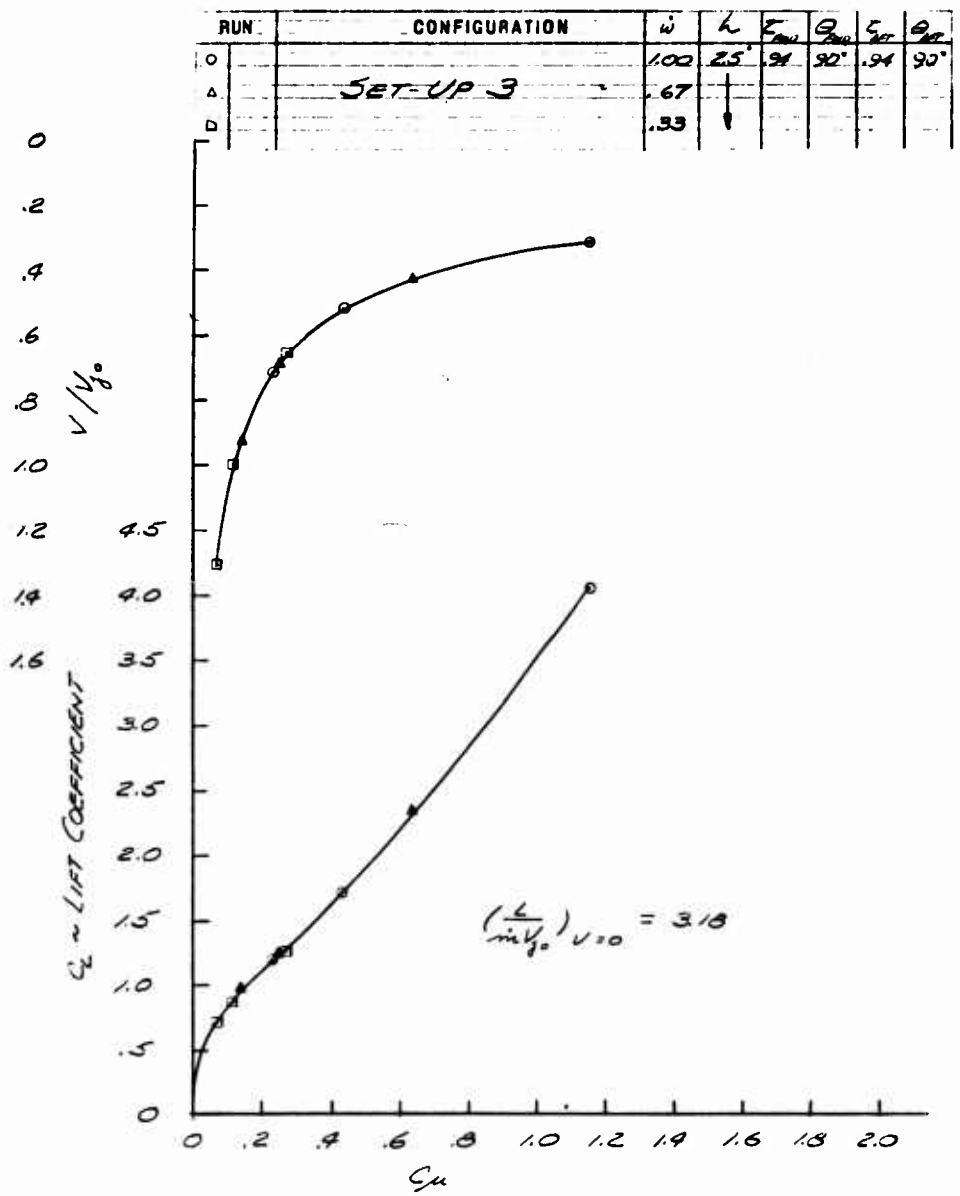

Fig. 12 C_L and V/V_{j_o} vs C_μ

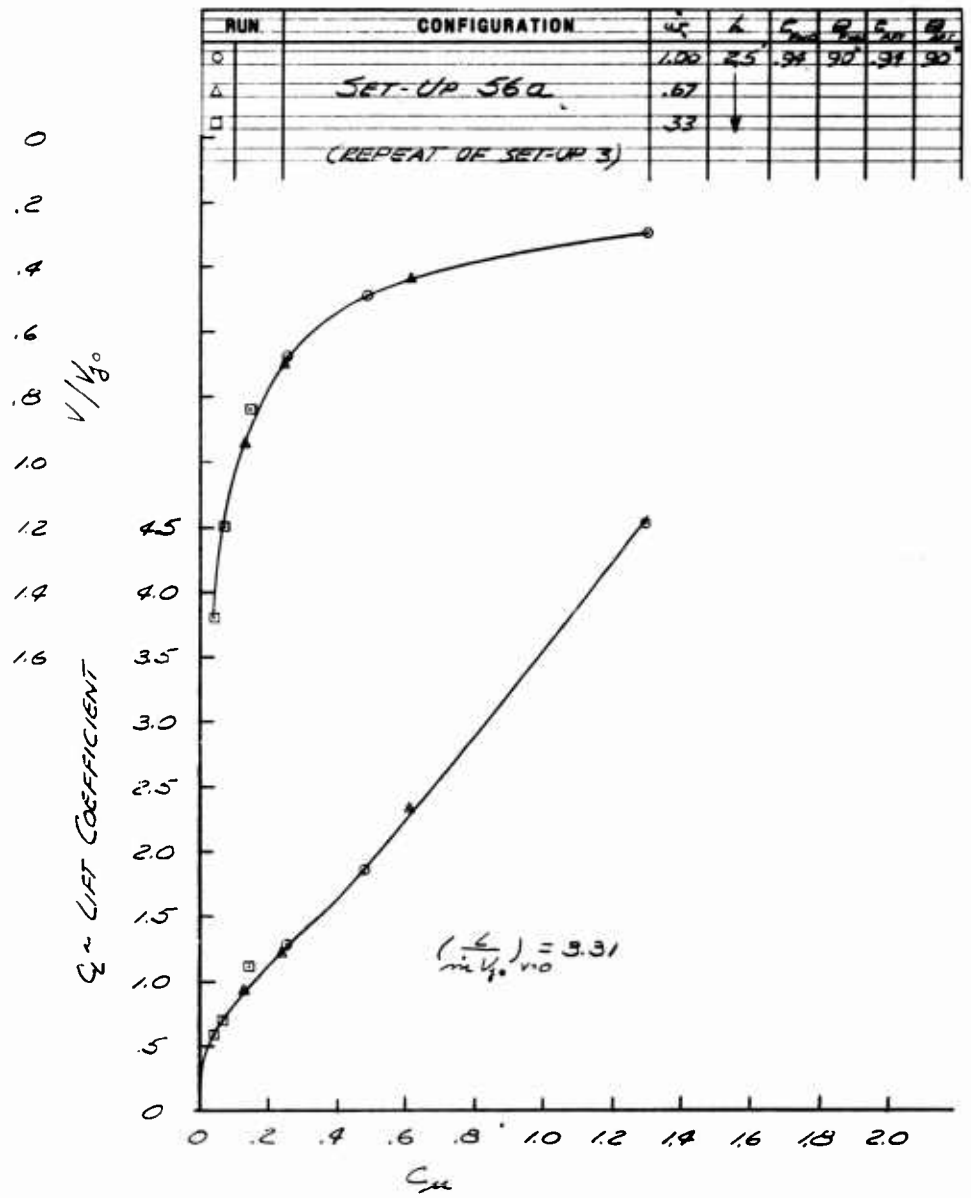

Fig. 12a C_L and V/V_{j_o} vs C_μ

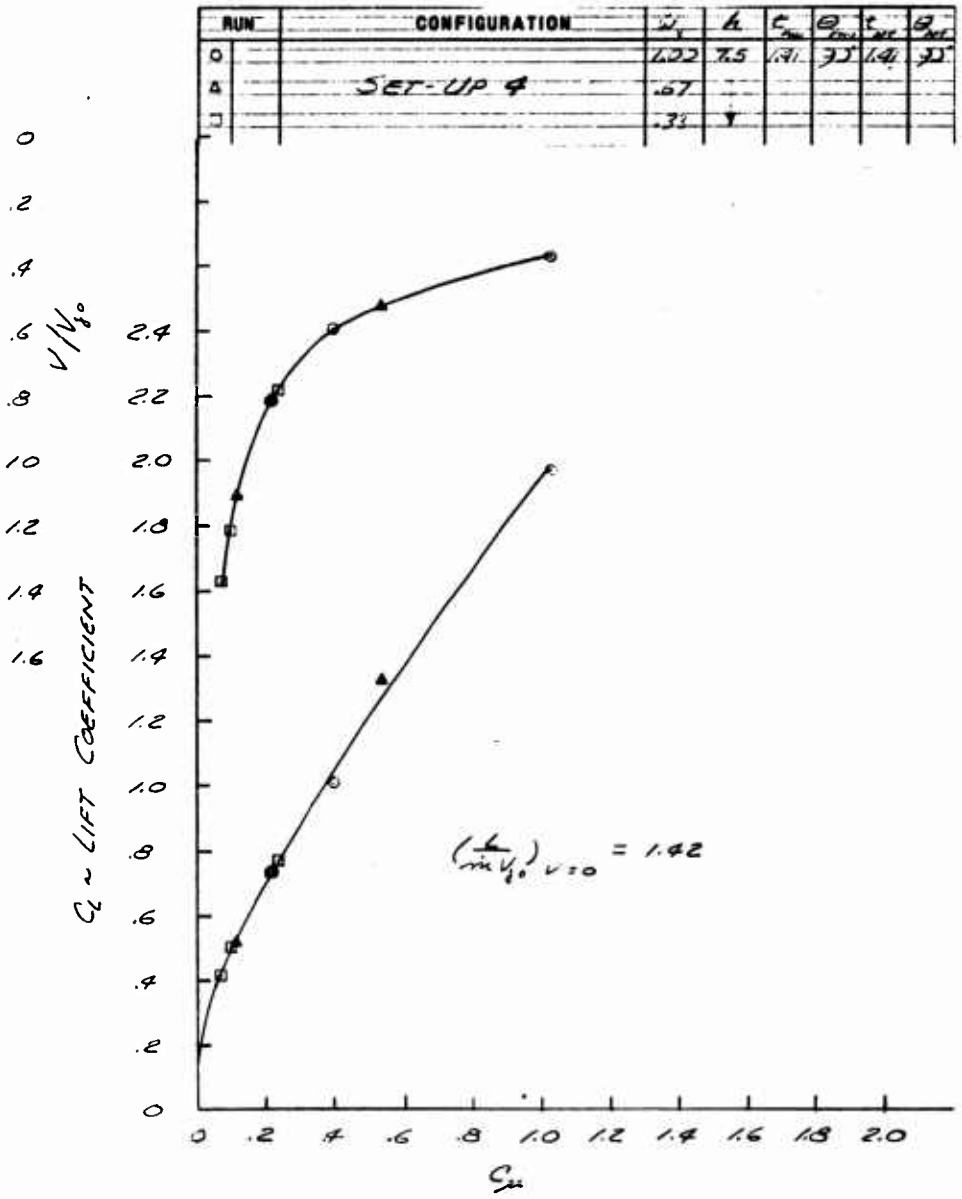

Fig. 13 C_L and V/V_{j_o} vs C_μ

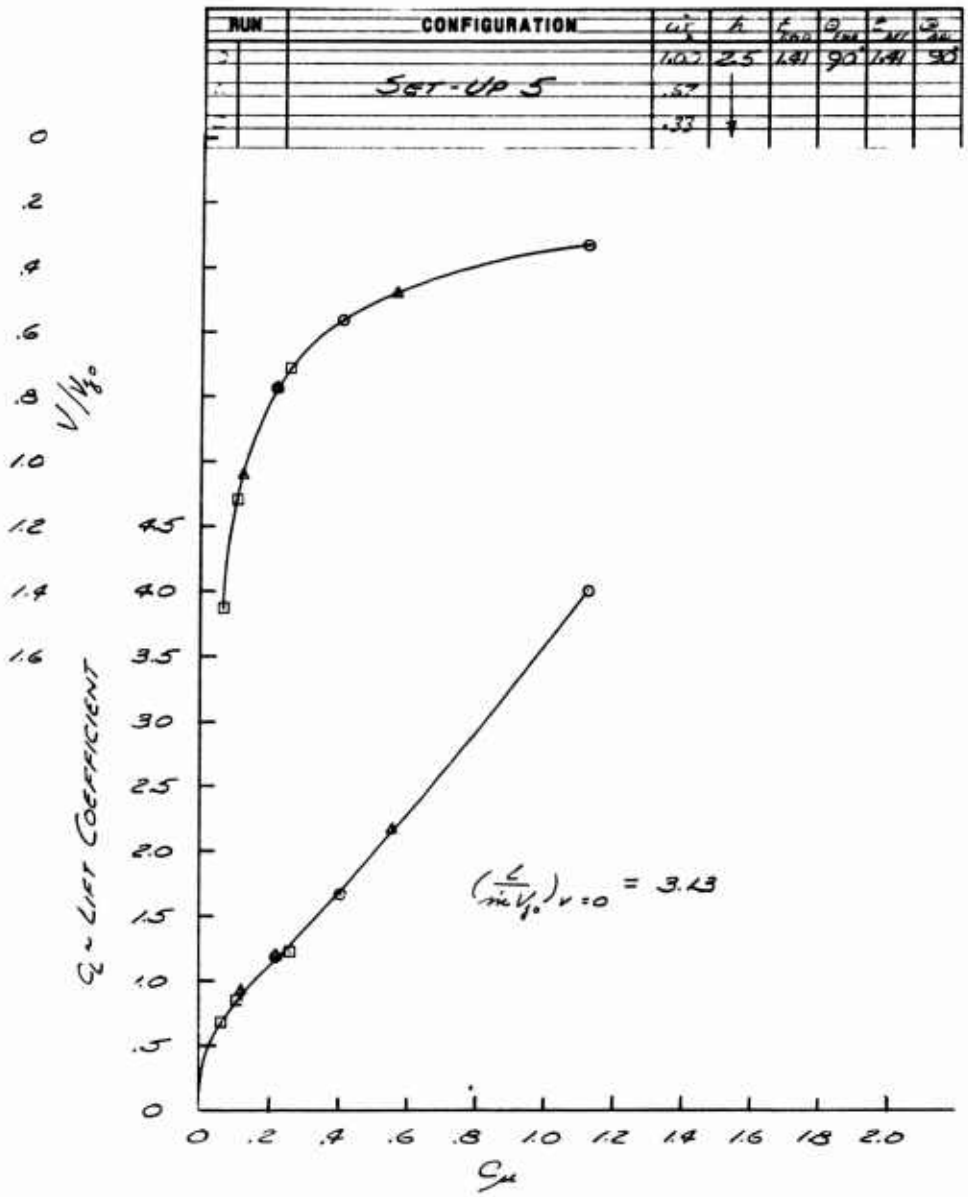

Fig. 14 C_L and V/V_{j_o} vs C_μ

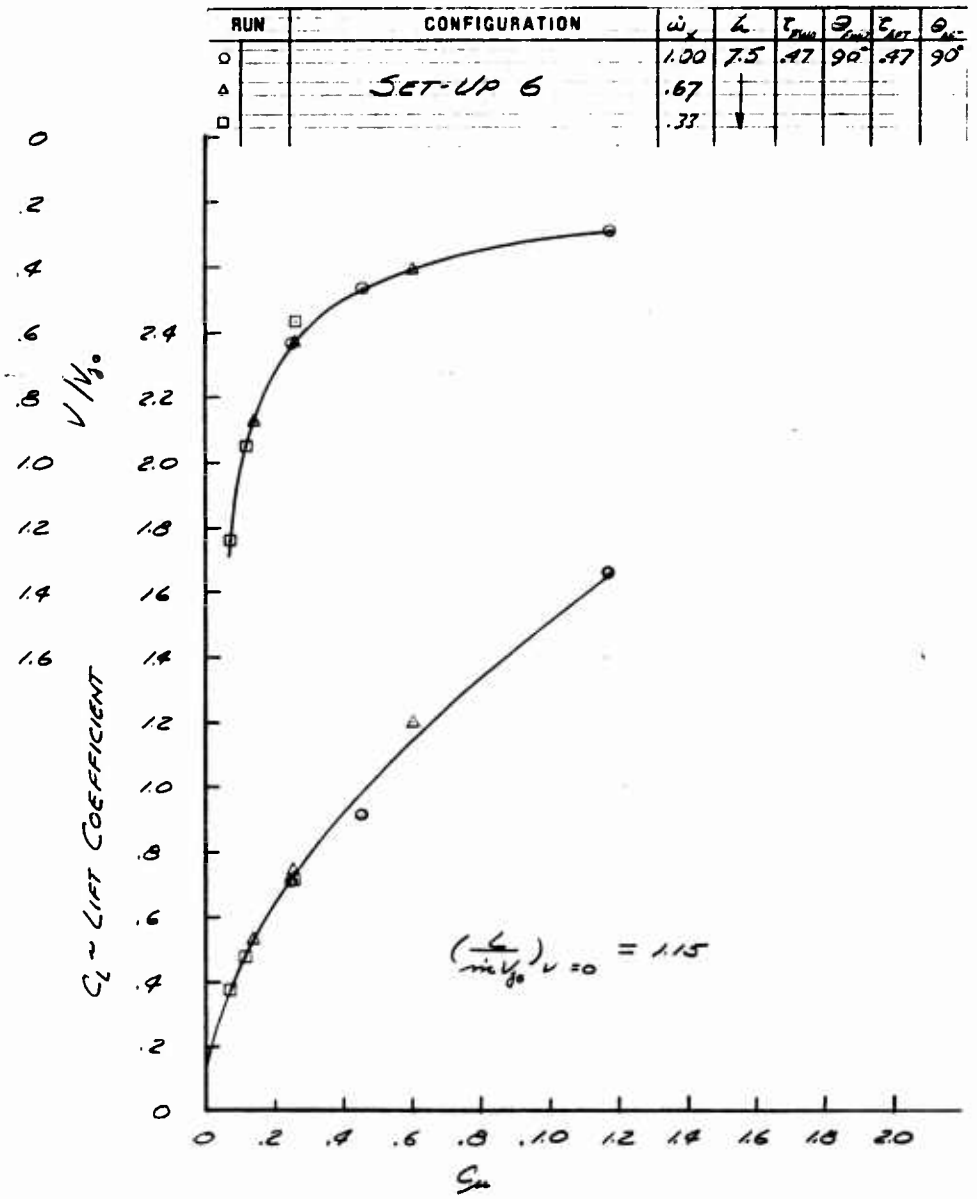

Fig. 15 C_L and V/V_{j_o} vs C_μ

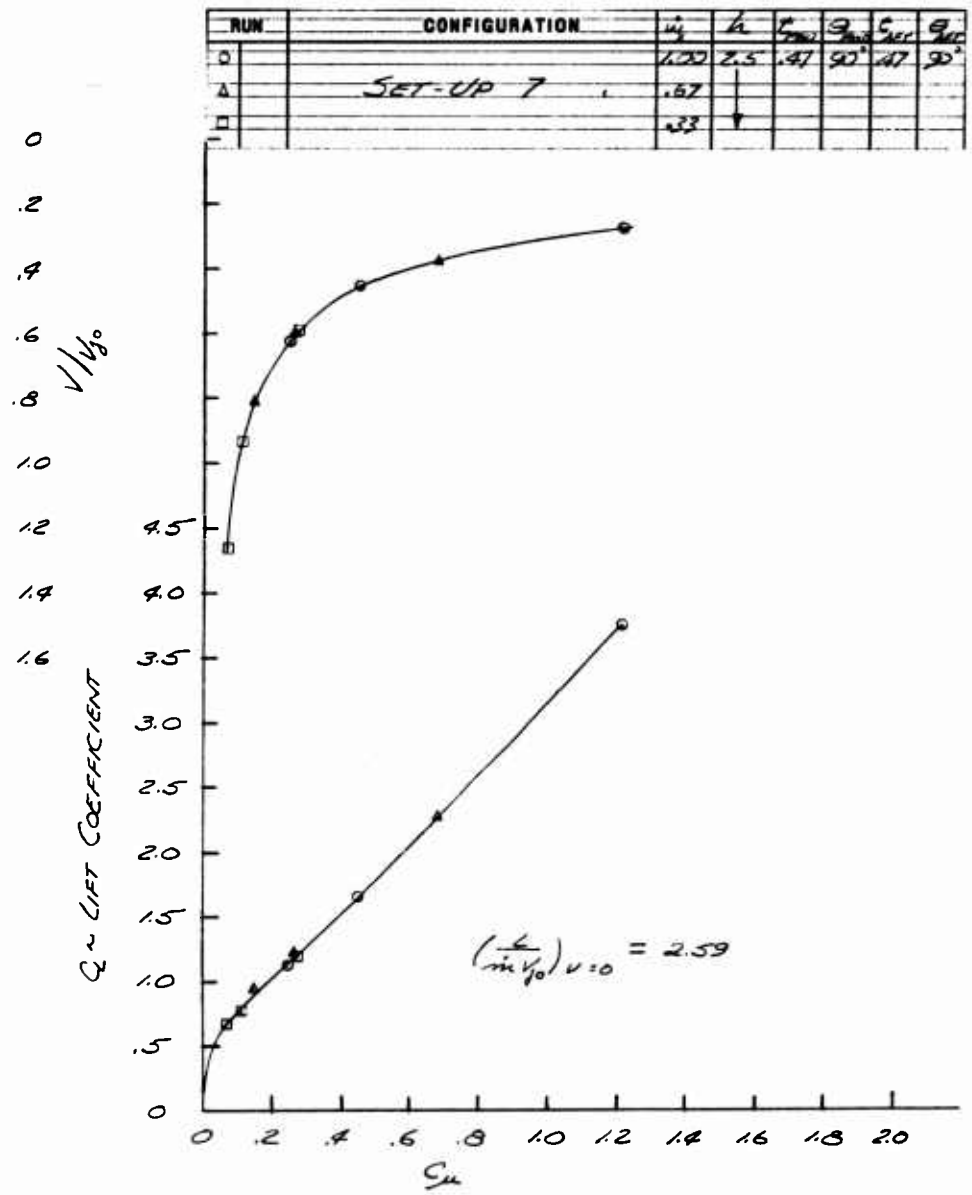

Fig. 16 C_L and V/V_{j_o} vs C_μ

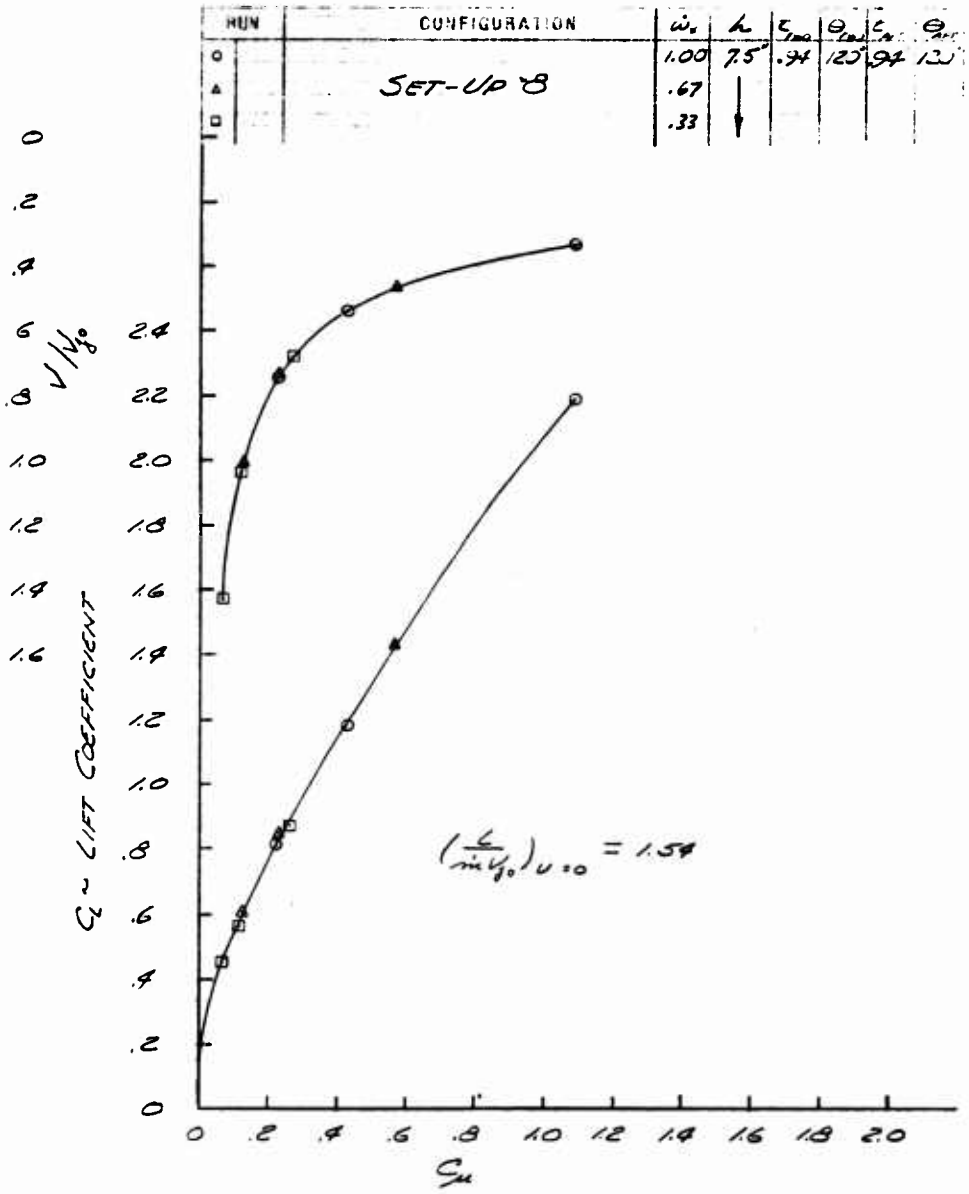

Fig. 17 C_L and V/V_{j_o} vs C_μ

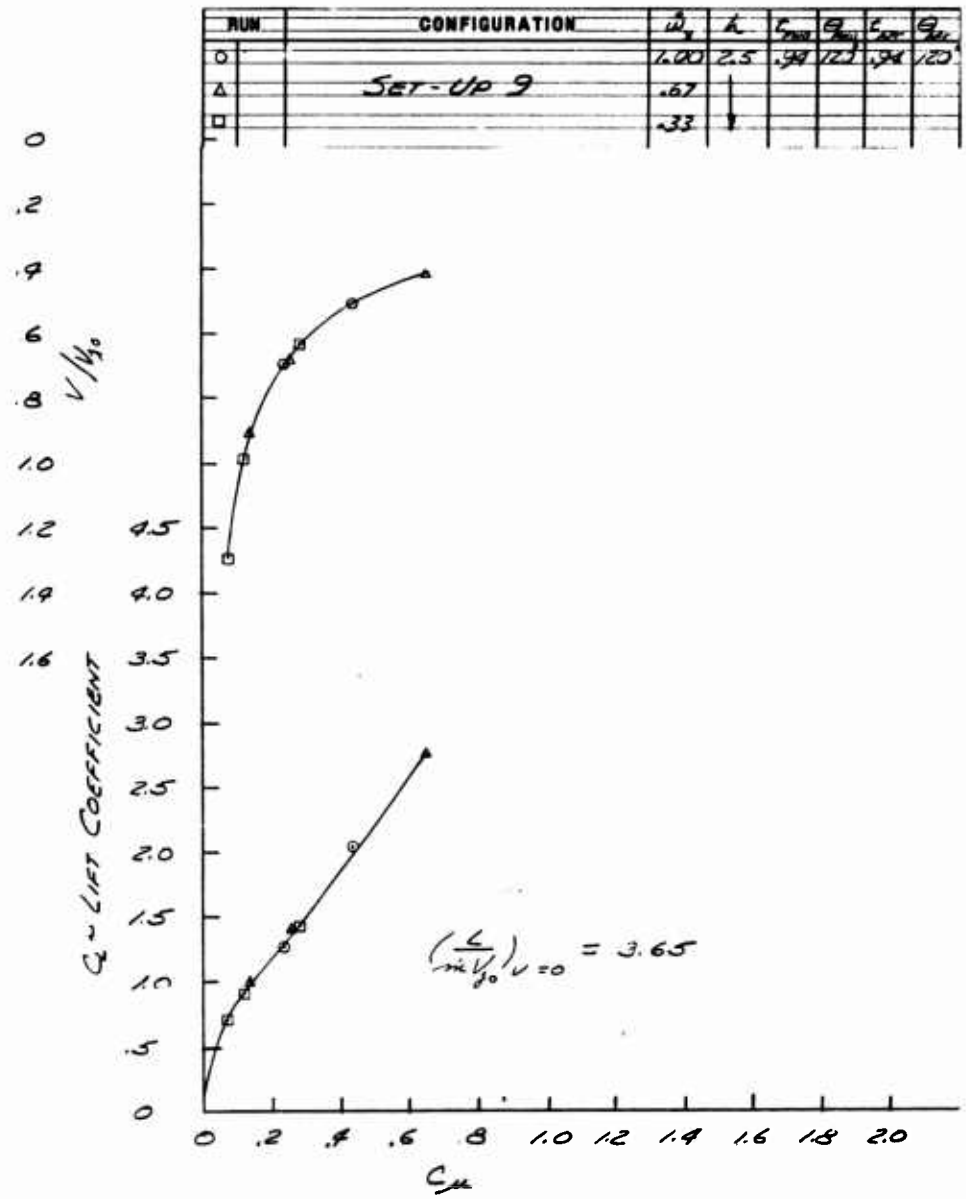

Fig. 18 C_L and V/V_{j_o} vs C_μ

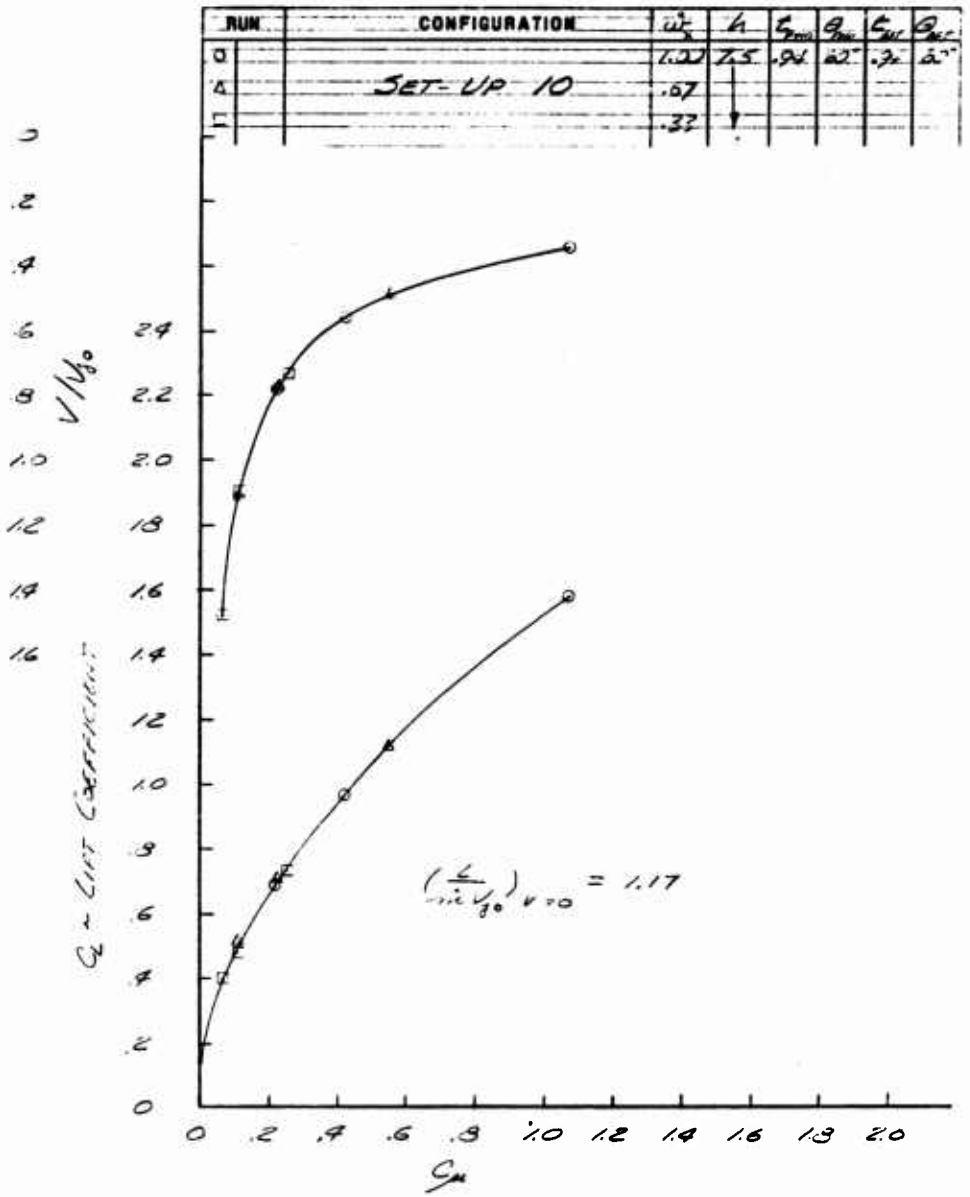

Fig. 19 C_L and V/V_{j_o} vs C_μ

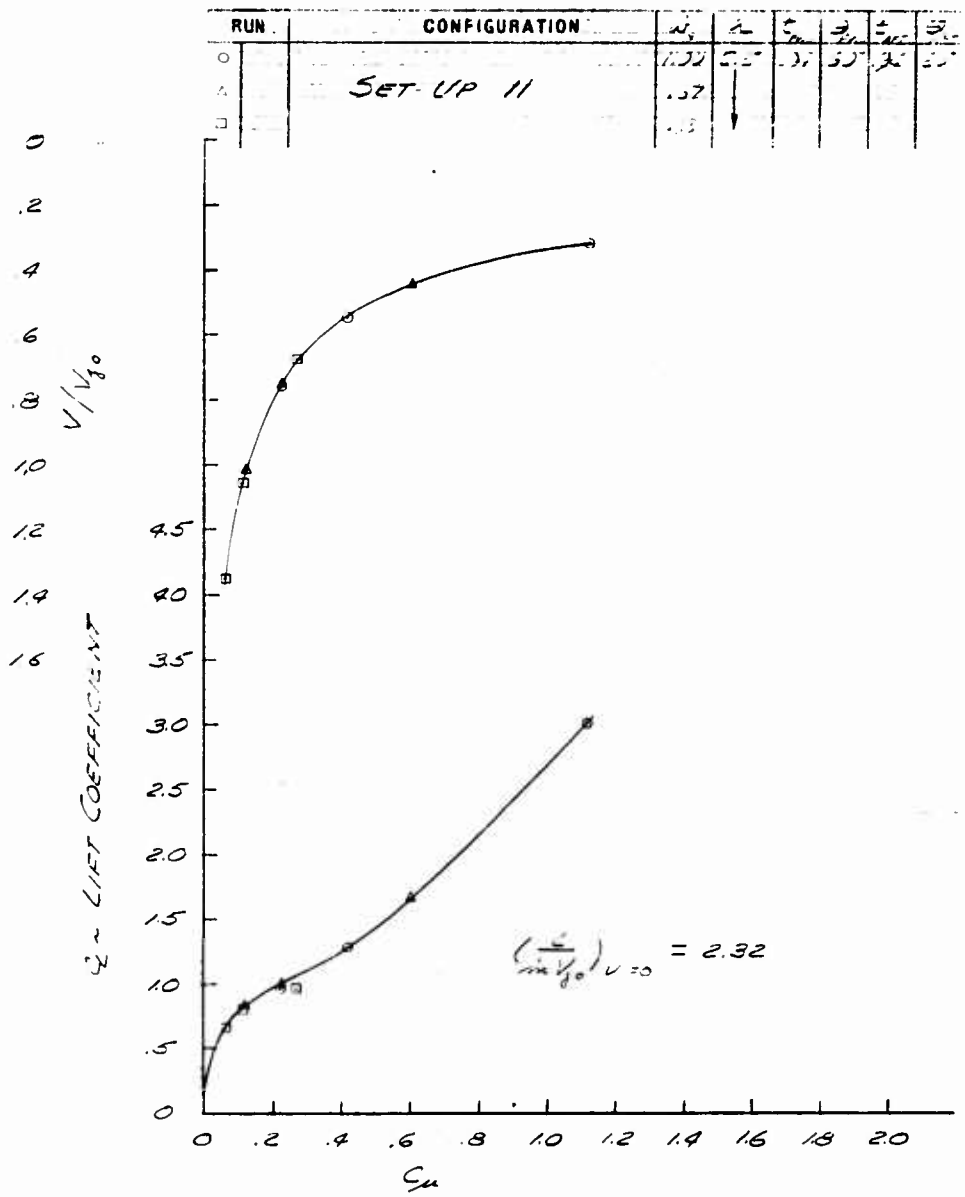

Fig. 20 C_L and V/V_{j_o} vs C_μ

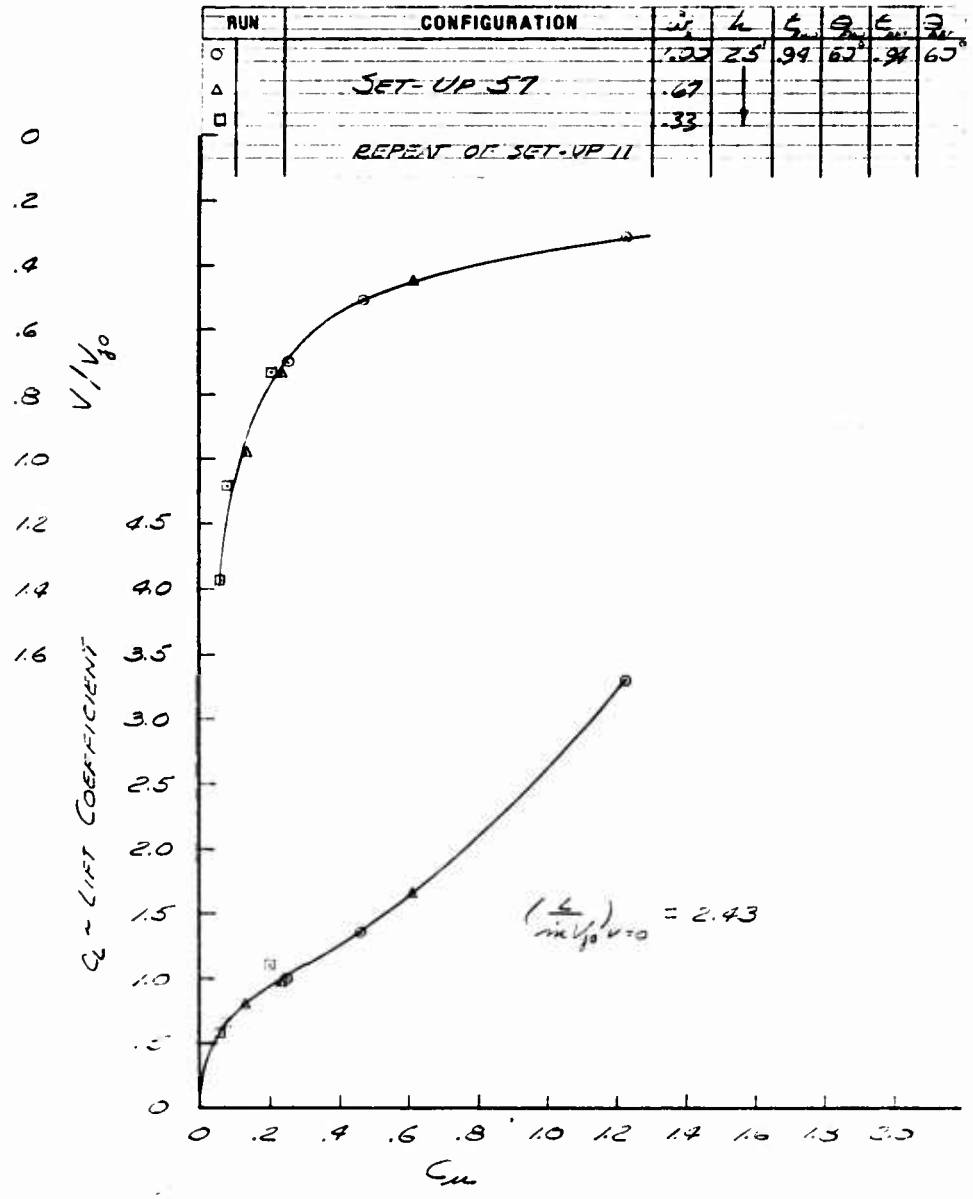

Fig. 20a C_L and V/V_{j_o} vs C_μ

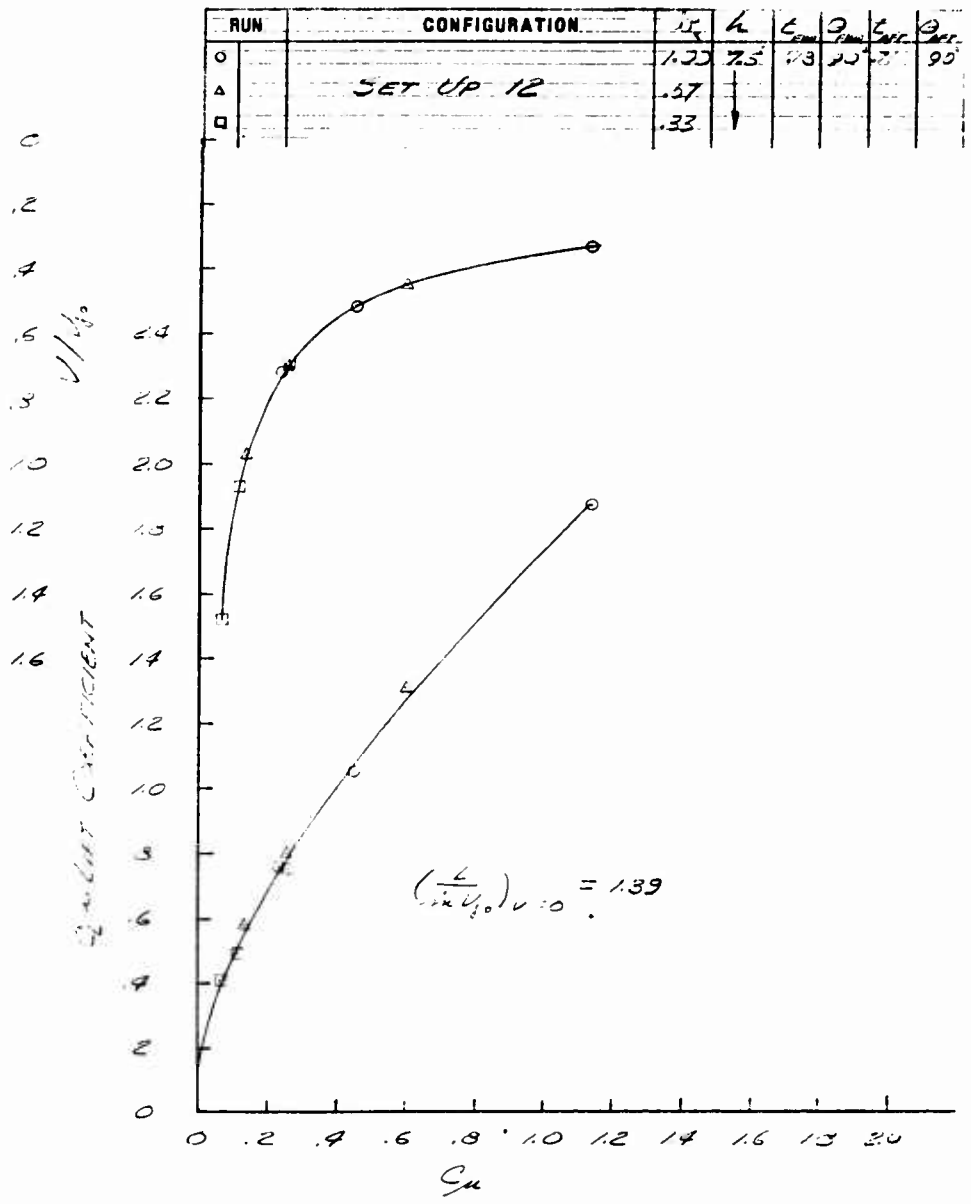

Fig. 21 C_L and V/V_{j_o} vs C_μ

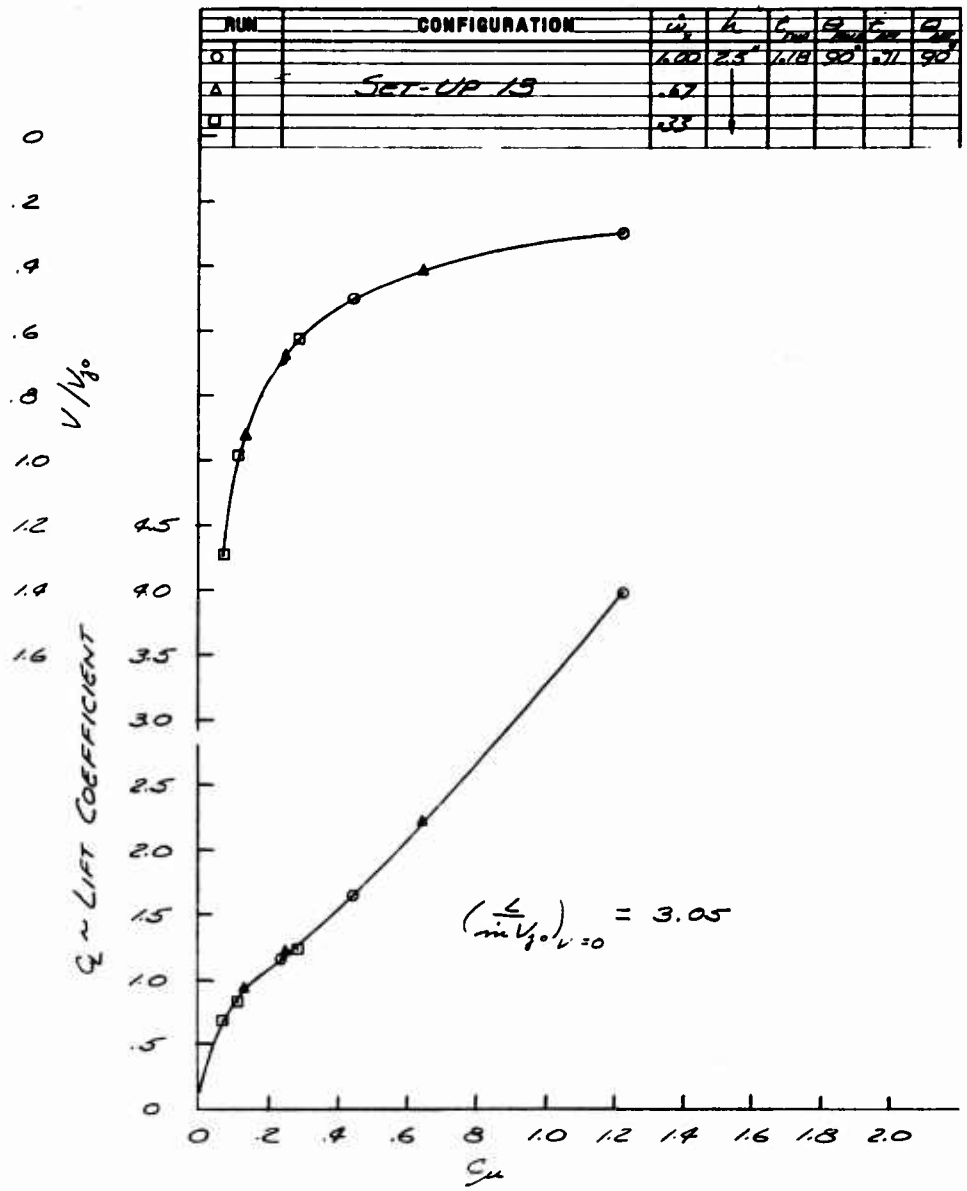

Fig. 22 C_L and V/V_{j_o} vs C_μ

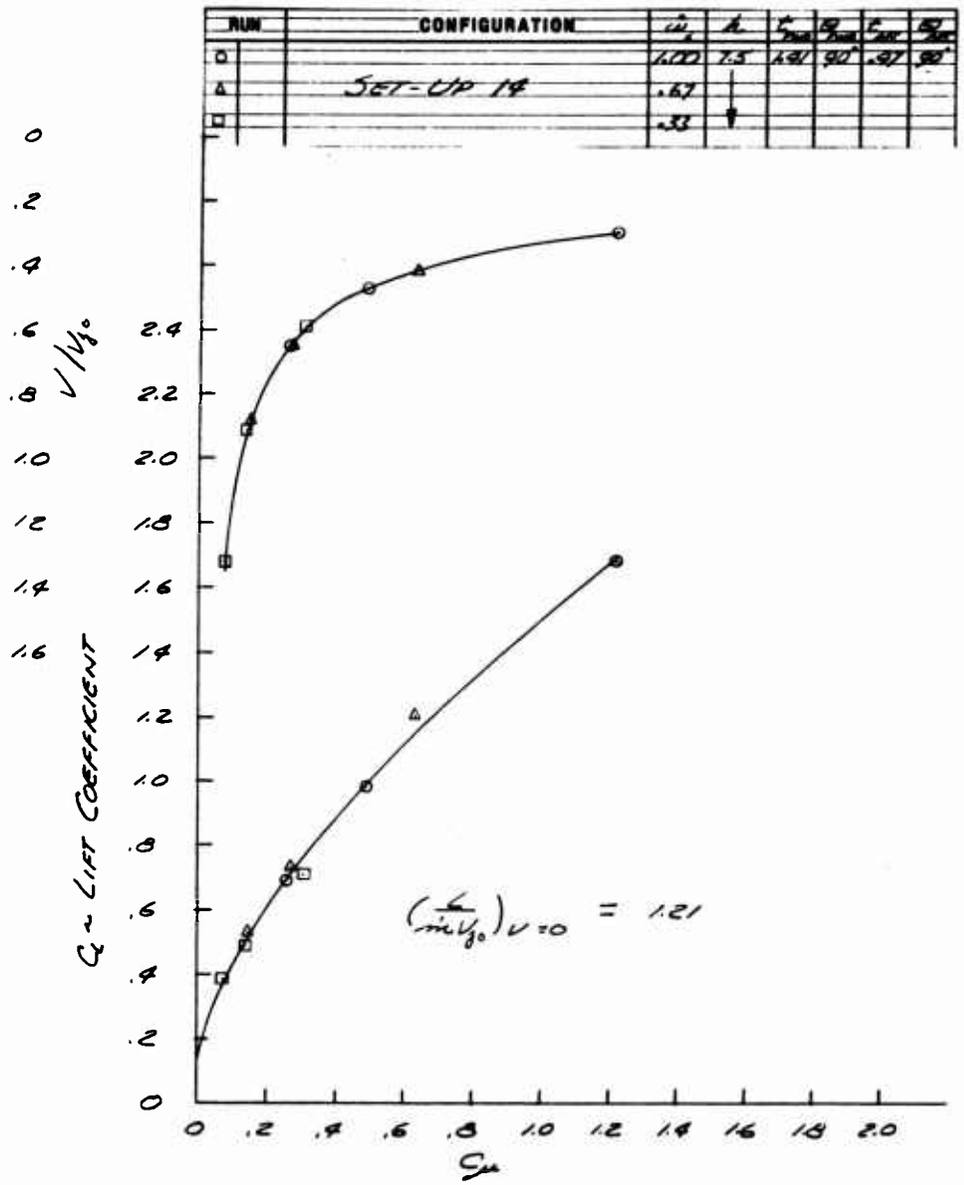

Fig. 23 C_L and V/V_{j_o} vs C_μ

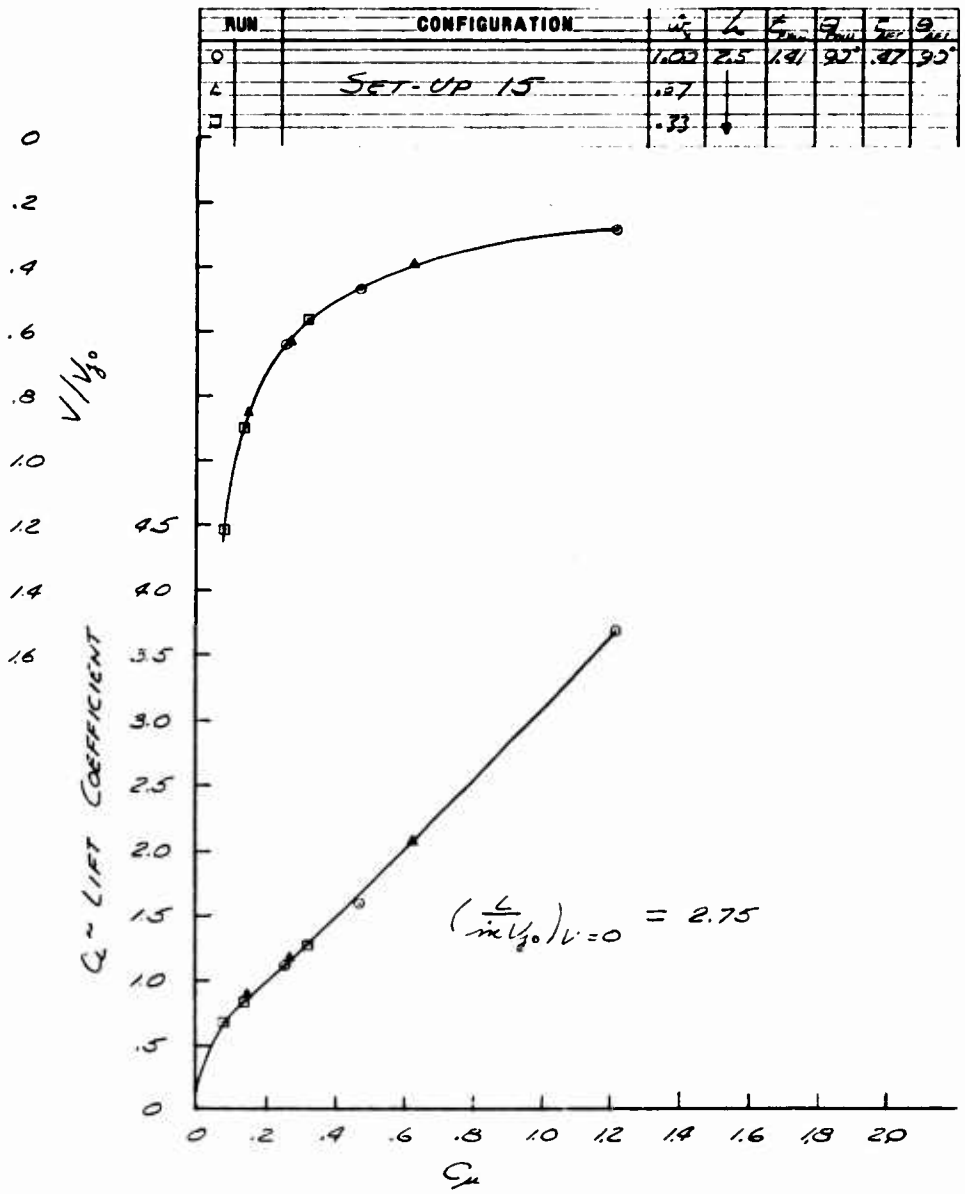

Fig. 24 C_L and V/V_{j_o} vs C_μ

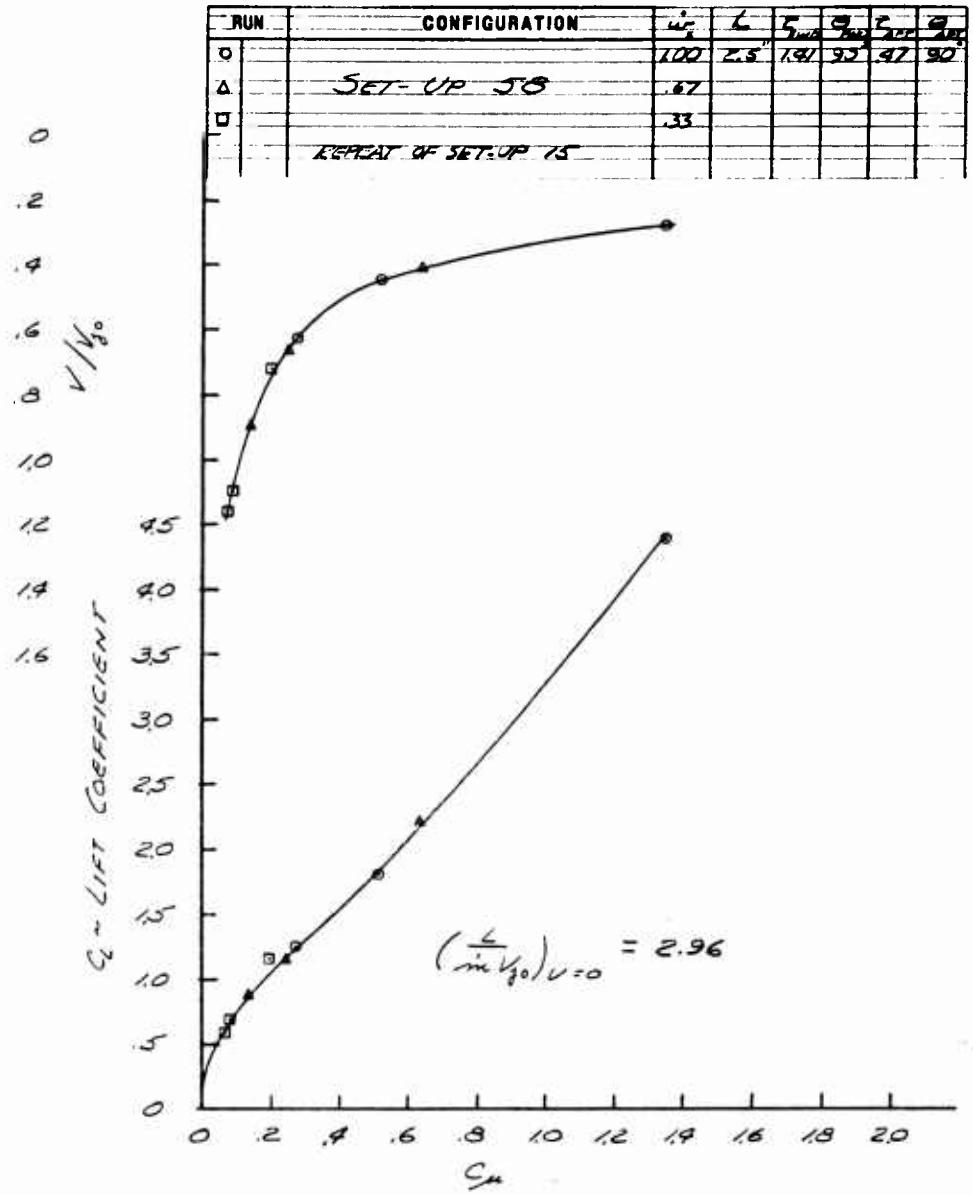

Fig. 24a C_L and V/V_{j_o} vs C_μ

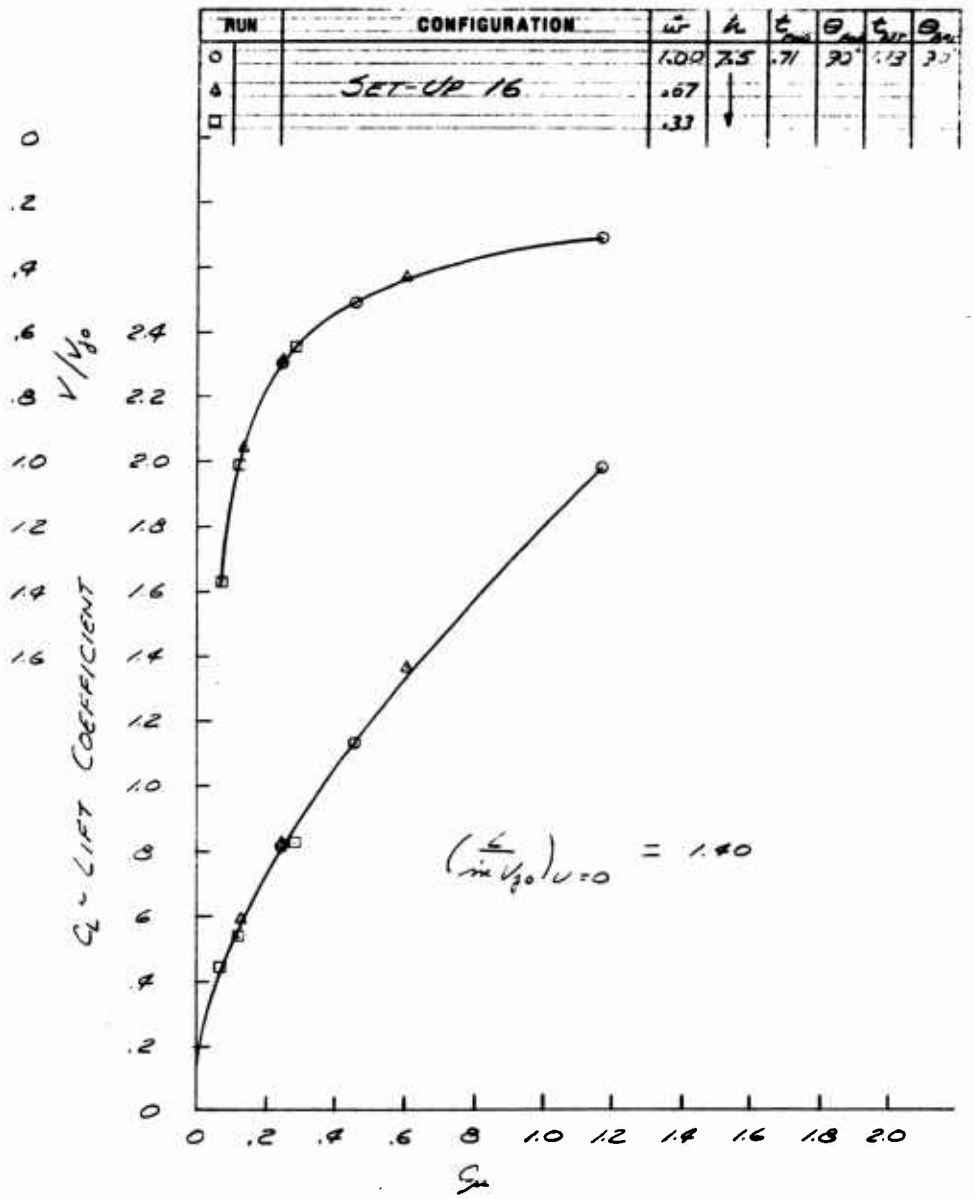

Fig. 25 C_L and V/V_{j_o} vs C_μ

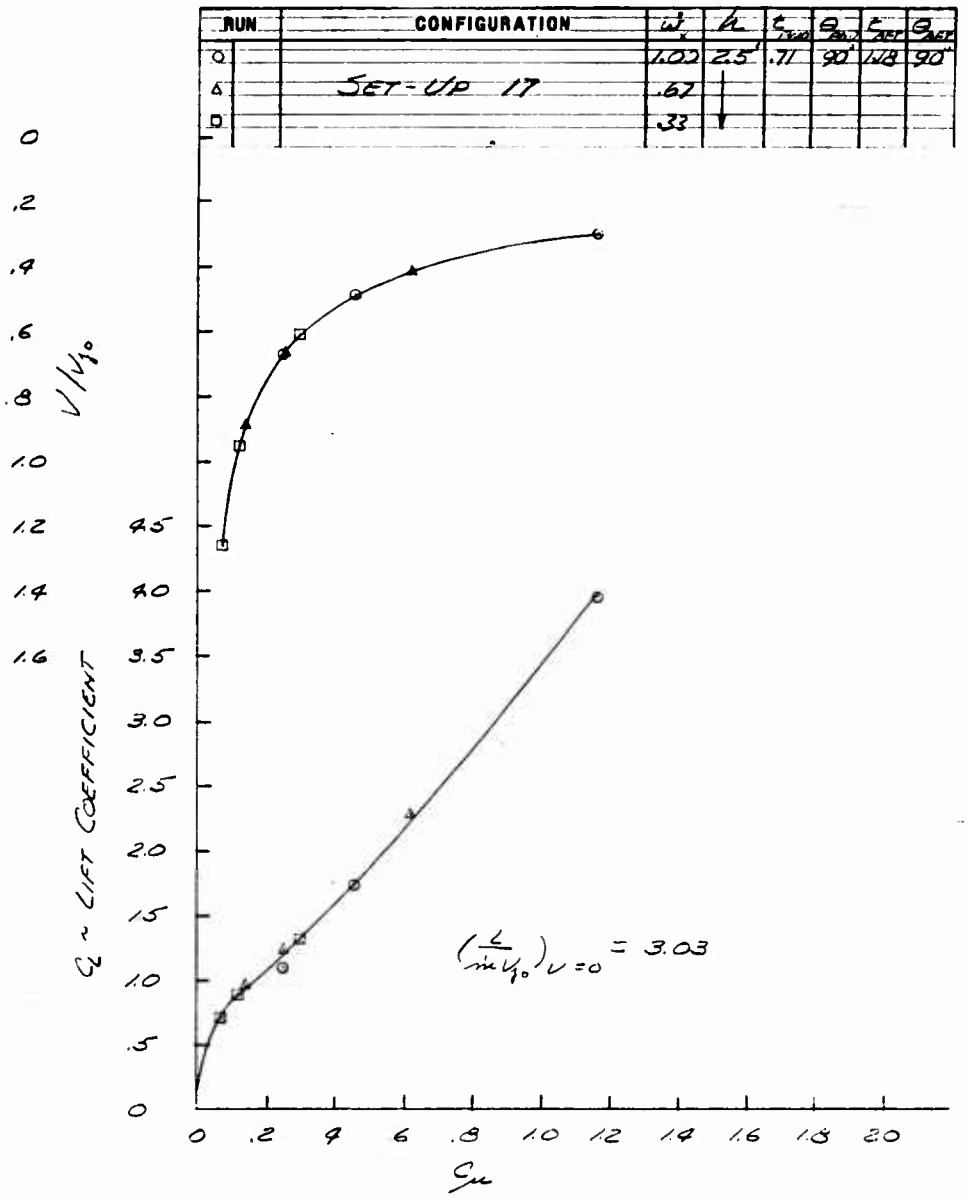

Fig. 26 C_L and V/V_{j_o} vs C_μ

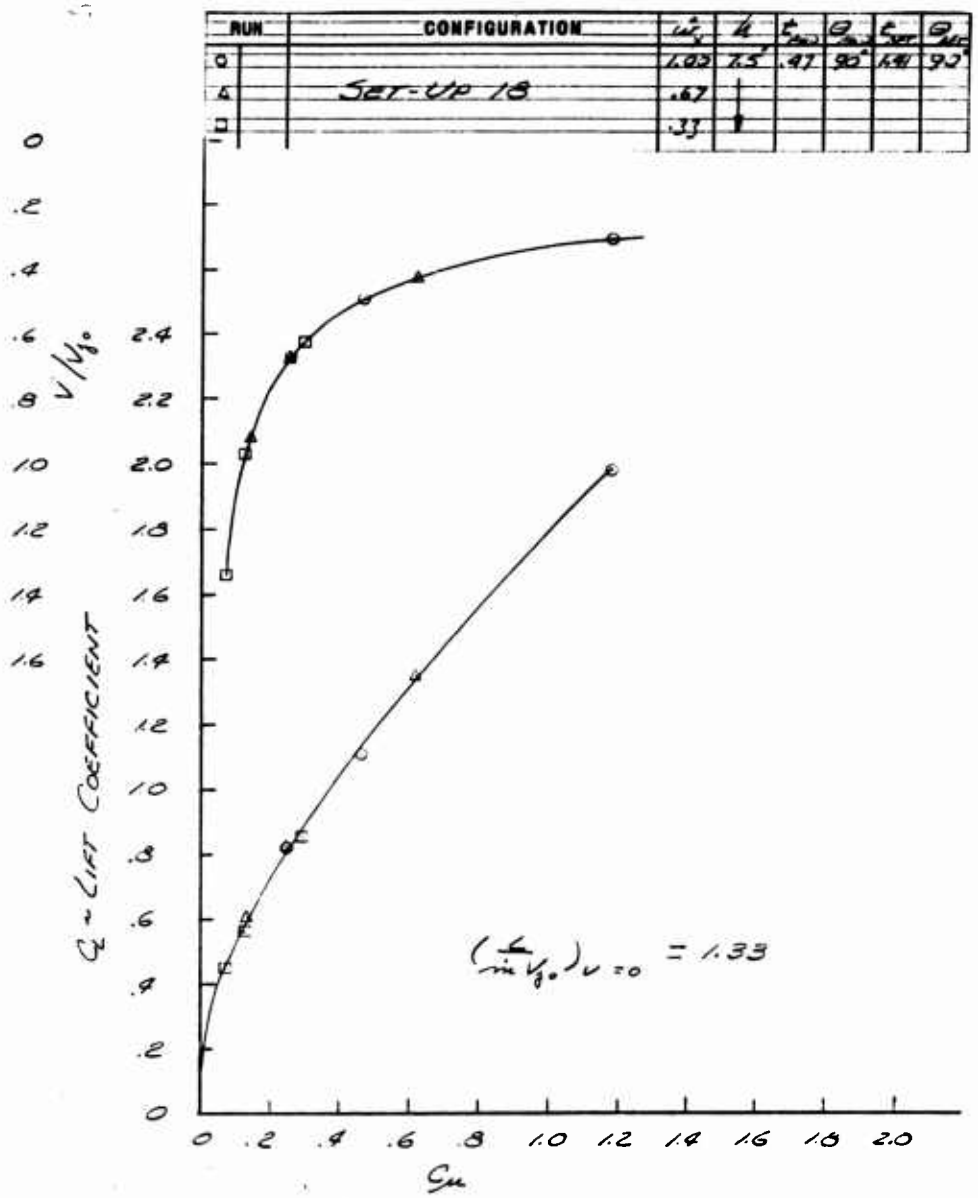

Fig. 27 C_L and V/V_{j_o} vs C_μ

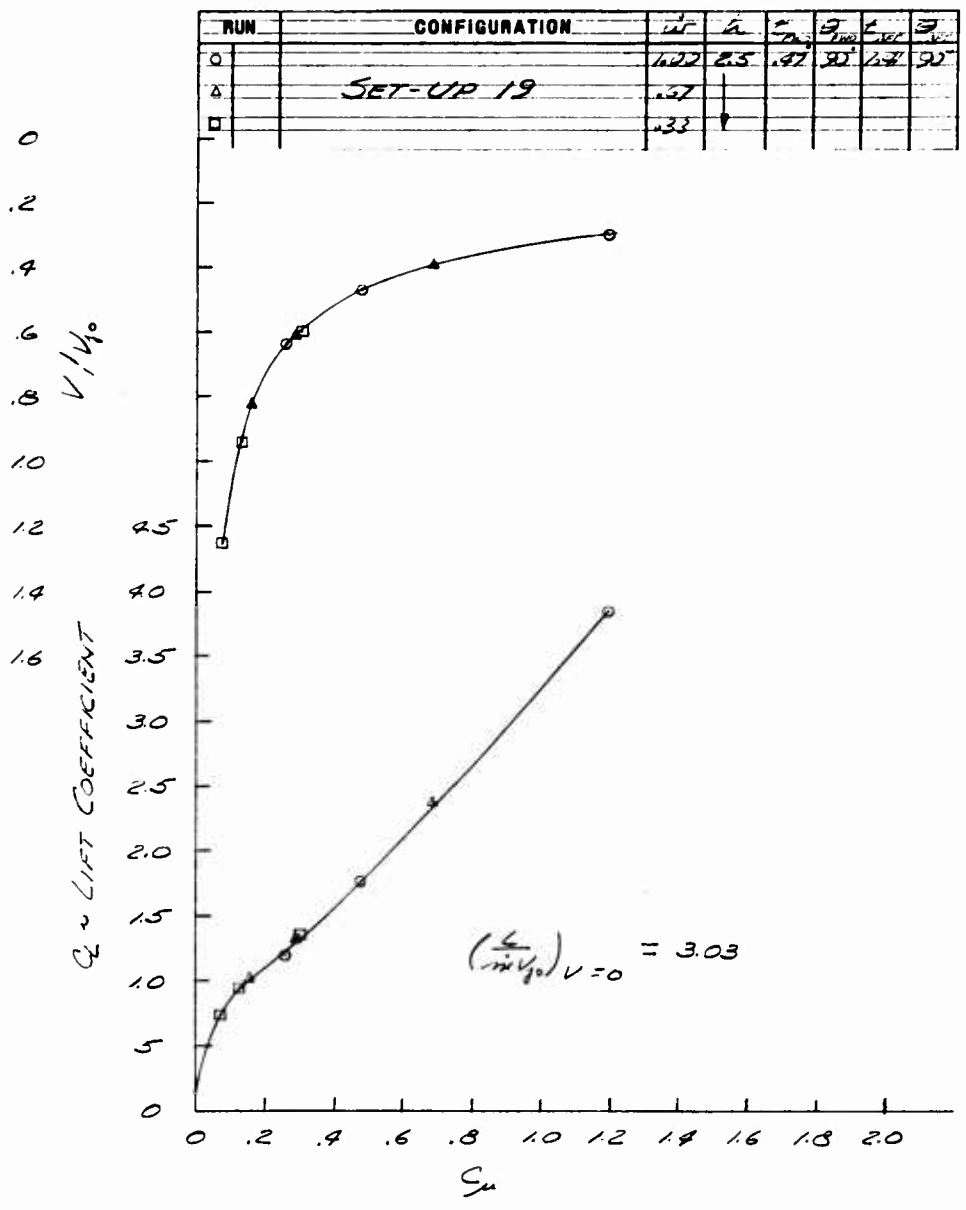

Fig. 28 C_L and V/V_{j_o} vs C_μ

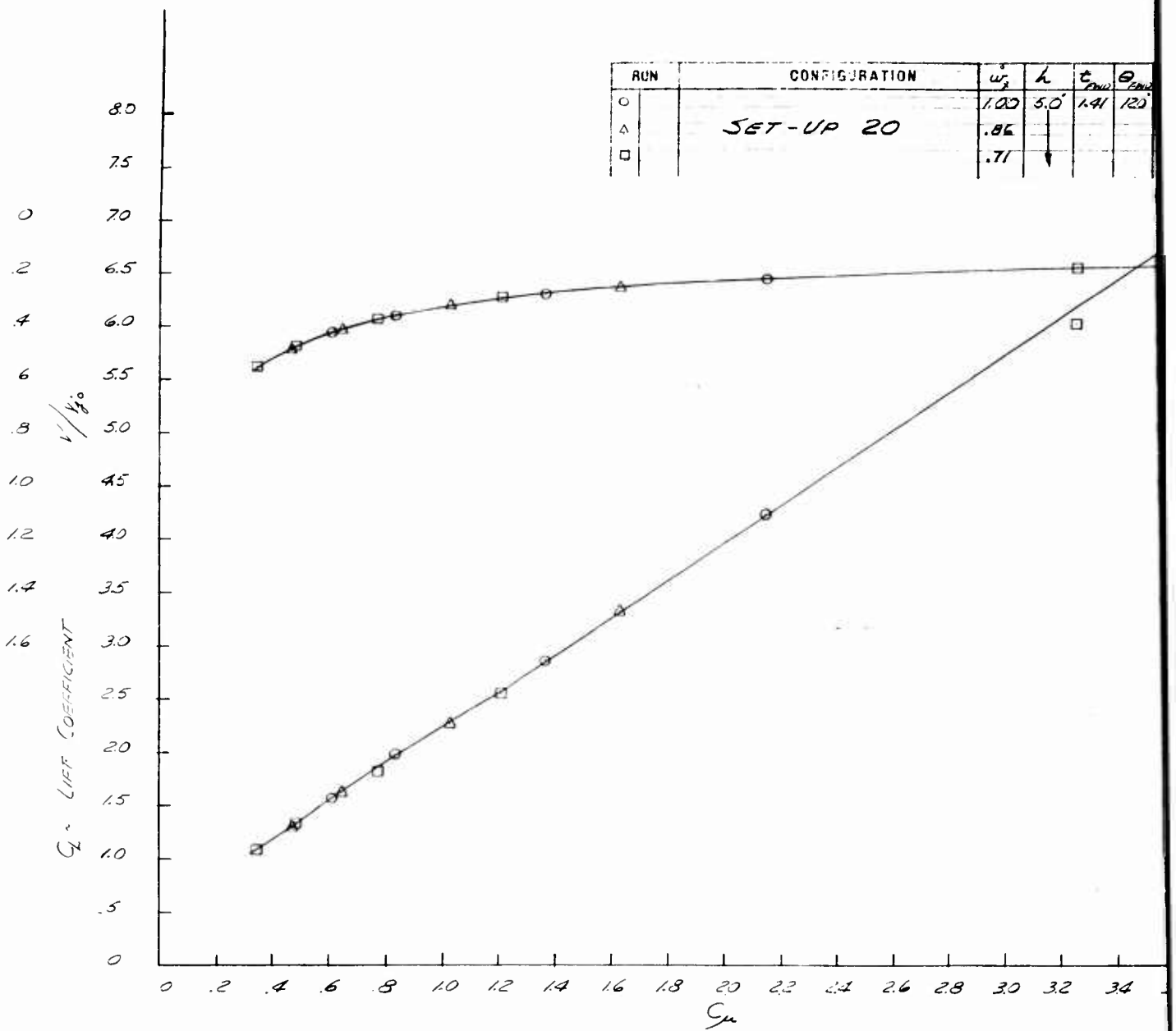

Fig. 29 C_L and V/V_{j_o} vs C_μ

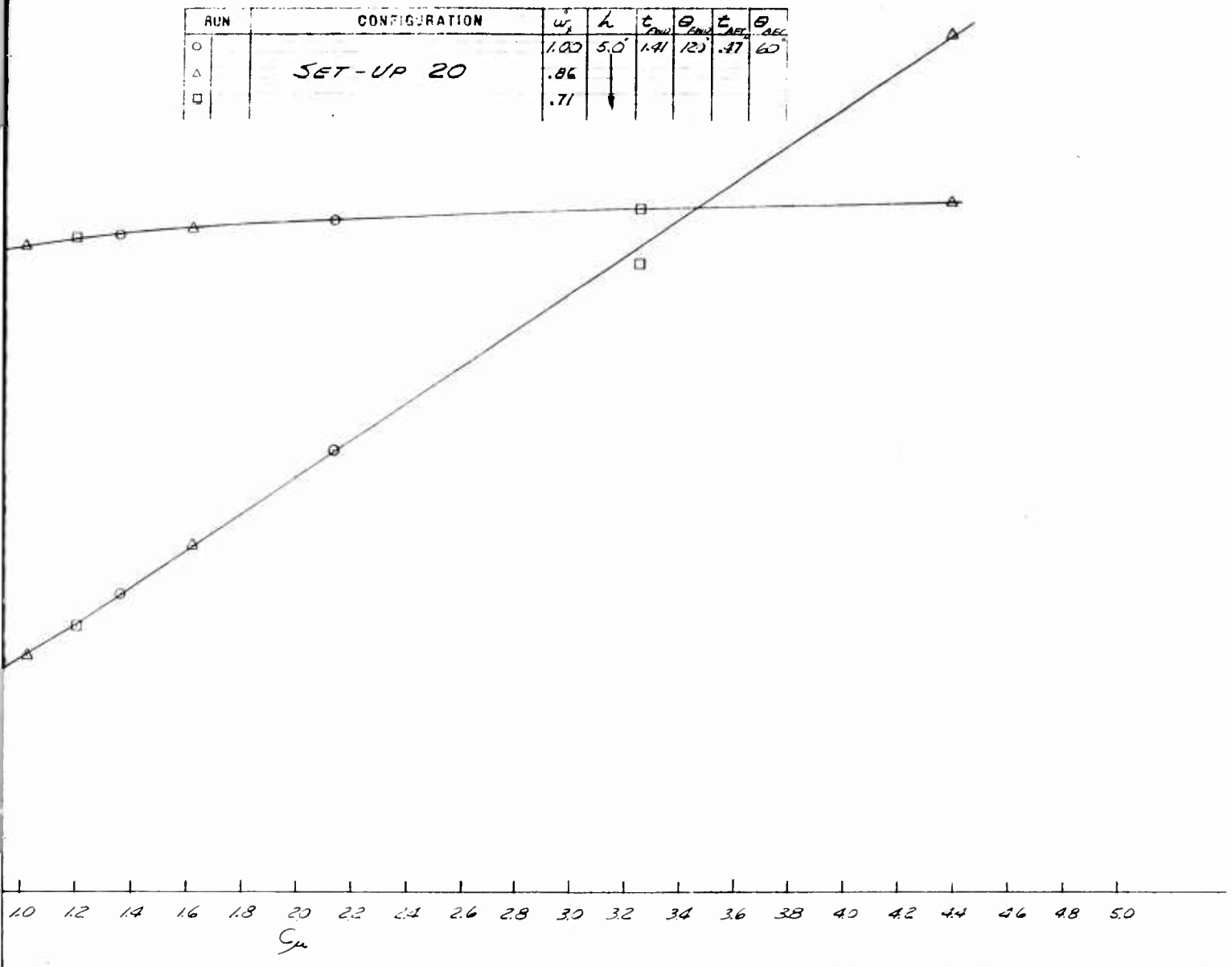

Fig. 29 C_L and V/V_{j_o} vs C_μ

2

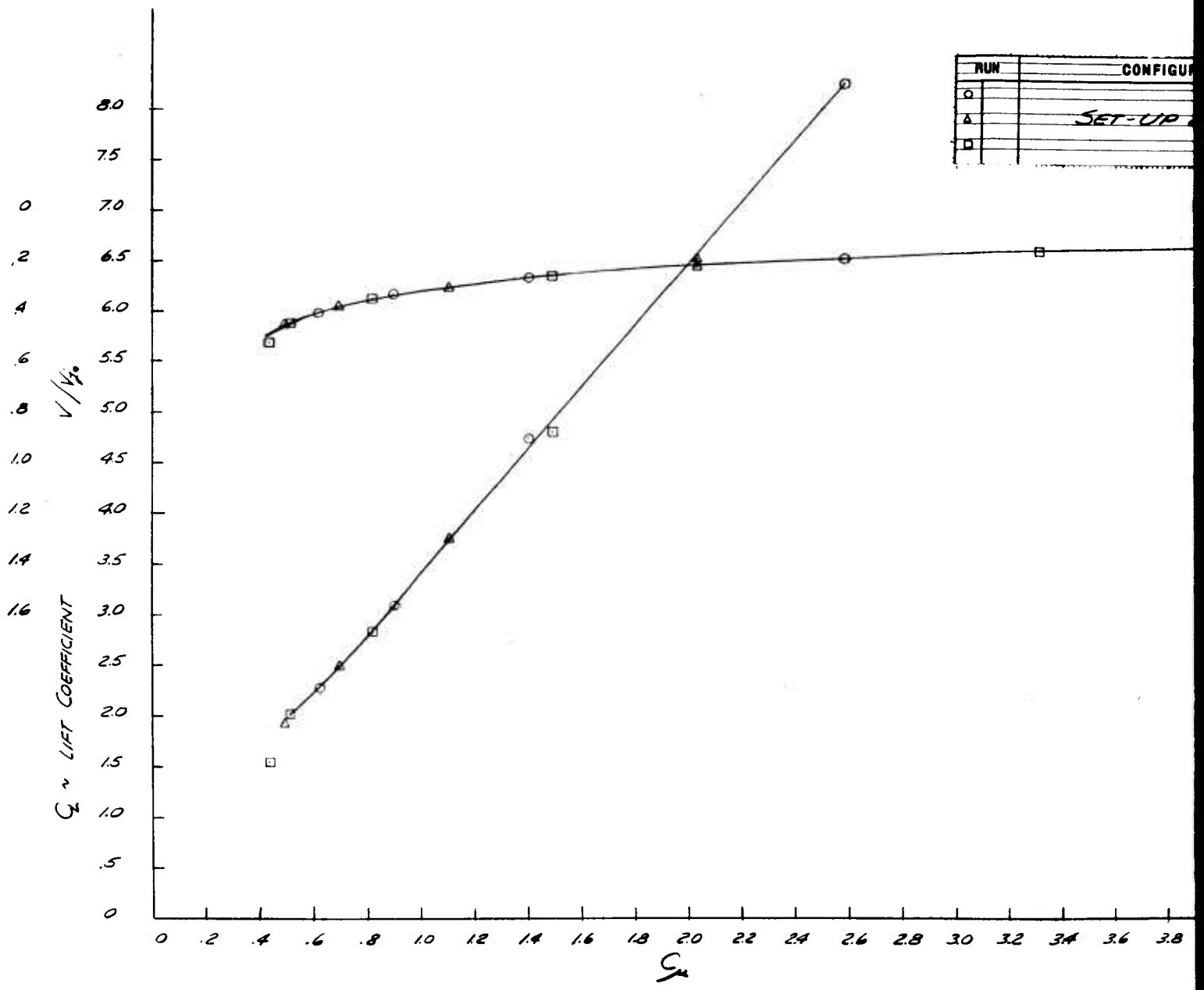

Fig. 30 C_L and V/V_{j_o} vs C_μ

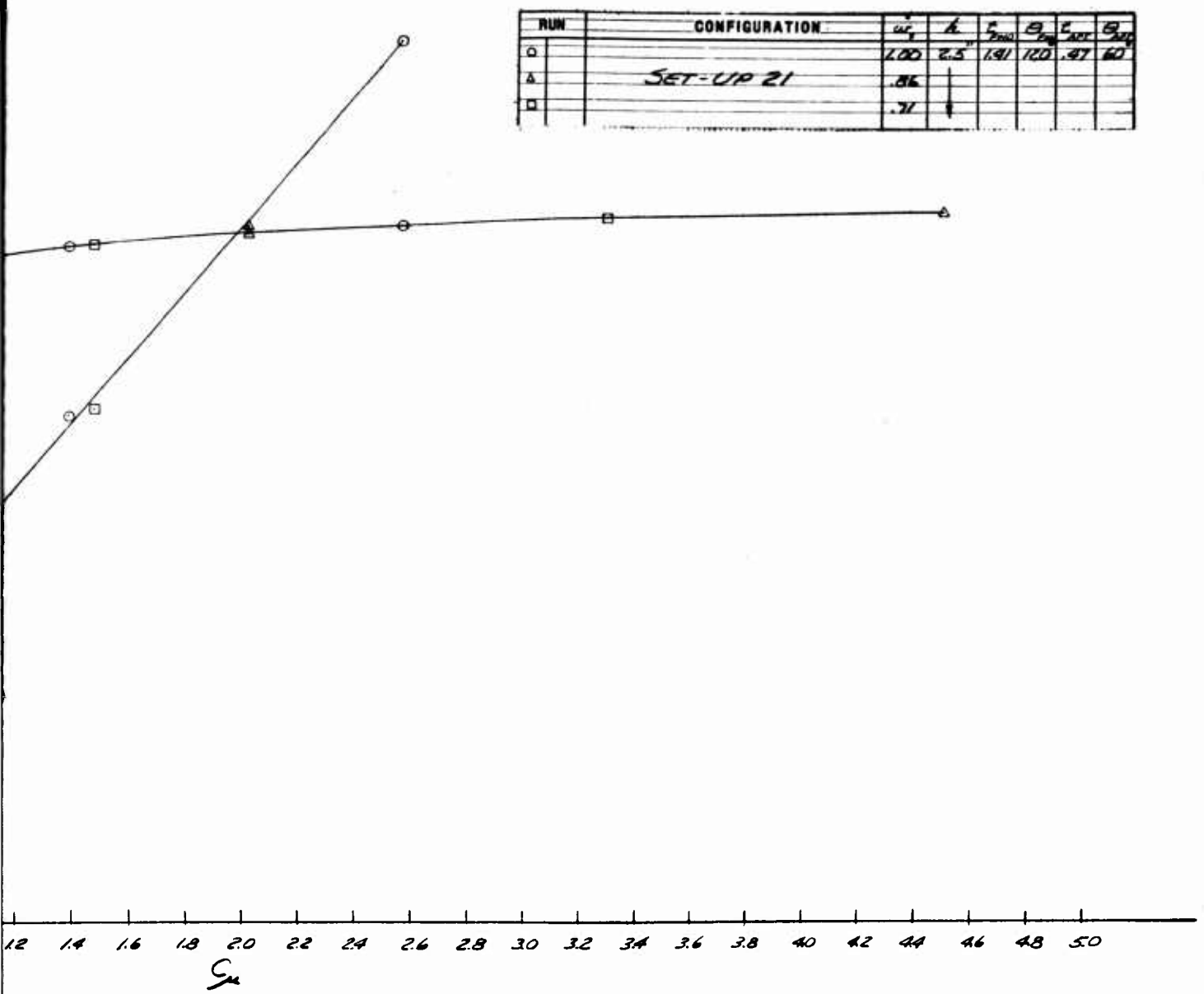

Fig. 30 C_L and V/V_{j_o} vs C_μ

2

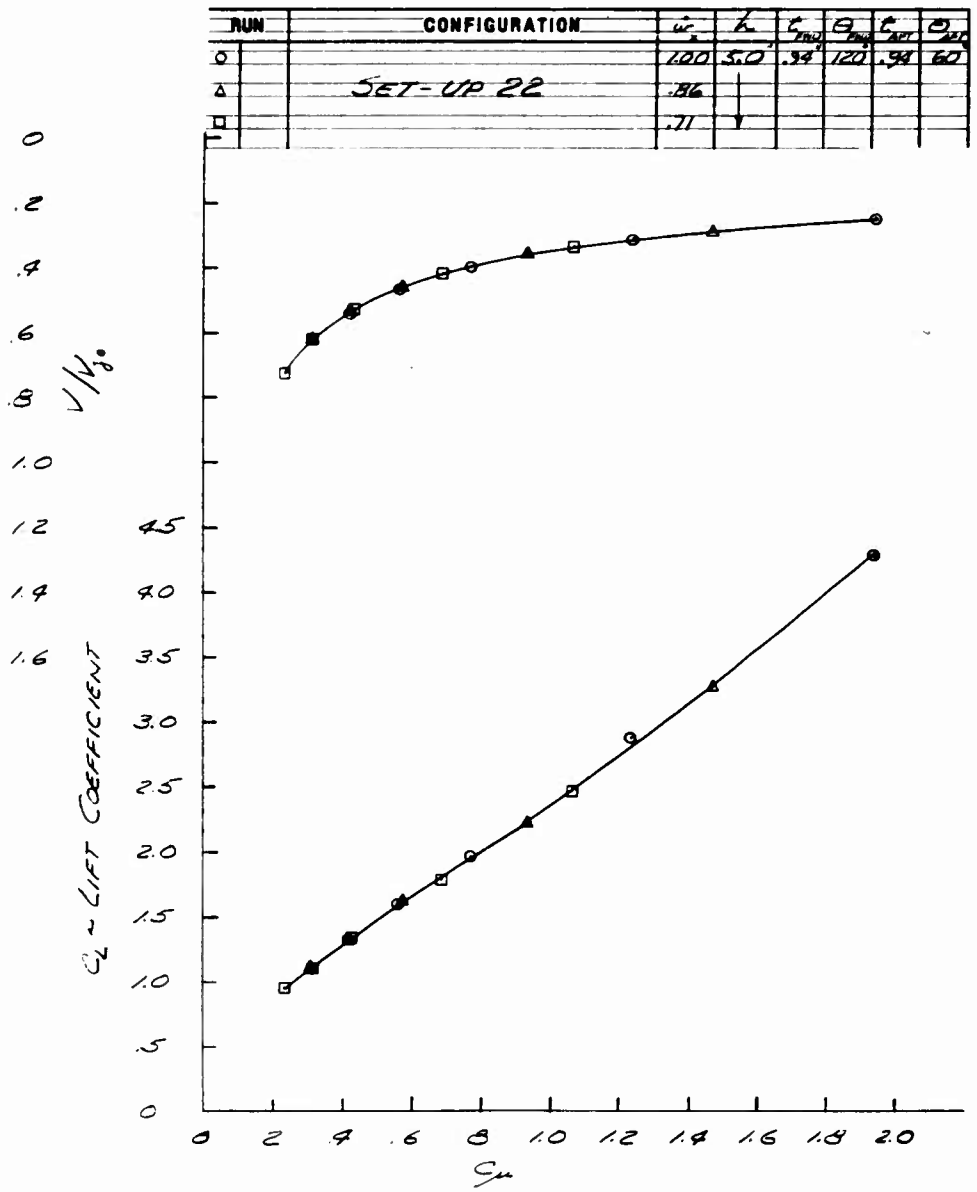

Fig. 31 C_L and V/V_{j_o} vs C_μ

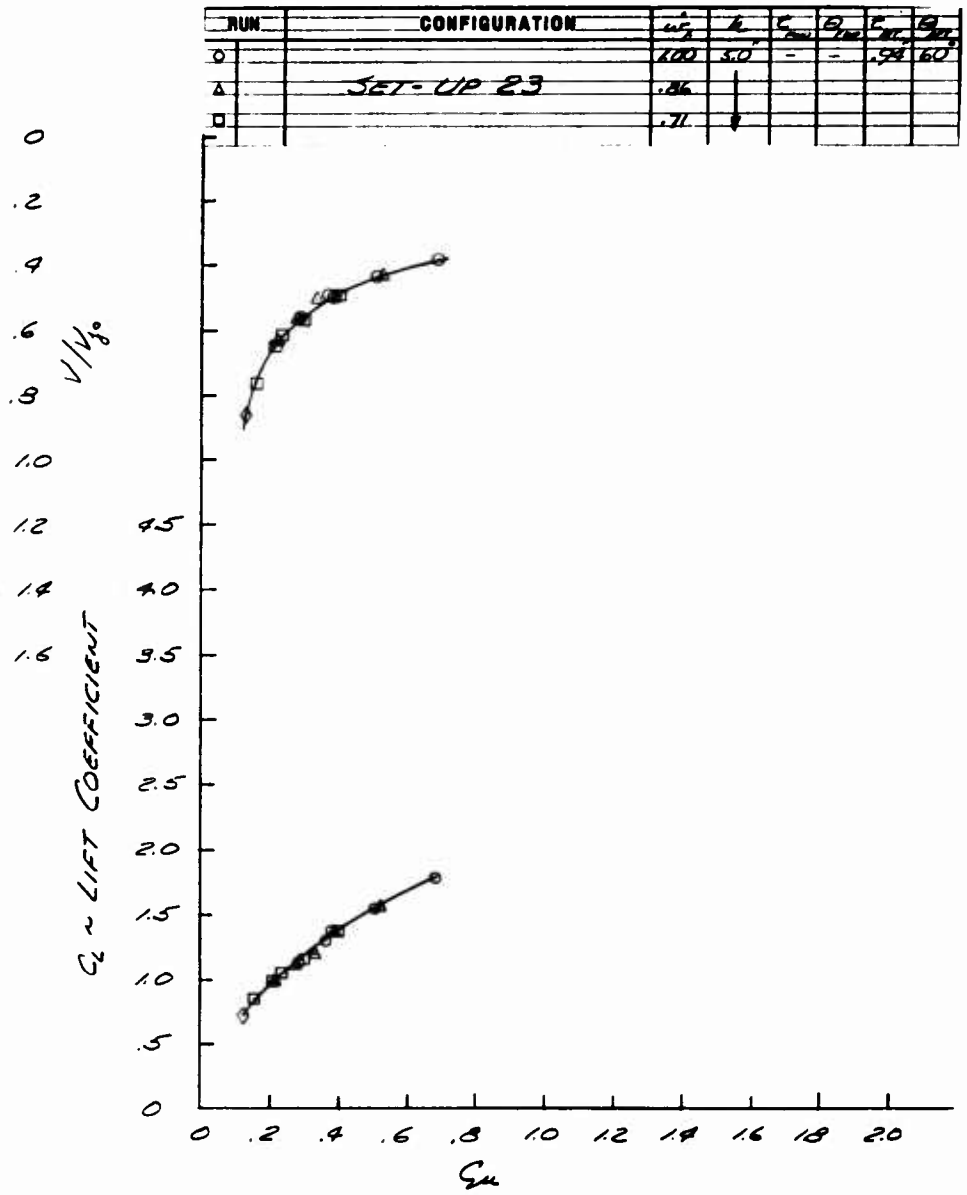

Fig. 32 C_L and V/V_{j_o} vs C_μ

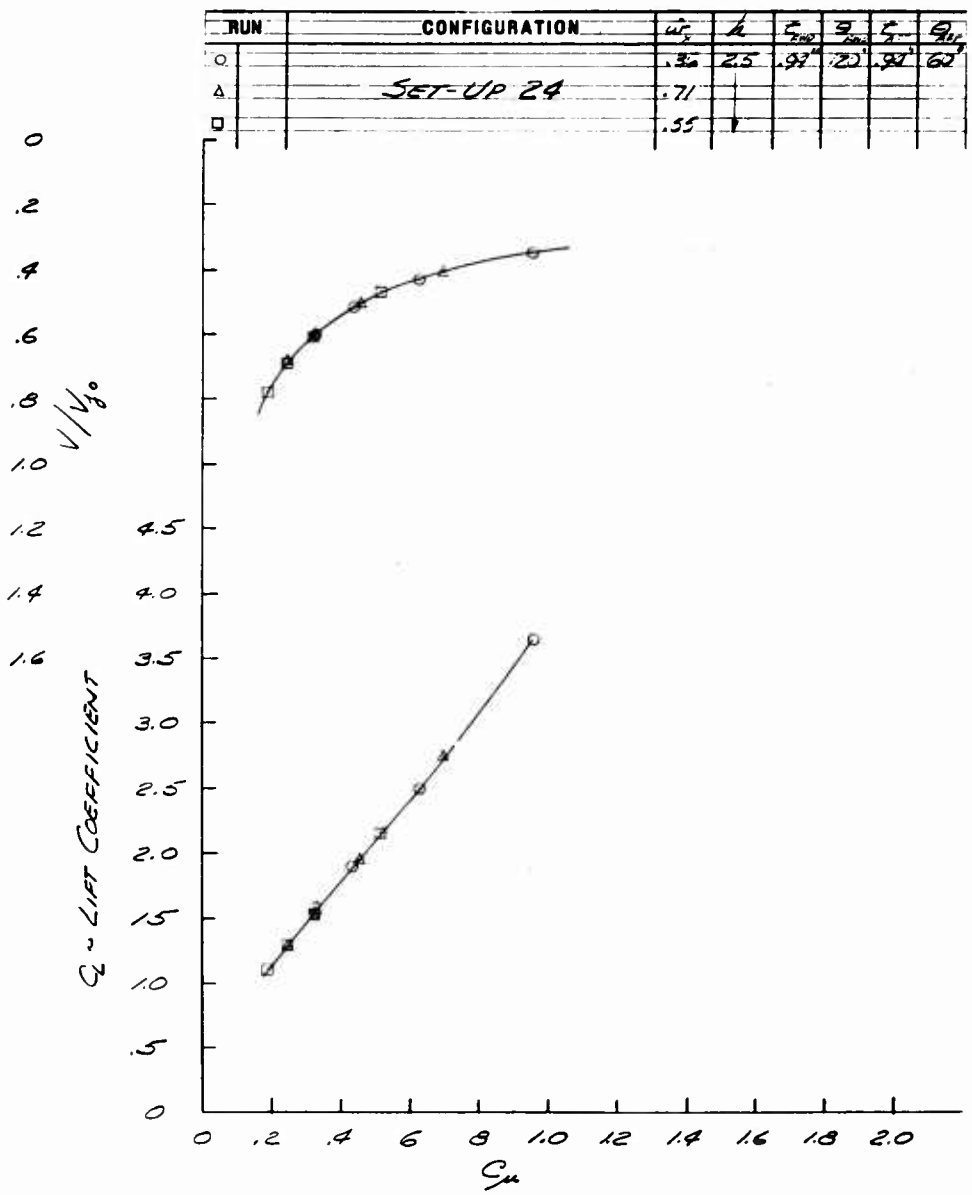

Fig. 33 C_L and V/V_{j_o} vs C_μ

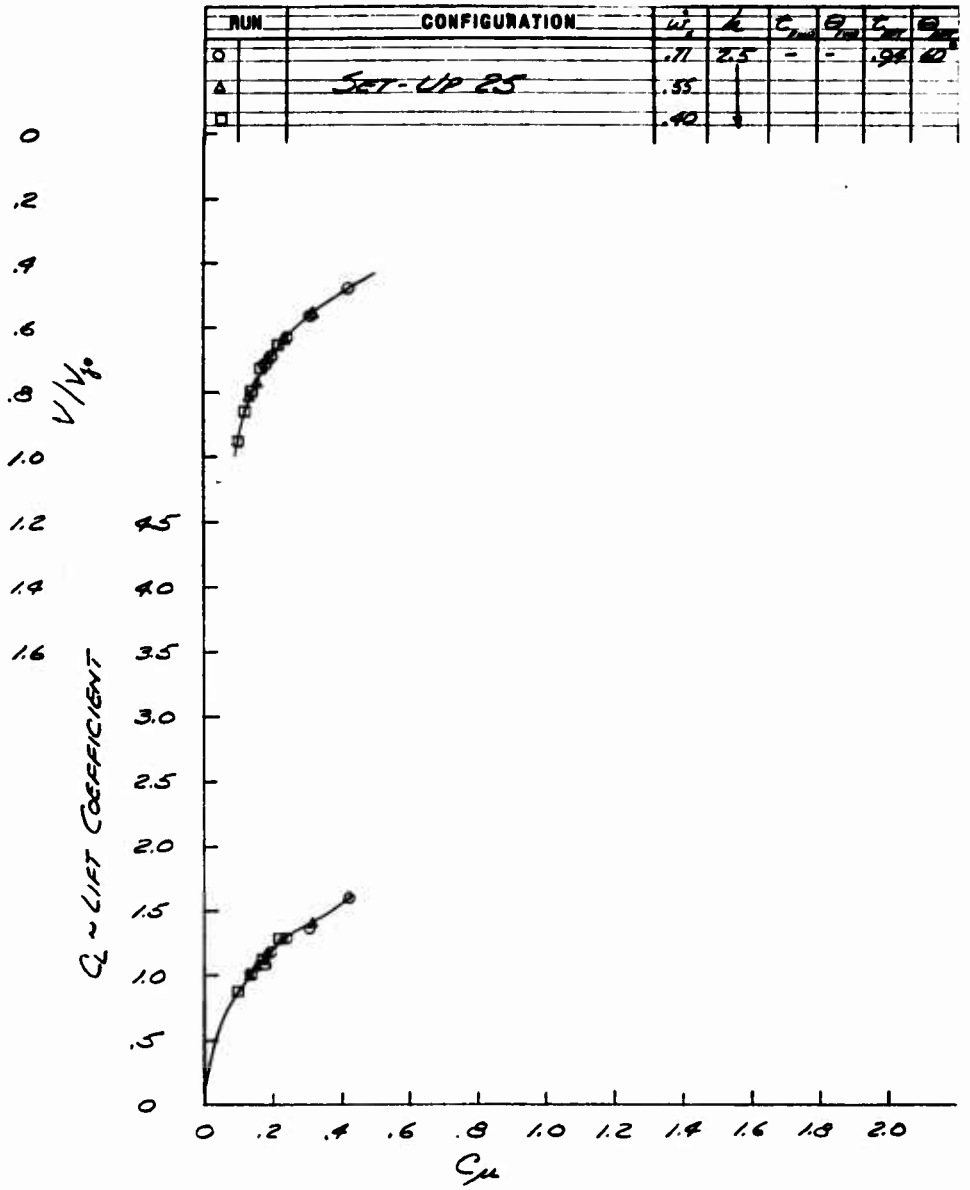

Fig. 34 C_L and V/V_{j_o} vs C_μ

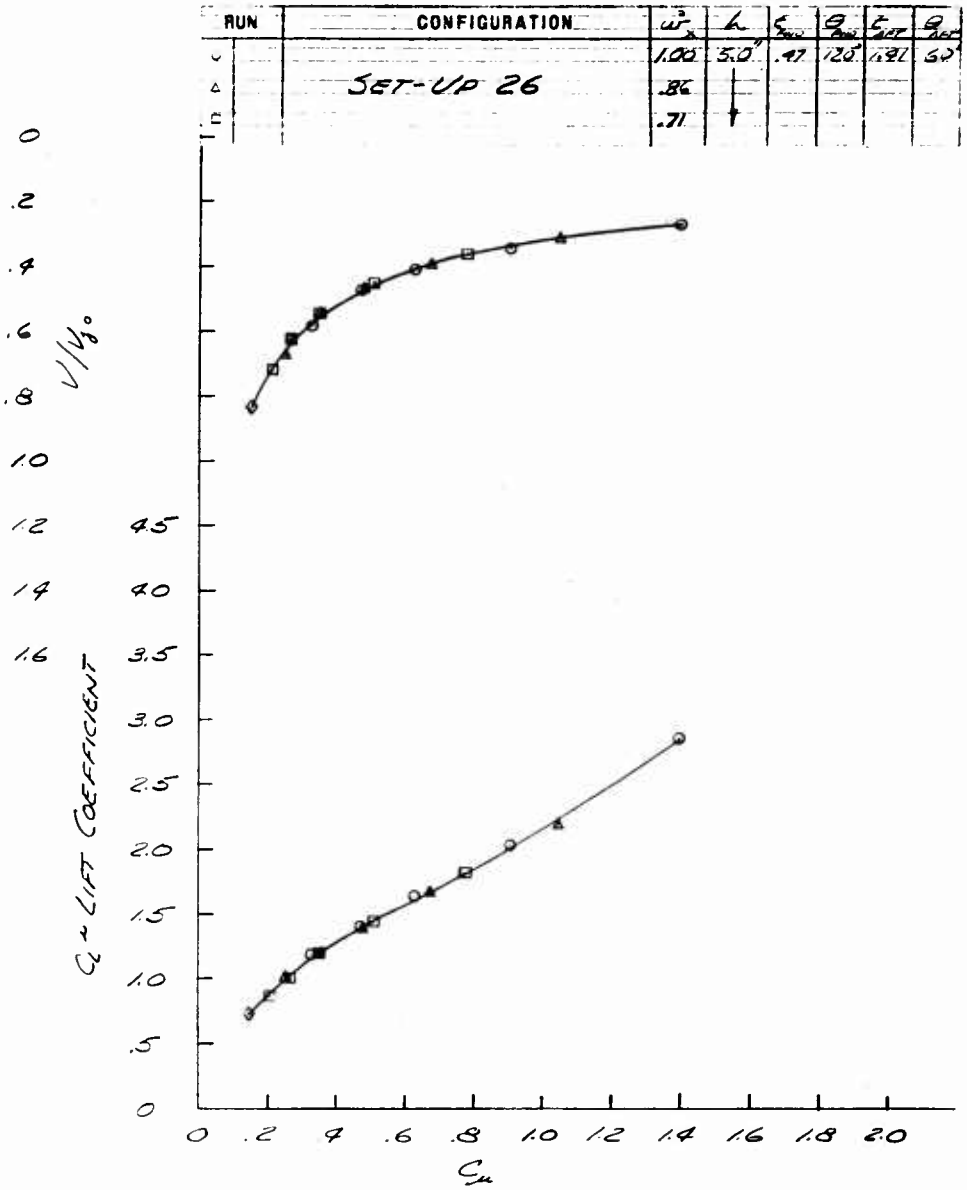

Fig. 35 C_L and V/V_{j_o} vs C_μ

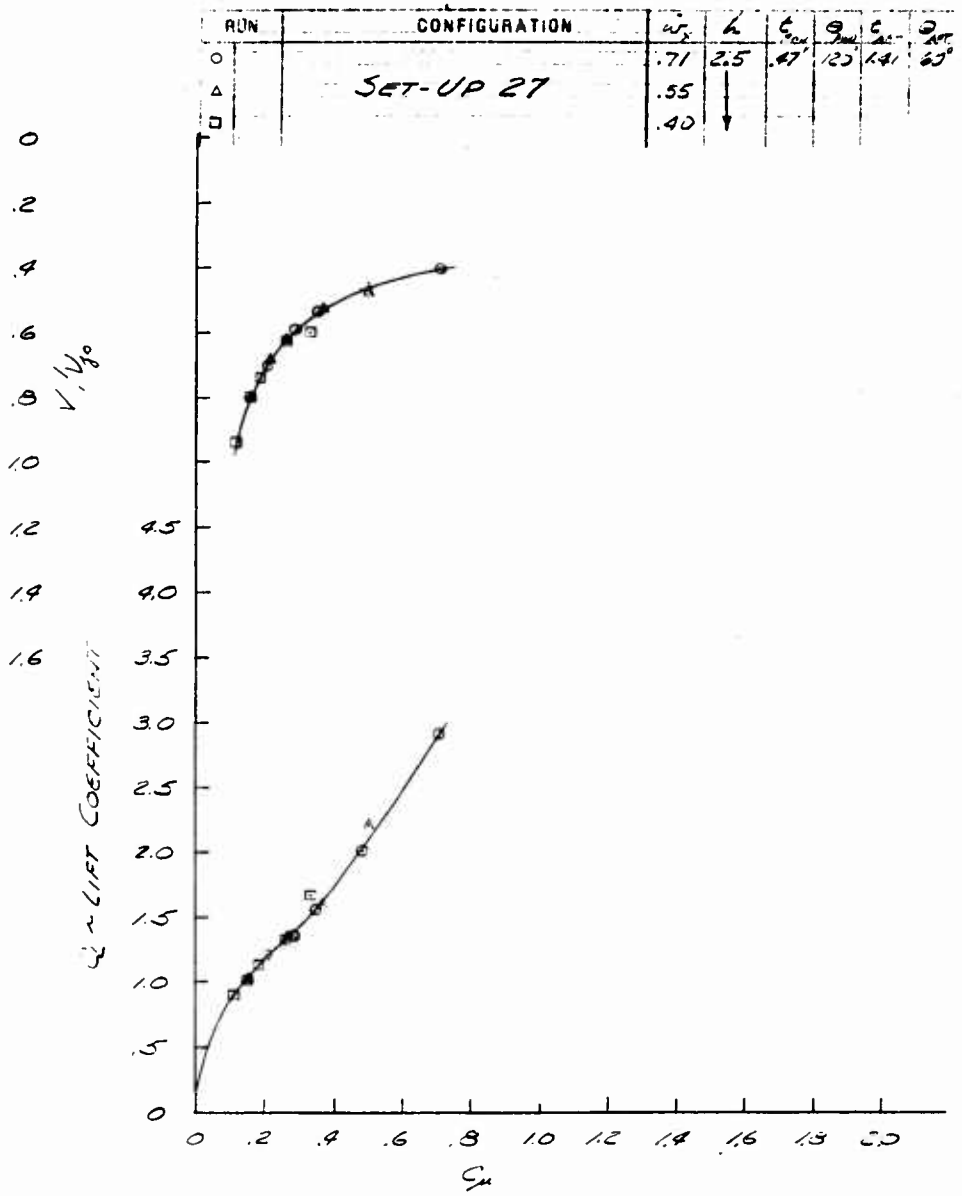

Fig. 36 C_L and V/V_{j_o} vs C_μ

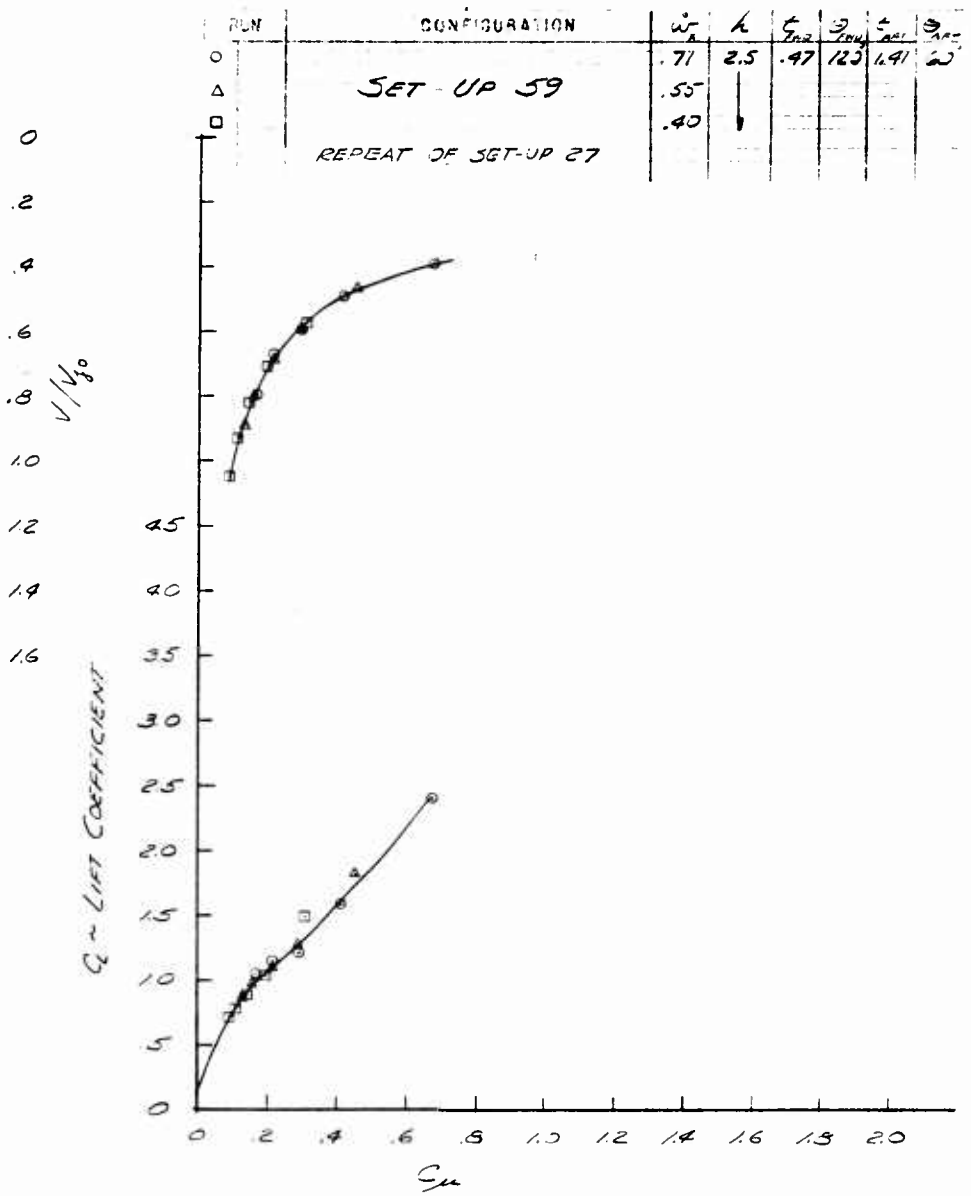

Fig. 36a C_L and V/V_{j_o} vs C_μ

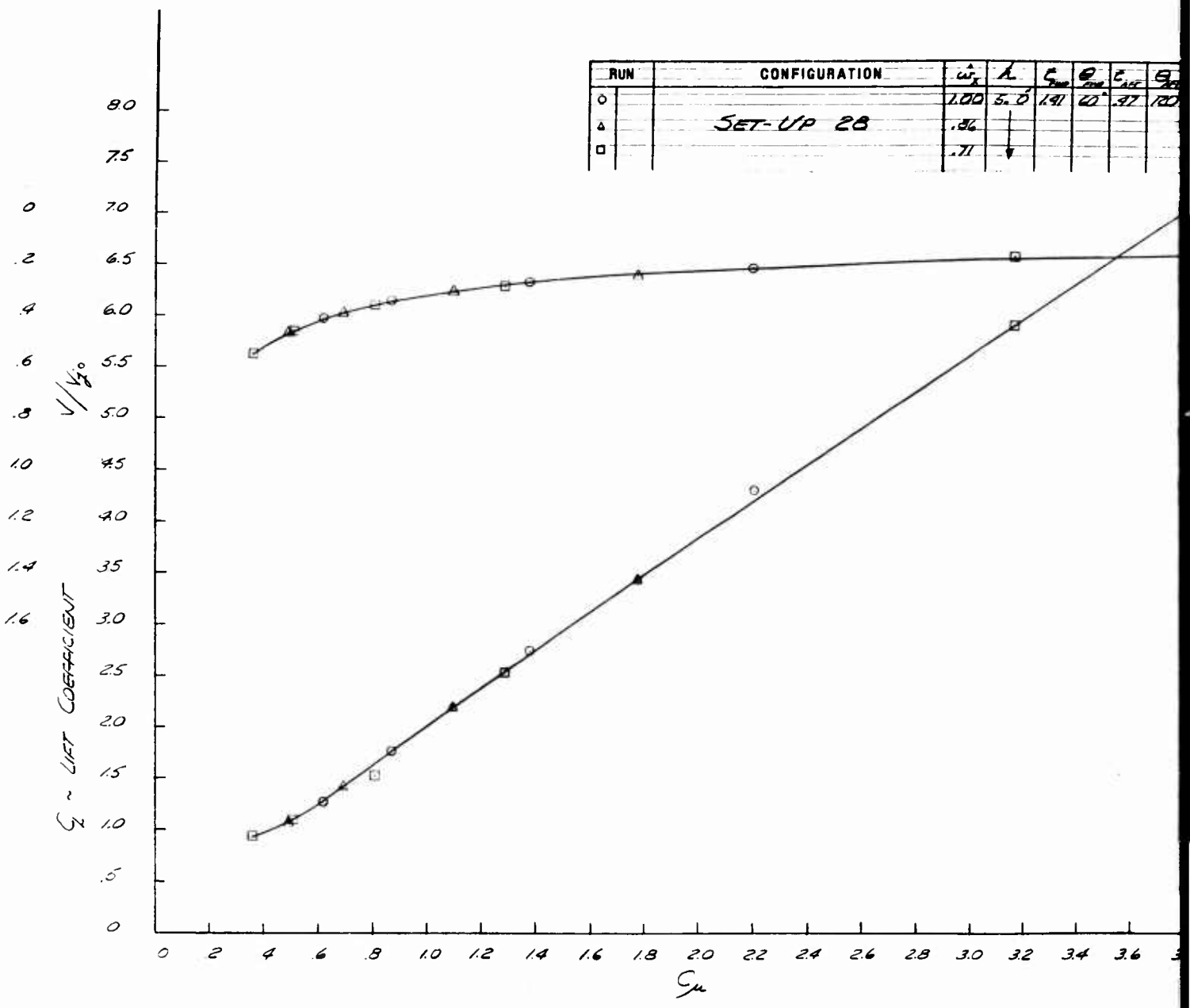

Fig. 37 C_L and V/V_{j_o} vs C_μ

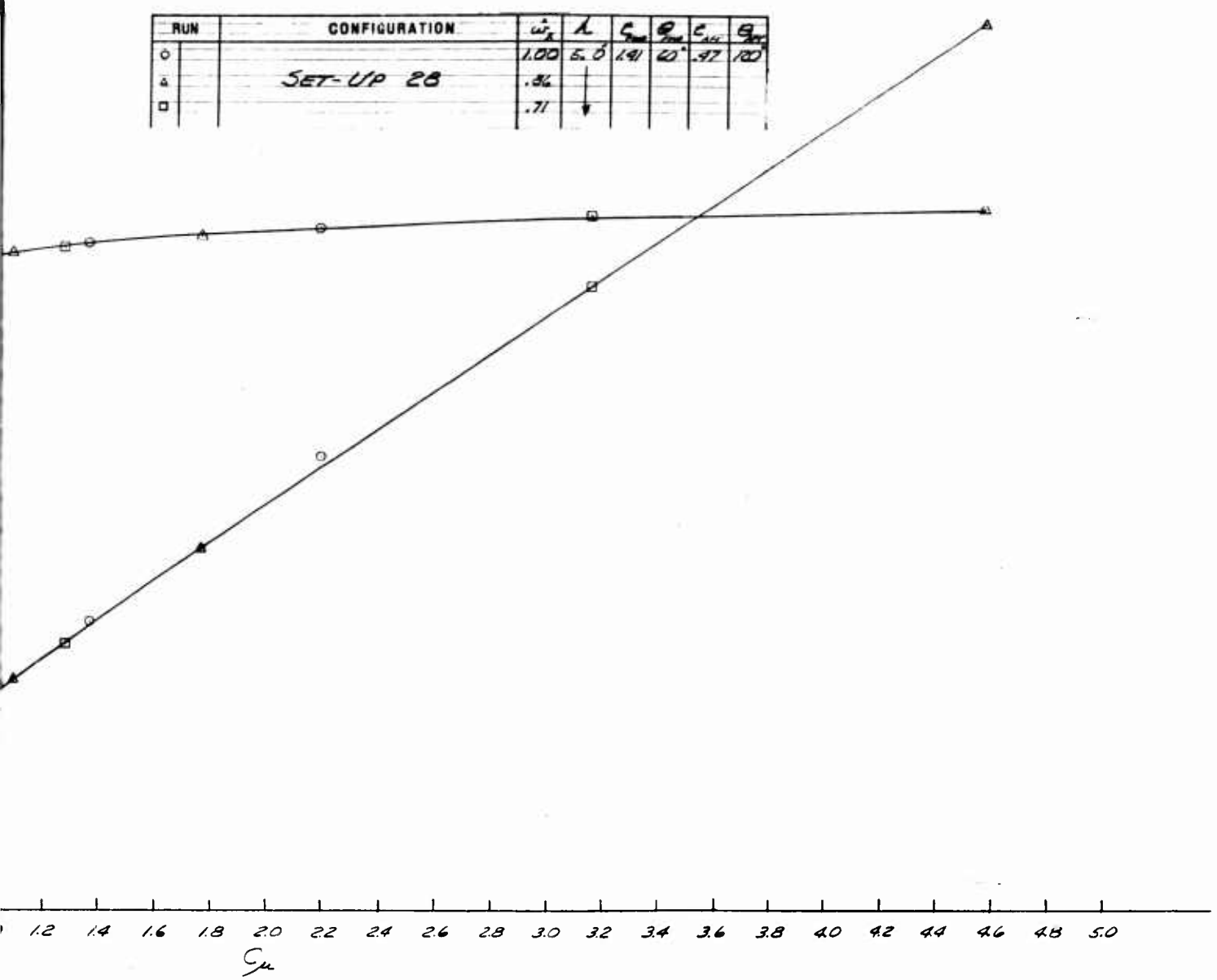

Fig. 37 C_L and V/V_{j_o} vs C_μ

2

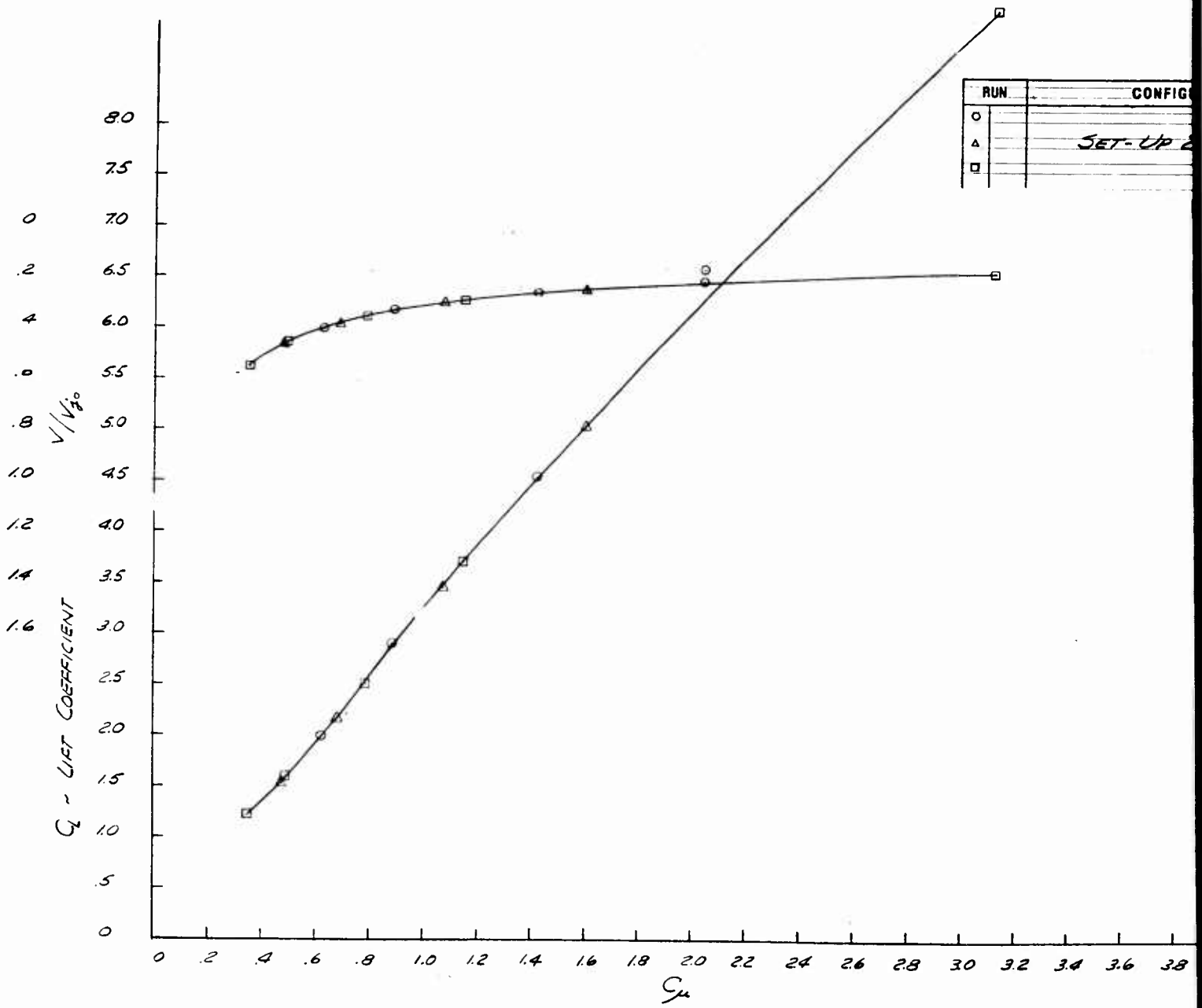

Fig. 38 C_L and V/V_{j_o} vs C_μ

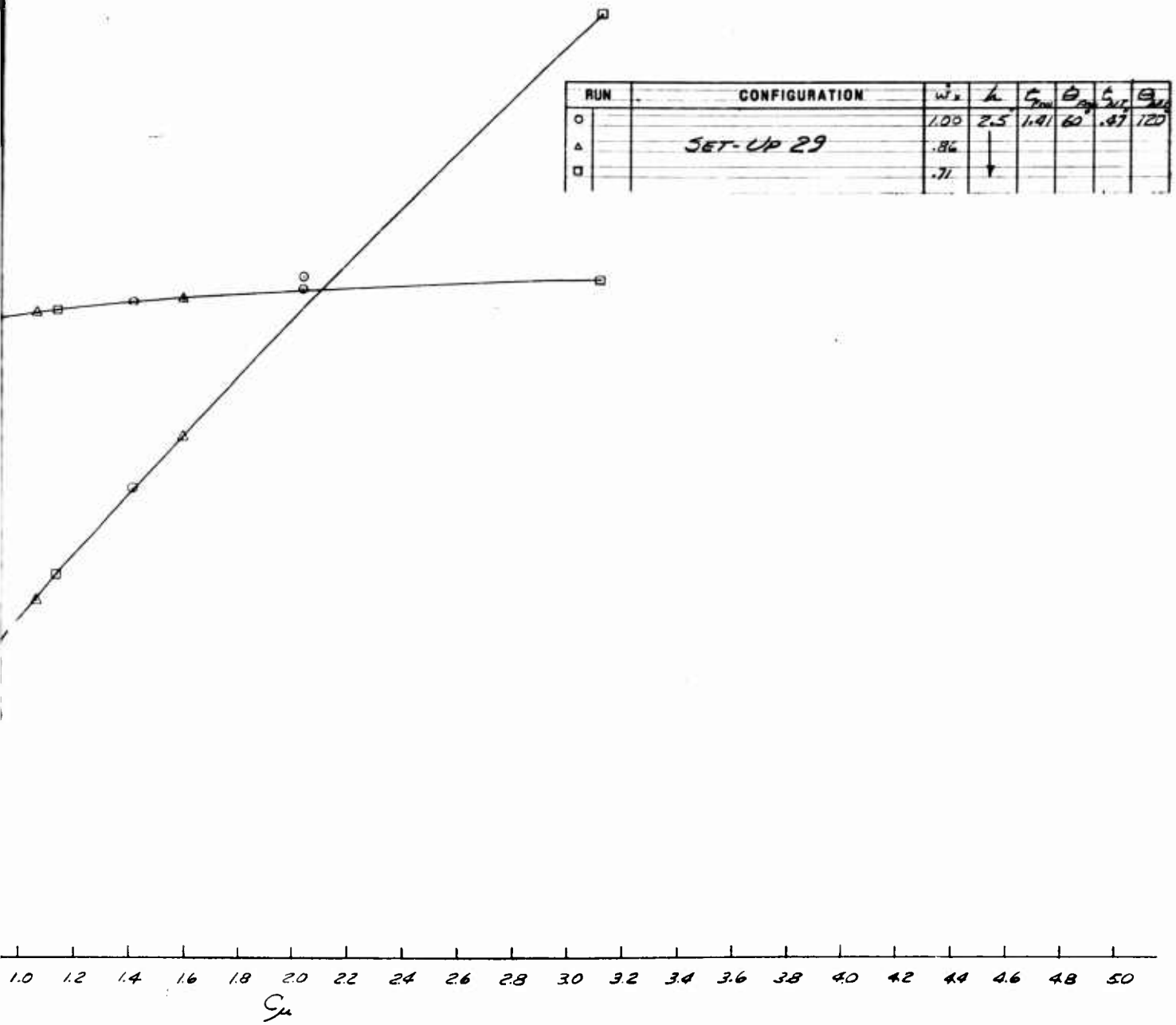

Fig. 38 C_L and V/V_{j_o} vs C_μ

2

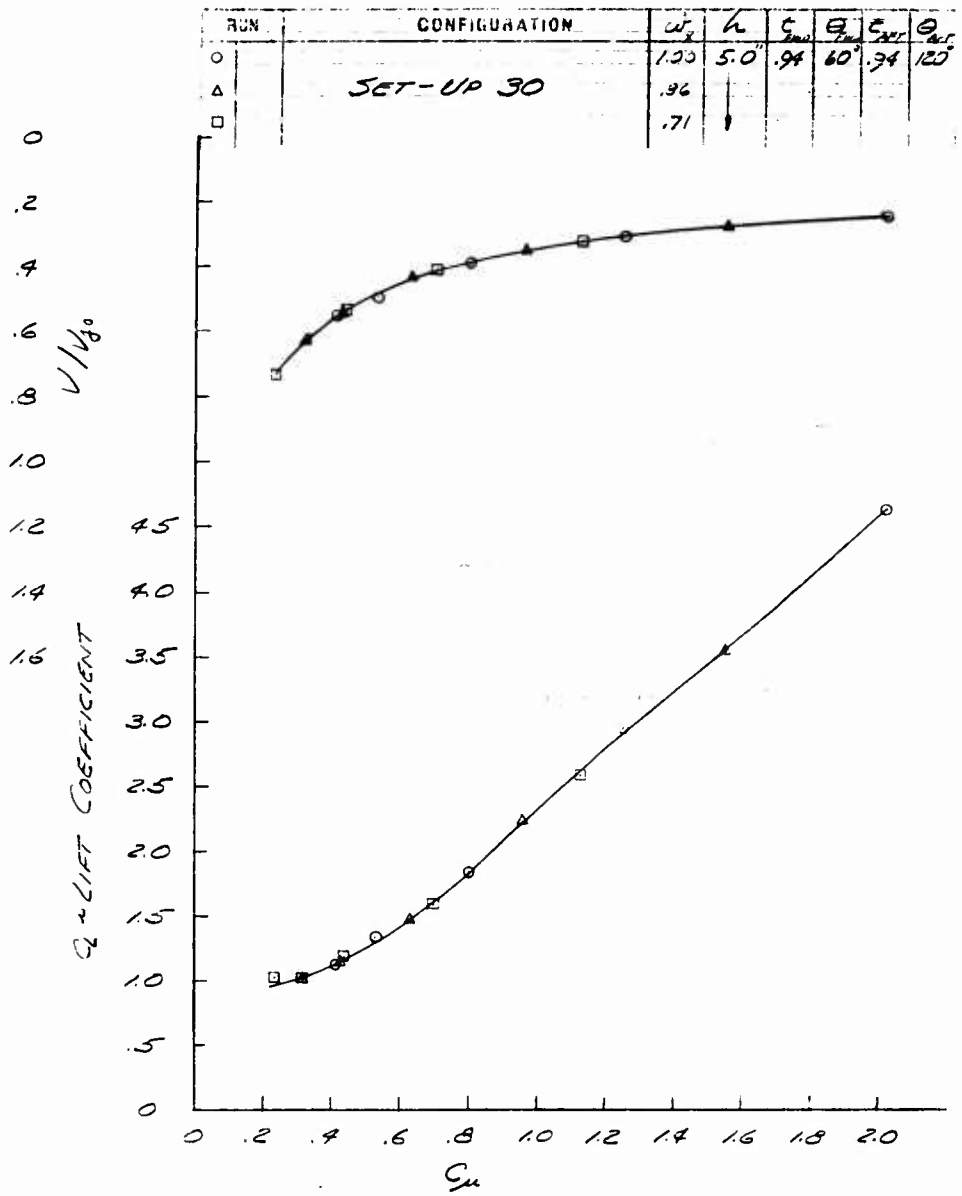

Fig. 39 C_L and V/V_{j_o} vs C_μ

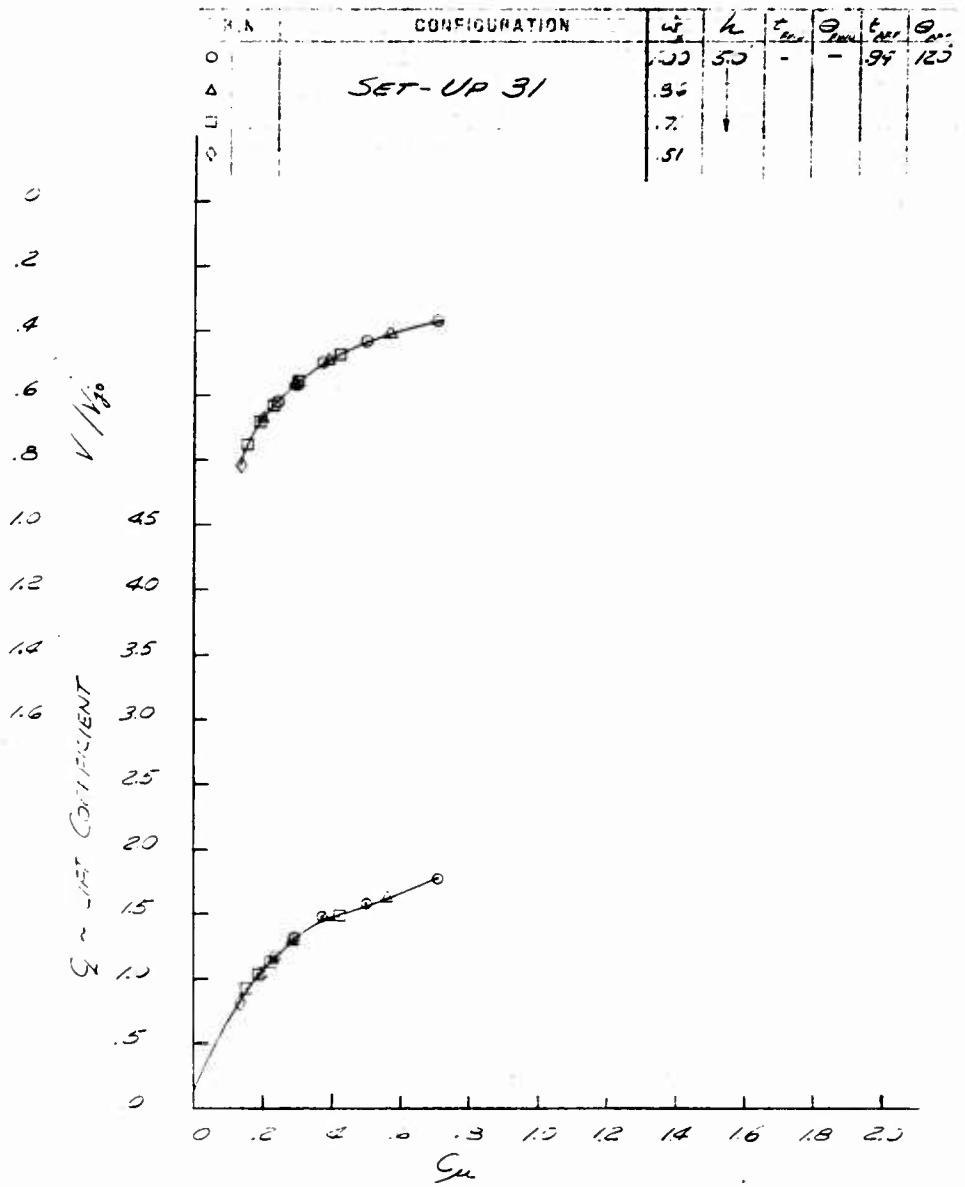

Fig. 40 C_L and V/V_{j_o} vs C_μ

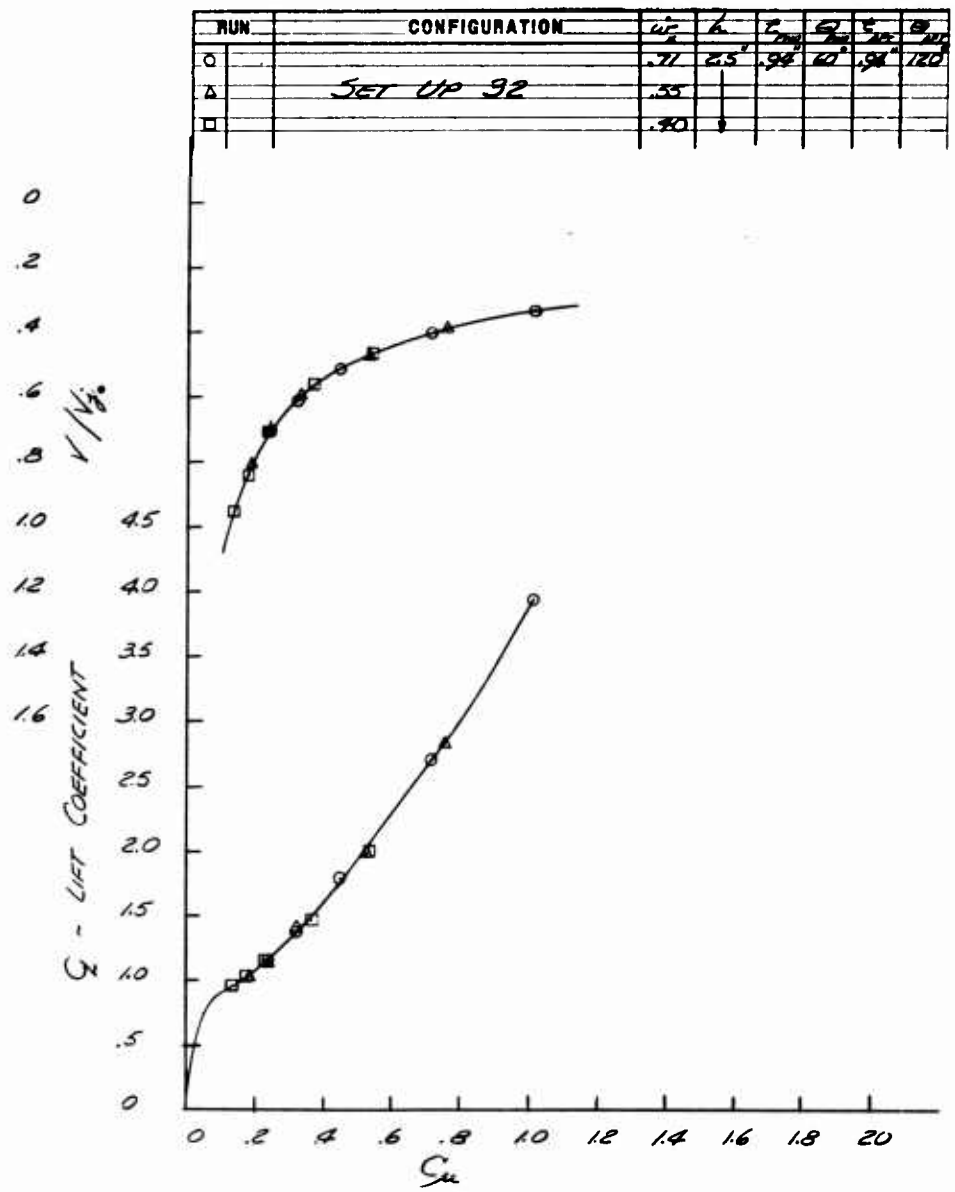

Fig. 41 C_L and V/V_{j_o} vs C_μ

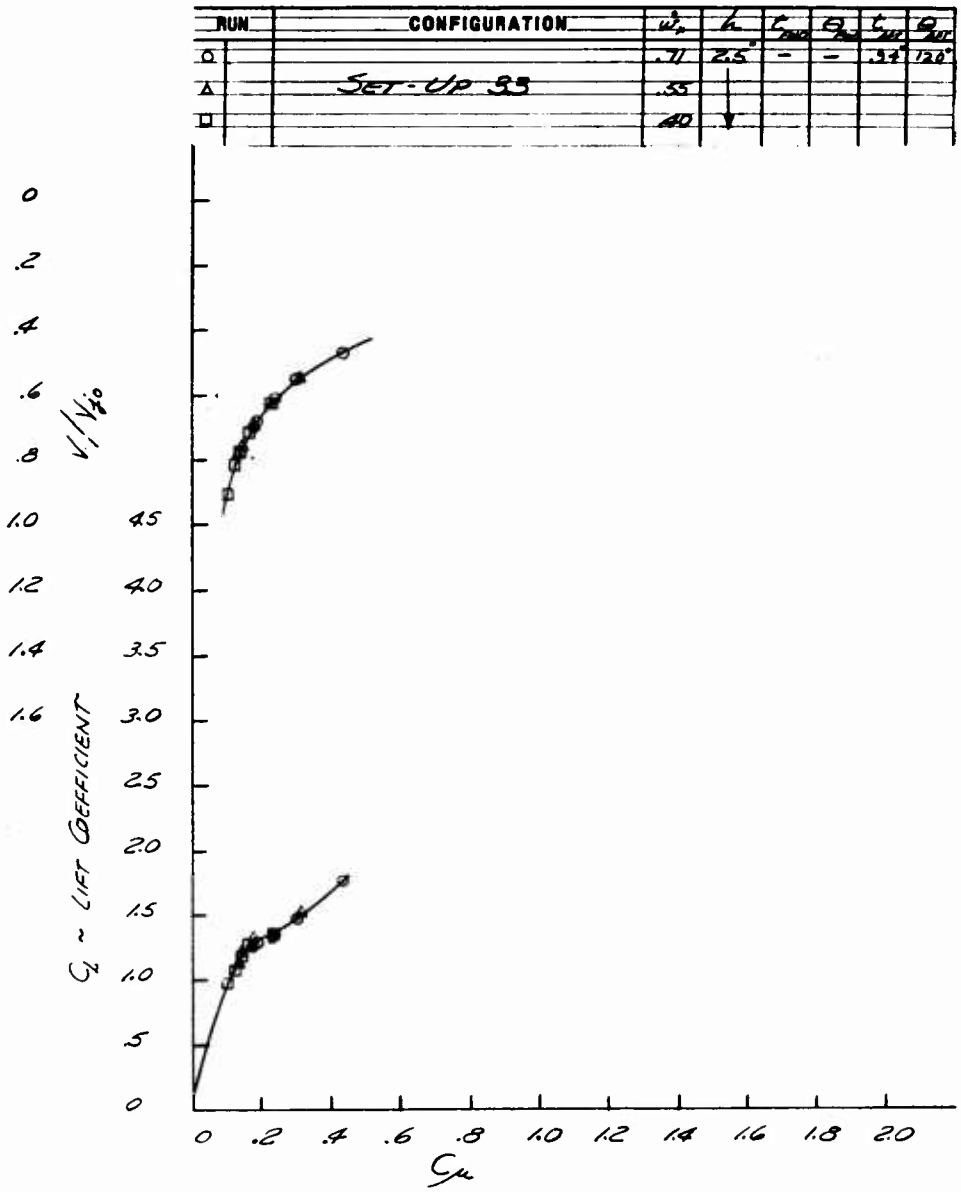

Fig. 42 C_L and V/V_{j_o} vs C_μ

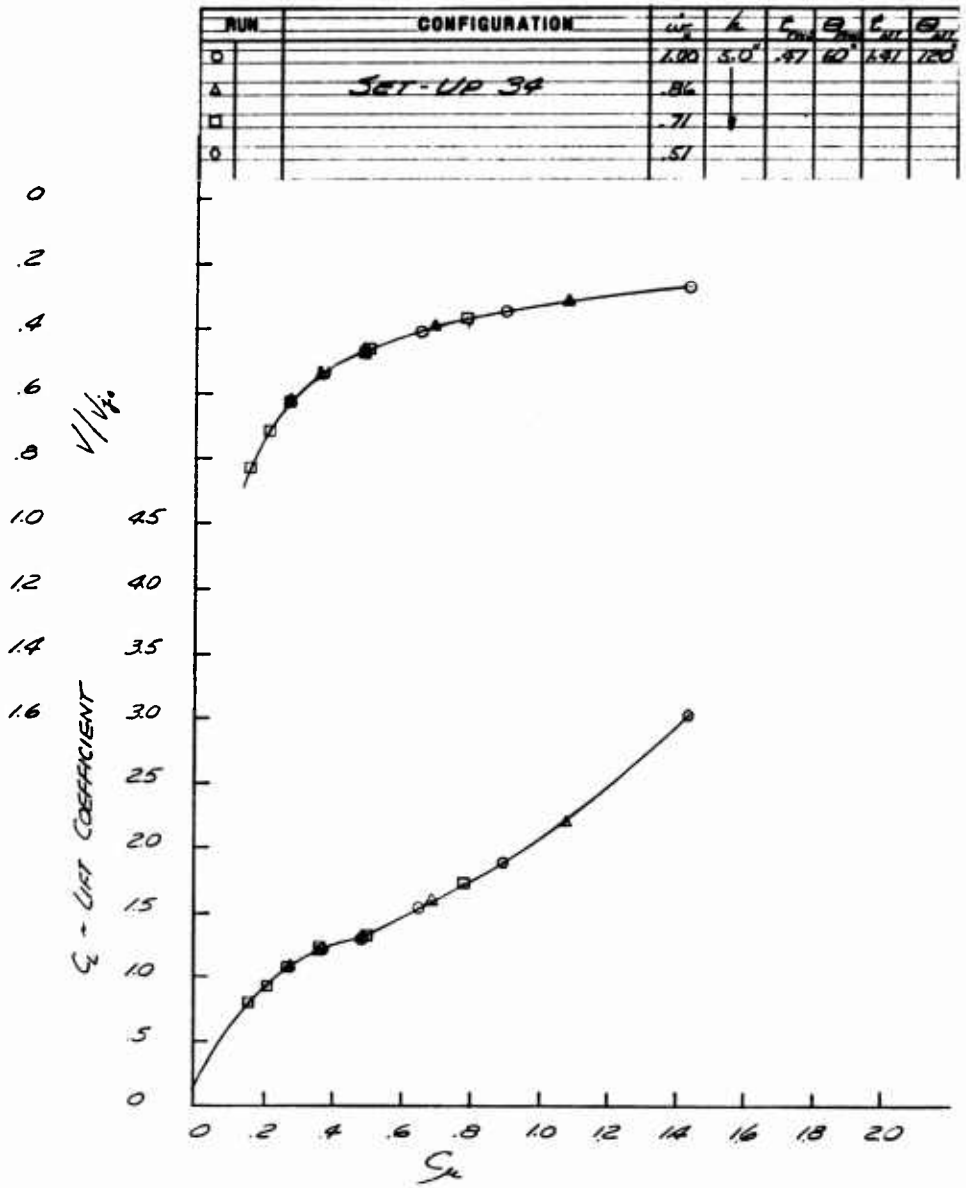

Fig. 43 C_L and V/V_{j_o} vs C_μ

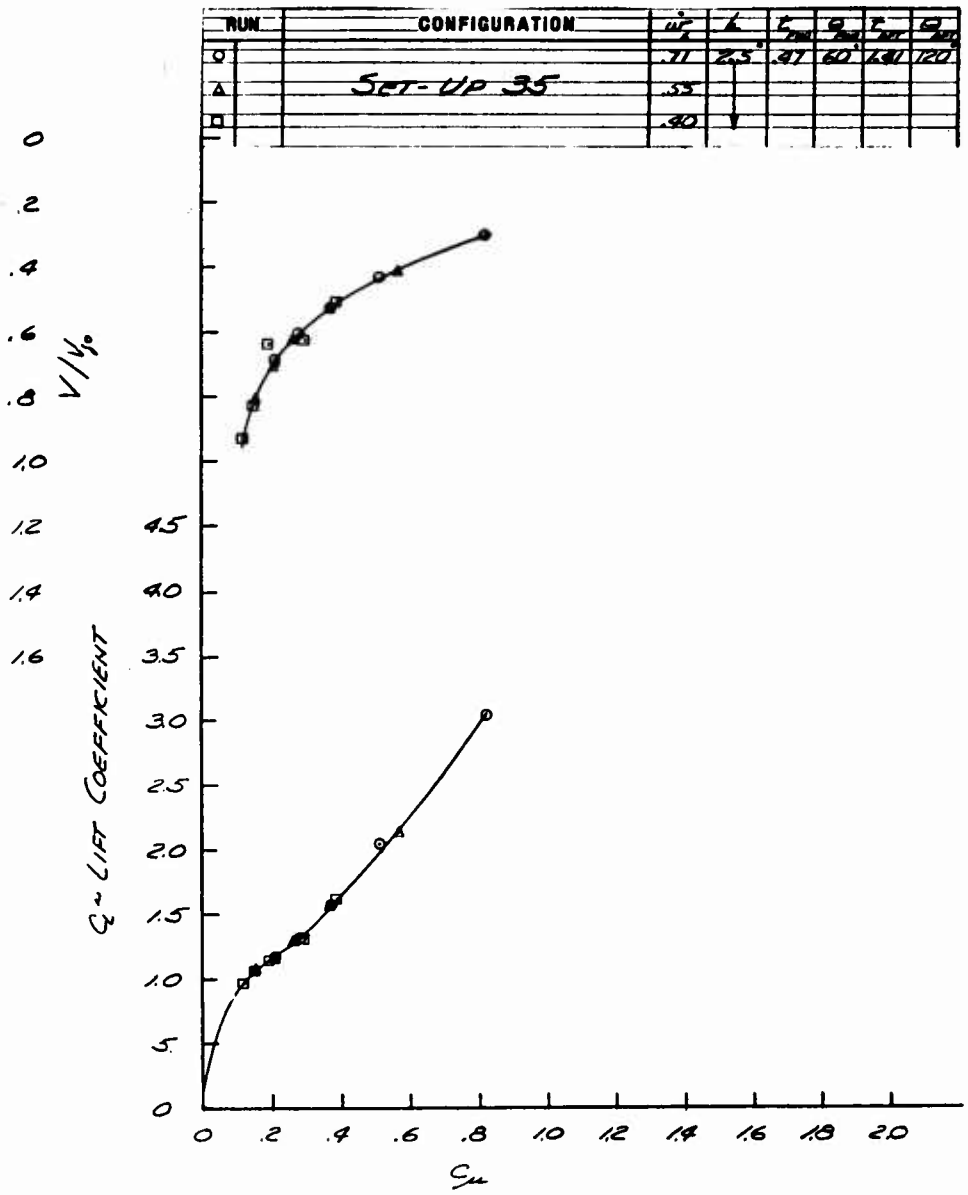

Fig. 44 C_L and V/V_{j_o} vs C_μ

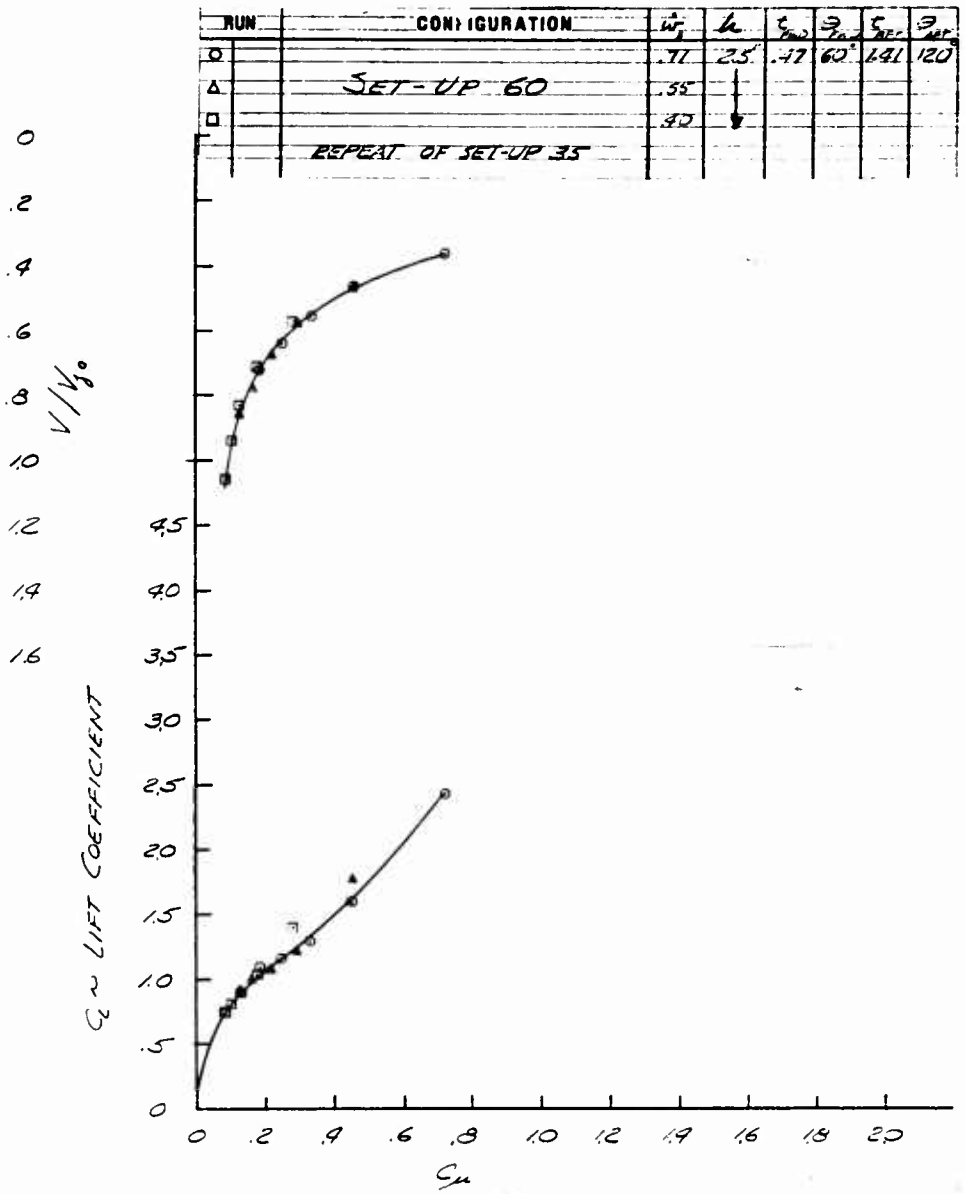

Fig. 44a C_L and V/V_{j_o} vs C_μ

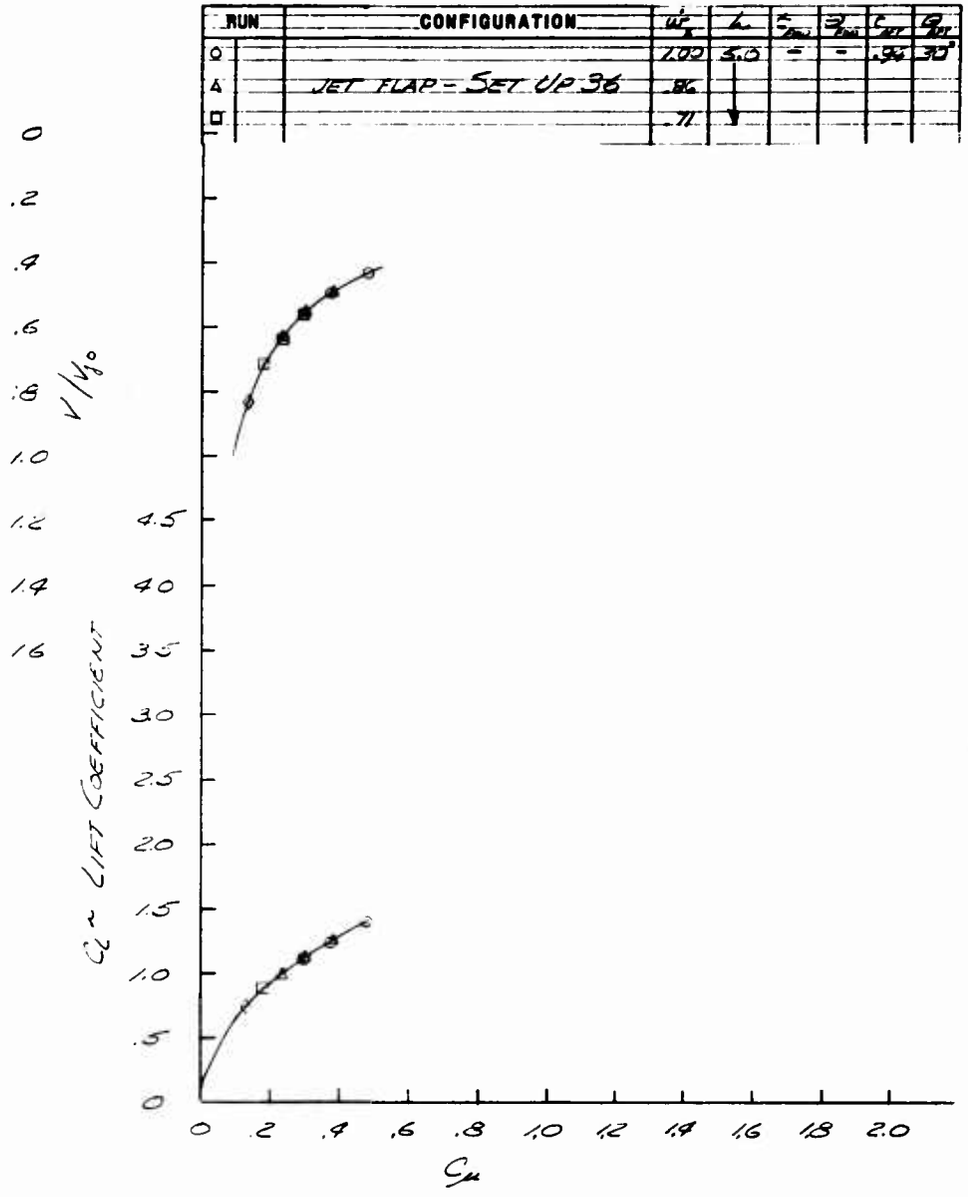

Fig. 45 C_L and V/V_{j_o} vs C_μ

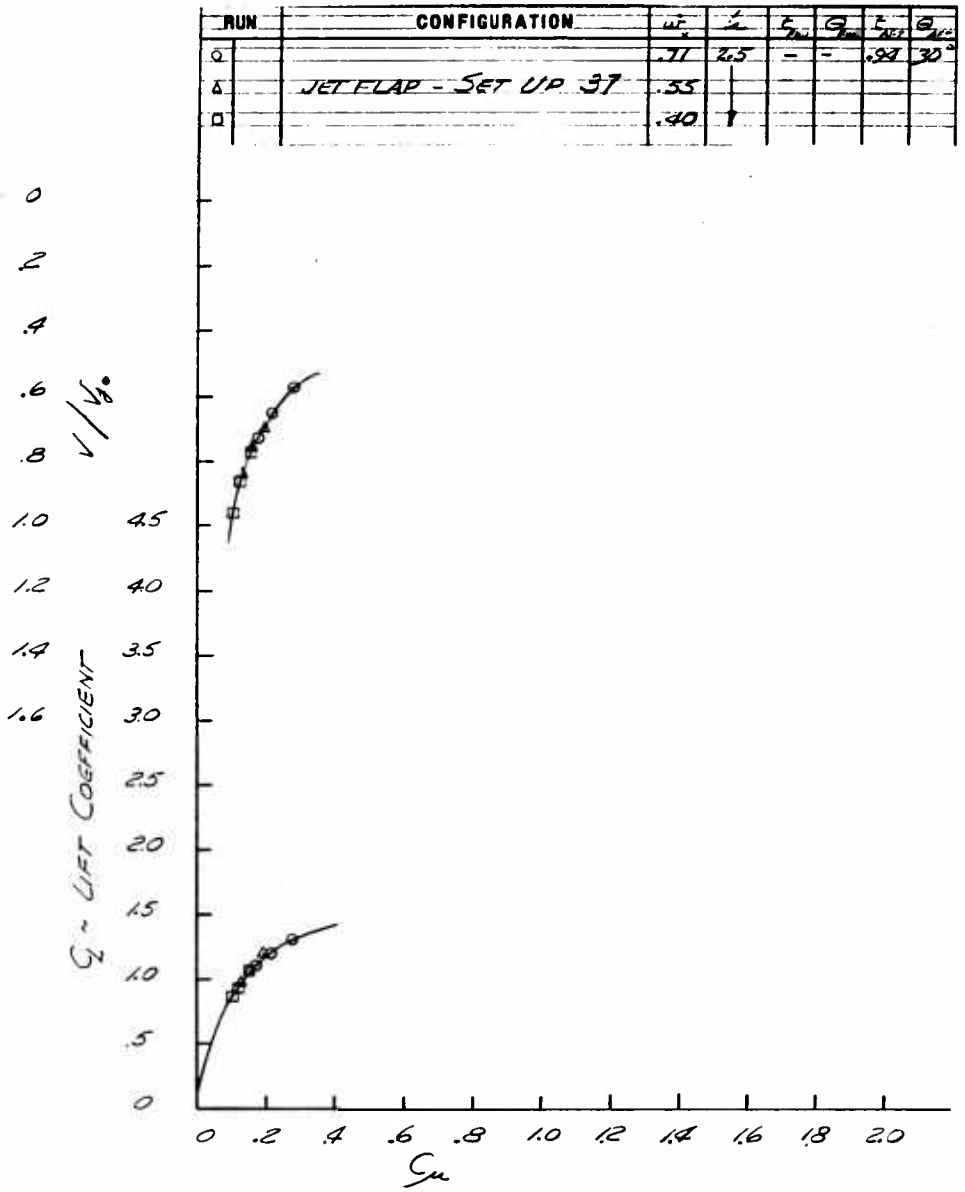

Fig. 46 C_L and V/V_{j_o} vs C_μ

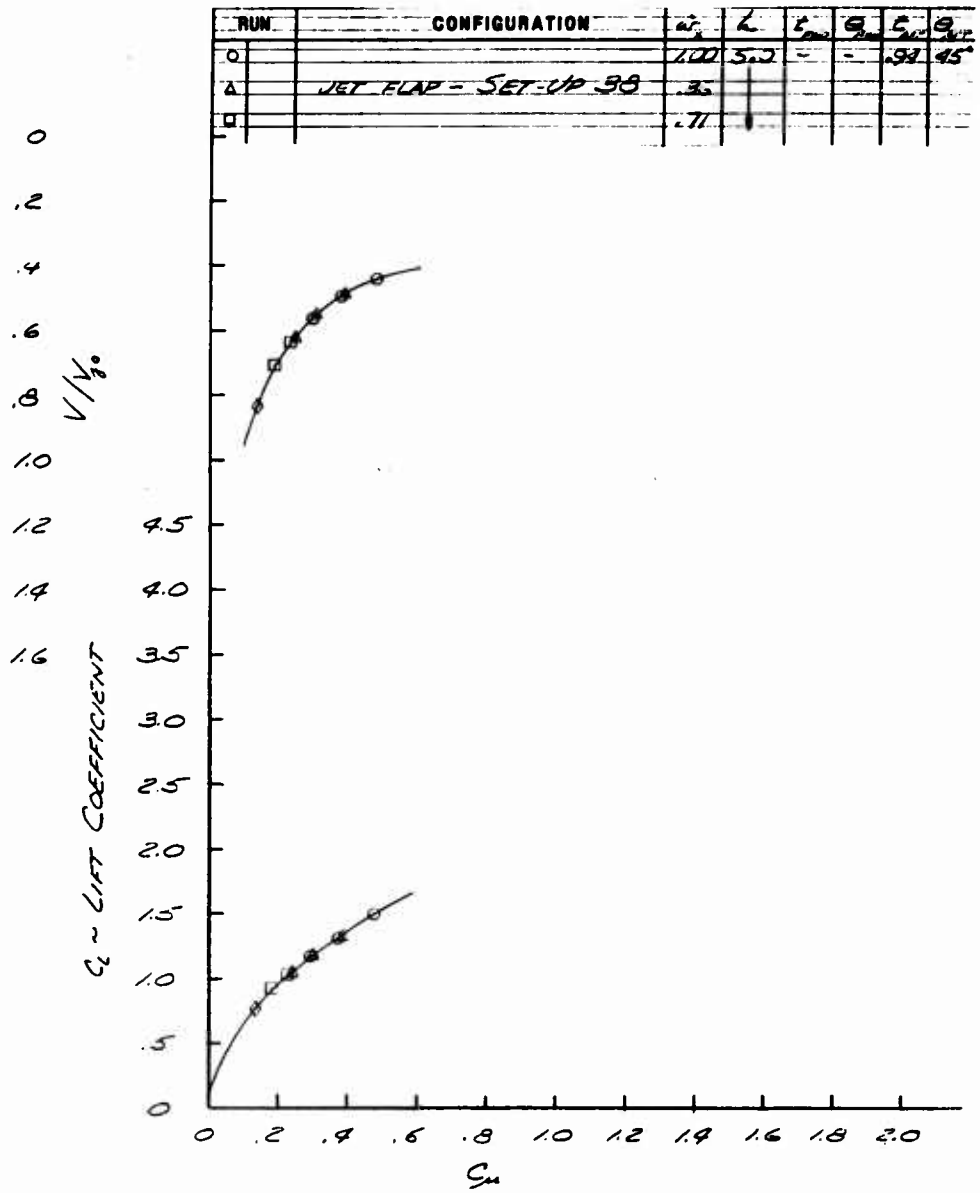

Fig. 47 C_L and V/V_{j_o} vs C_μ

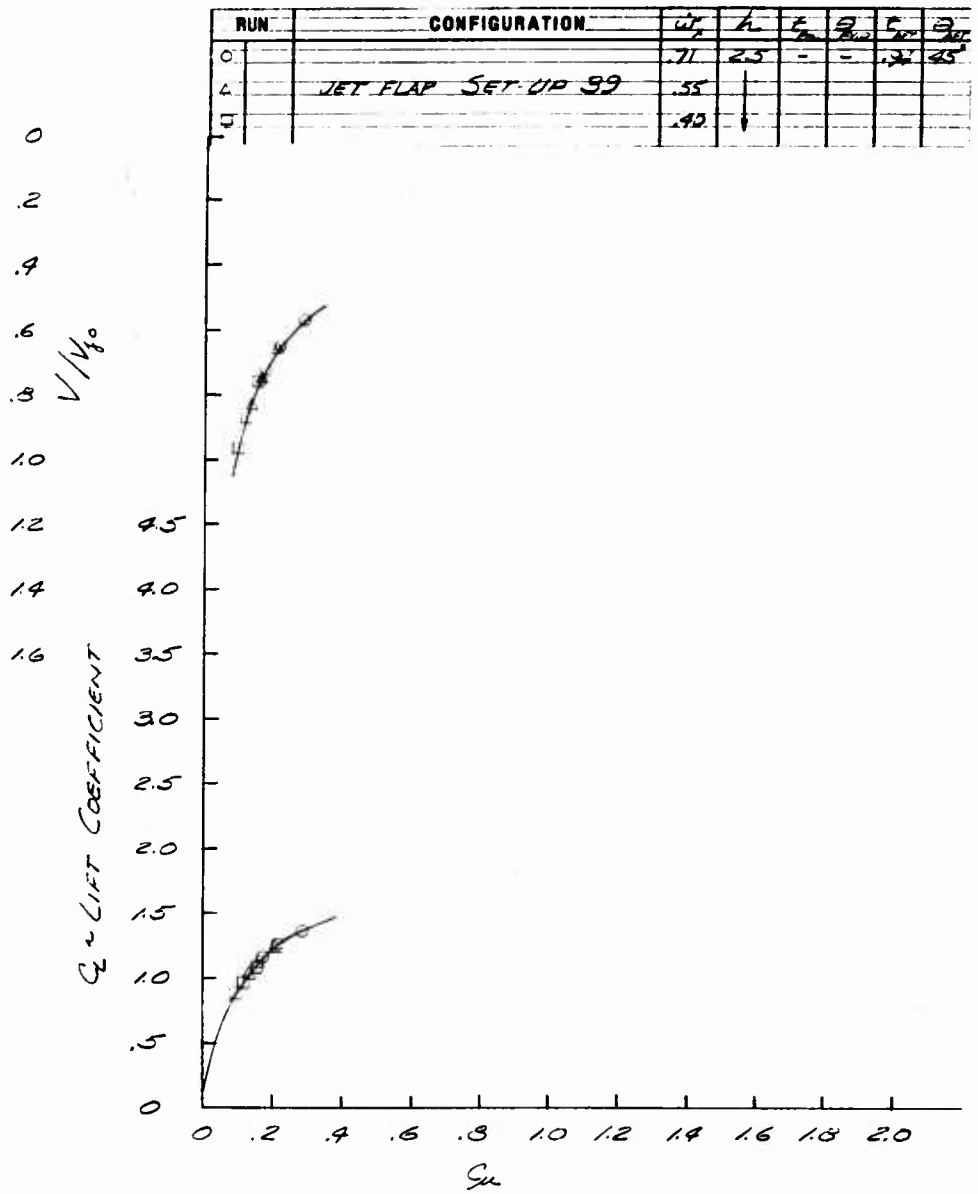

Fig. 48 C_L and V/V_{j_o} vs C_μ

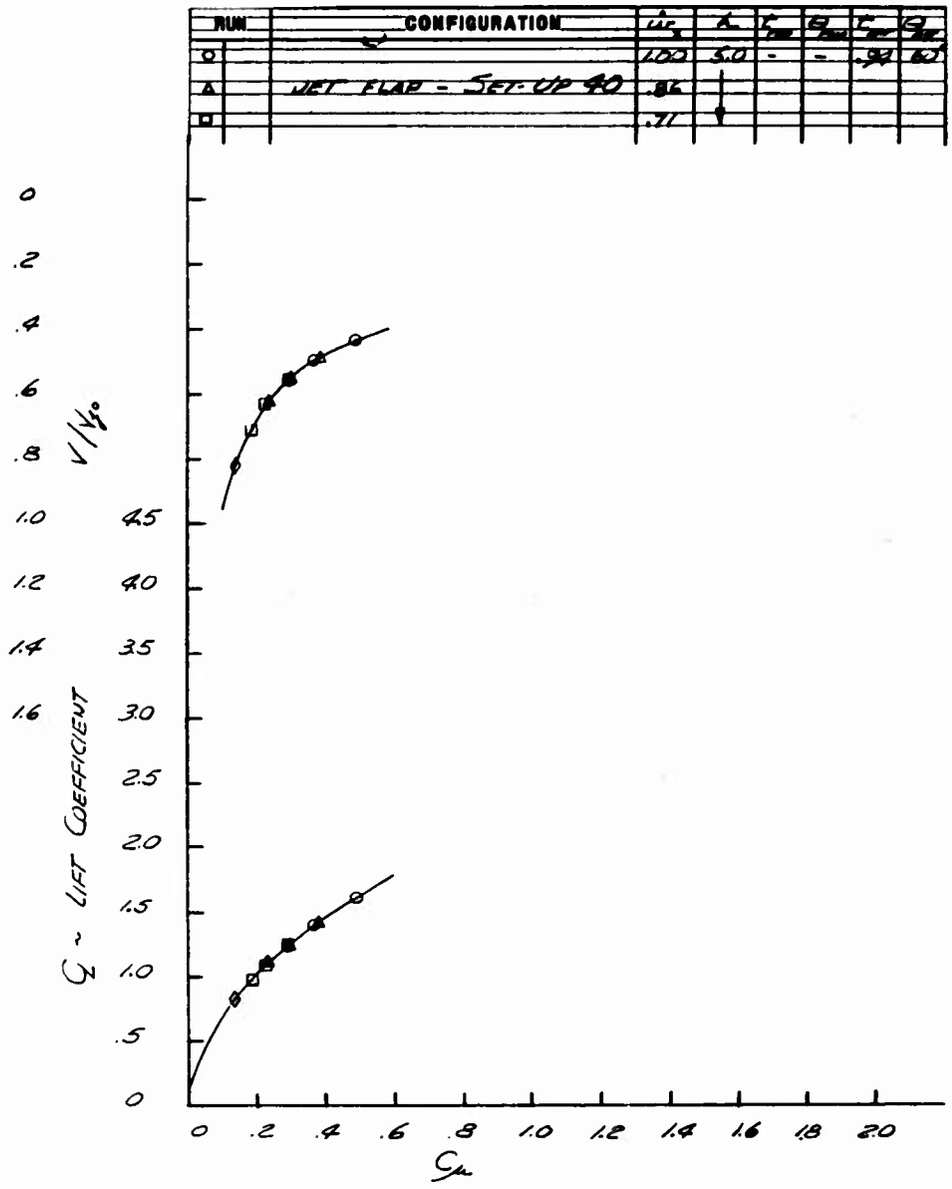

Fig. 49 C_L and V/V_{j_o} vs C_μ

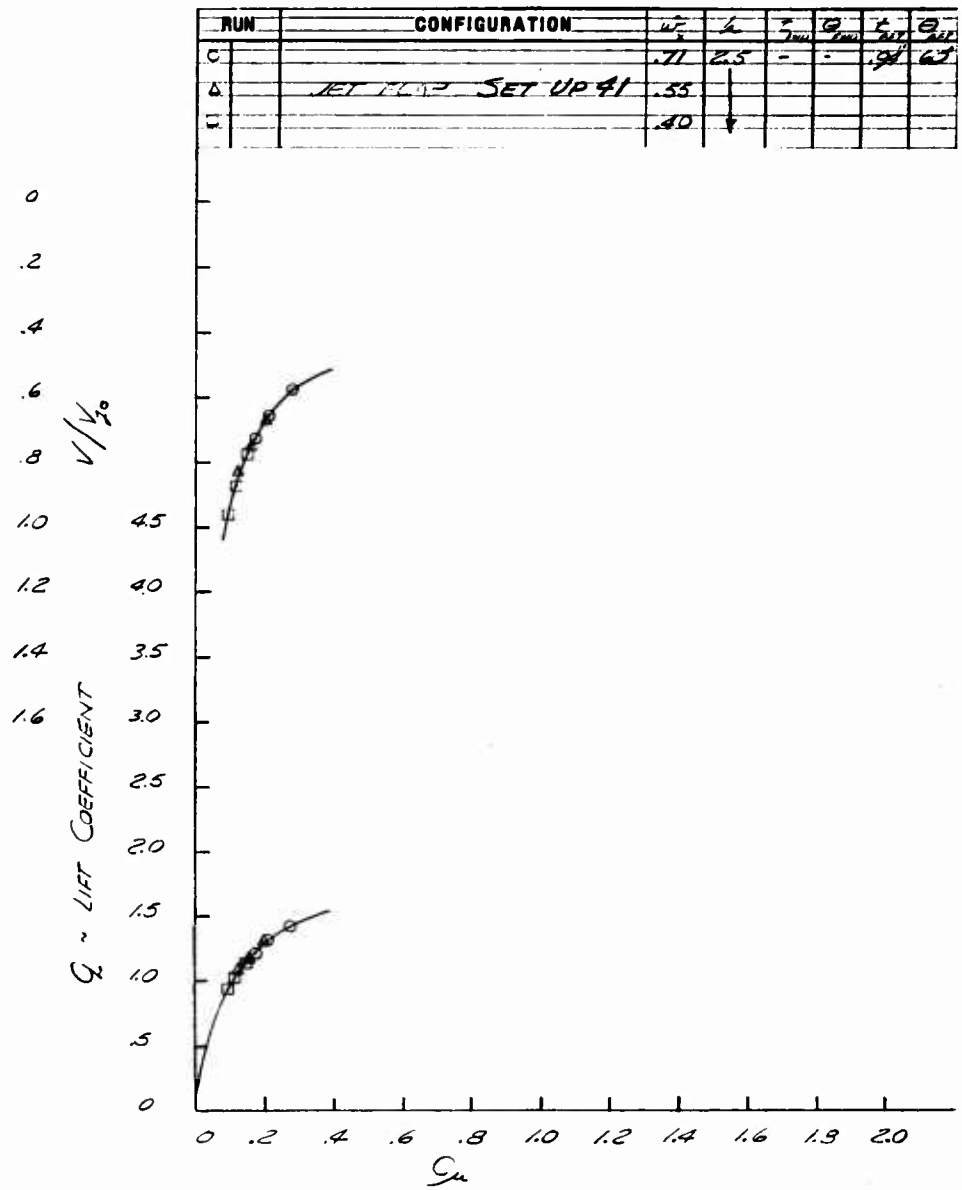

Fig. 50 C_L and V/V_{j_o} vs C_μ

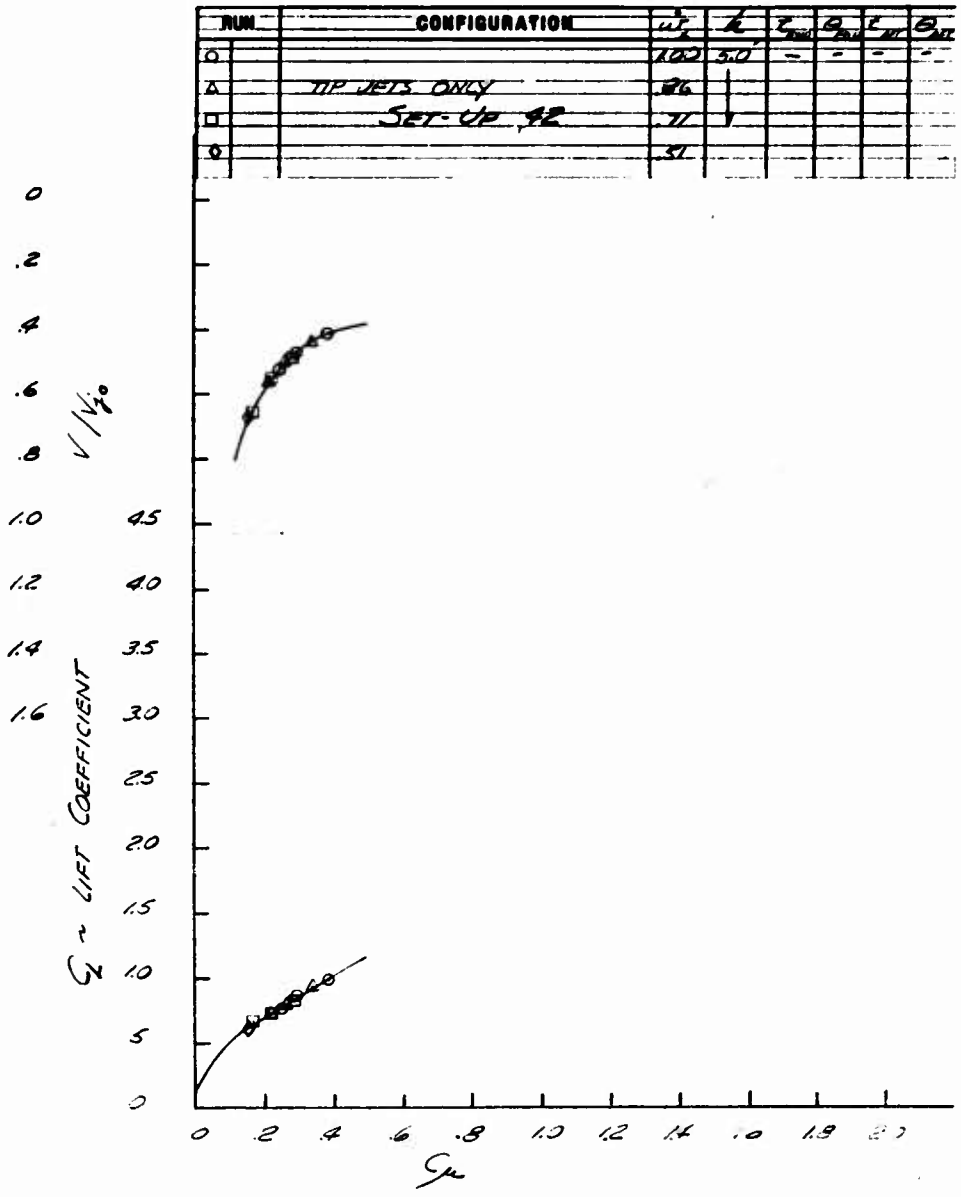

Fig. 51 C_L and V/V_{j_o} vs C_μ

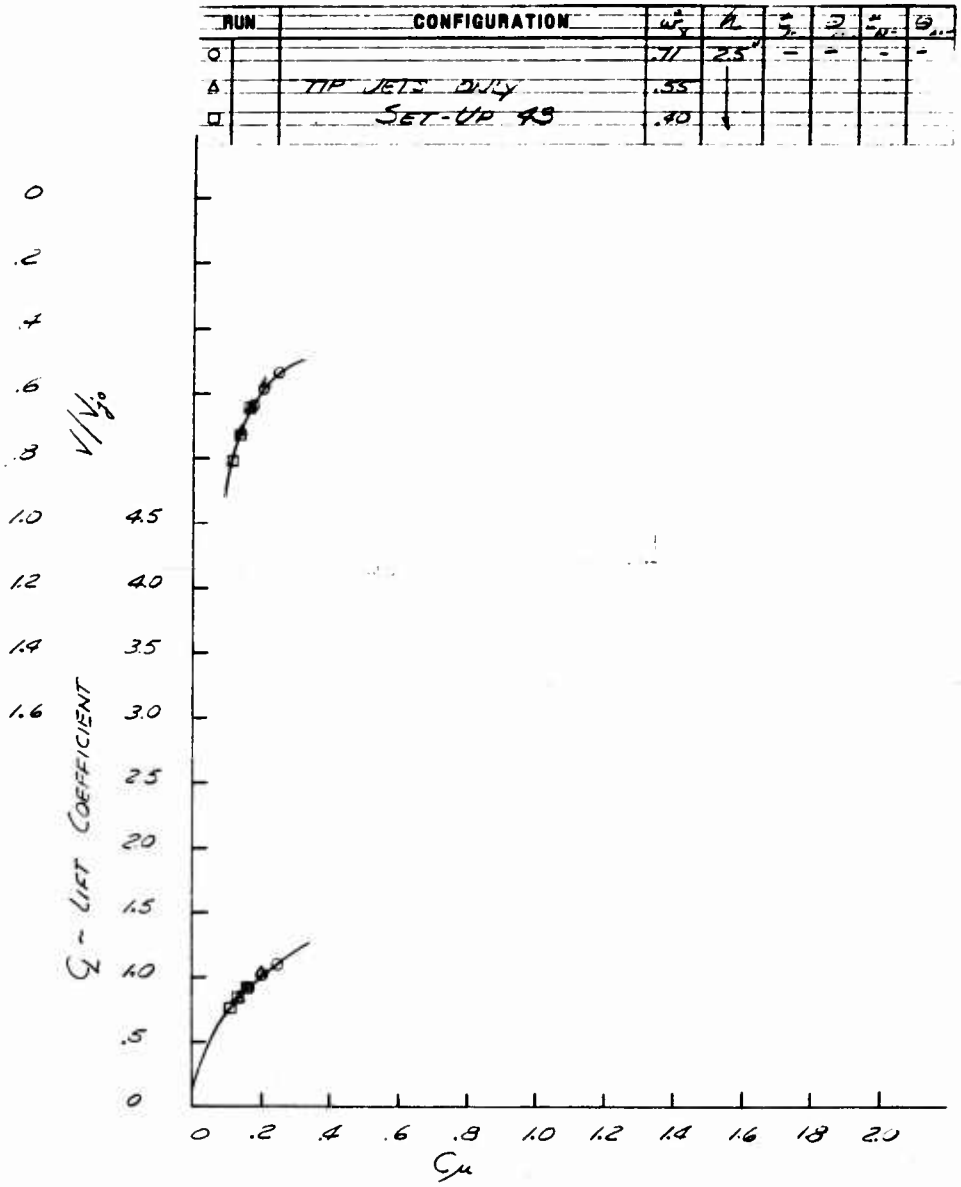

Fig. 52 C_L and V/V_{j_o} vs C_μ

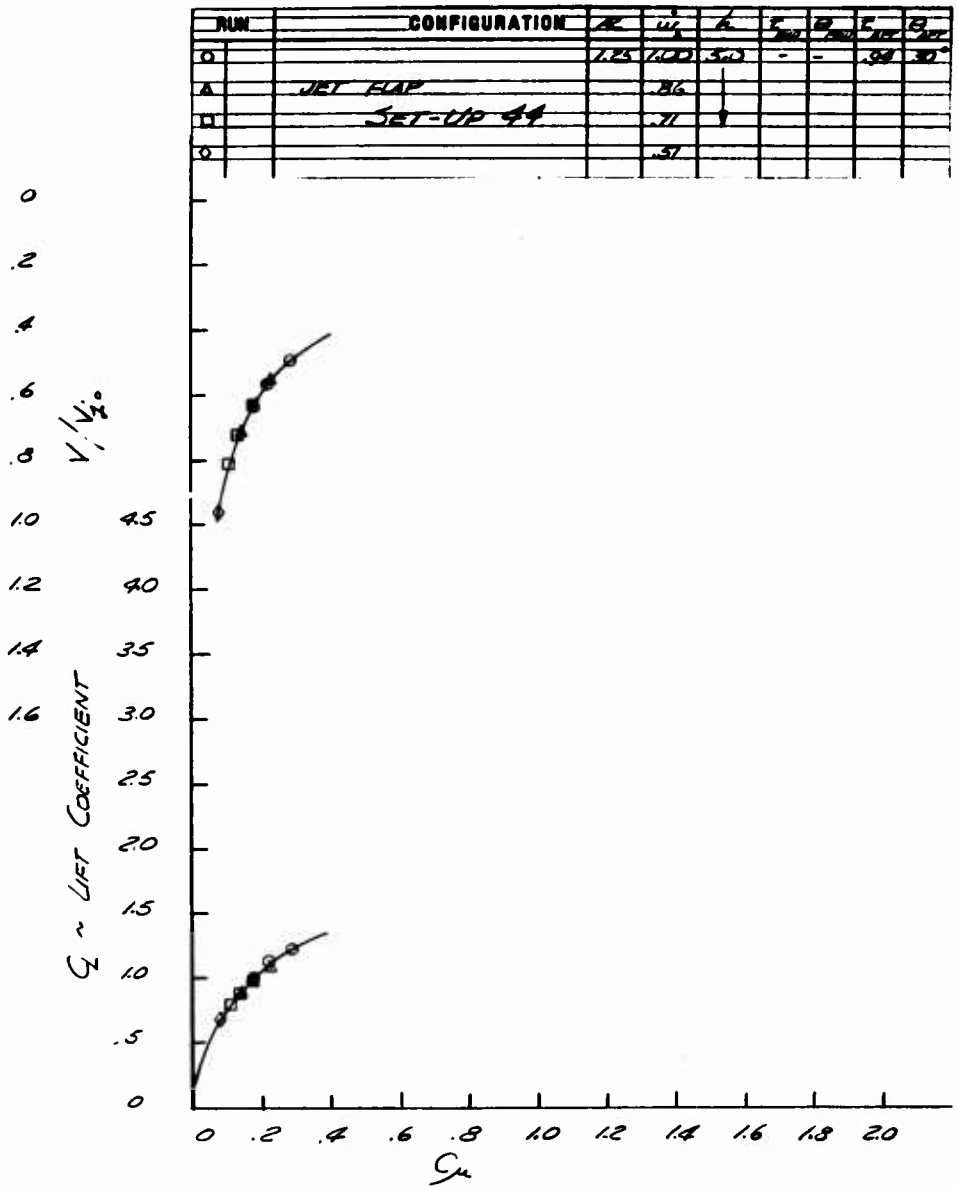

Fig. 53 C_L and V/V_{j_o} vs C_μ

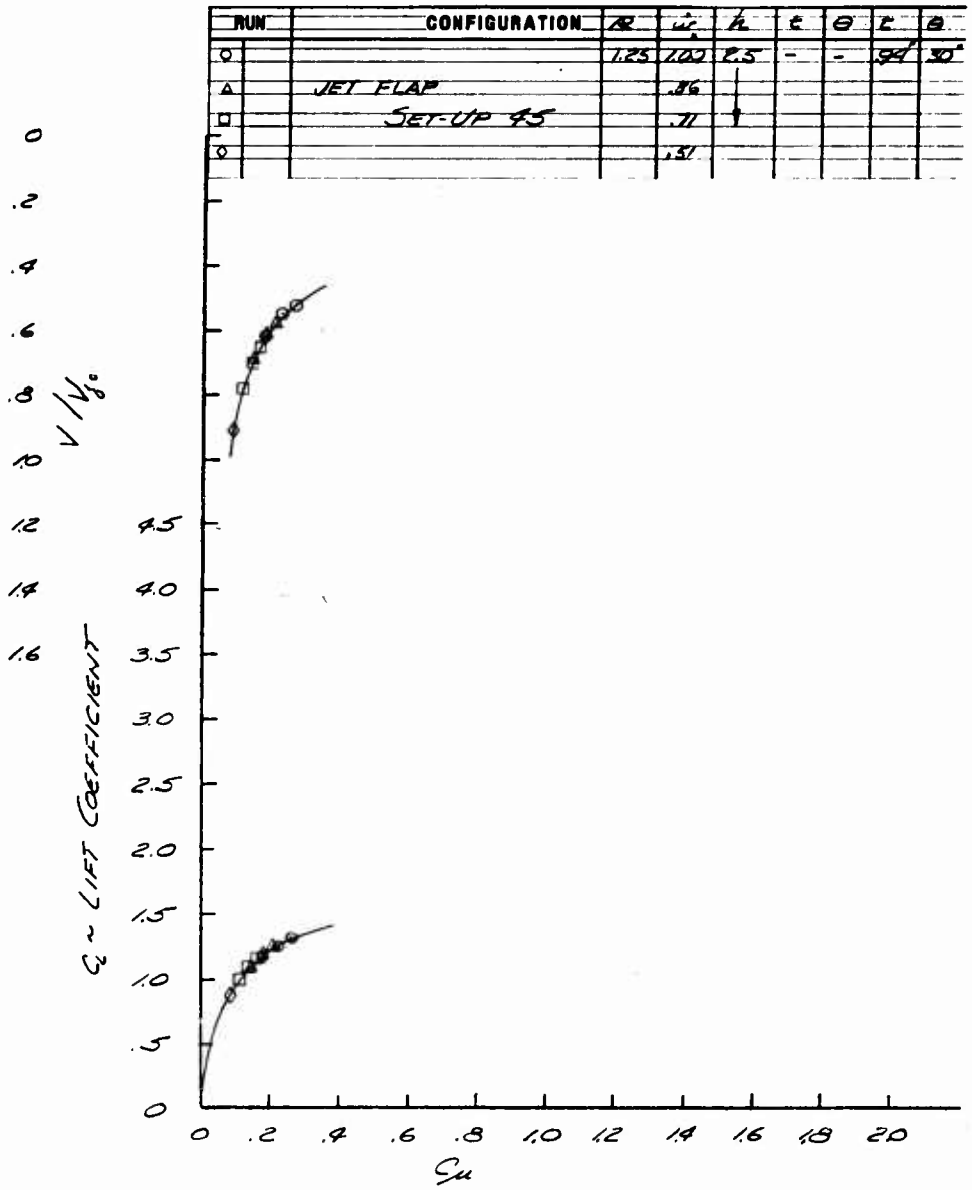

Fig. 54 C_L and V/V_{j_o} vs C_μ

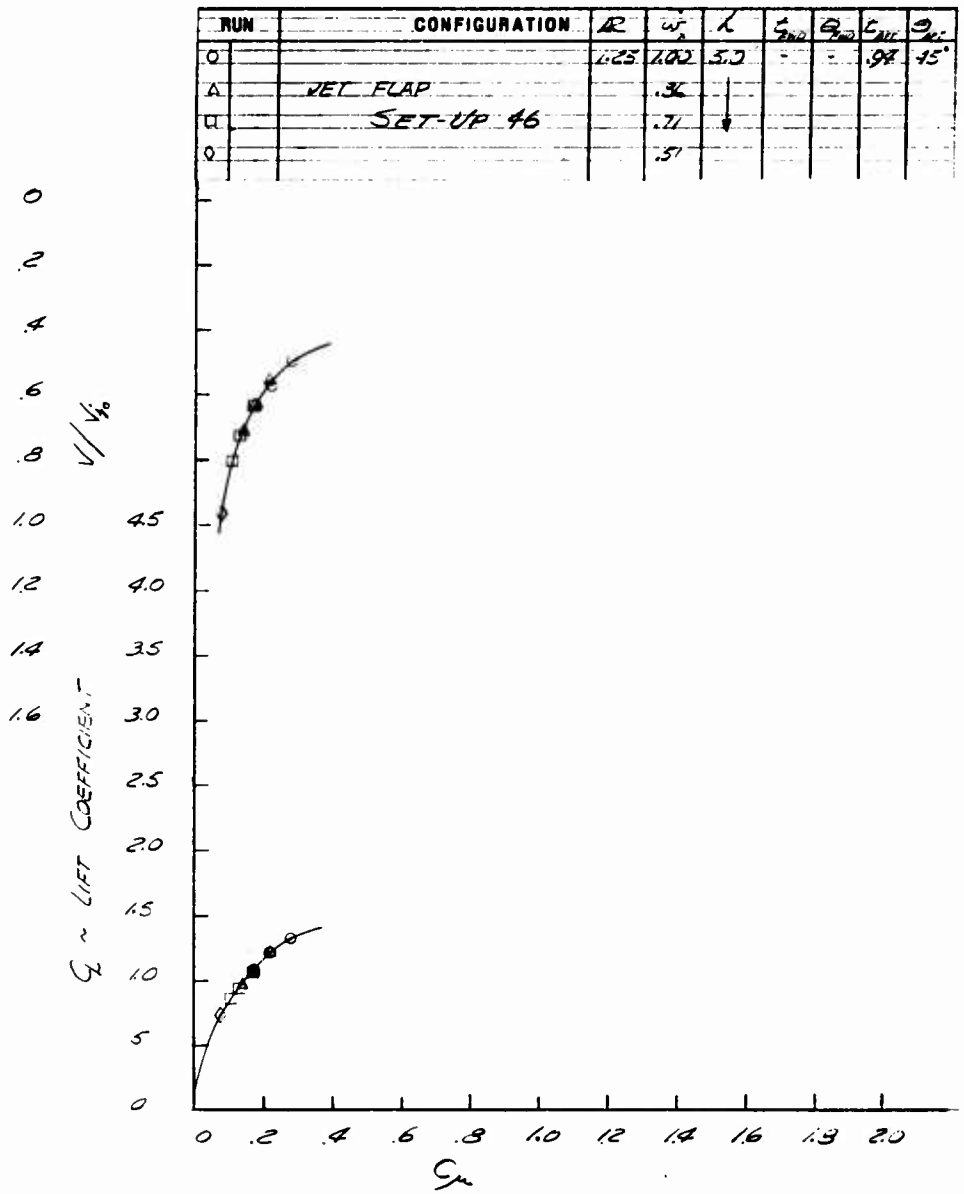

Fig. 55 C_L and V/V_{j_o} vs C_μ

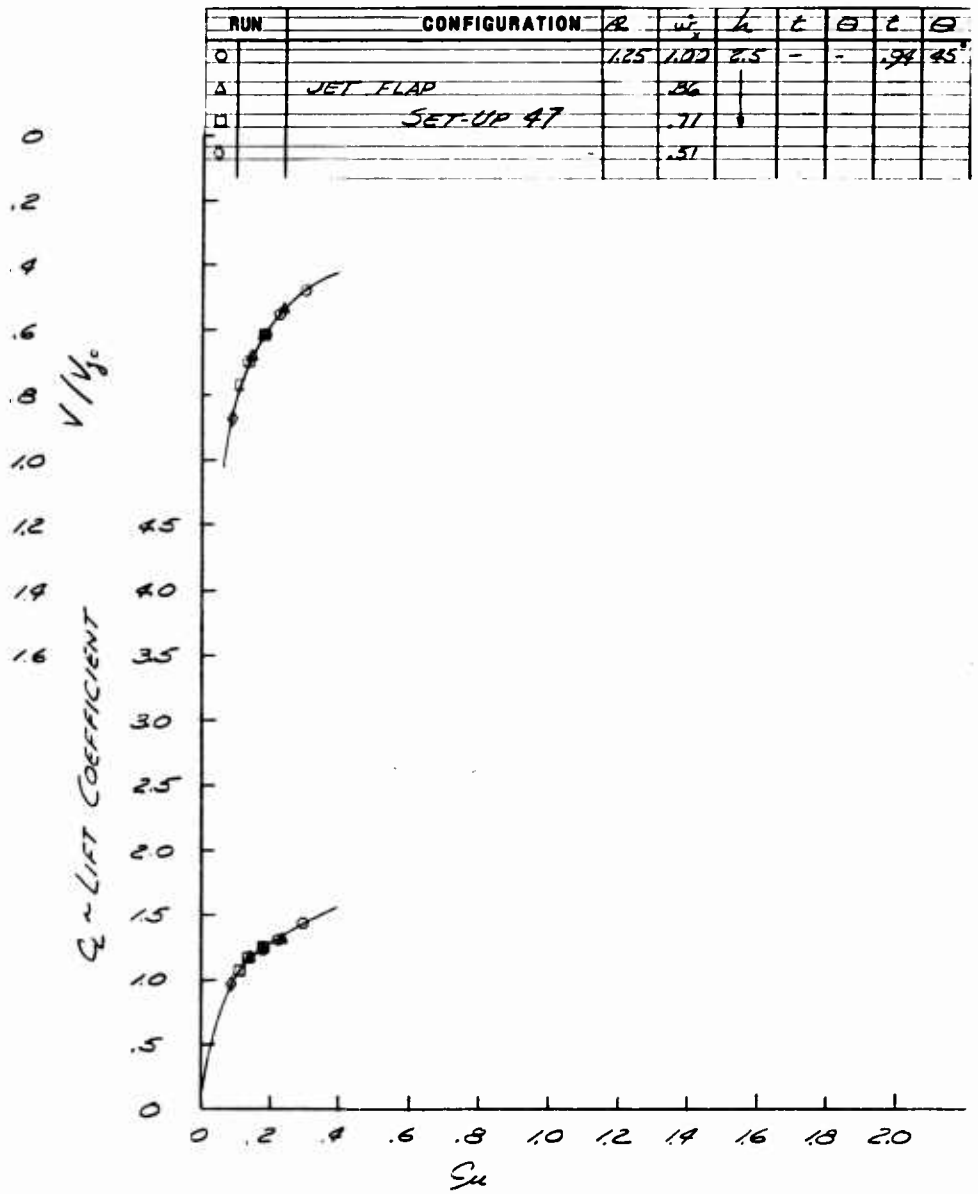

Fig. 56 C_L and V/V_{j_o} vs C_μ

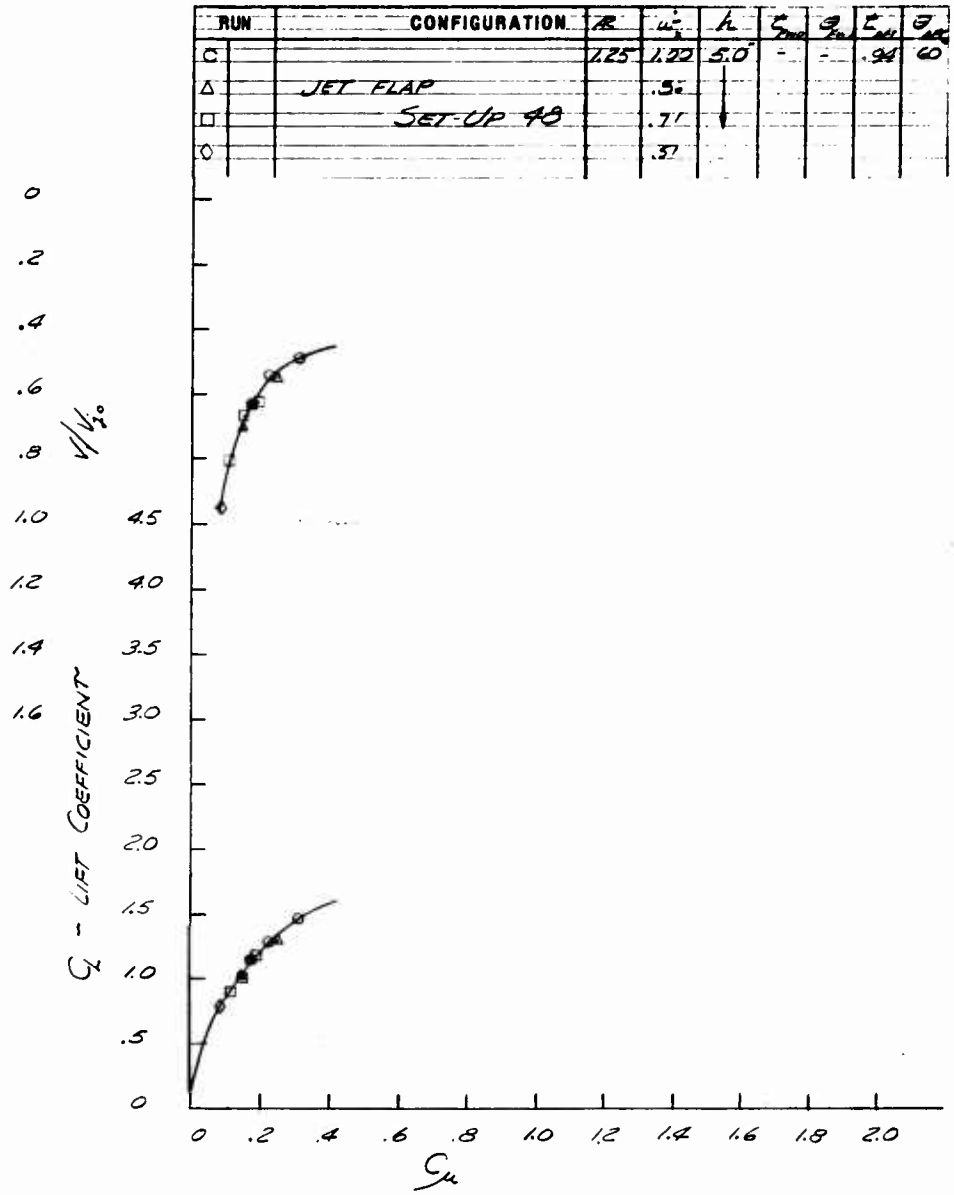

Fig. 57 C_L and V/V_{j_o} vs C_μ

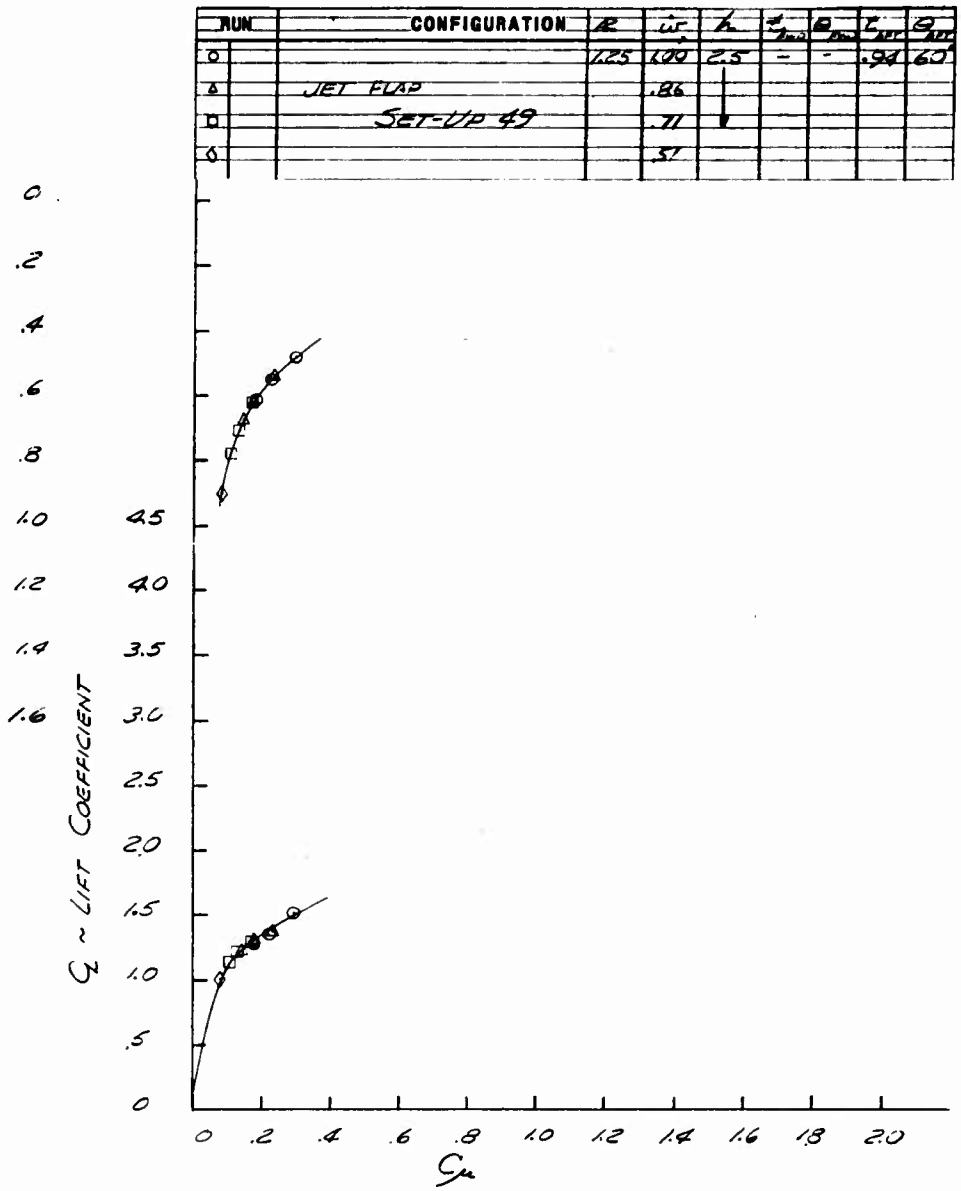

Fig. 58 C_L and V/V_{j_o} vs C_μ

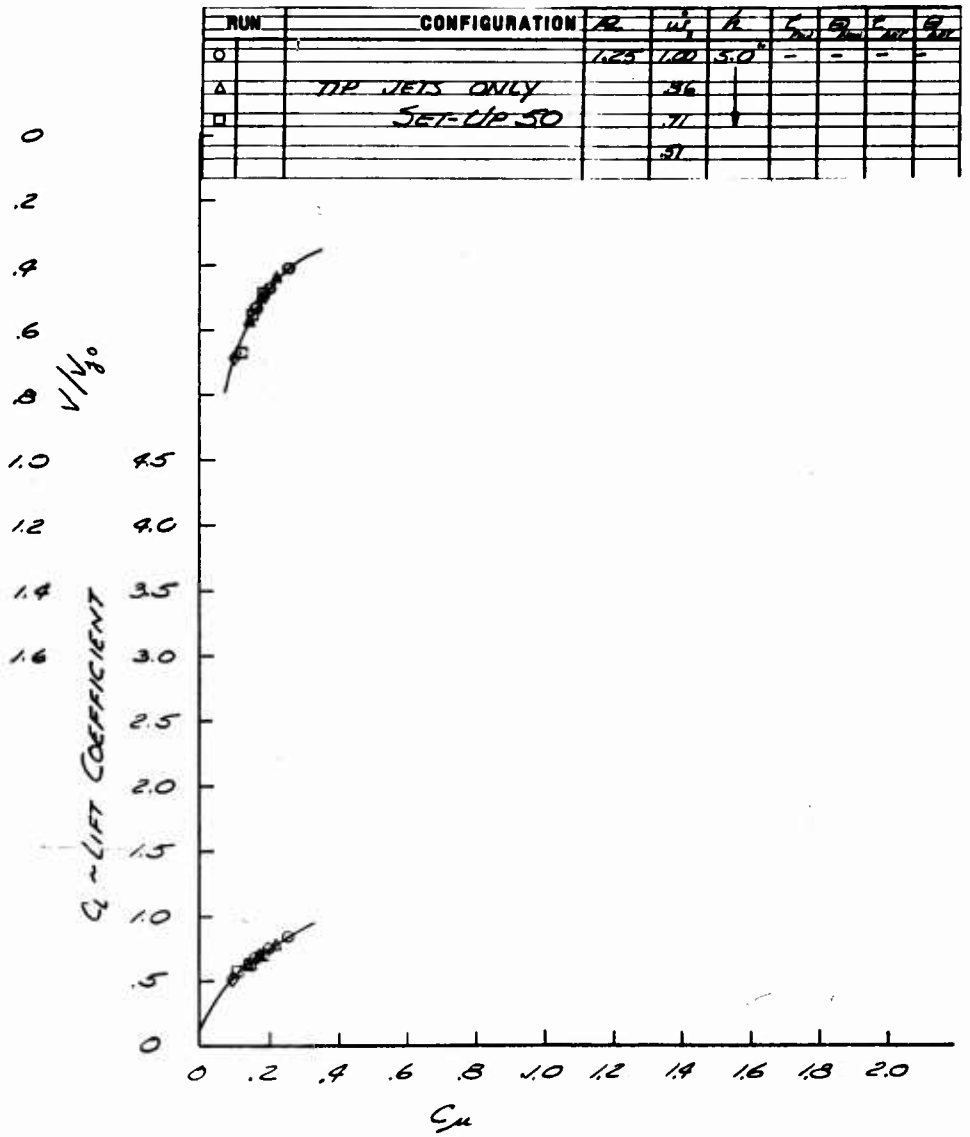

Fig. 59 C_L and V/V_{j_o} vs C_μ

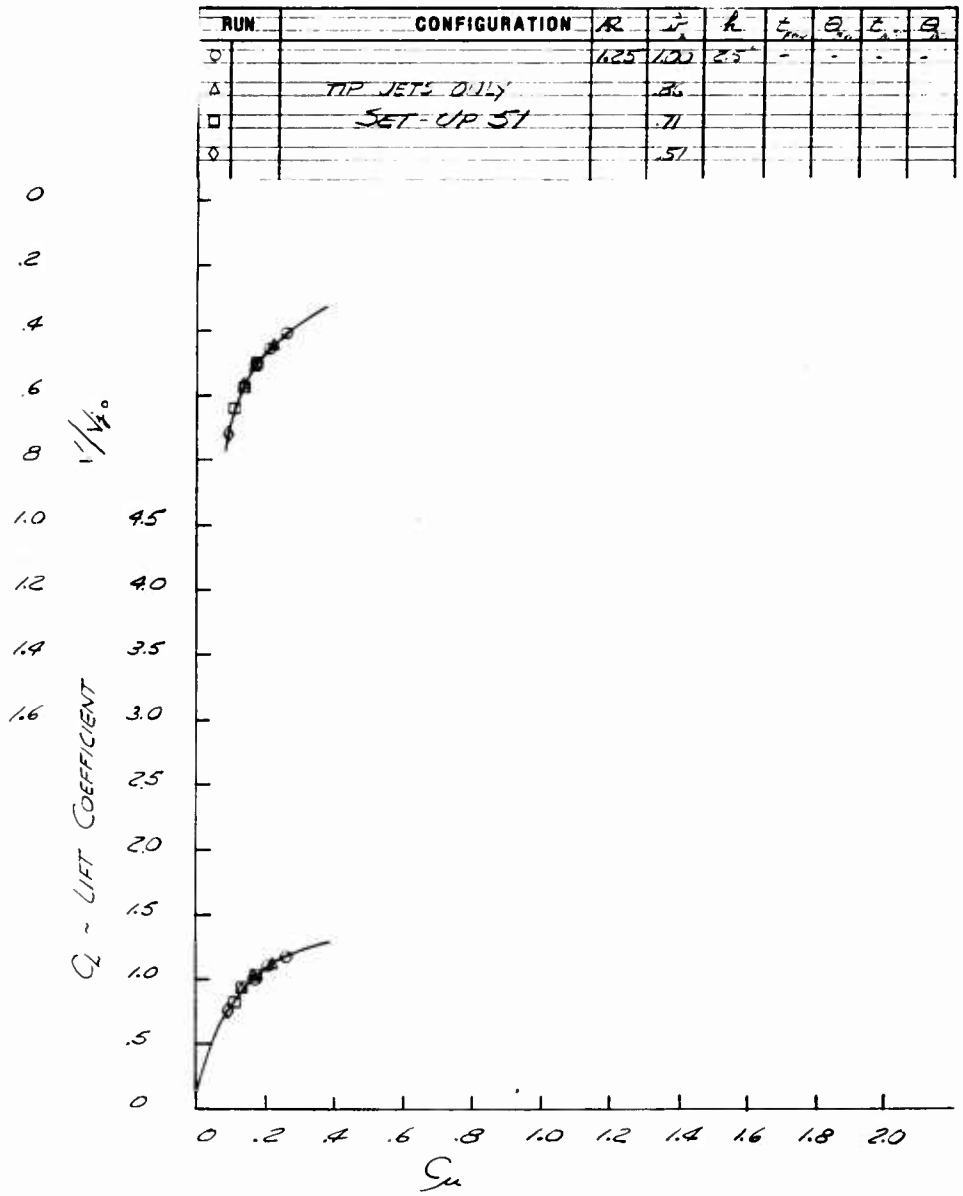

Fig. 60 C_L and V/V_{j_o} vs C_μ

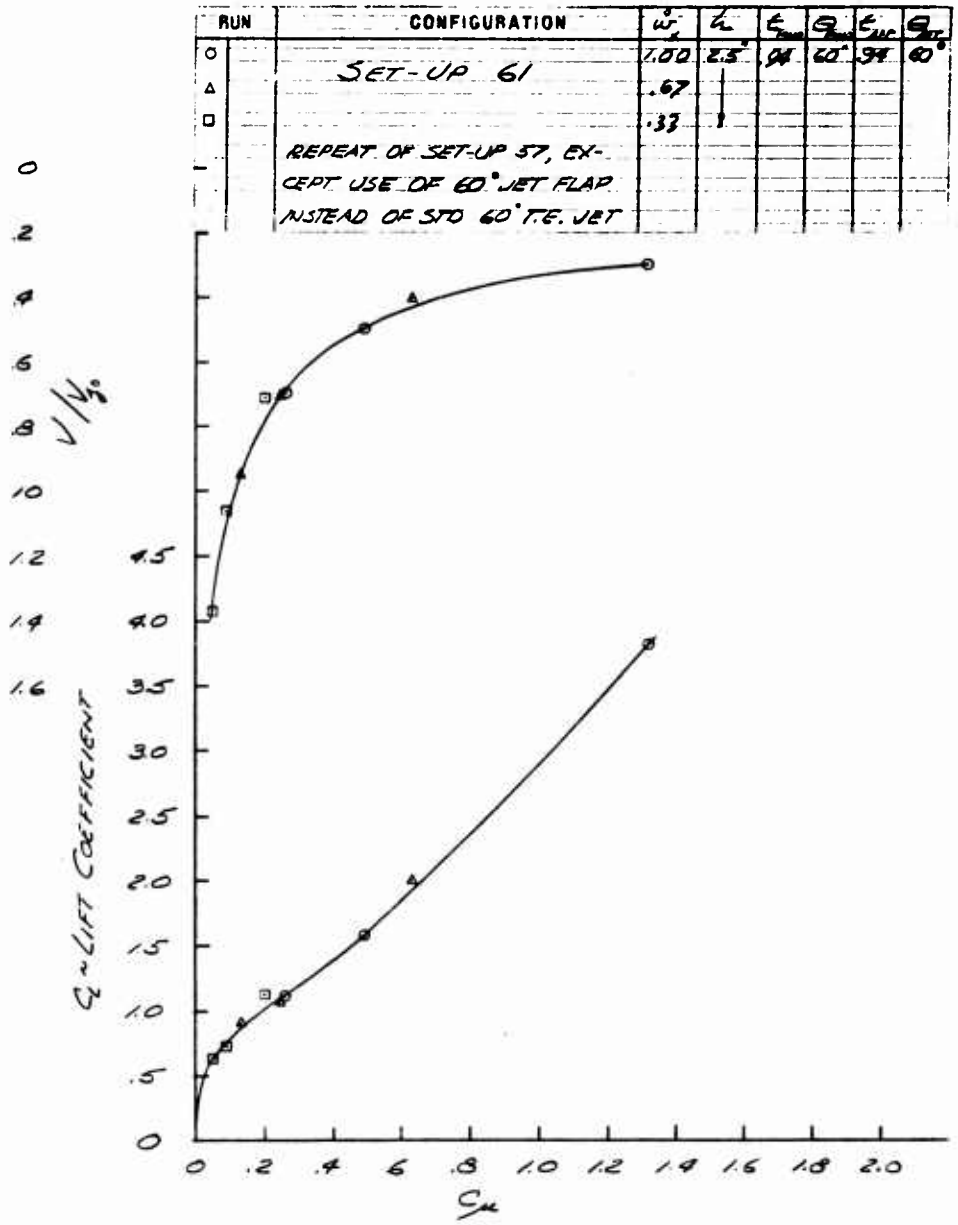

Fig. 61 C_L and V/V_{j_o} vs C_μ

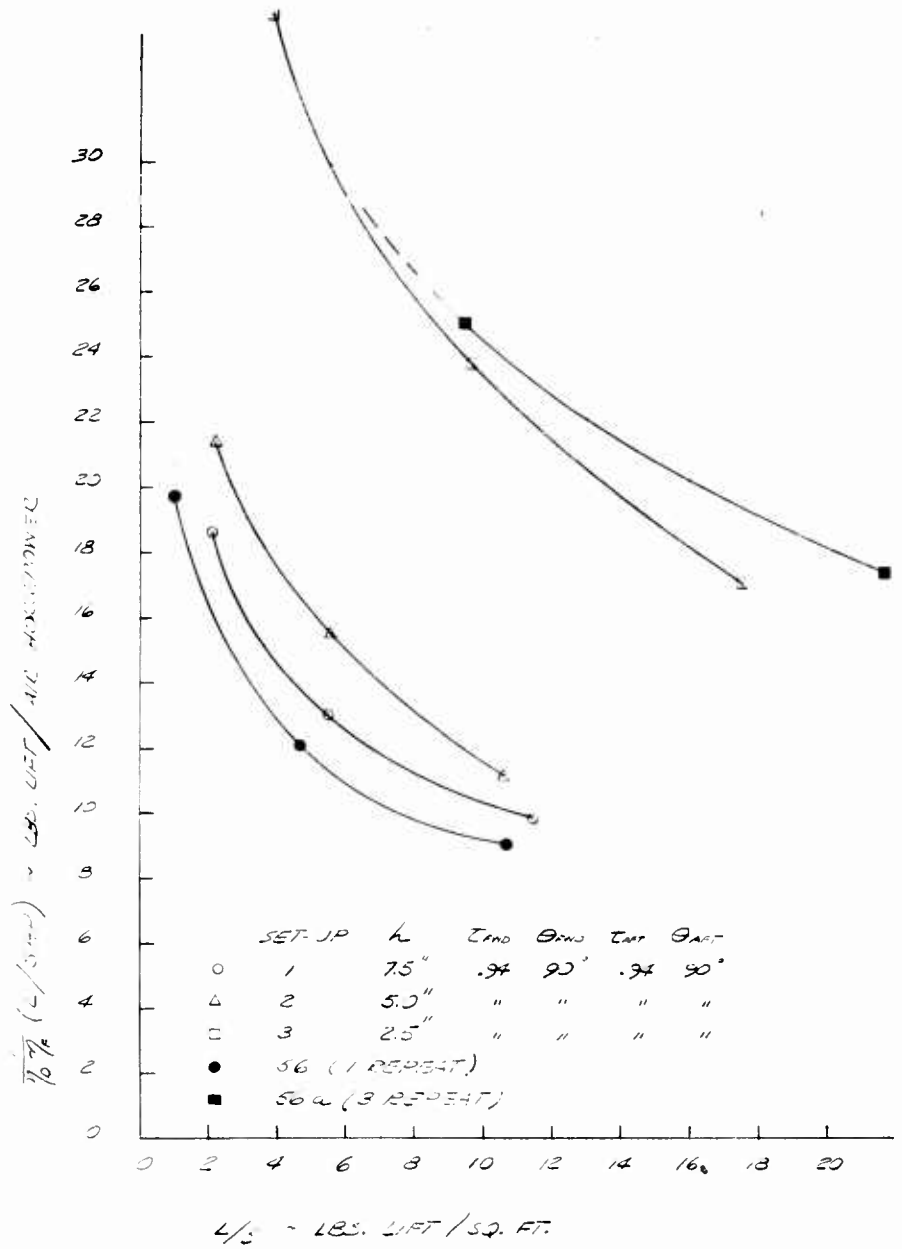

Fig. 62 Hover Lift/Shaft Horsepower versus Base Loading

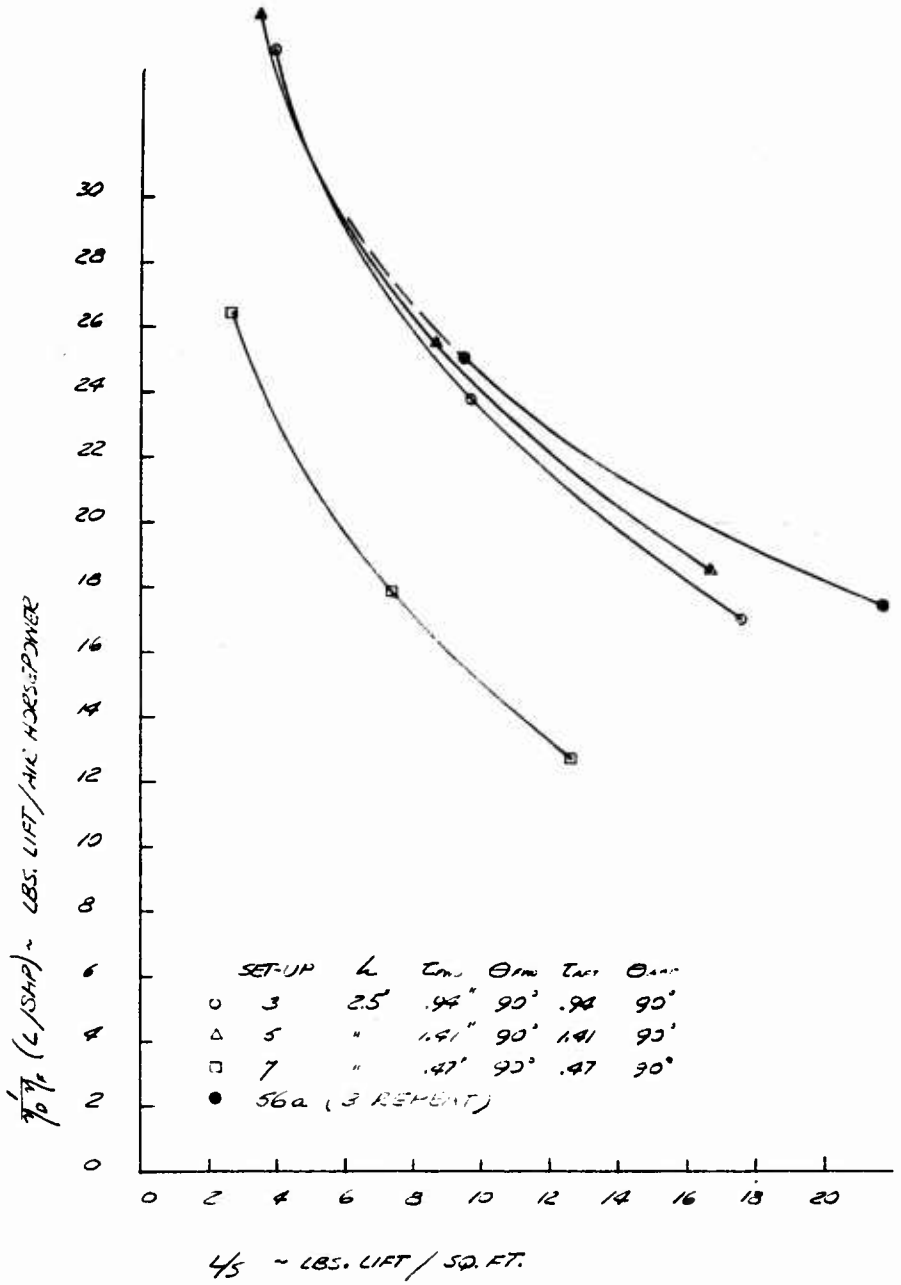

Fig. 63 Hover Lift/Shaft Horsepower versus Base Loading

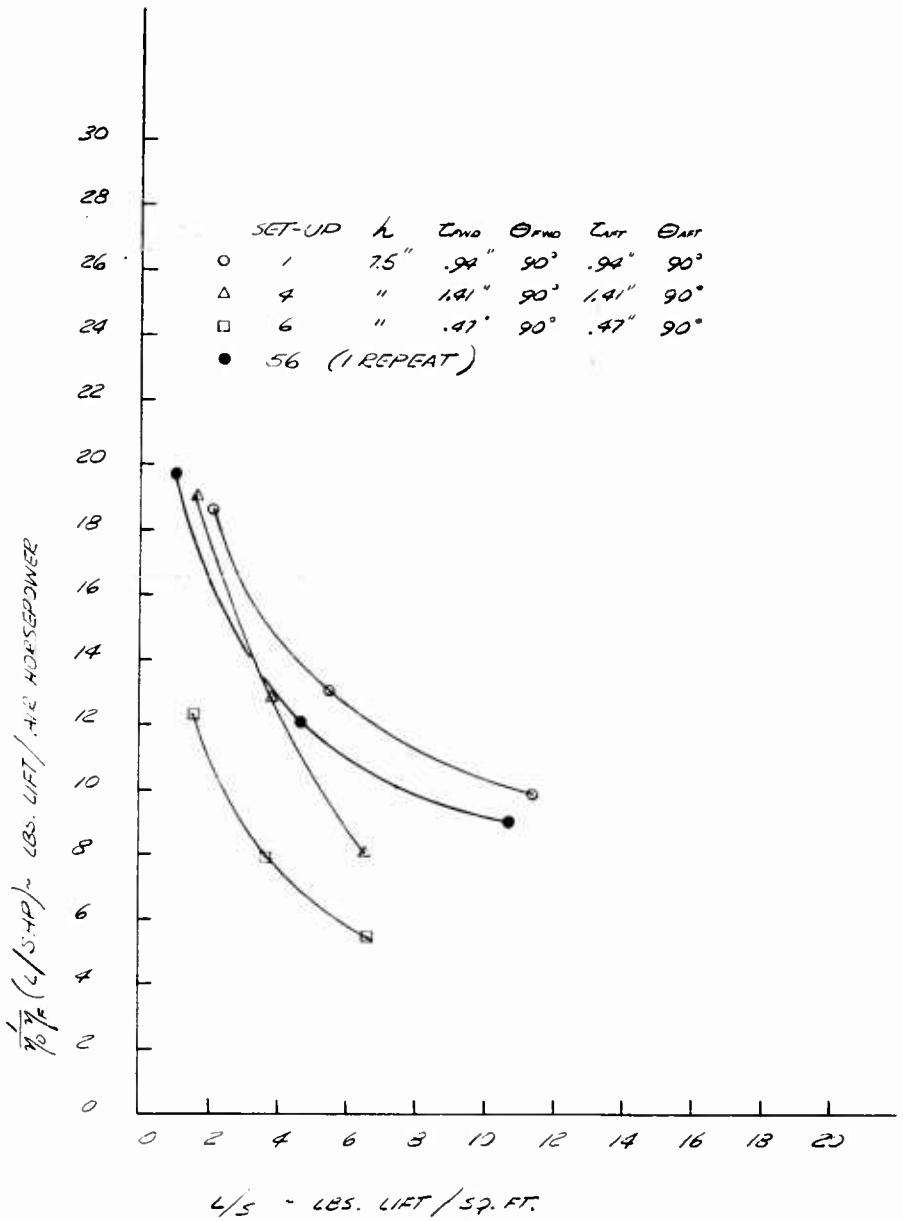

Fig. 64 Hover Lift/Shaft Horsepower versus Base Loading

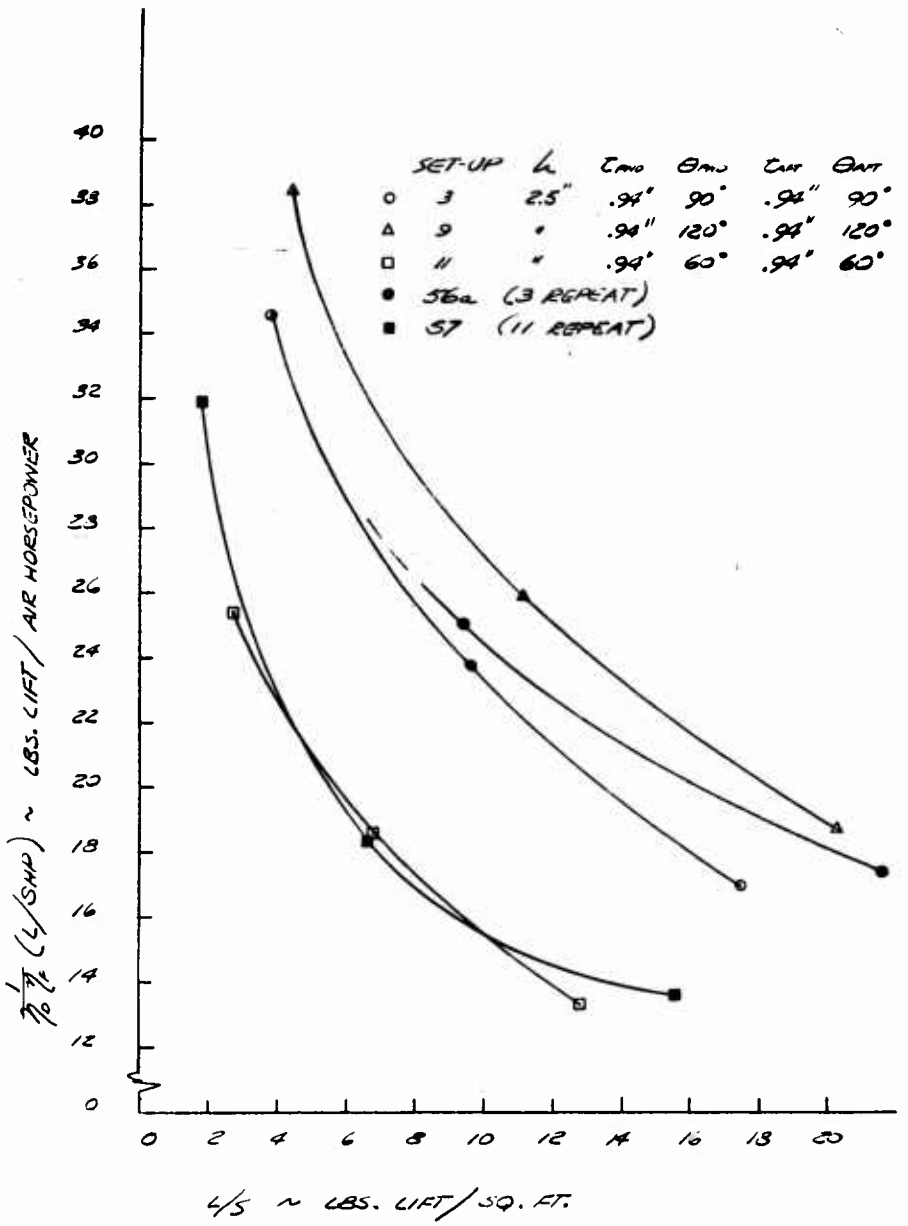

Fig. 65 Hover Lift/Shaft Horsepower versus Base Loading

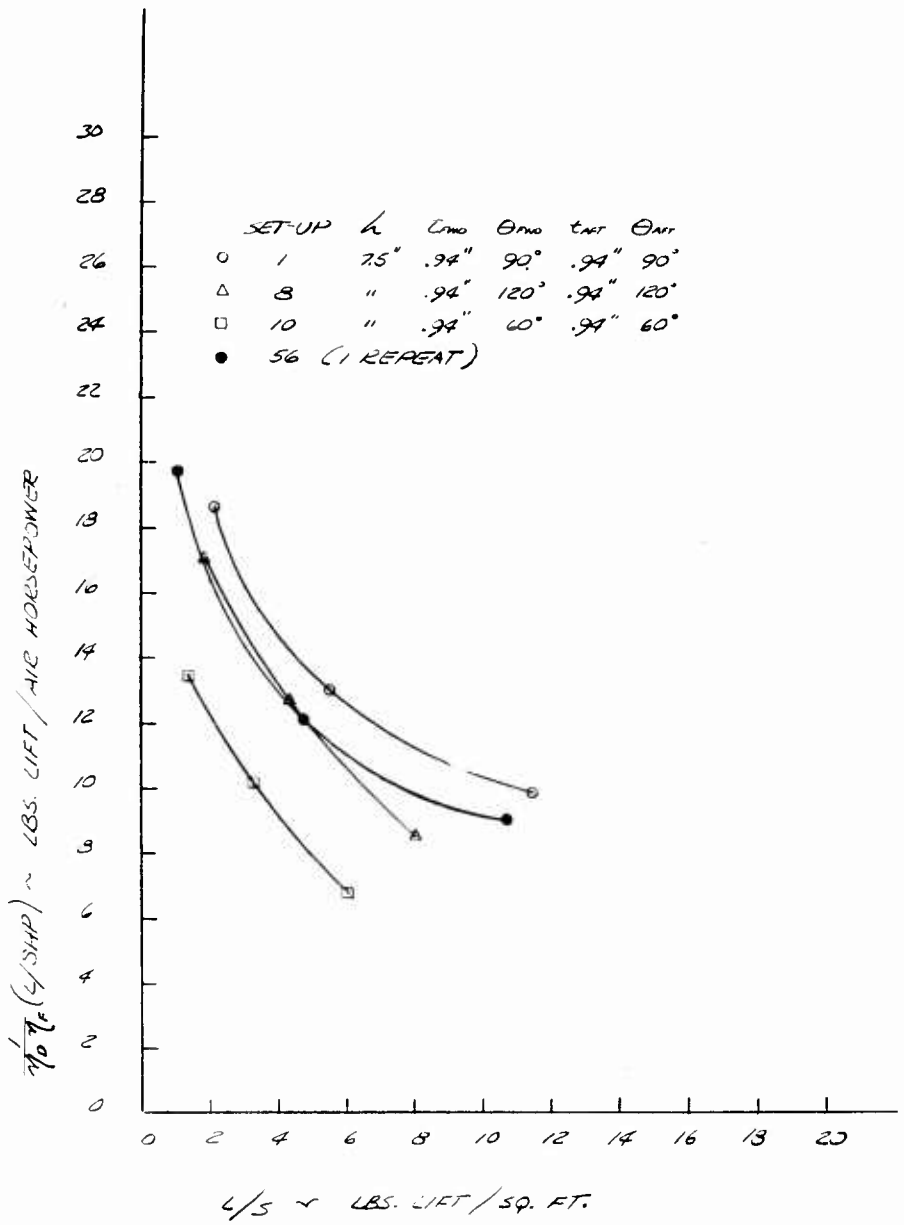

Fig. 66 Hover Lift/Shaft Horsepower versus Base Loading

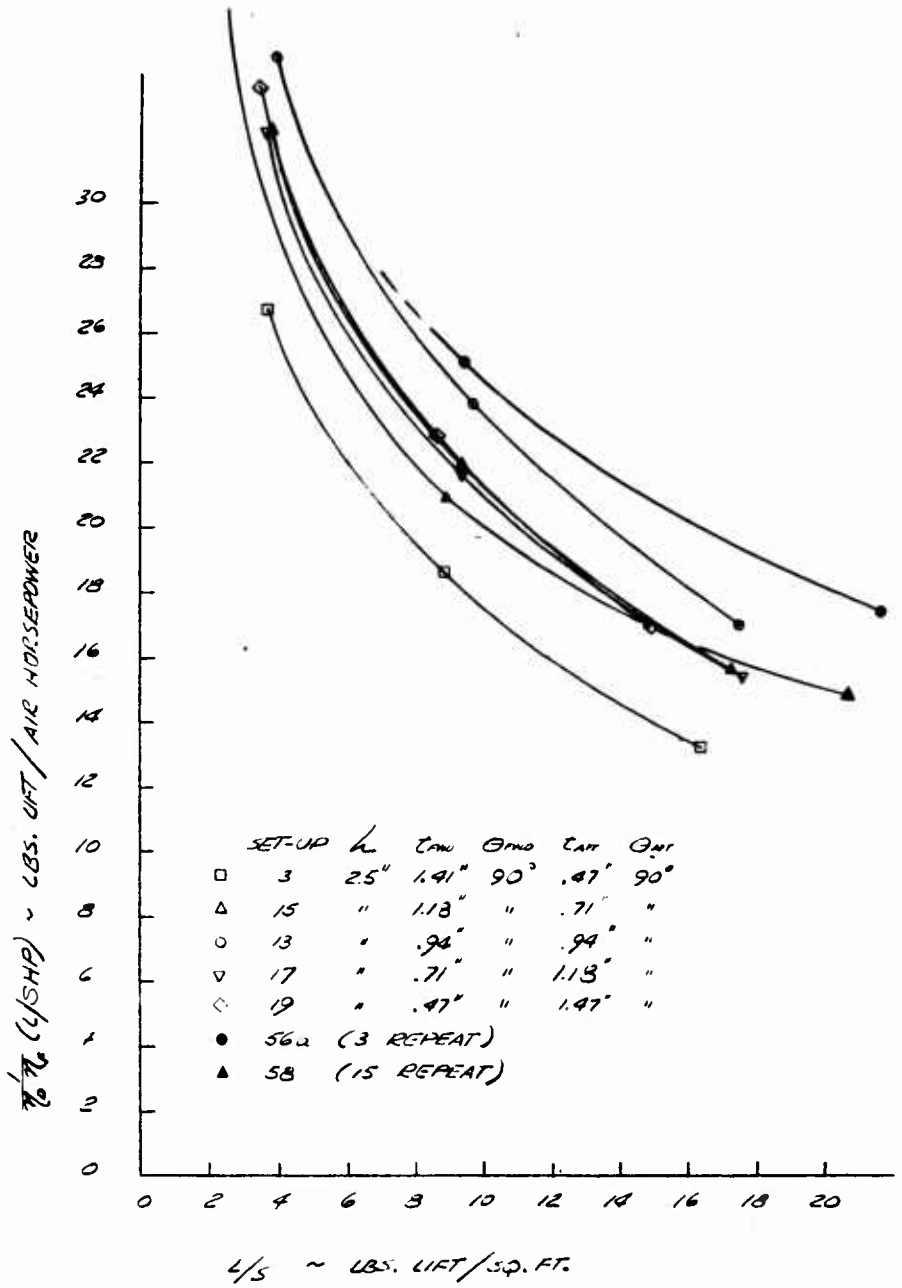

Fig. 67 Hover Lift/Shaft Horsepower versus Base Loading

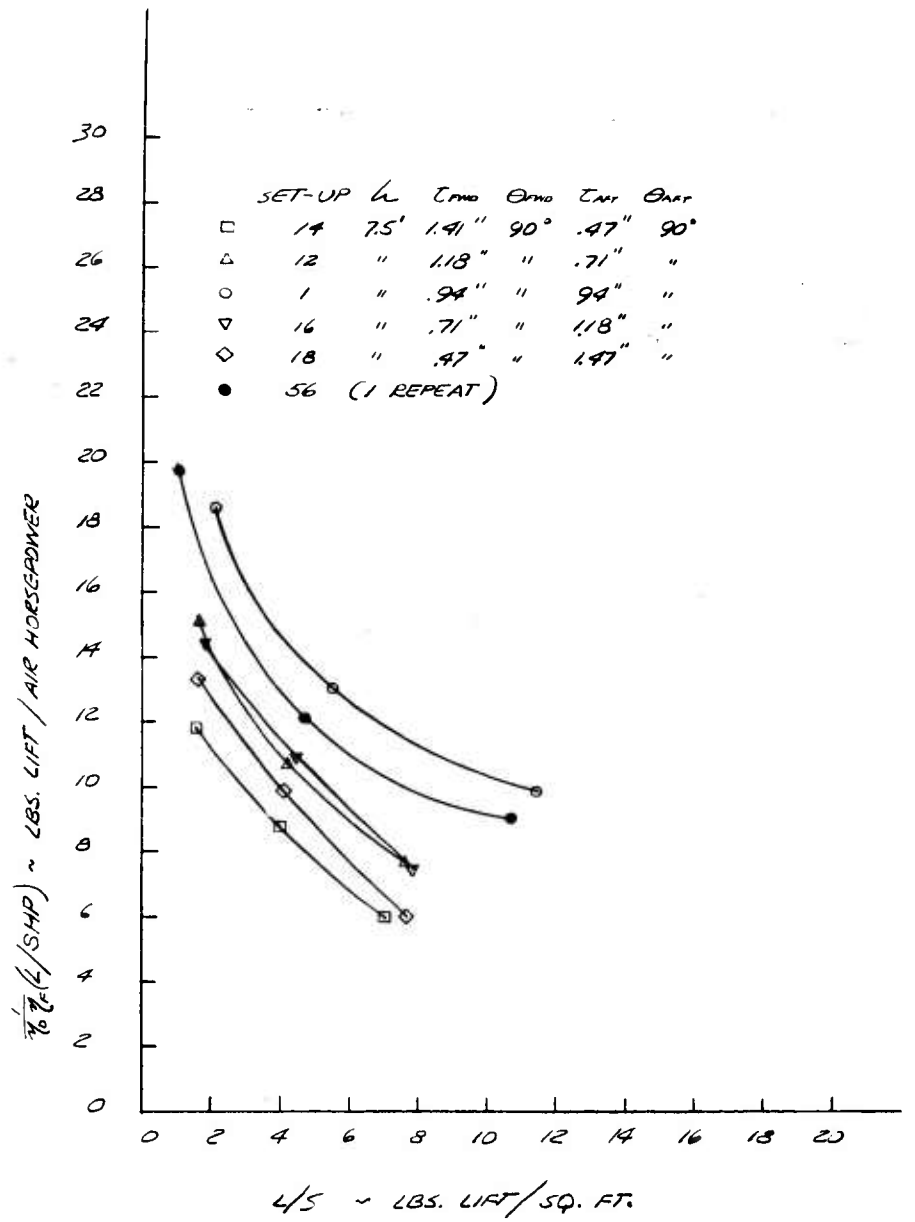

Fig. 68 Hover Lift/Shaft Horsepower versus Base Loading

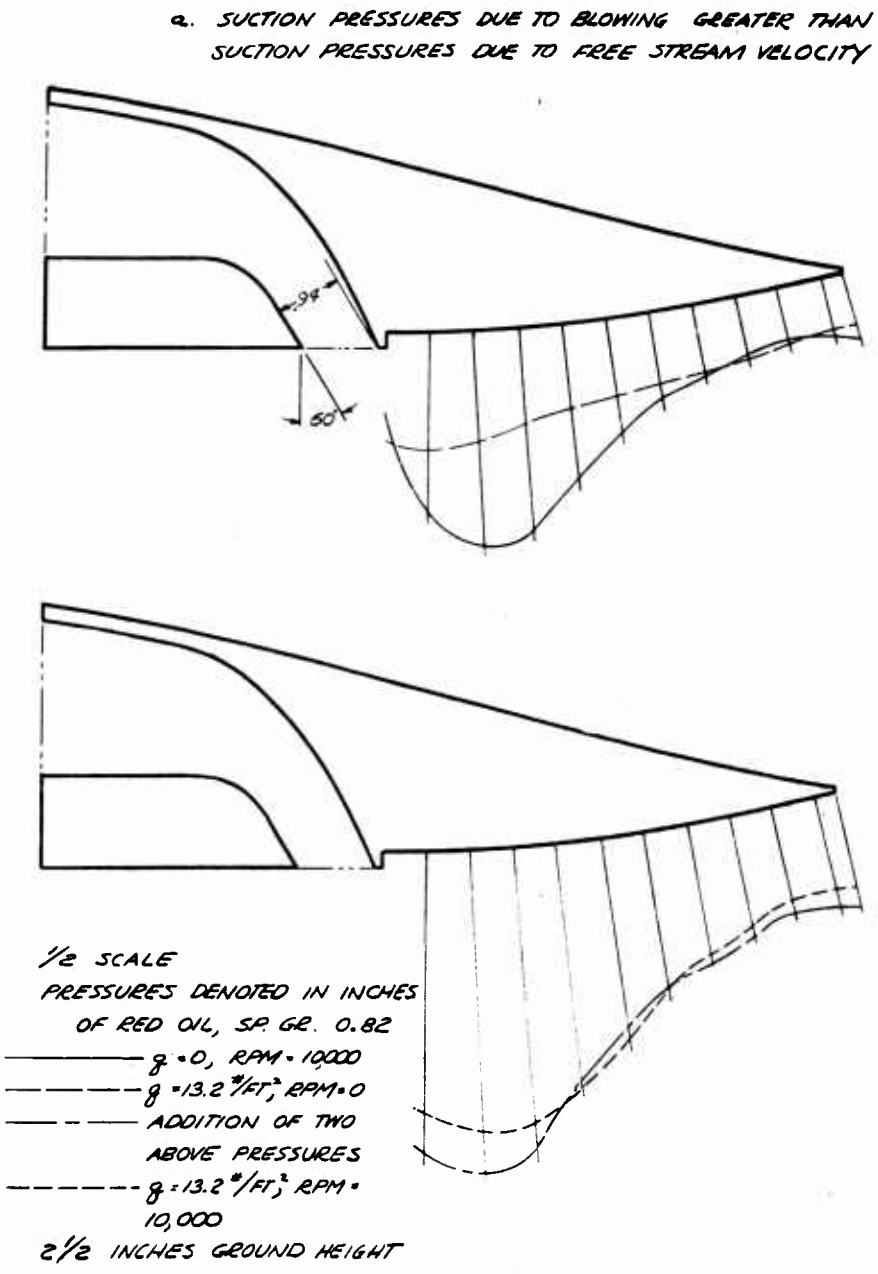

Fig. 69 Pressure Survey of Trailing Edge - 10000 rpm

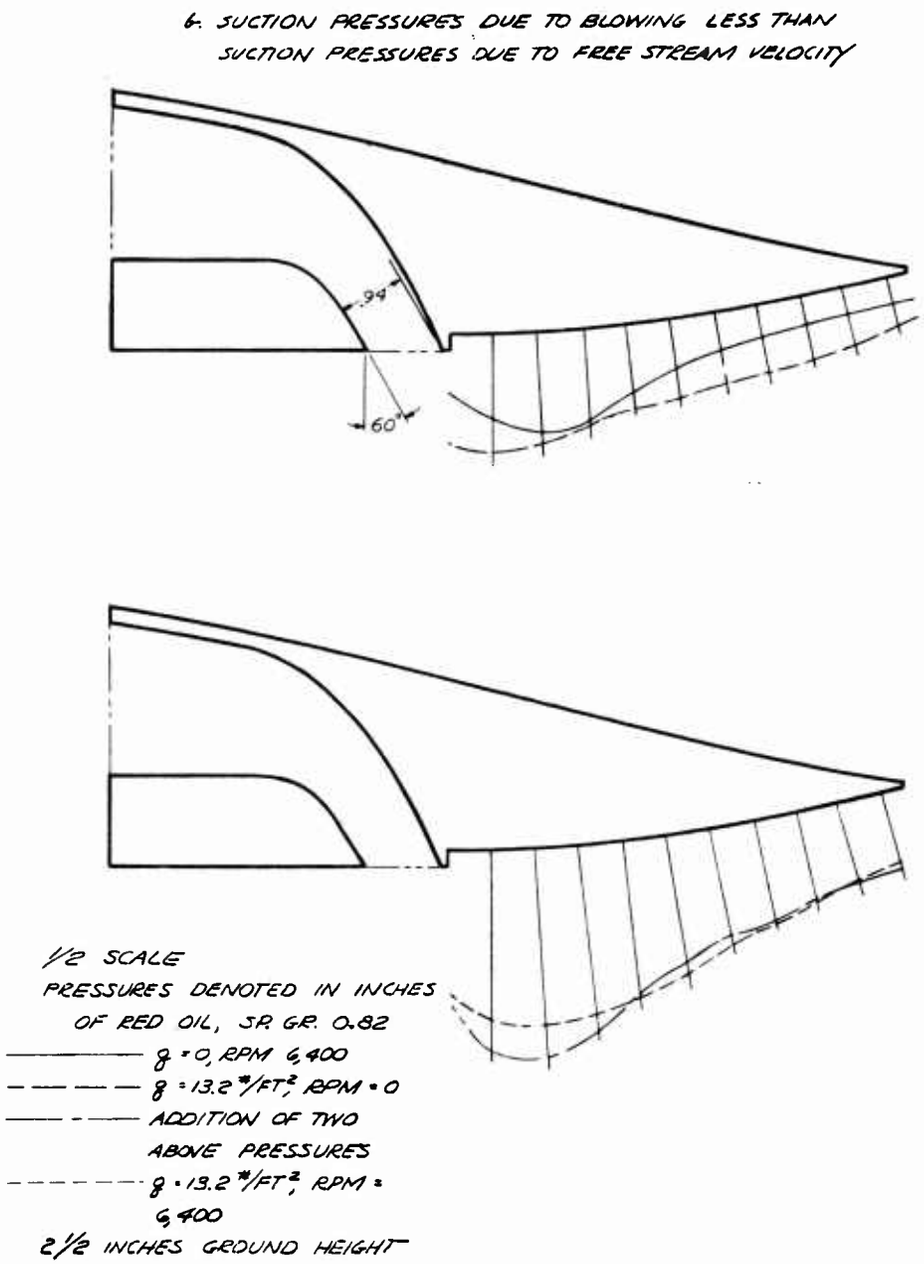

Fig. 70 Pressure Survey of Trailing Edge - 6400 rpm

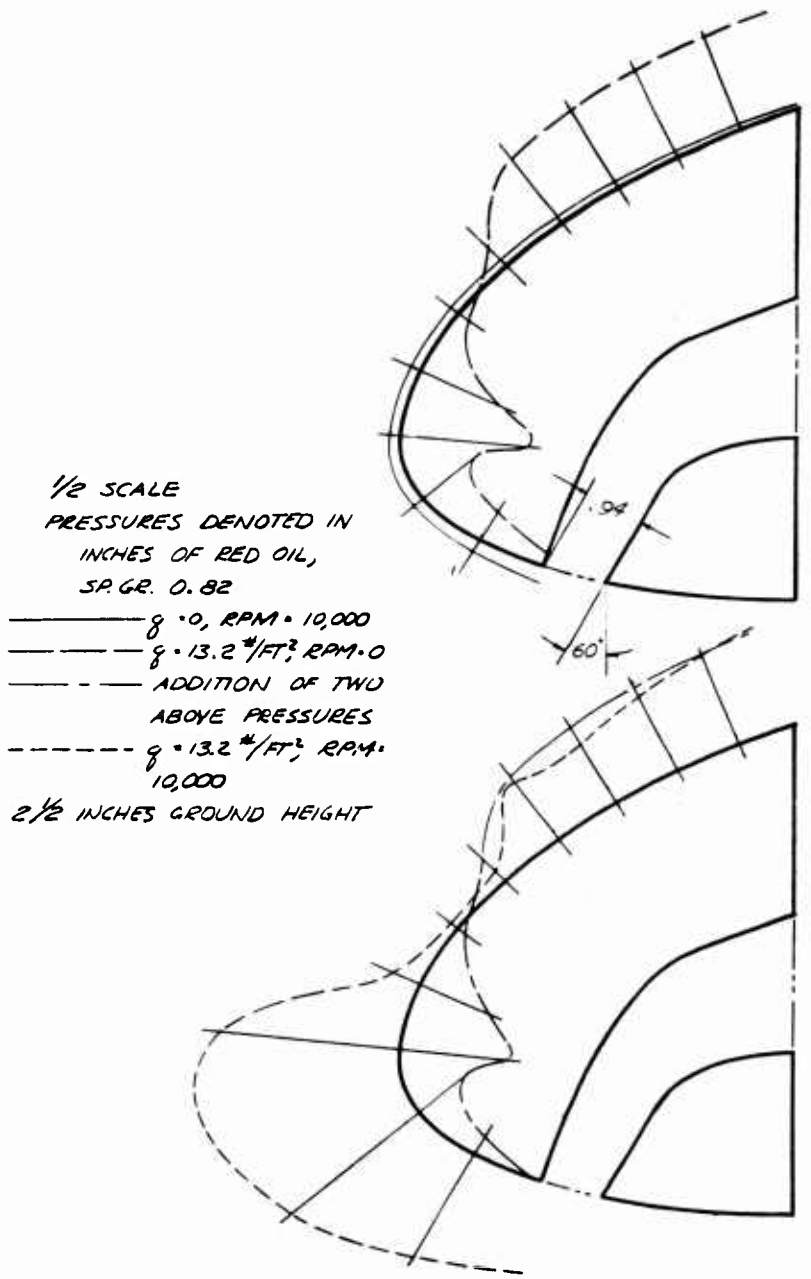

Fig. 71 Pressure Survey of Leading Edge - 10000 rpm

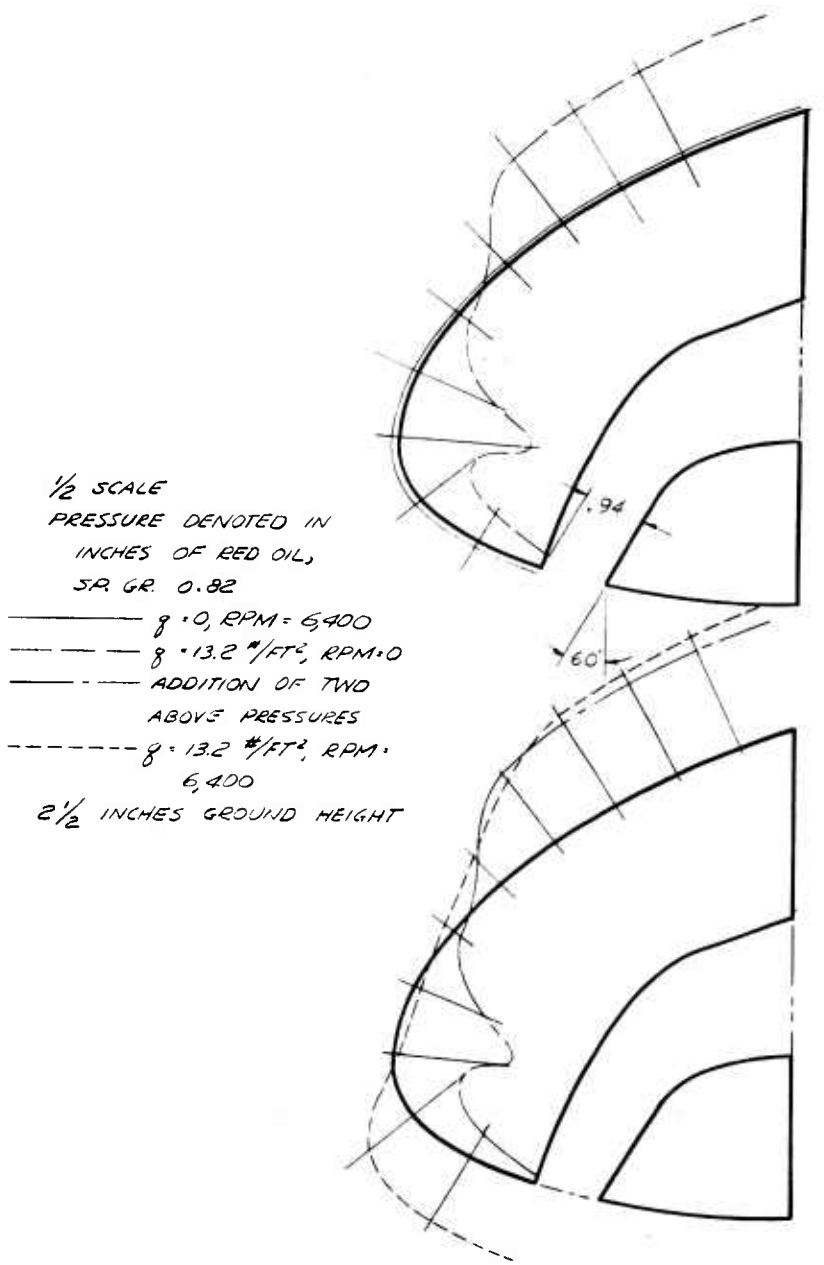

Fig. 72 Pressure Survey of Leading Edge - 6400 rpm

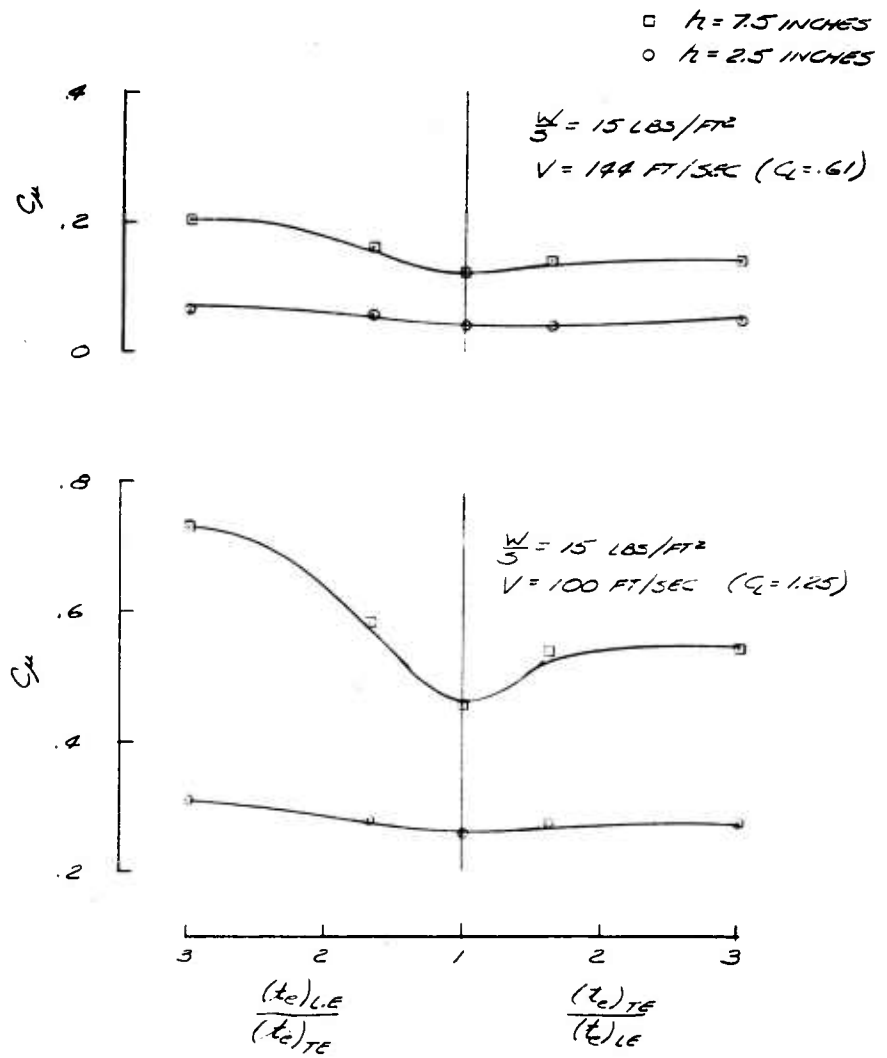

Fig. 73 Effect of Differential Air Flow - Constant Total Jet Area

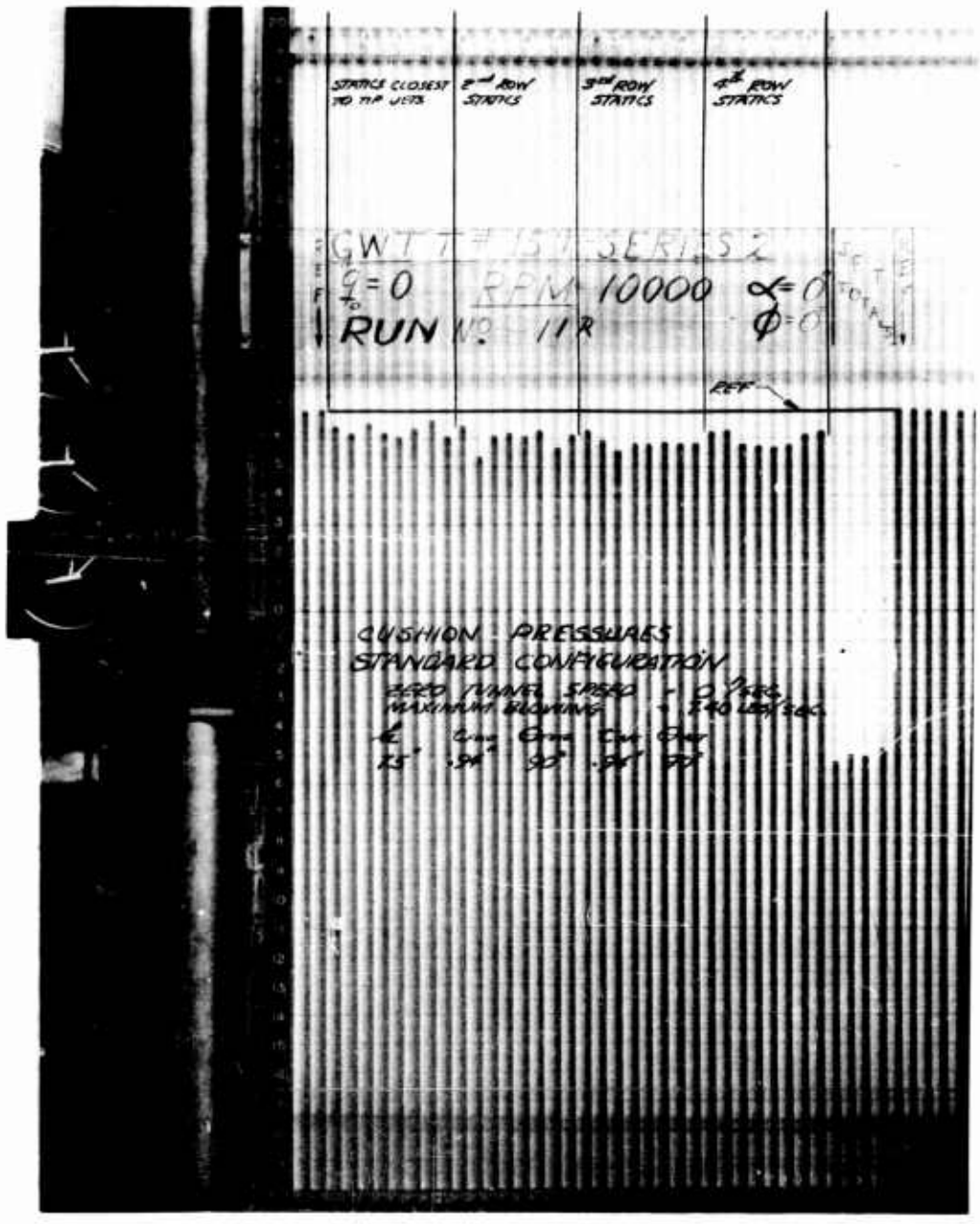

Fig. 74 Cushion Pressures - Standard Configuration; h = 7.5 inches, V = 0 ft/sec

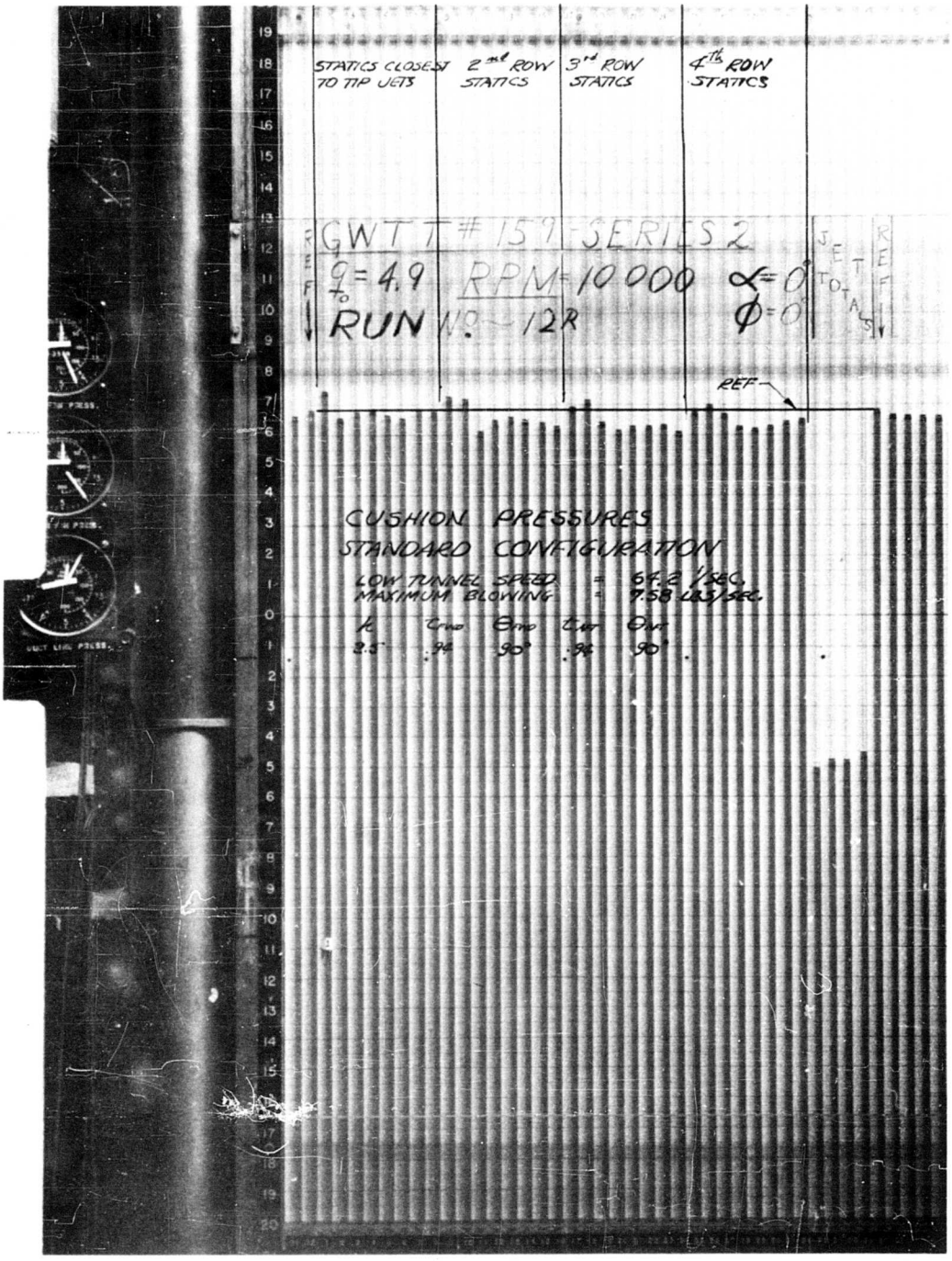

Fig. 75 Cushion Pressures - Standard Configuration; h = 7.5 inches, V = 64 ft/sec

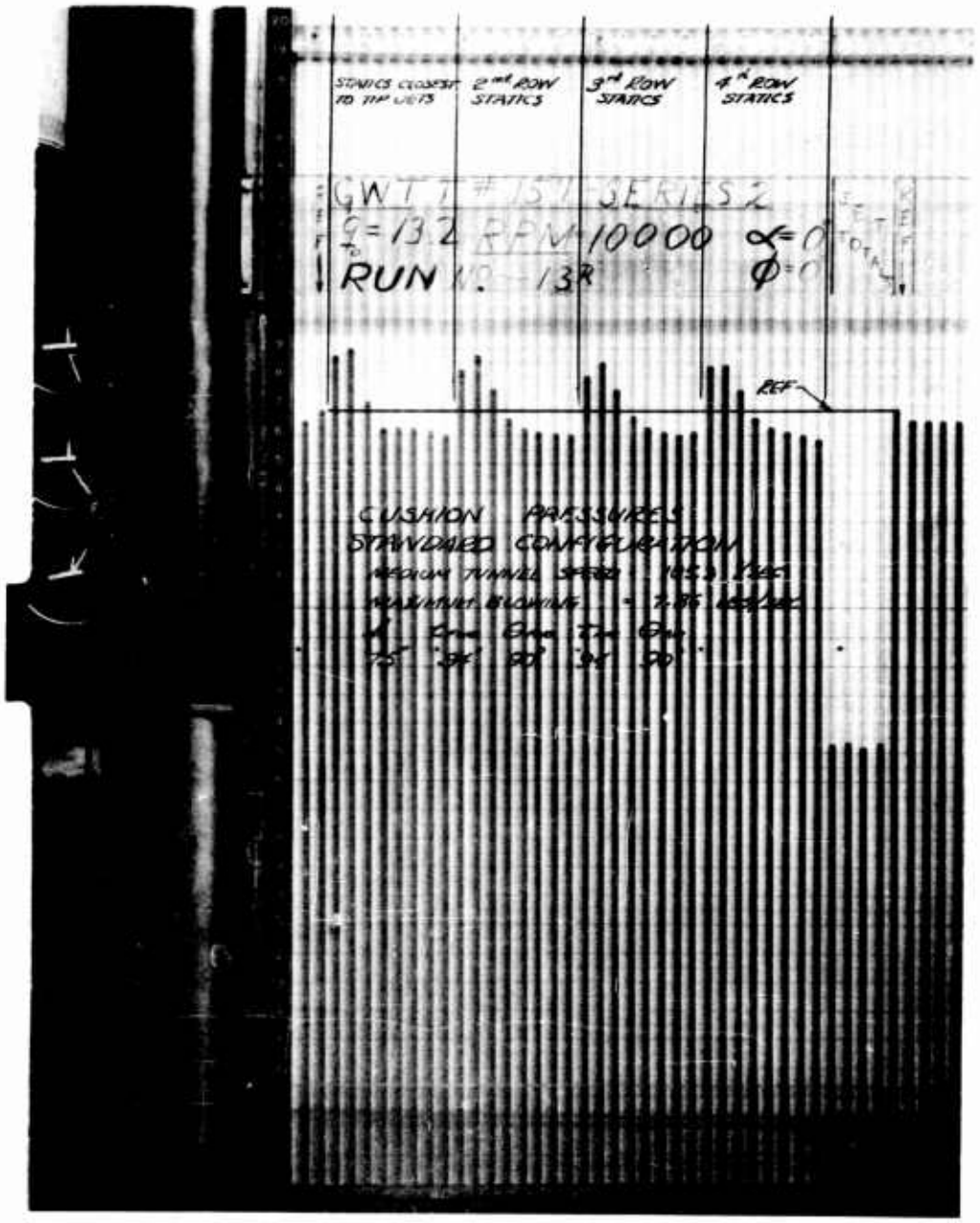

Fig. 76 Cushion Pressures - Standard Configuration; h = 7.5 inches, V = 105 ft/sec

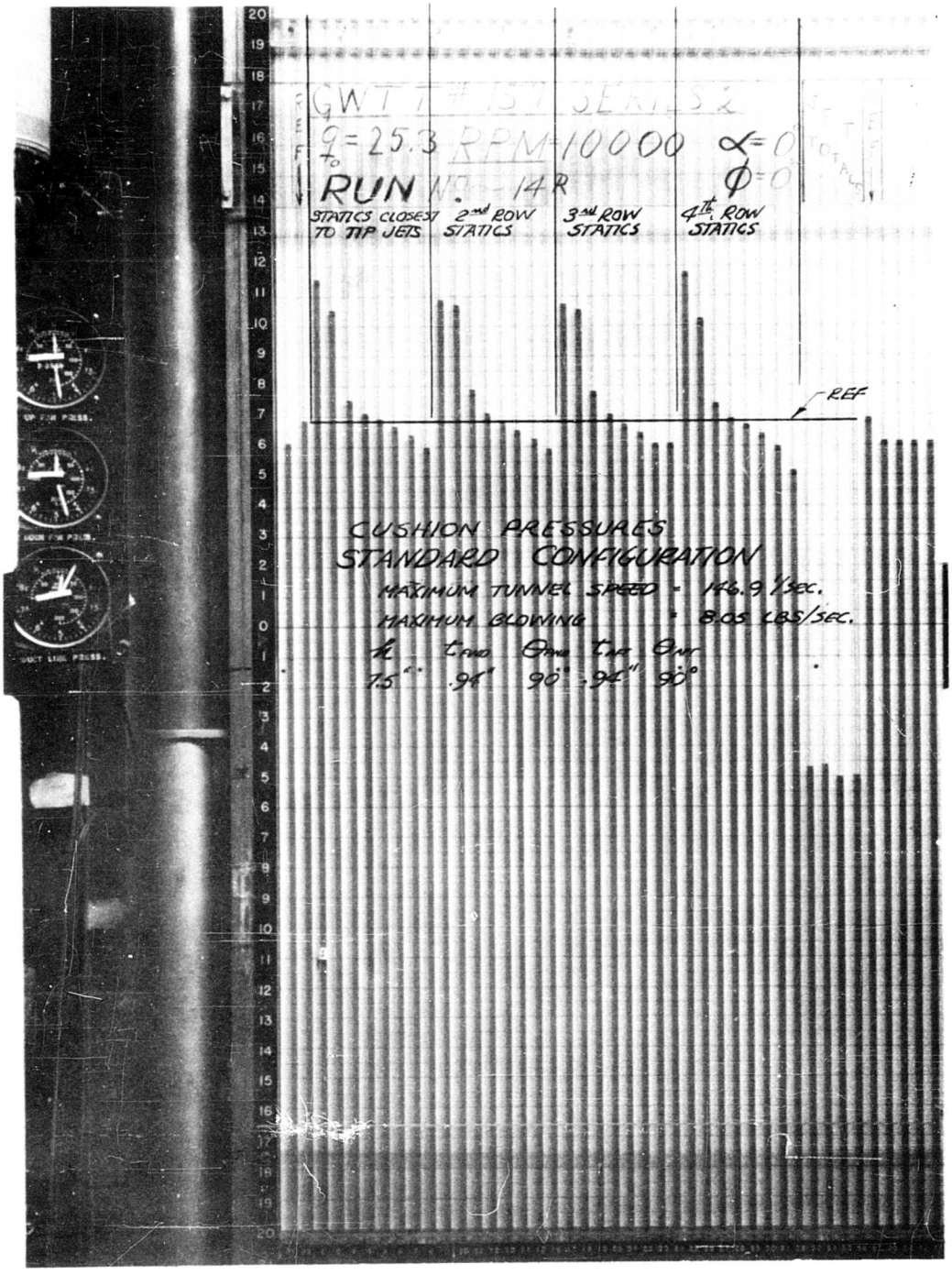

Fig. 77 Cushion Pressures - Standard Configuration; h = 7.5 inches, V = 147 ft/sec

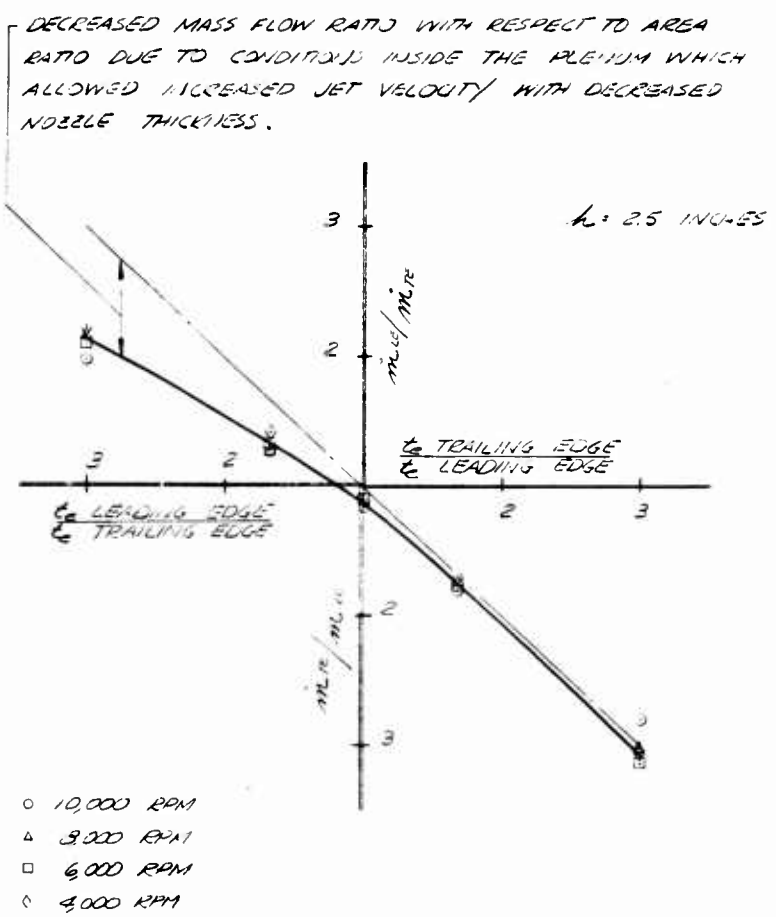

Fig. 78 Mass Flow Distribution With Differential Nozzle Thickness; θ_j = 90 degrees, h = 2.5 inches

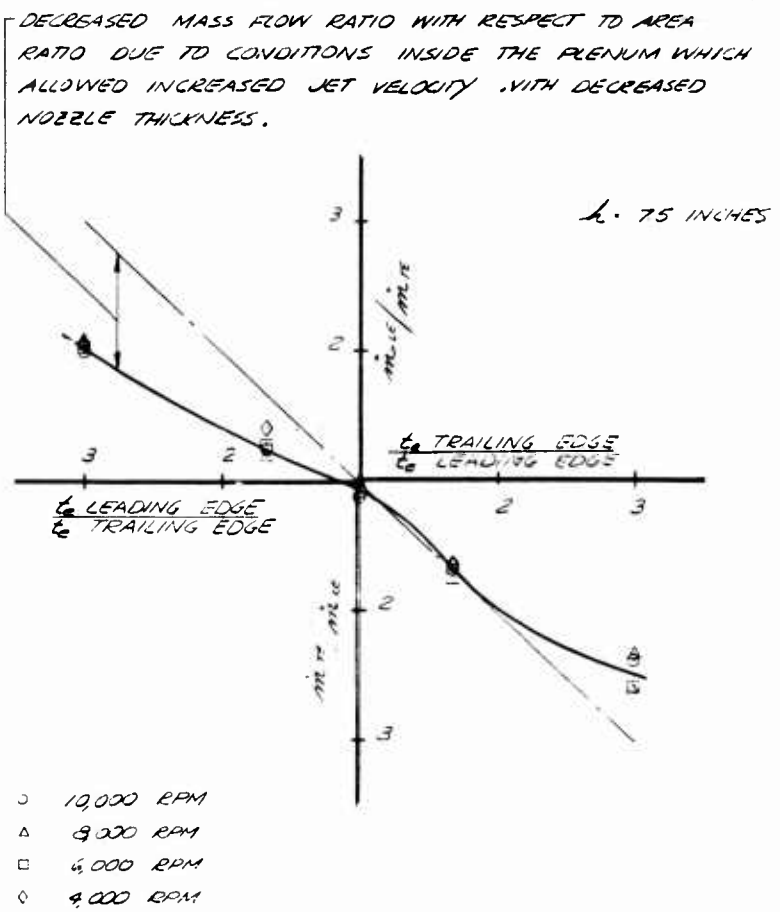

Fig. 79 Mass Flow Distribution With Differential Nozzle Thickness; θ_j = 90 degrees, h = 7.5 inches

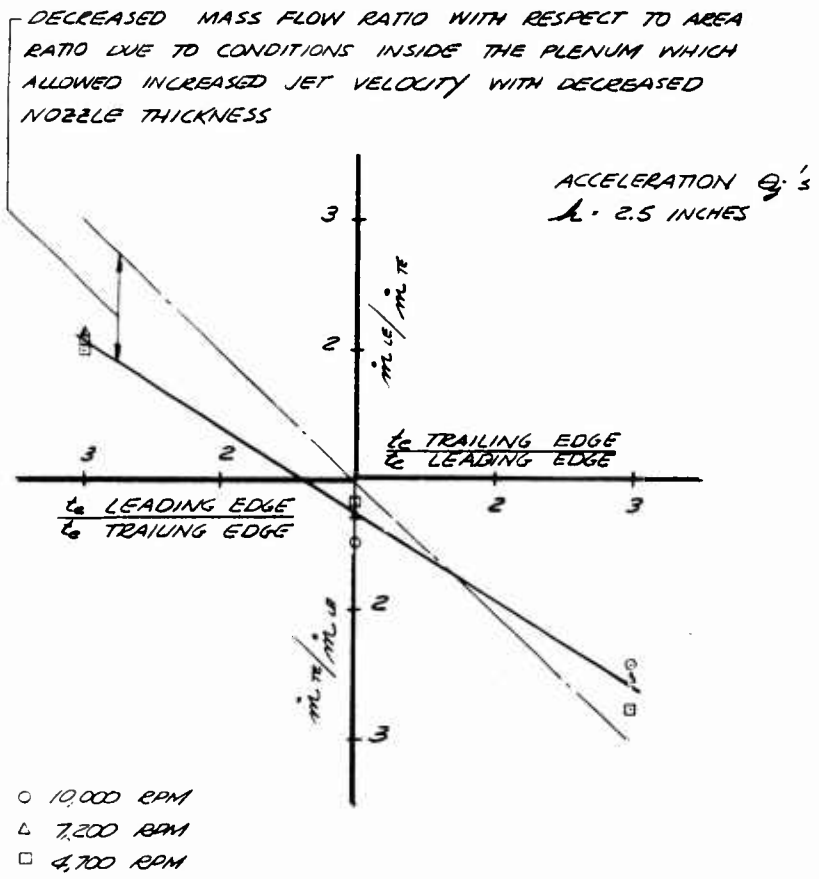

Fig. 80 Mass Flow Distribution With Differential Nozzle Thickness — Acceleration Configuration; h = 2.5 inches

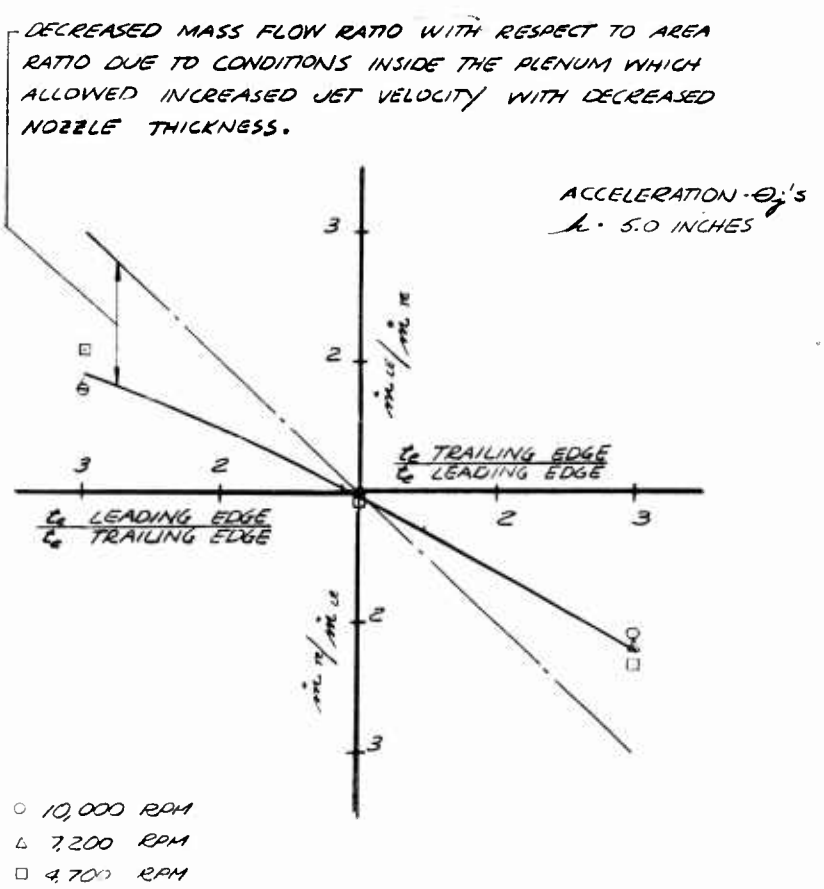

Fig. 81 Mass Flow Distribution With Differential Nozzle Thickness — Acceleration Configuration; h = 5.0 inches

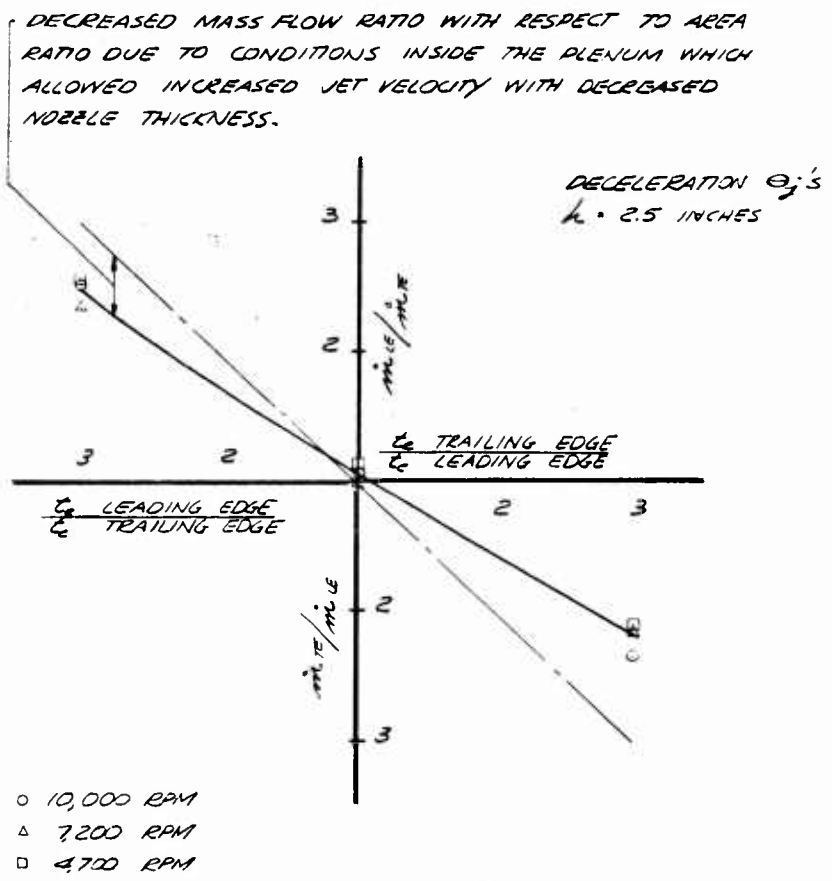

Fig. 82 Mass Flow Distribution With Differential Nozzle Thickness — Deceleration Configuration; h = 2.5 inches

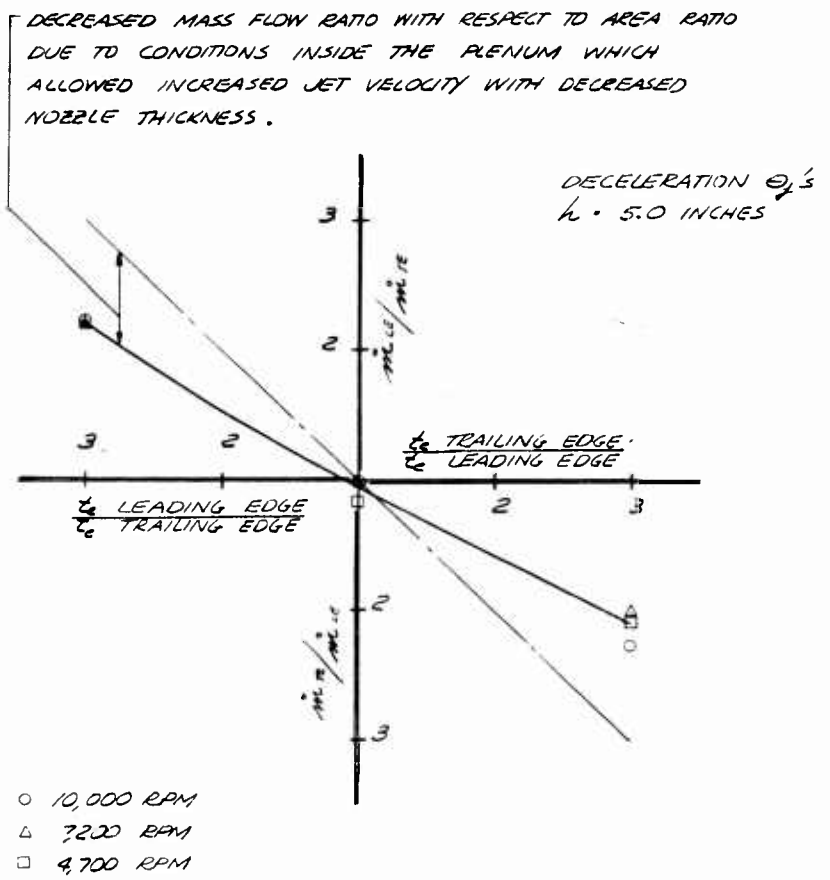

Fig. 83 Mass Flow Distribution With Differential Nozzle Thickness — Deceleration Configuration; h = 5.0 inches

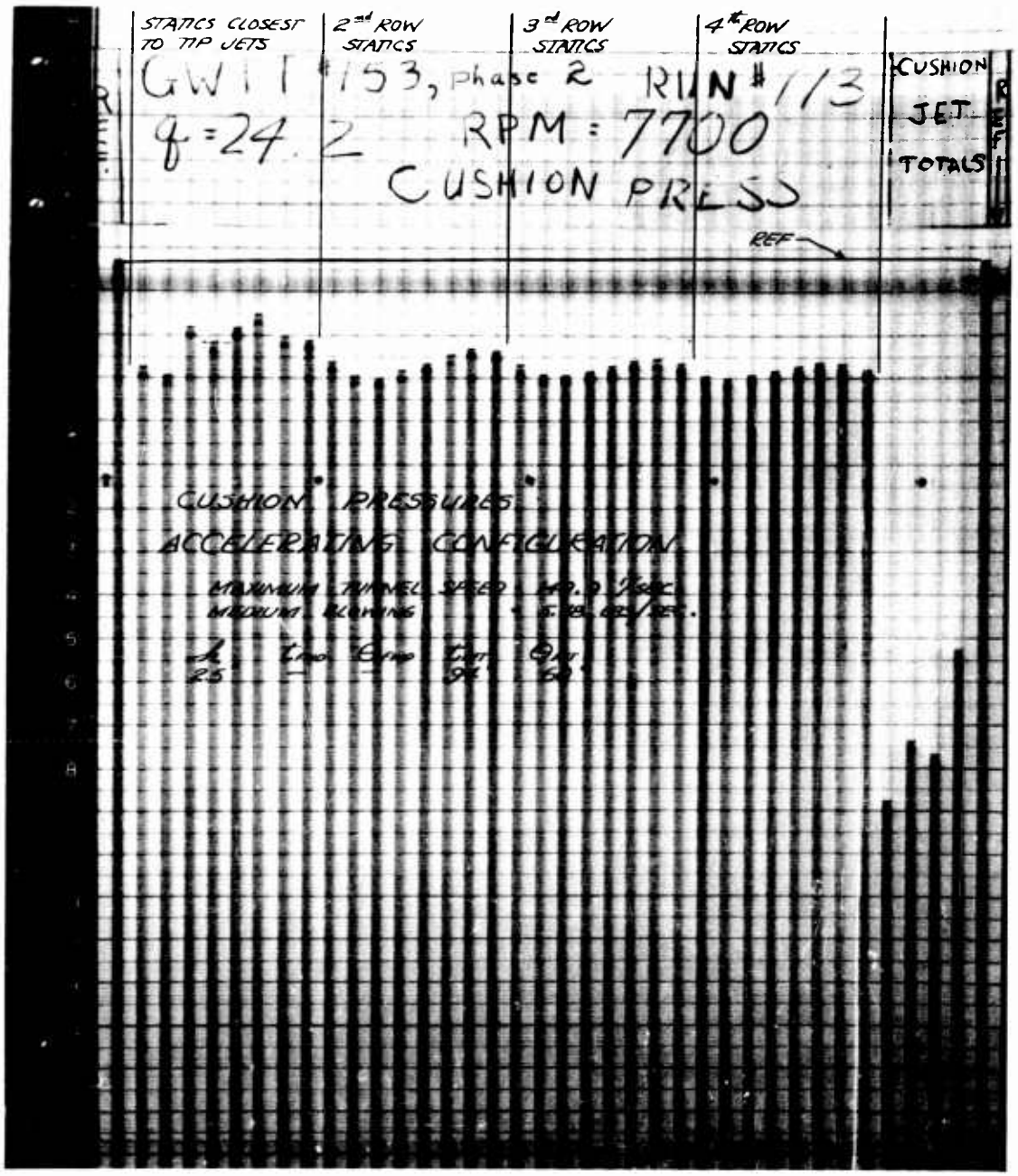

Fig. 84 Cushion Pressures — Acceleration Configuration With Leading Edge Blocked; h = 2.5 inches

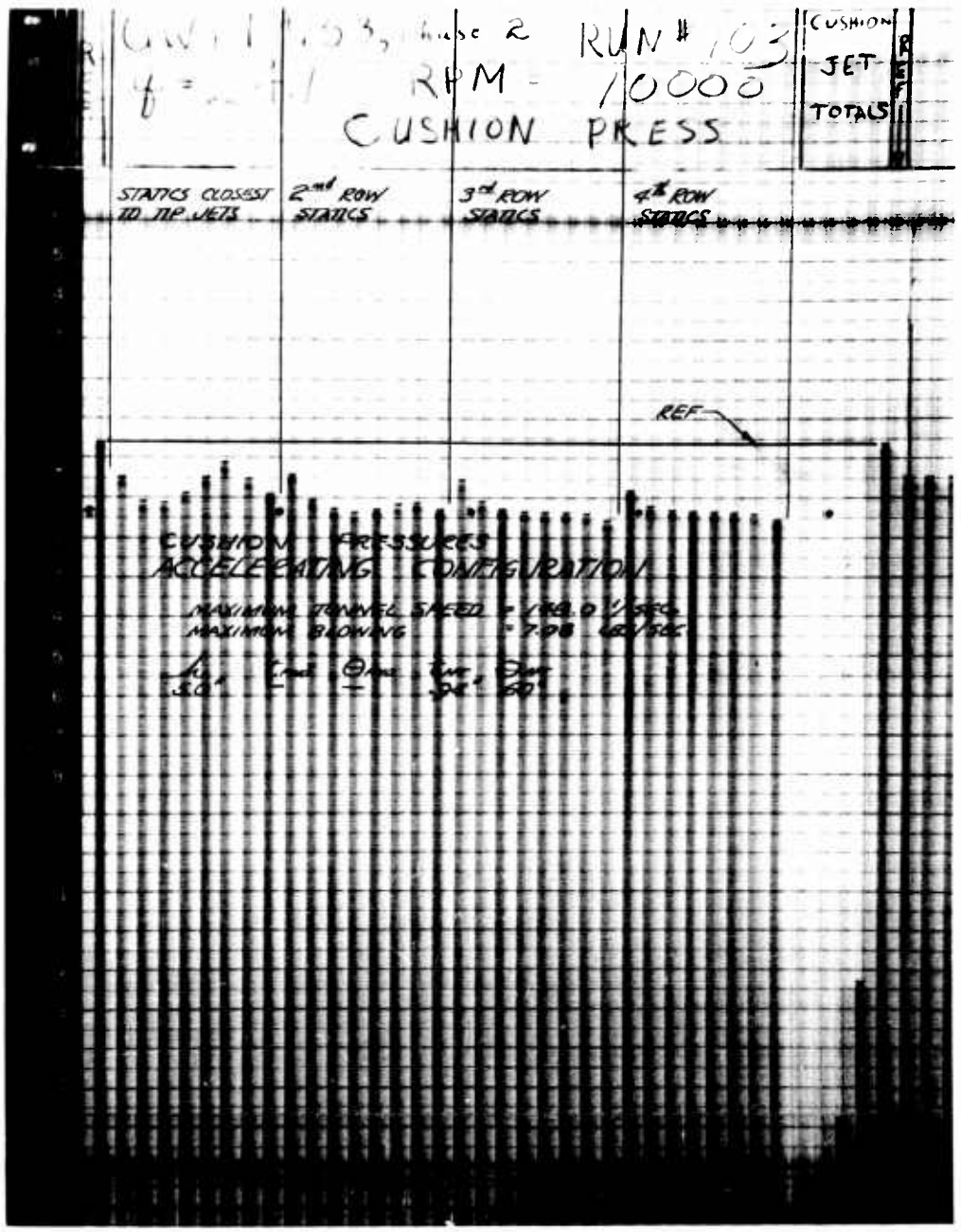

Fig. 85 Cushion Pressures — Acceleration Configuration With Leading Edge Blocked: h = 5.0 inches

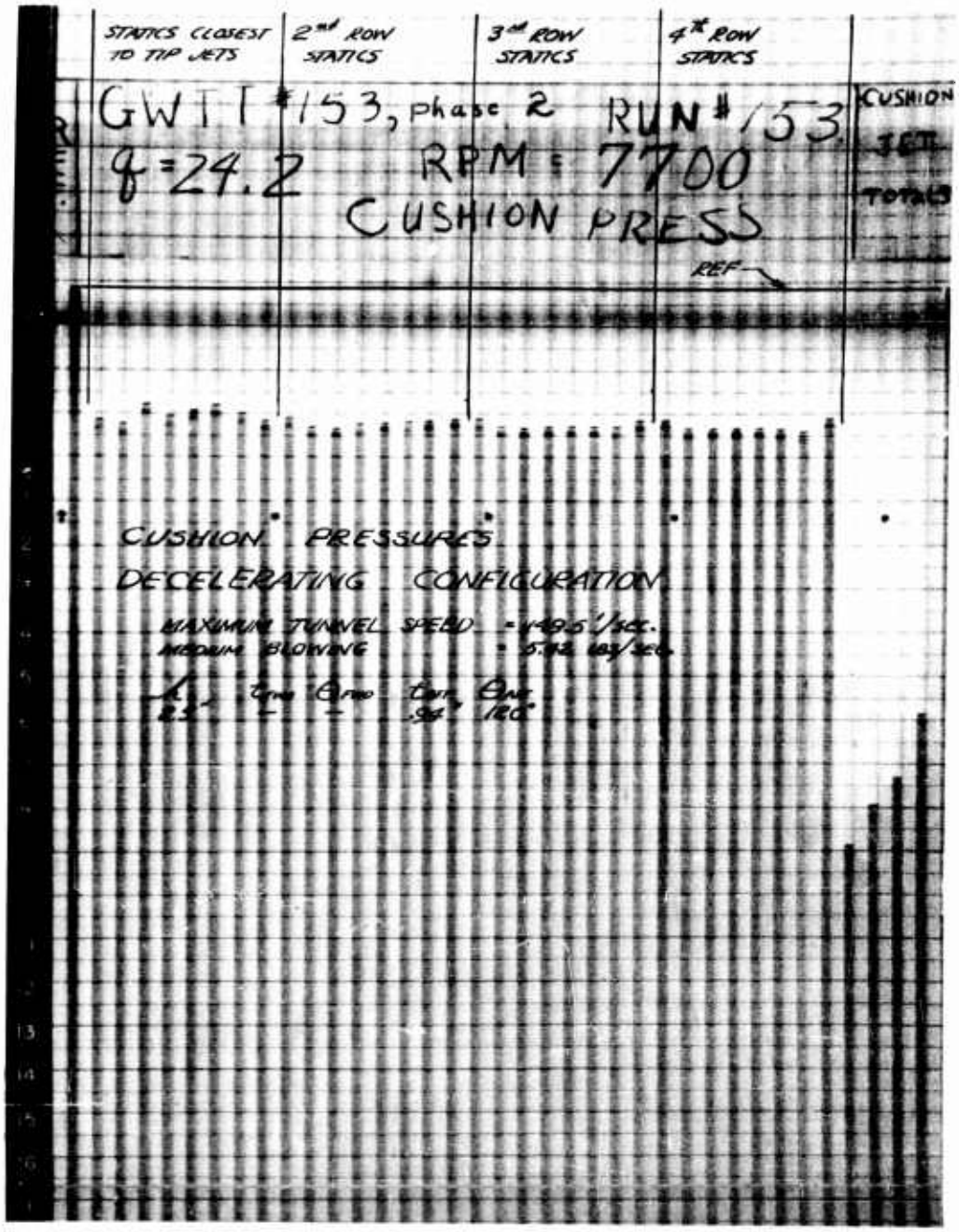

Fig. 86 Cushion Pressures — Deceleration Configuration With Leading Edge Blocked; h = 2.5 inches

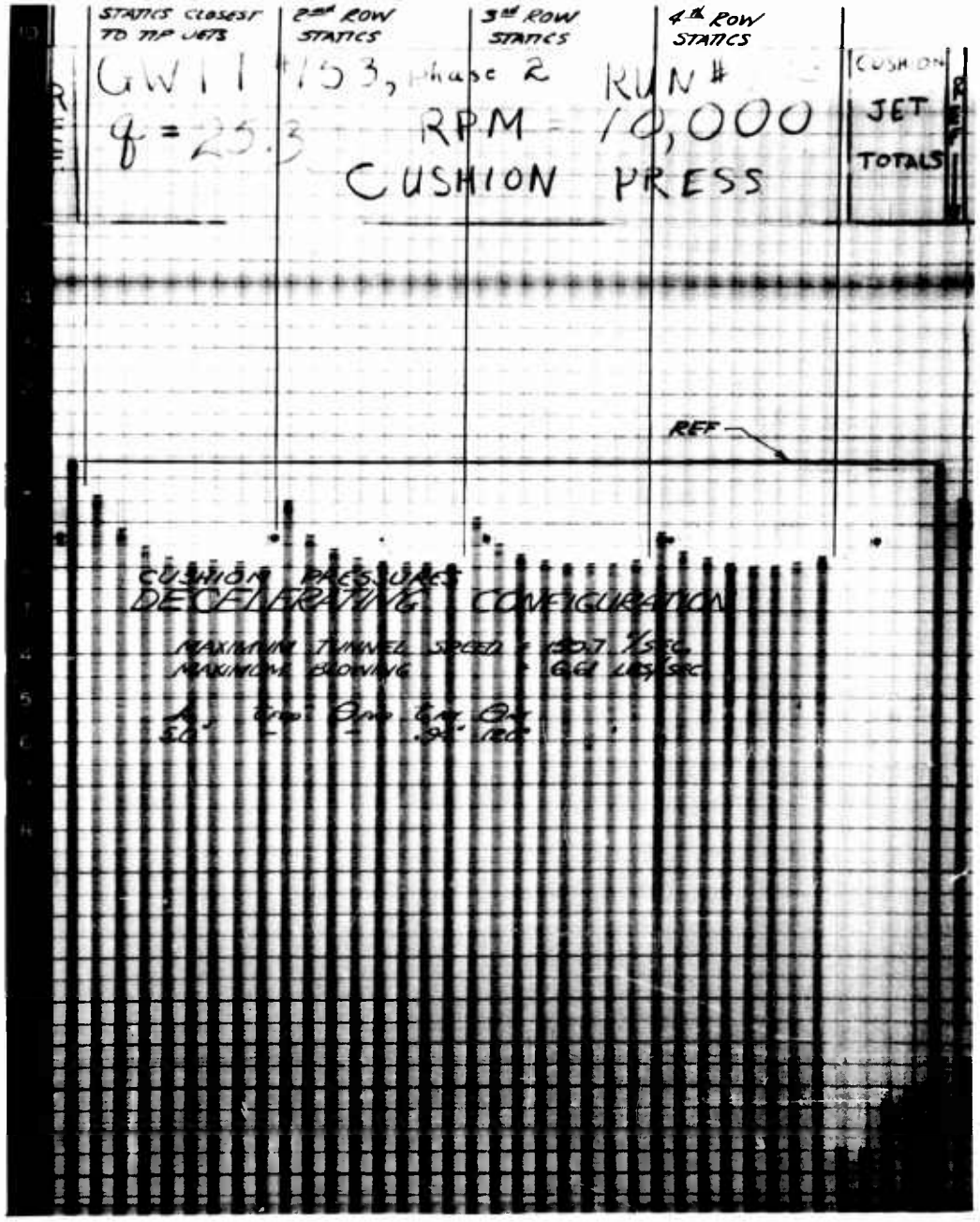

Fig. 87 Cushion Pressures — Deceleration Configuration With Leading Edge Blocked; h = 5.0 inches

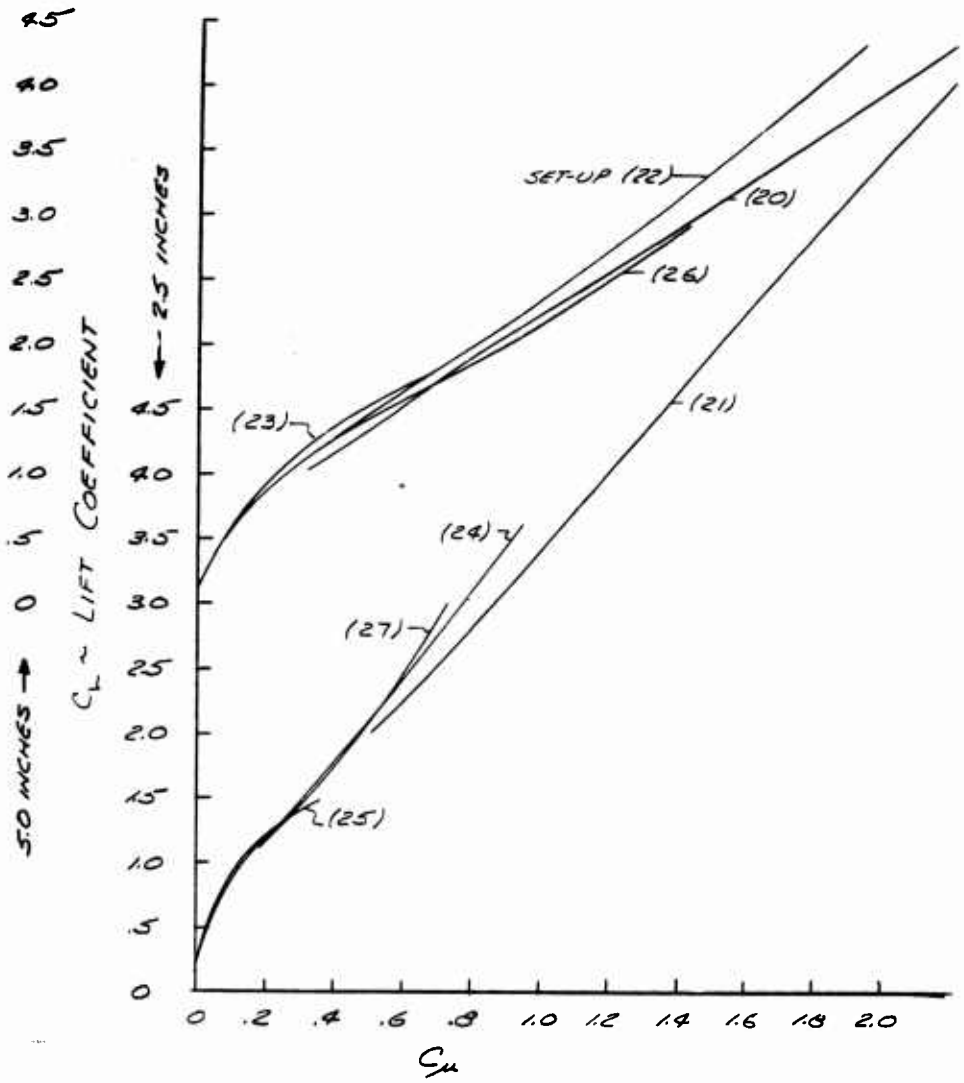

Fig. 88 Effect of Differential Mass Flow In Acceleration

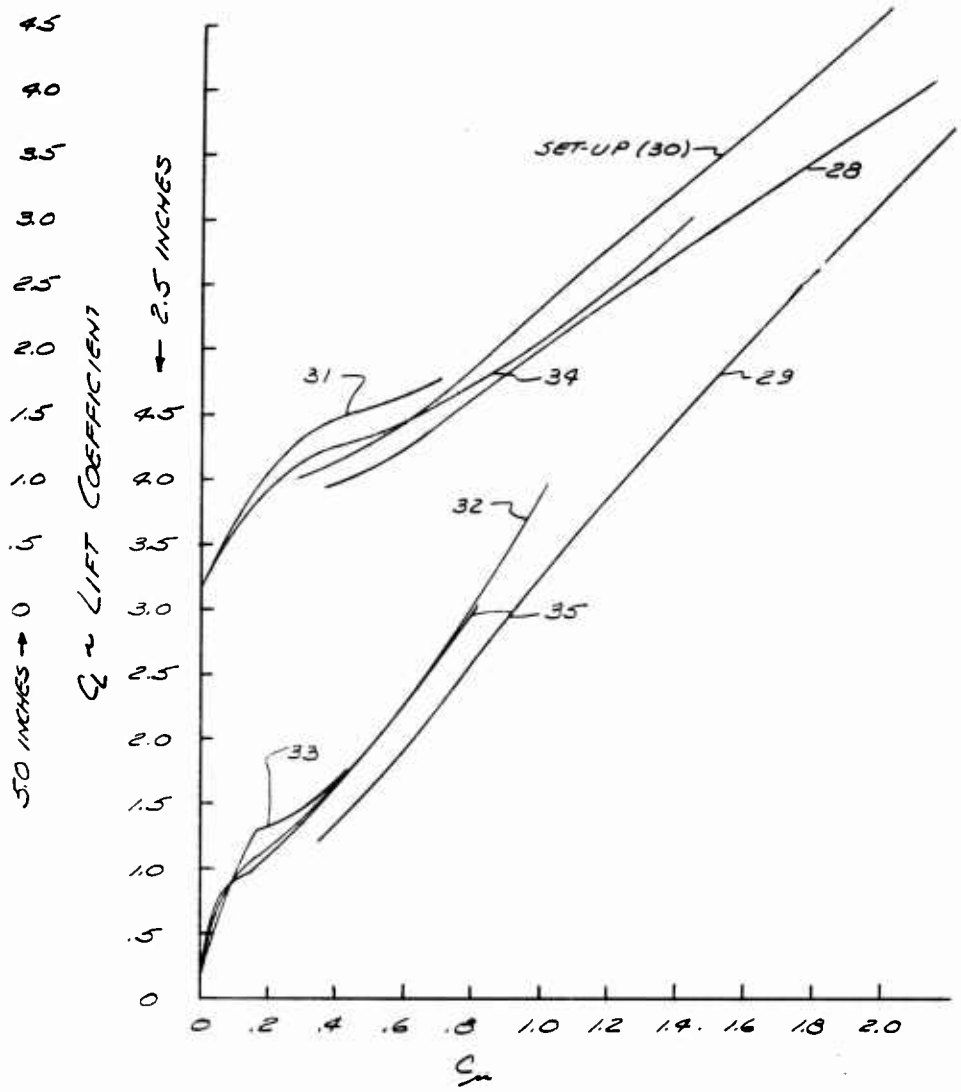

Fig. 89 Effect of Differential Mass Flow In Deceleration

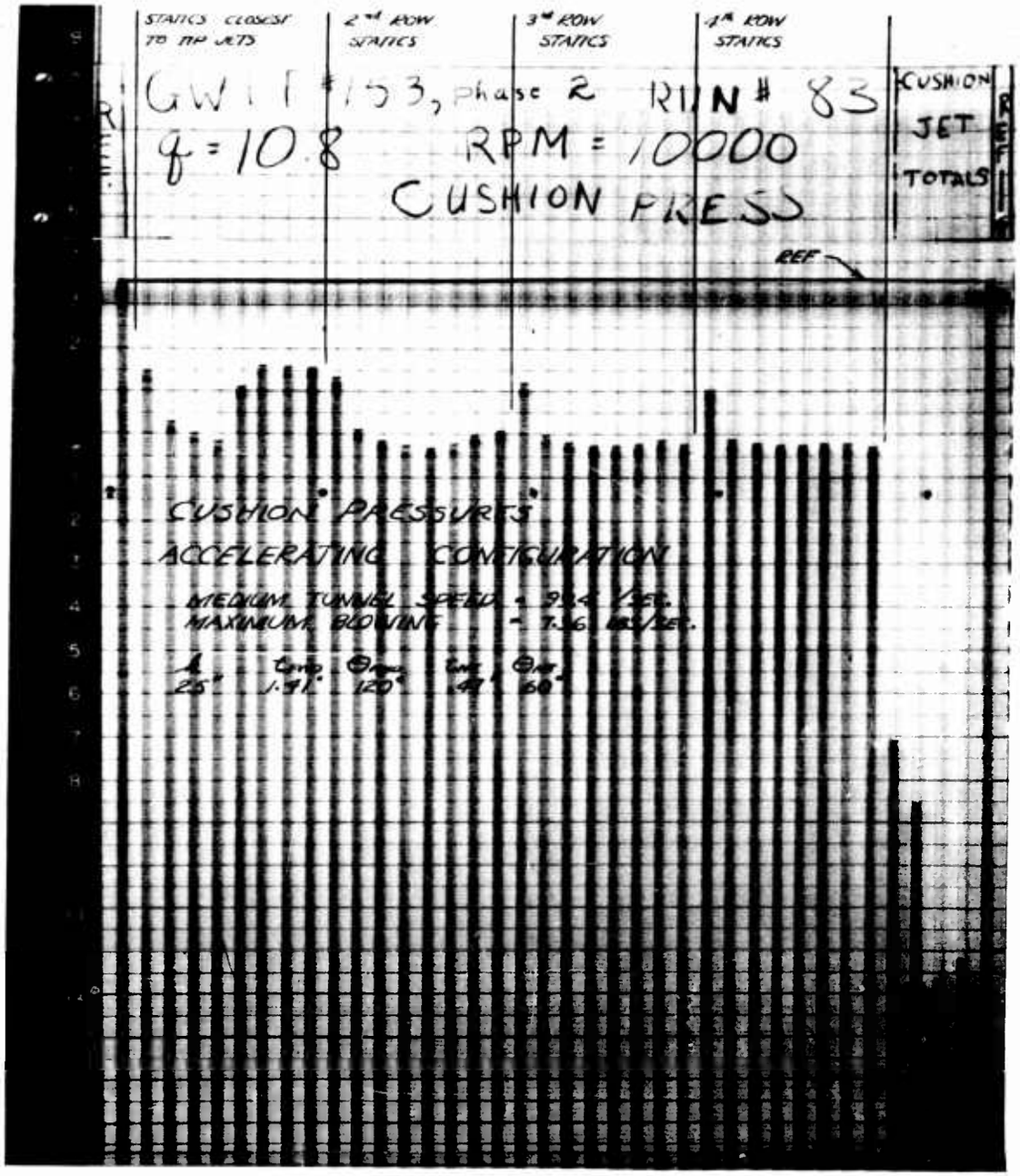

Fig. 90 Cushion Pressures — Acceleration; V = 99 ft/sec, $\dot{w}$ = 7.4 lbs/sec, h = 2.5 inches

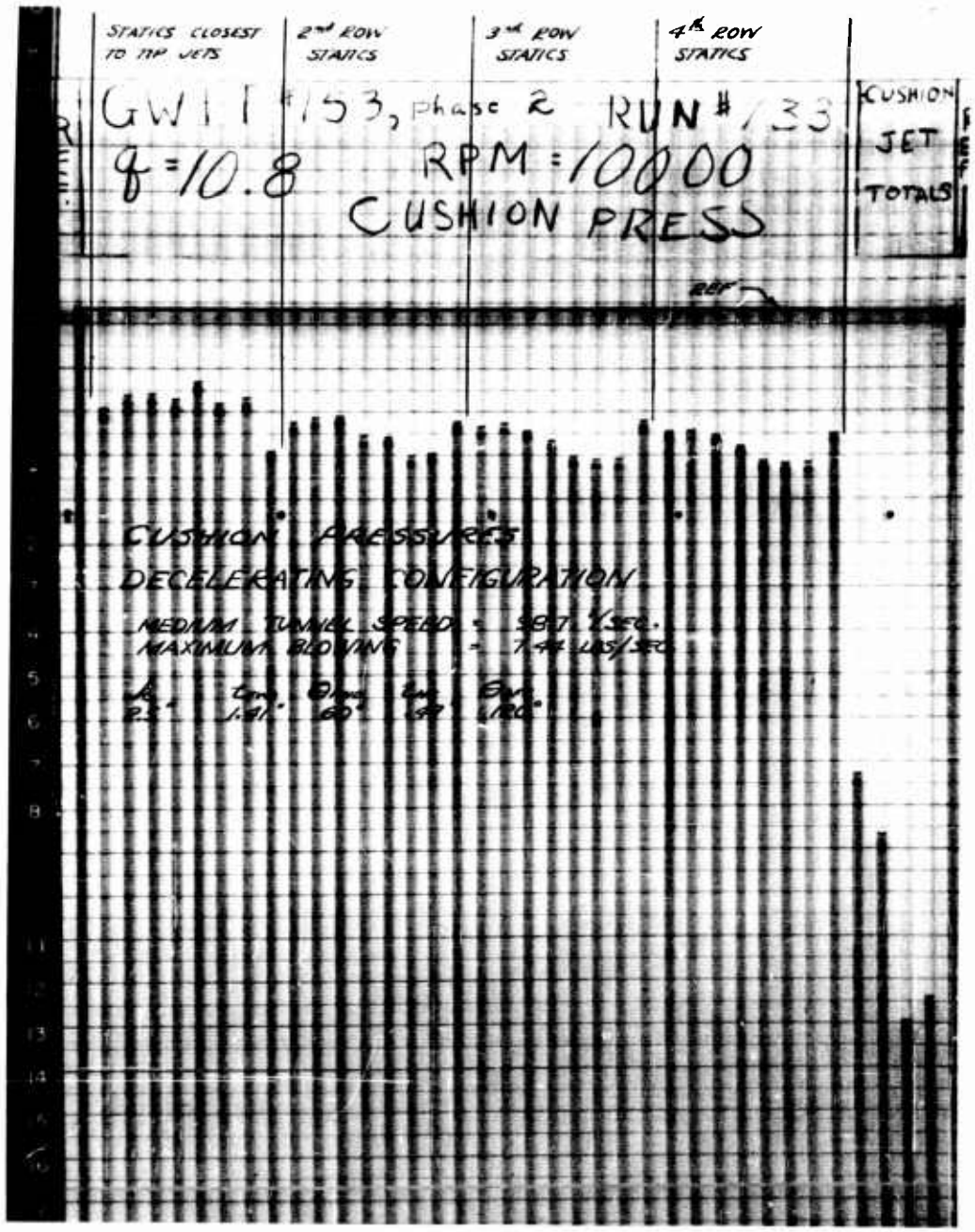

Fig. 91 Cushion Pressures — Deceleration; V = 99 ft/sec, $\dot{w}$ = 7.4 lbs/sec, h = 2.5 inches

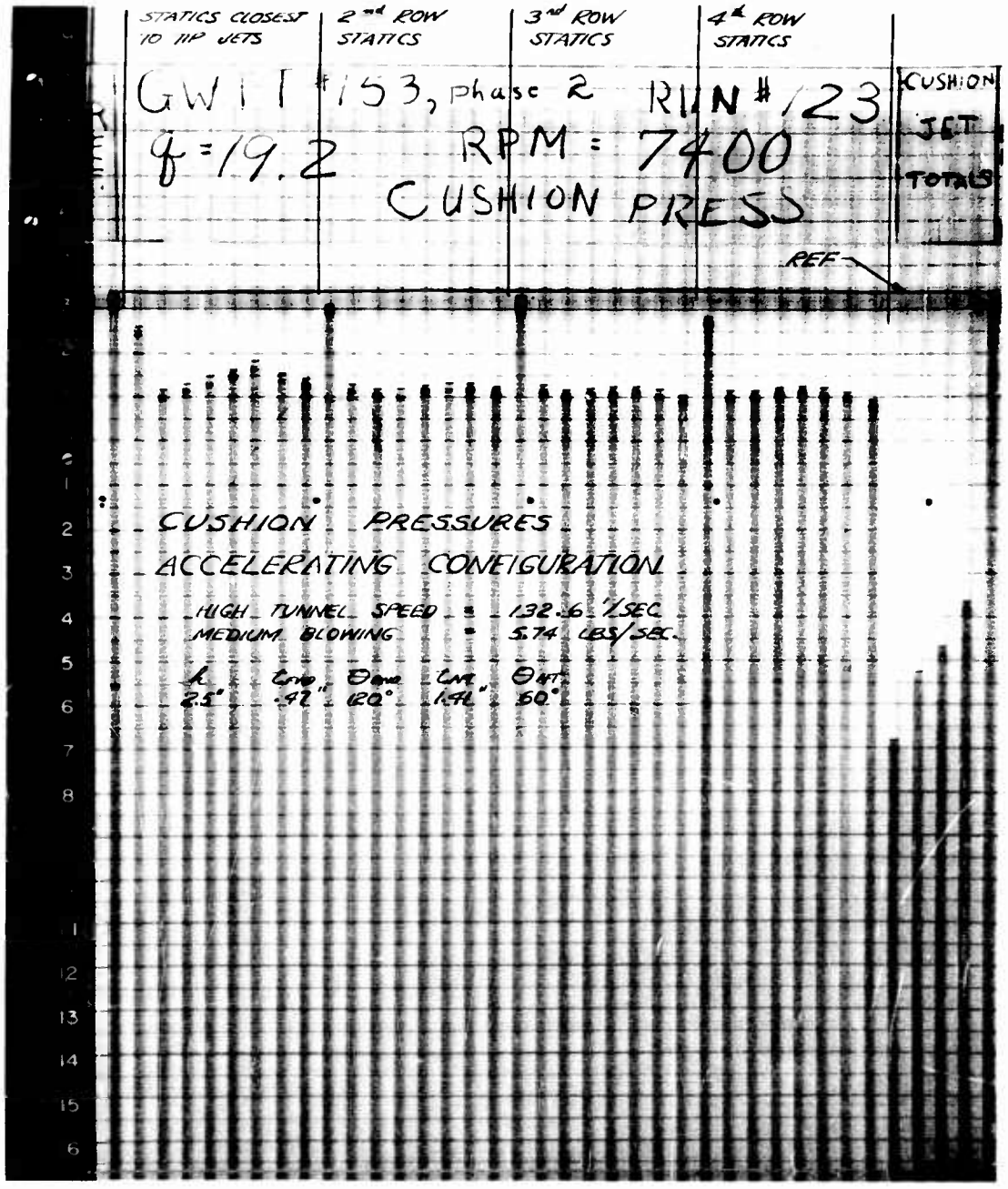

Fig. 92 Cushion Pressures — Acceleration; V = 132 ft/sec $\dot{w}$ = 5.7 lbs/sec, h = 2.5 inches

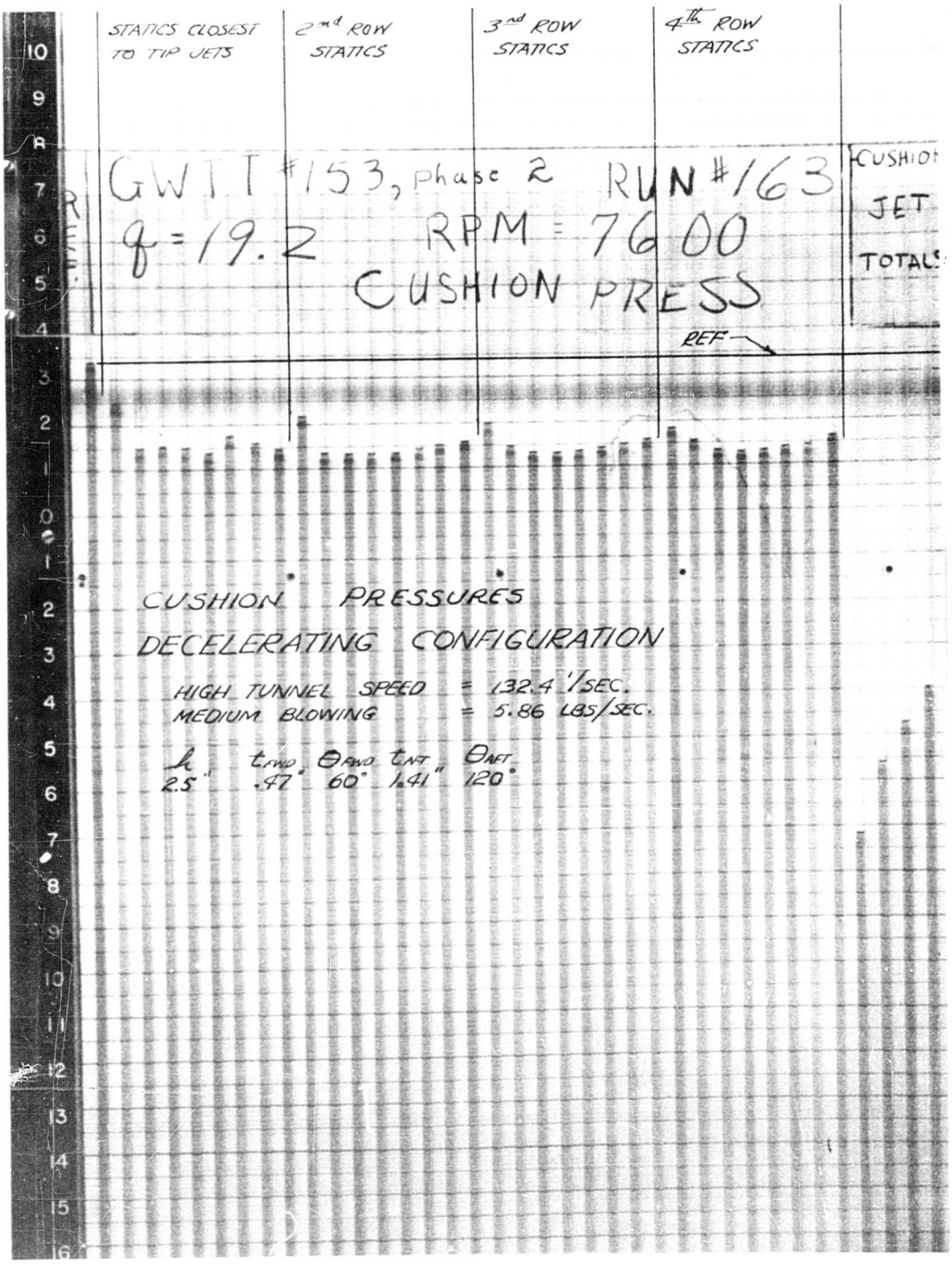

Fig. 93 Cushion Pressures – Deceleration; V = 132 ft/sec $\dot{w}$ = 5.7 lbs/sec, h = 2.5 inches

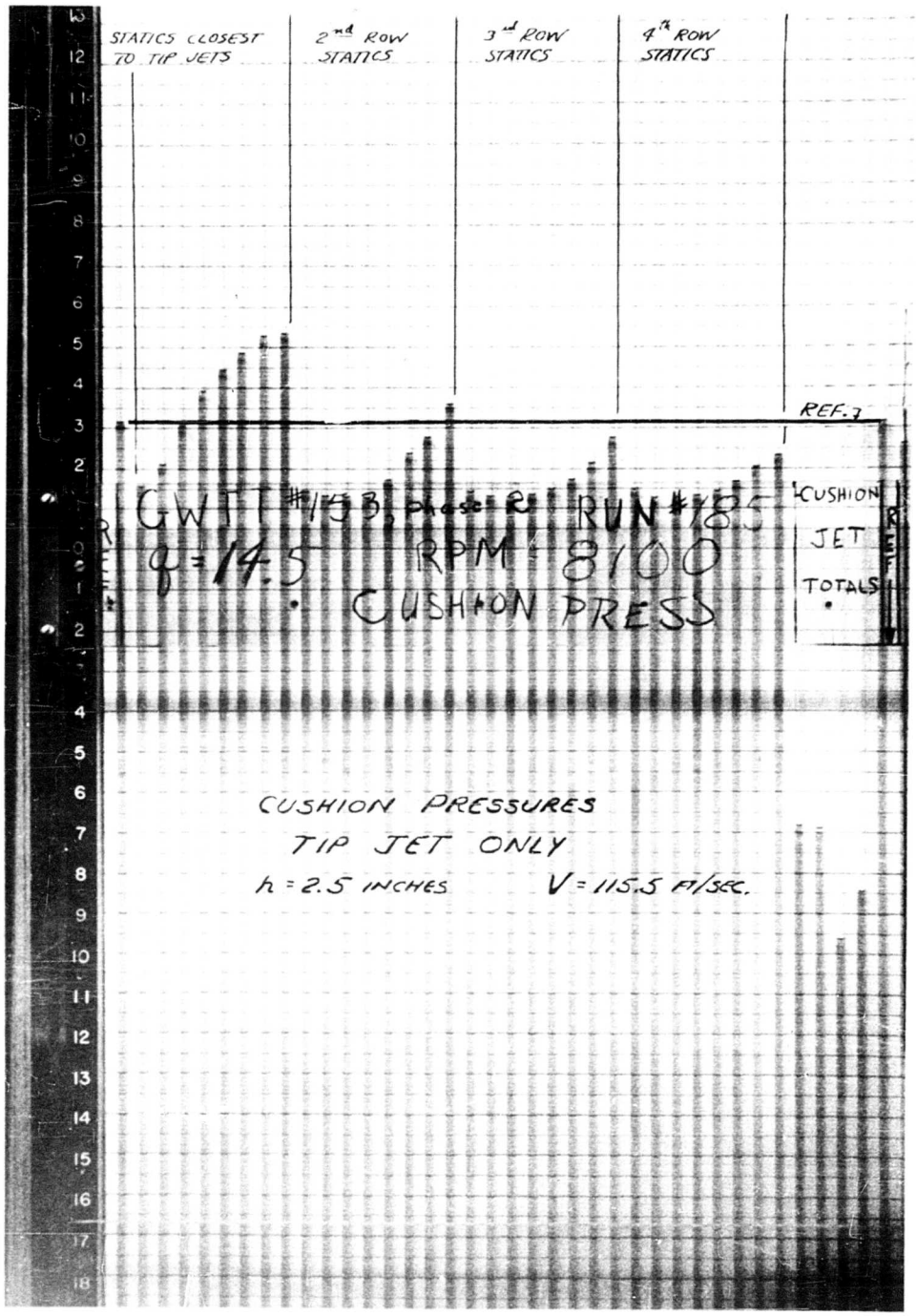

Fig. 94 Cushion Pressures — Tip Jet Only; h = 2.5 inches, V = 115.5 ft/sec

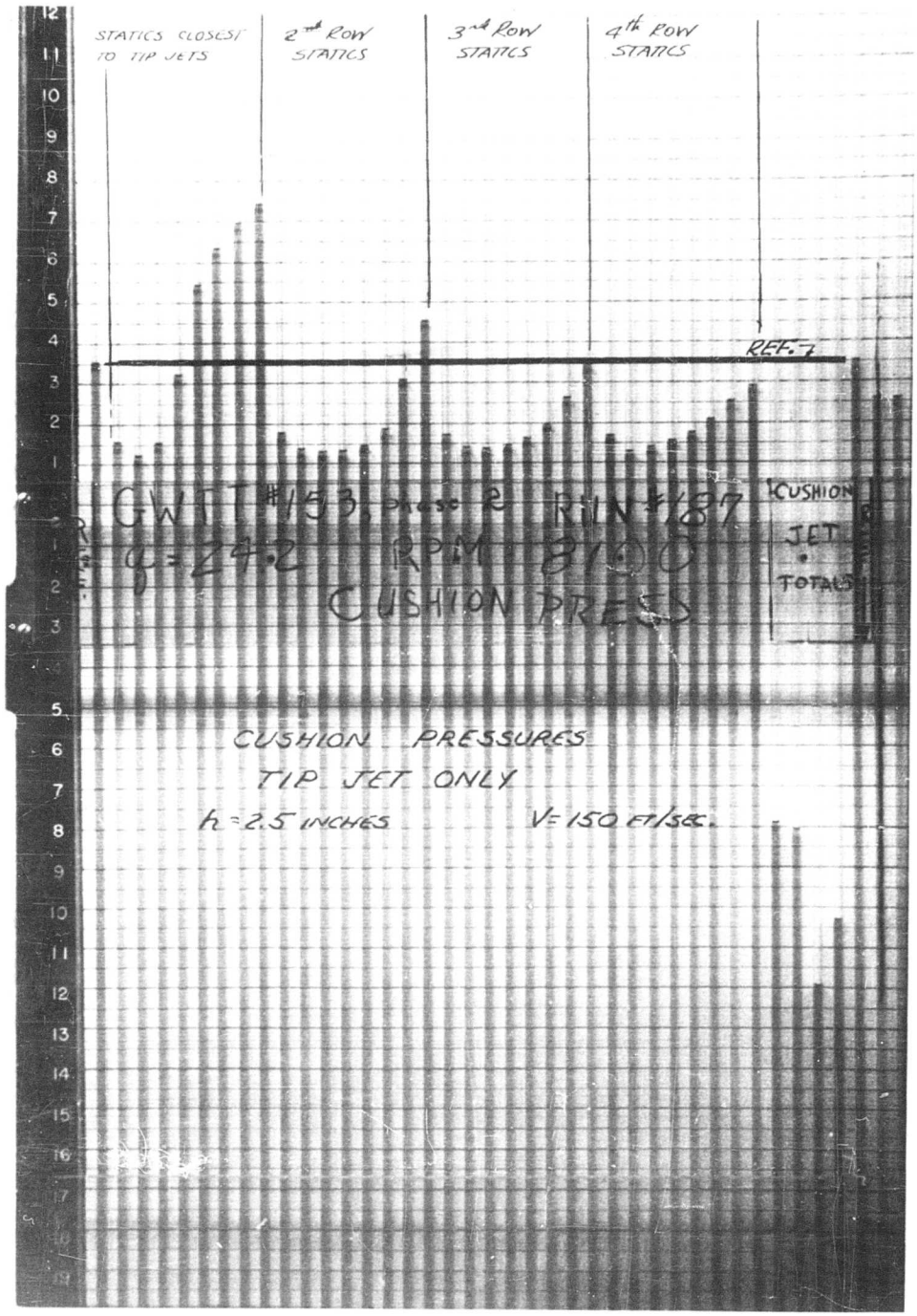

Fig. 95 Cushion Pressures - Tip Jet Only; h = 2.5 inches, V = 150 ft/sec

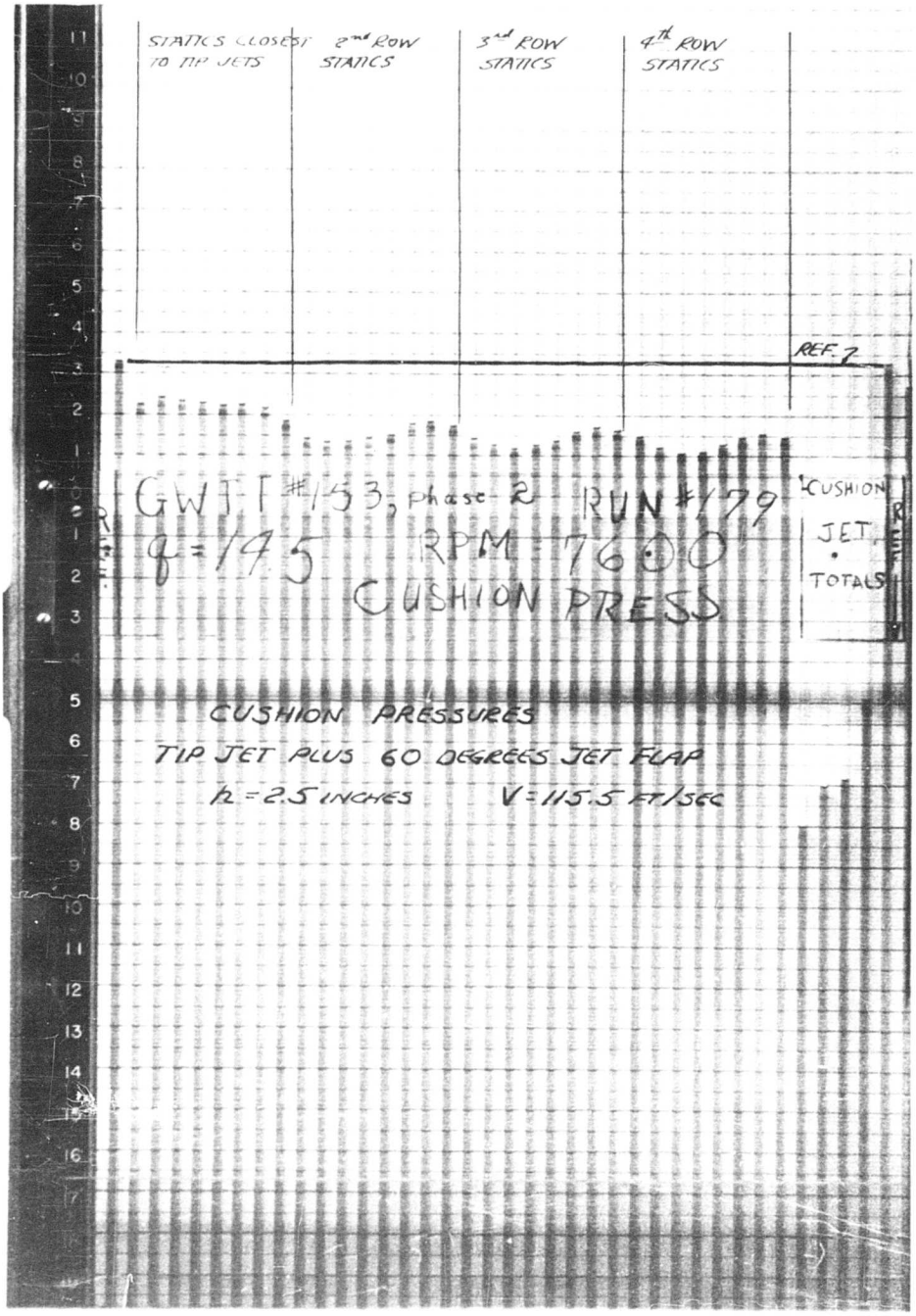

Fig. 96 Cushion Pressures — Tip Jet plus 60-degree Jet Flap; h = 2.5 inches, V = 115.5 ft/sec

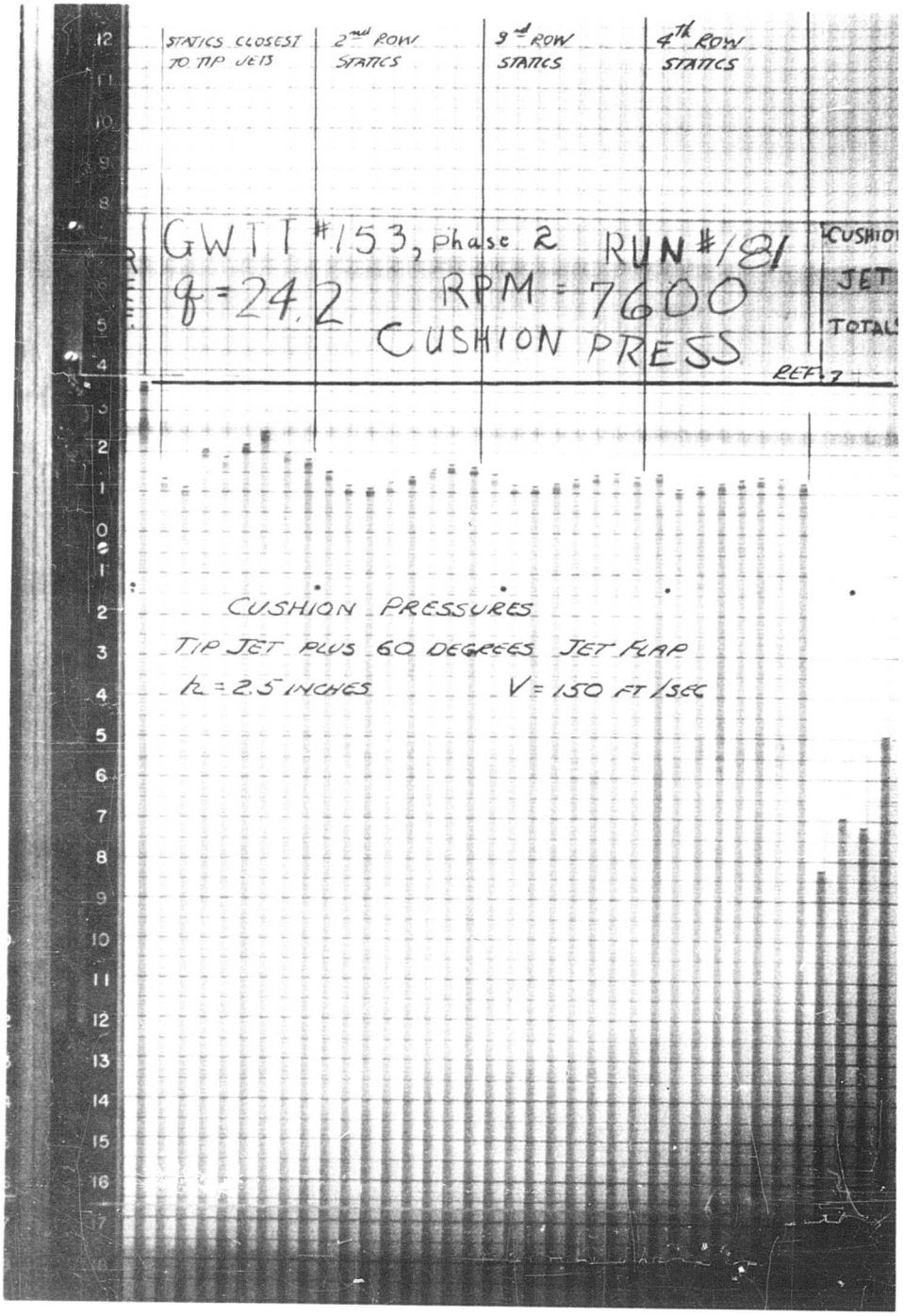

Fig. 97 Cushion Pressures — Tip Jet plus 60-degree Jet Flap; h = 2.5 inches, V = 150 ft/sec

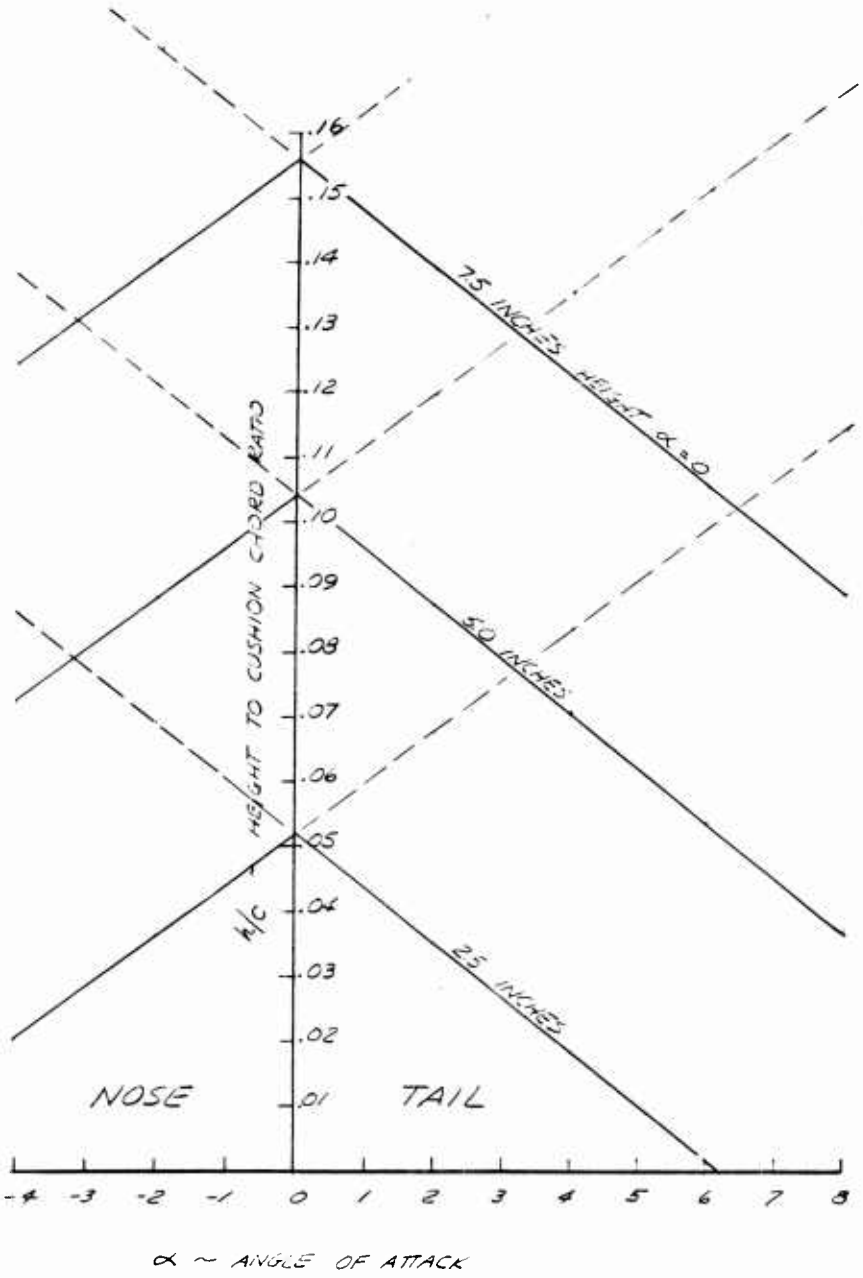

Fig. 98 Height-to-Cushion-Chord Ratio vs. Angle of Attack

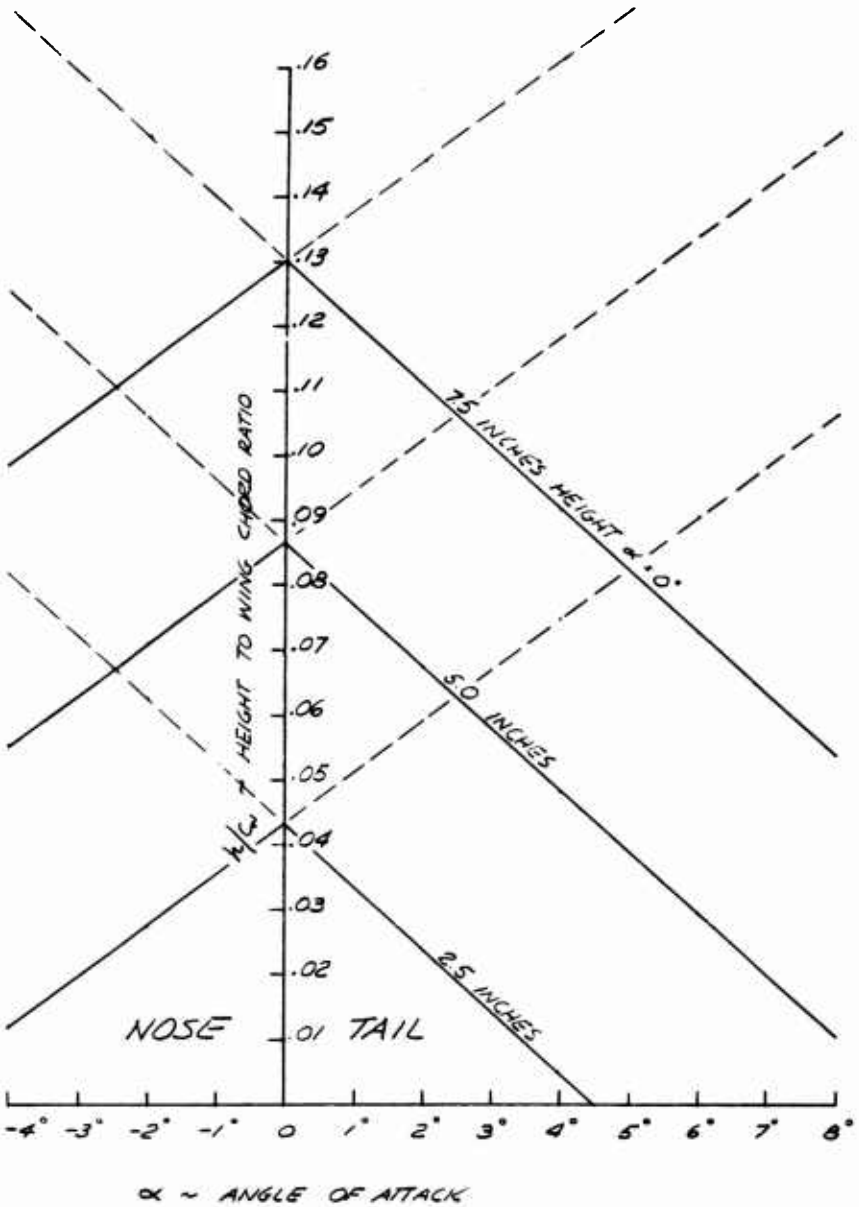

Fig. 99 Height-to-Wing-Chord Ratio vs. Angle of Attack

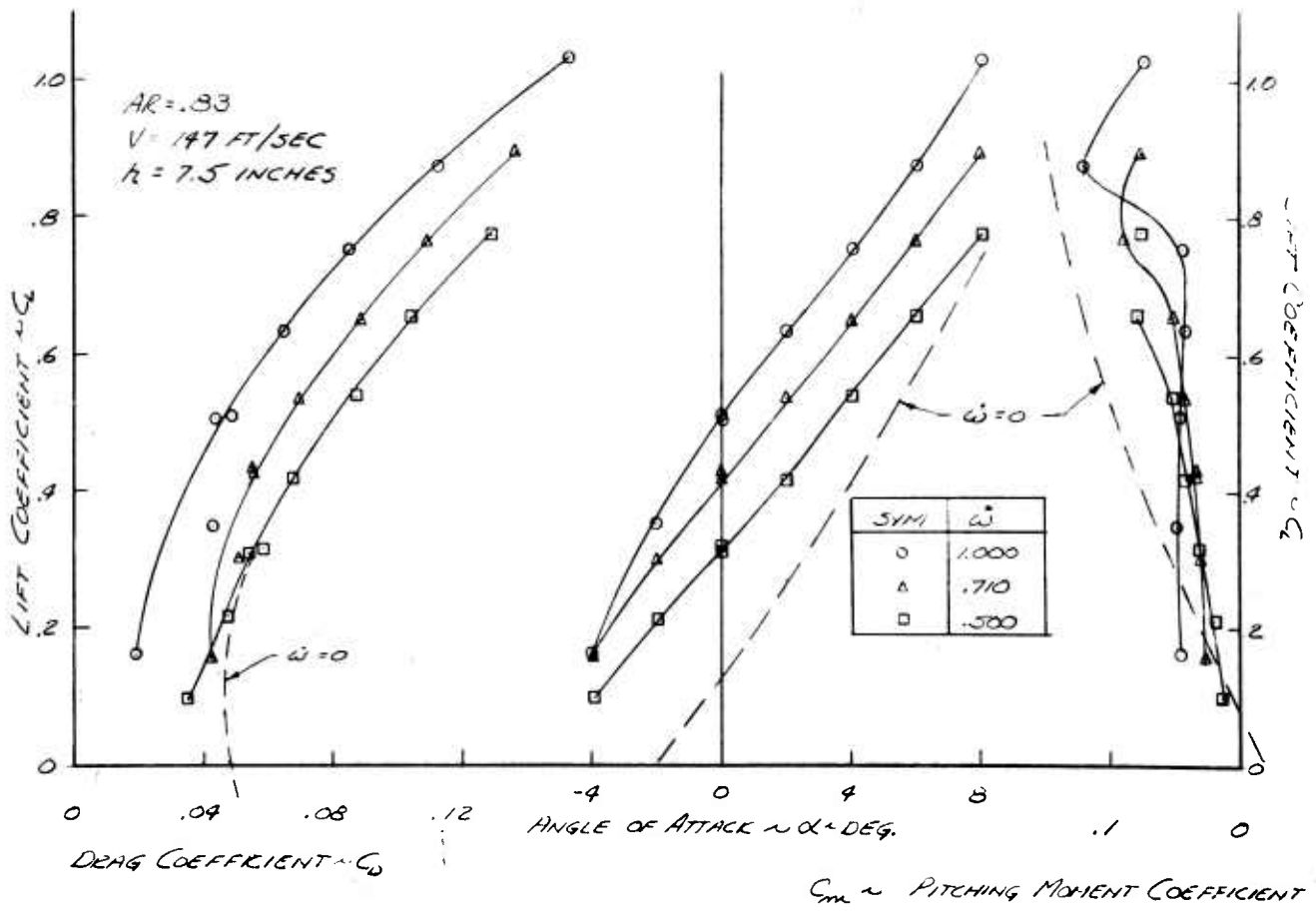

Fig. 100 Effect of Weight Flow With Tip Jet to High Angles of Attack

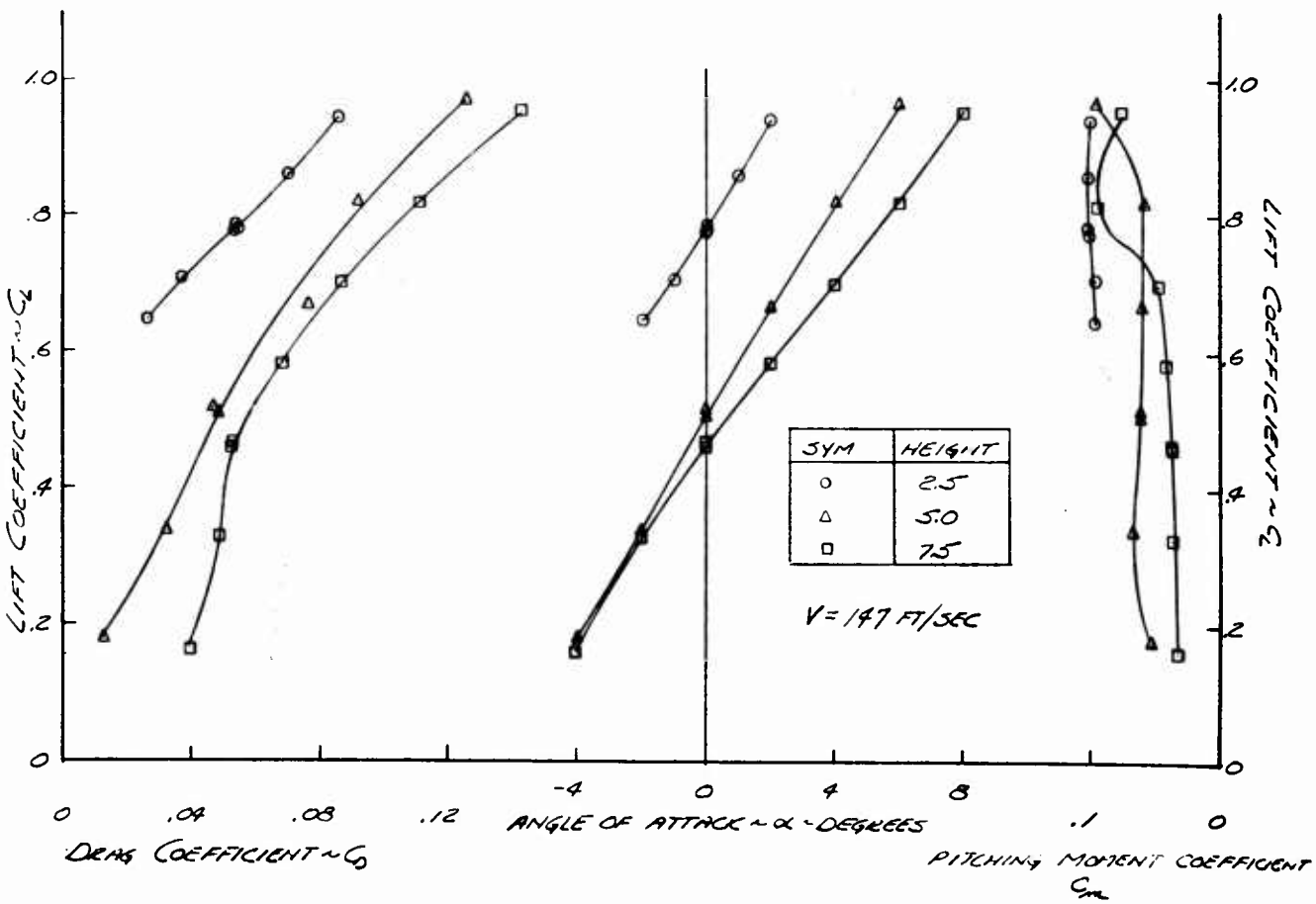

Fig. 101 Effect of Ground Height with Tip Jet to High Angles of Attack

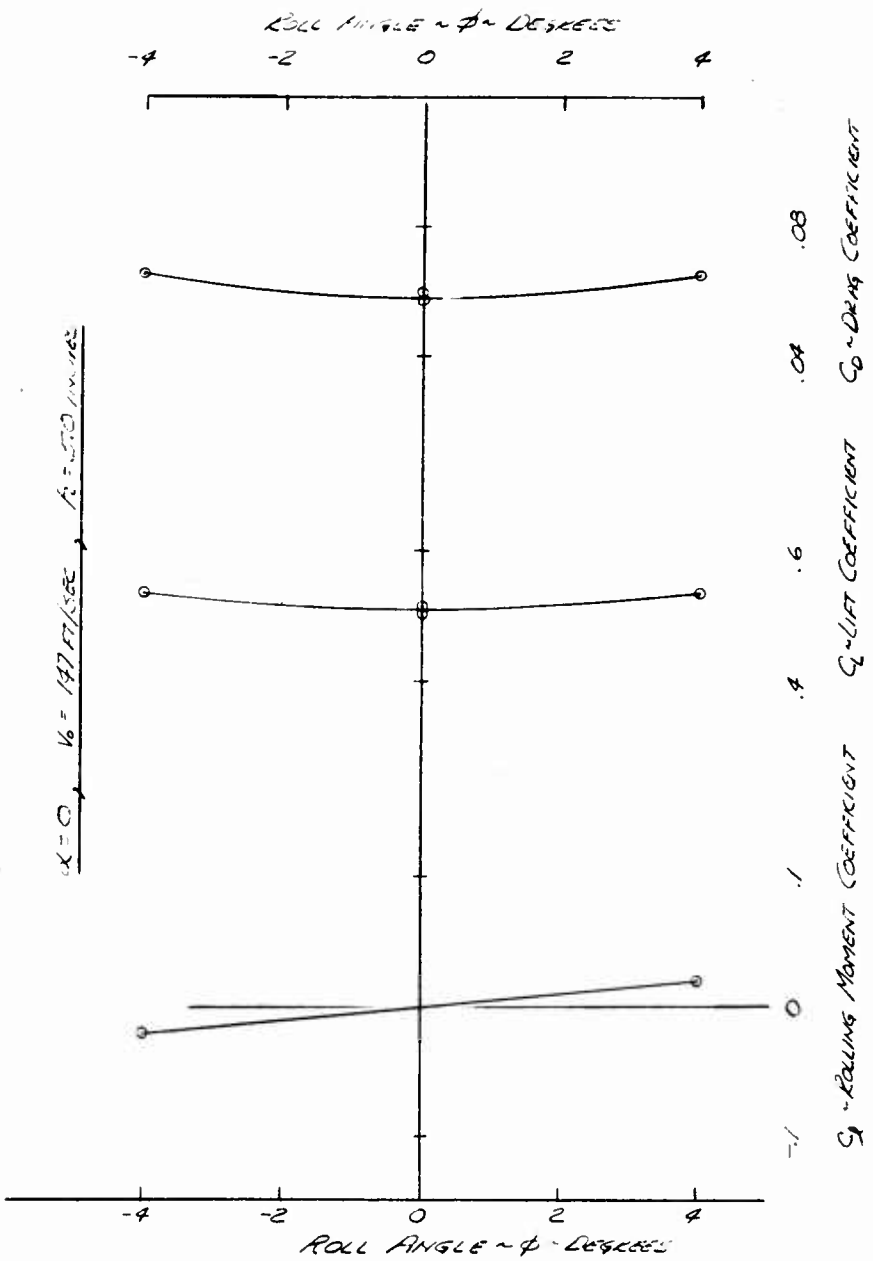

Fig. 102 Effect of Roll Angle With Tip Jet Only Configuration

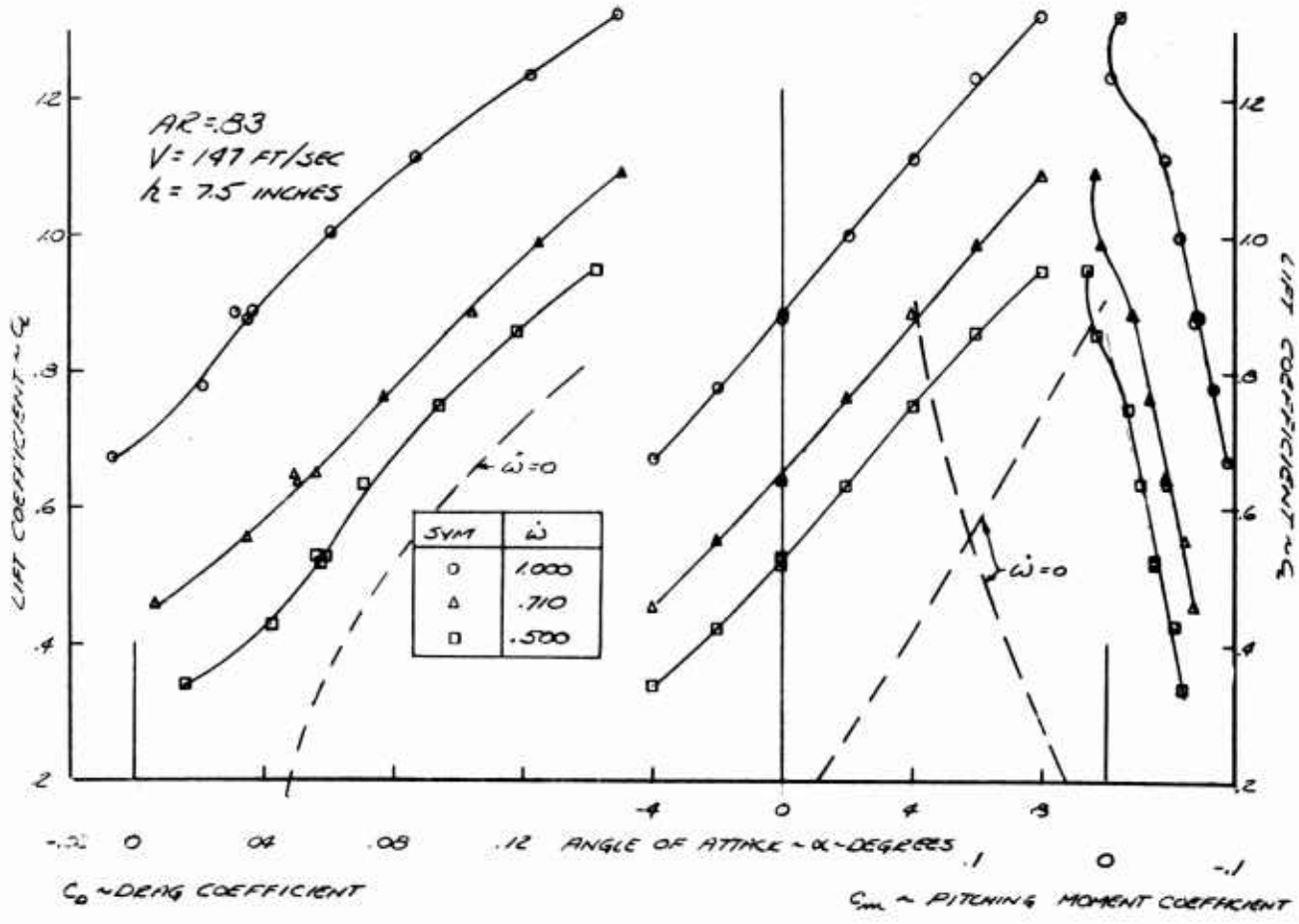

Fig. 103 Effect of Weight Flow With Tip Jet plus 60-degree Jet Flap Configuration to High Angles of Attack

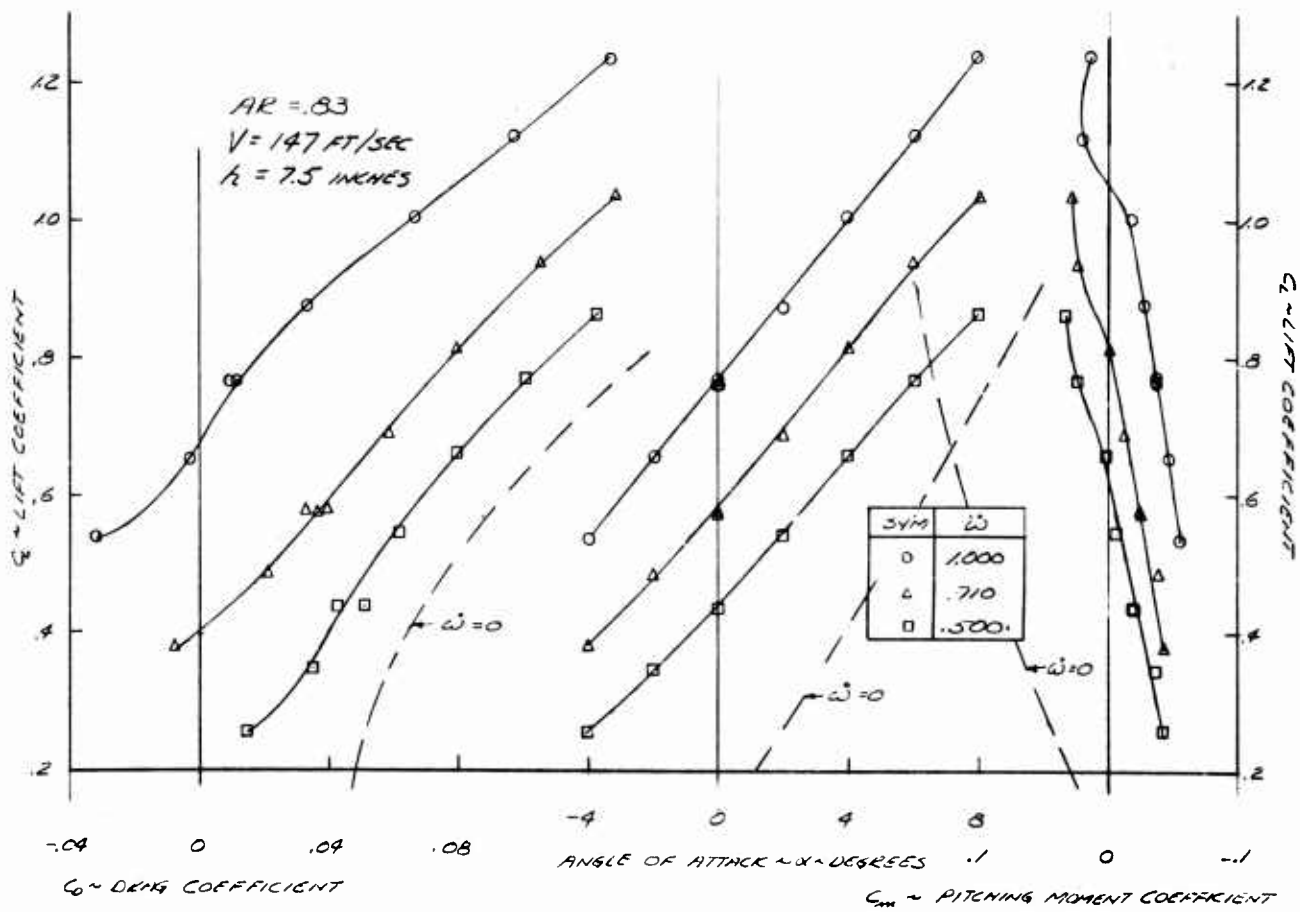

Fig. 104 Effect of Weight Flow With Tip Jet plus 30-degree Jet Flap Configuration to High Angles of Attack

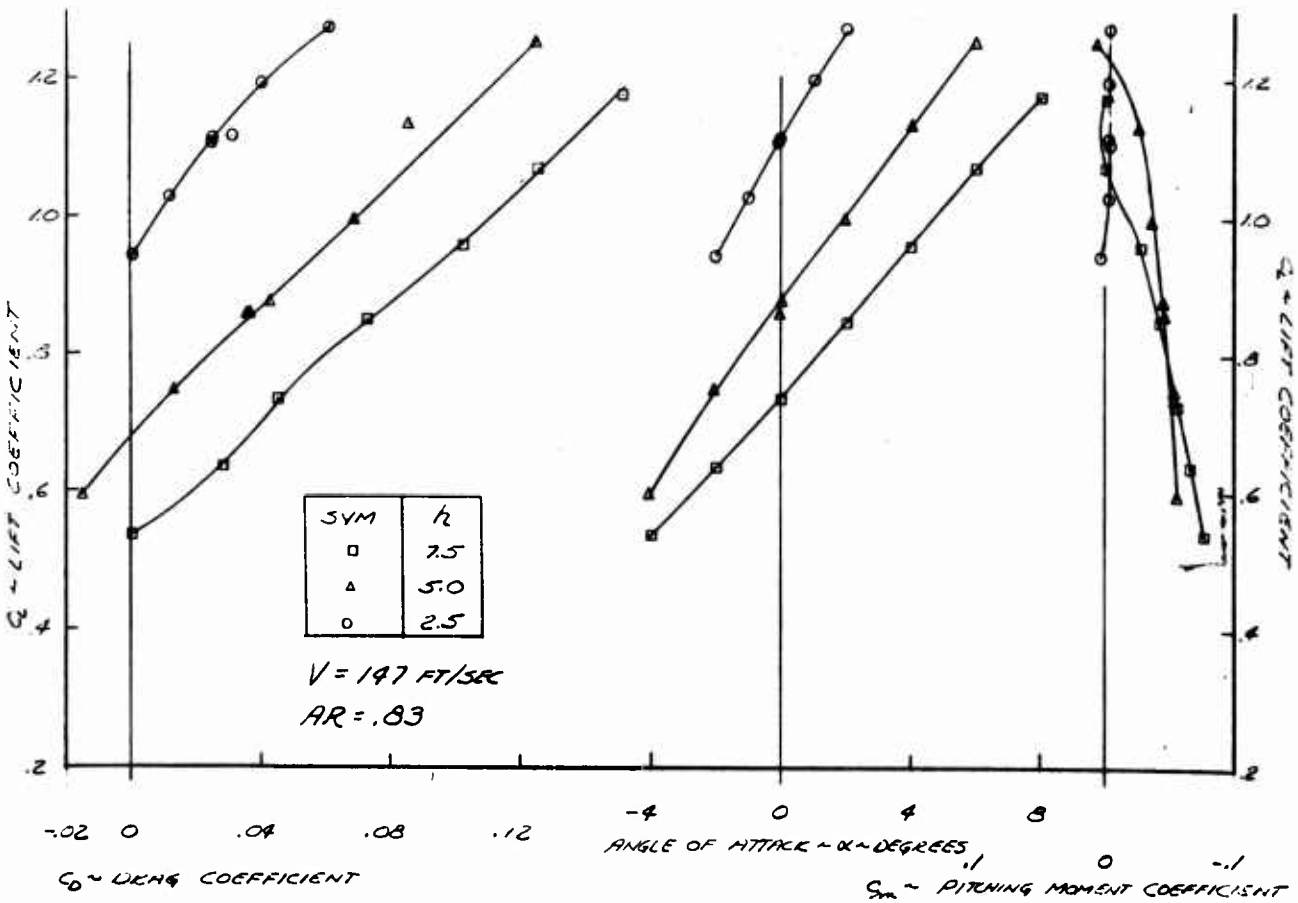

Fig. 105 Effect of Ground Height With Tip Jet plus 60-degree Jet Flap to High Angles of Attack

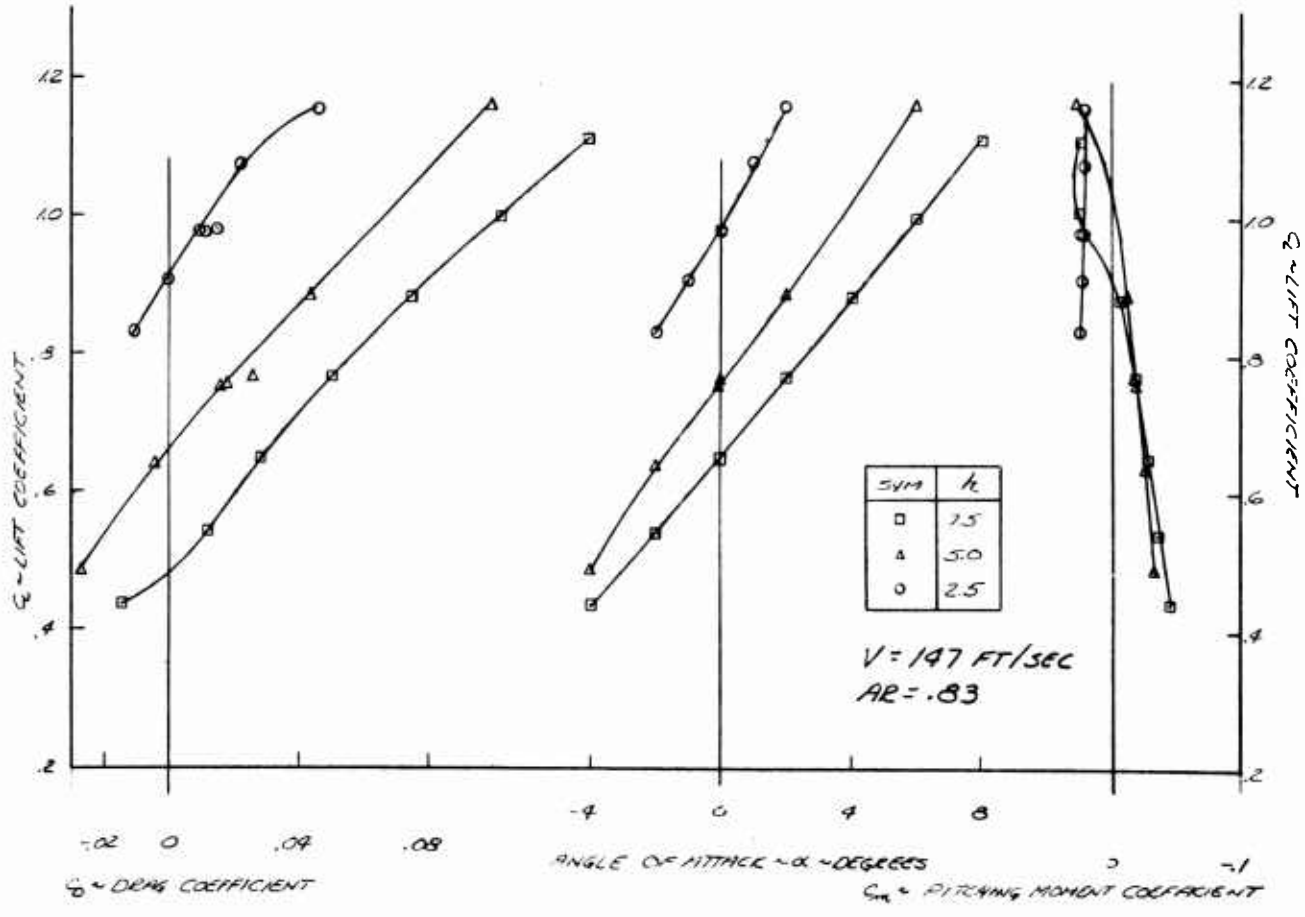

Fig. 106 Effect of Ground Height With Tip Jet plus 30-degree Jet Flap to High Angles of Attack

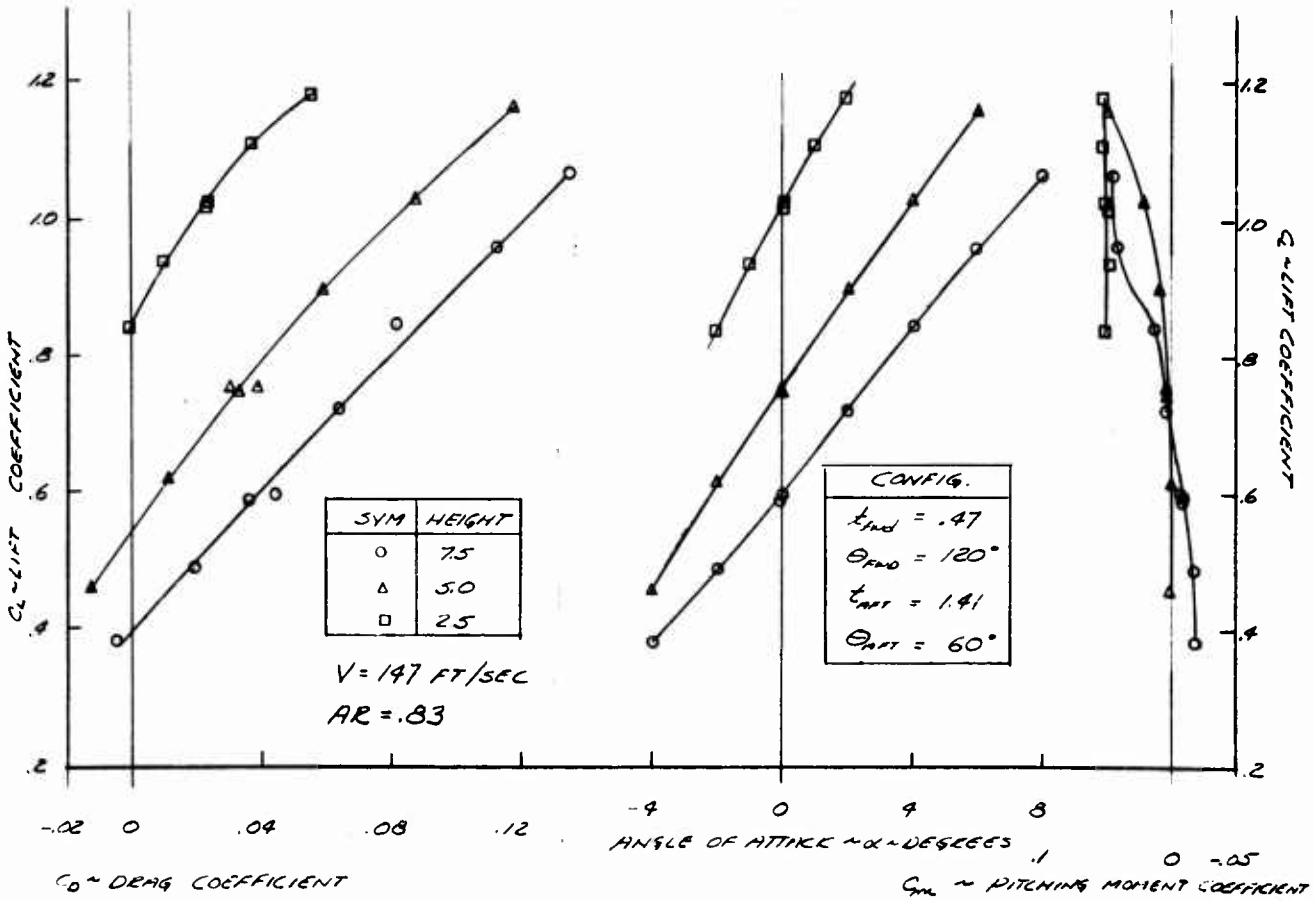

Fig. 107 Effect of Height on "Near Cruise Speed" Configuration to High Angles of Attack

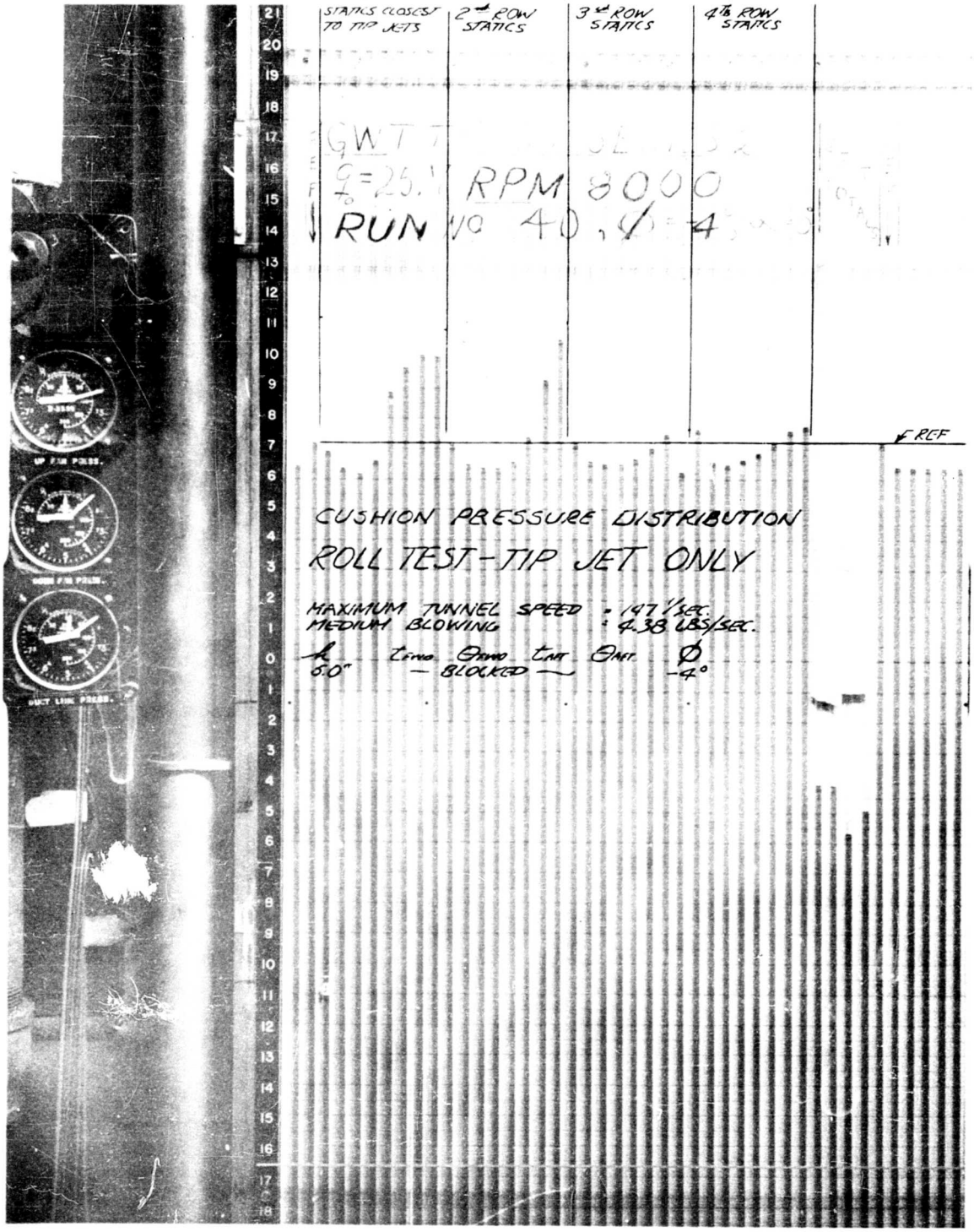

Fig. 103 Cushion Pressure Distribution During Roll Tests

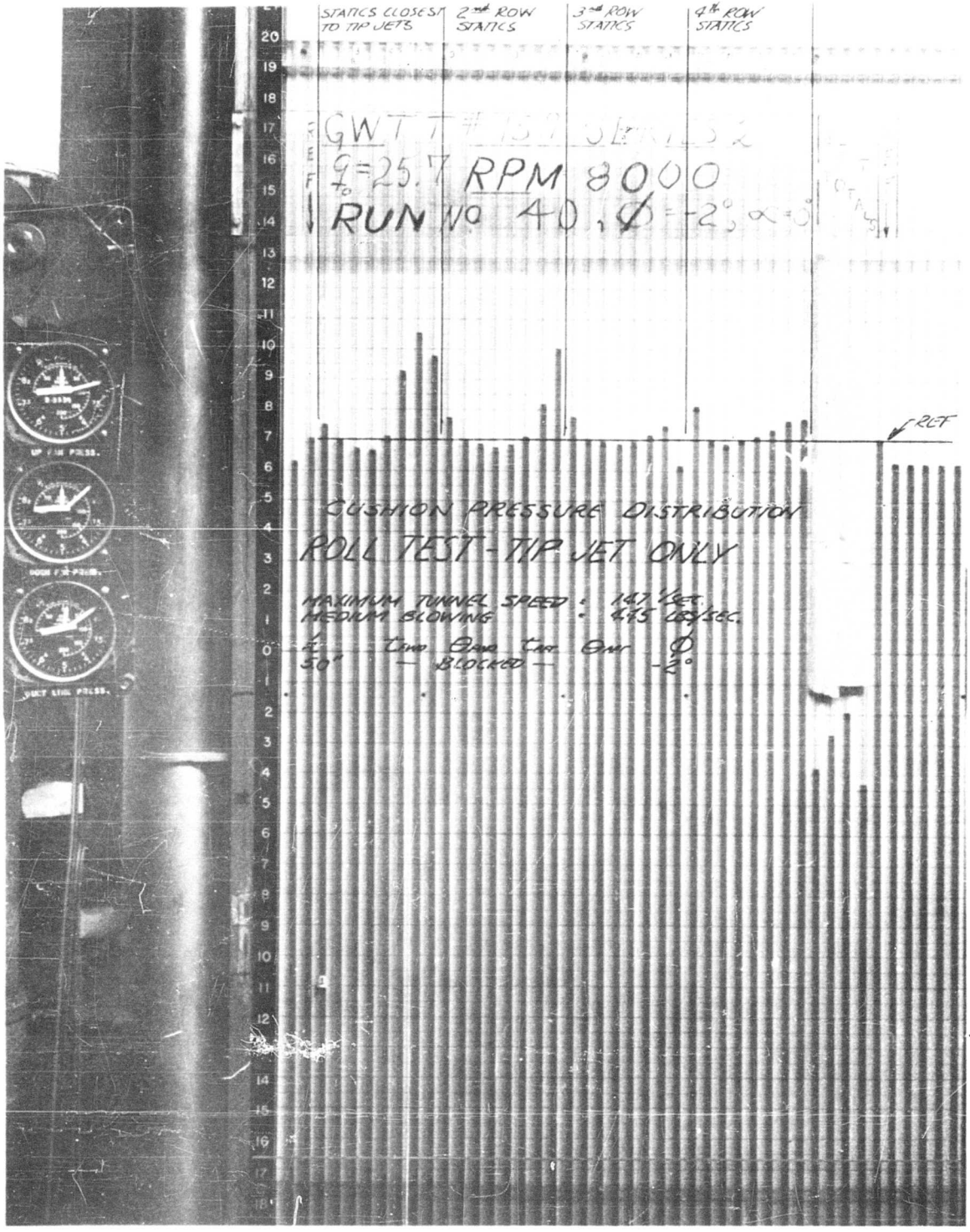

Fig. 109 Cushion Pressure Distribution During Roll Tests

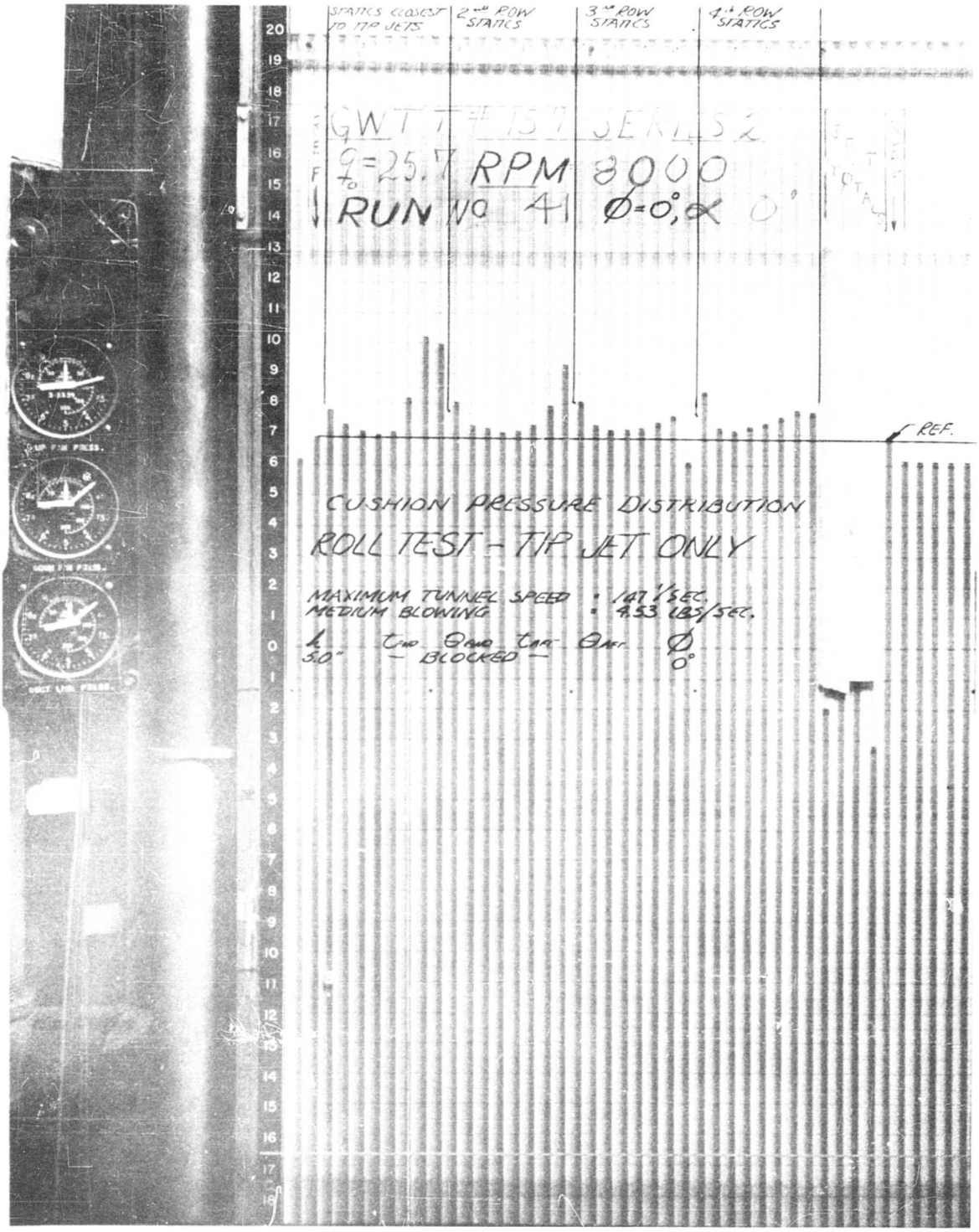

Fig. 110 Cushion Pressure Distribution During Roll Tests

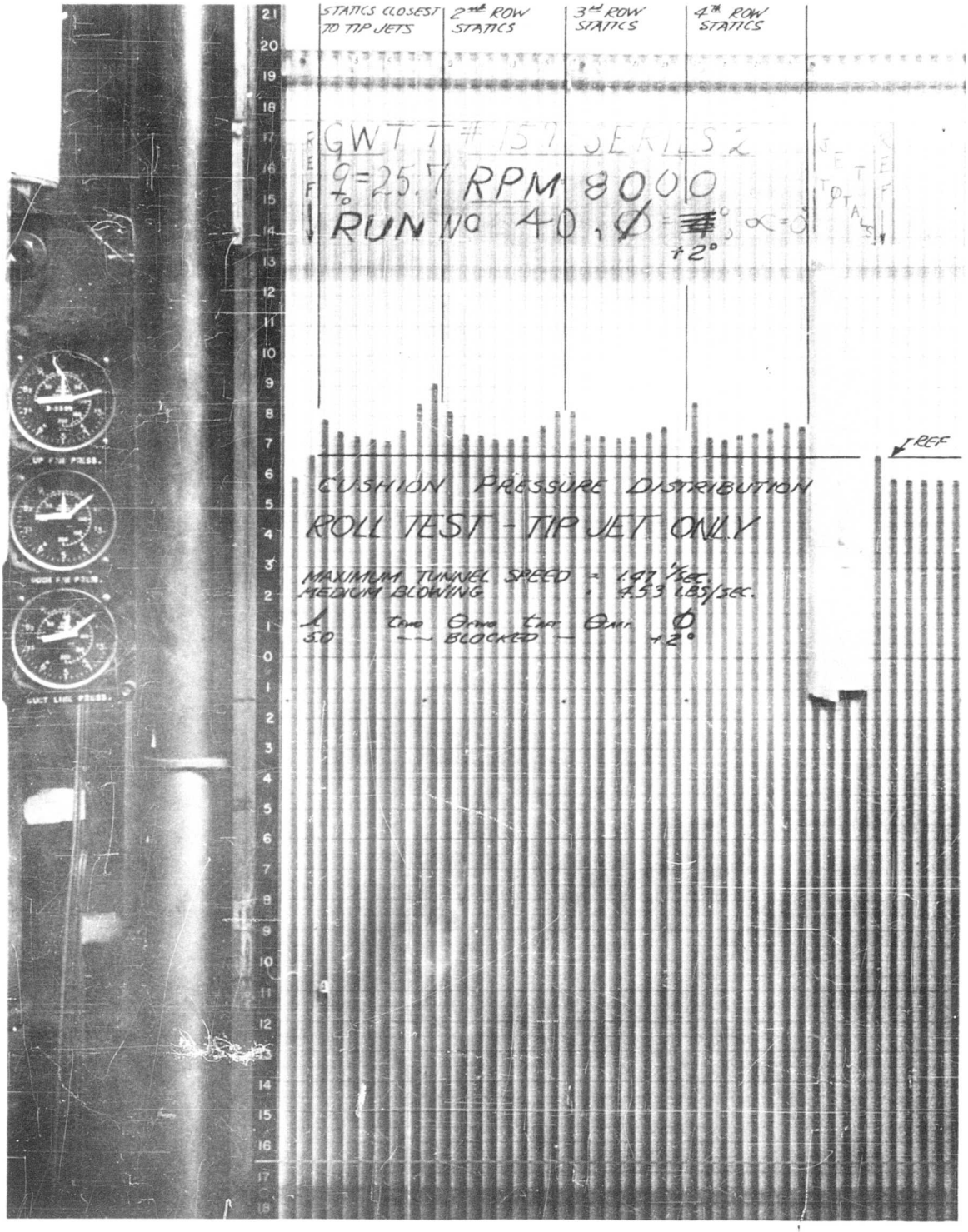

Fig. 111 Cushion Pressure Distribution During Roll Tests

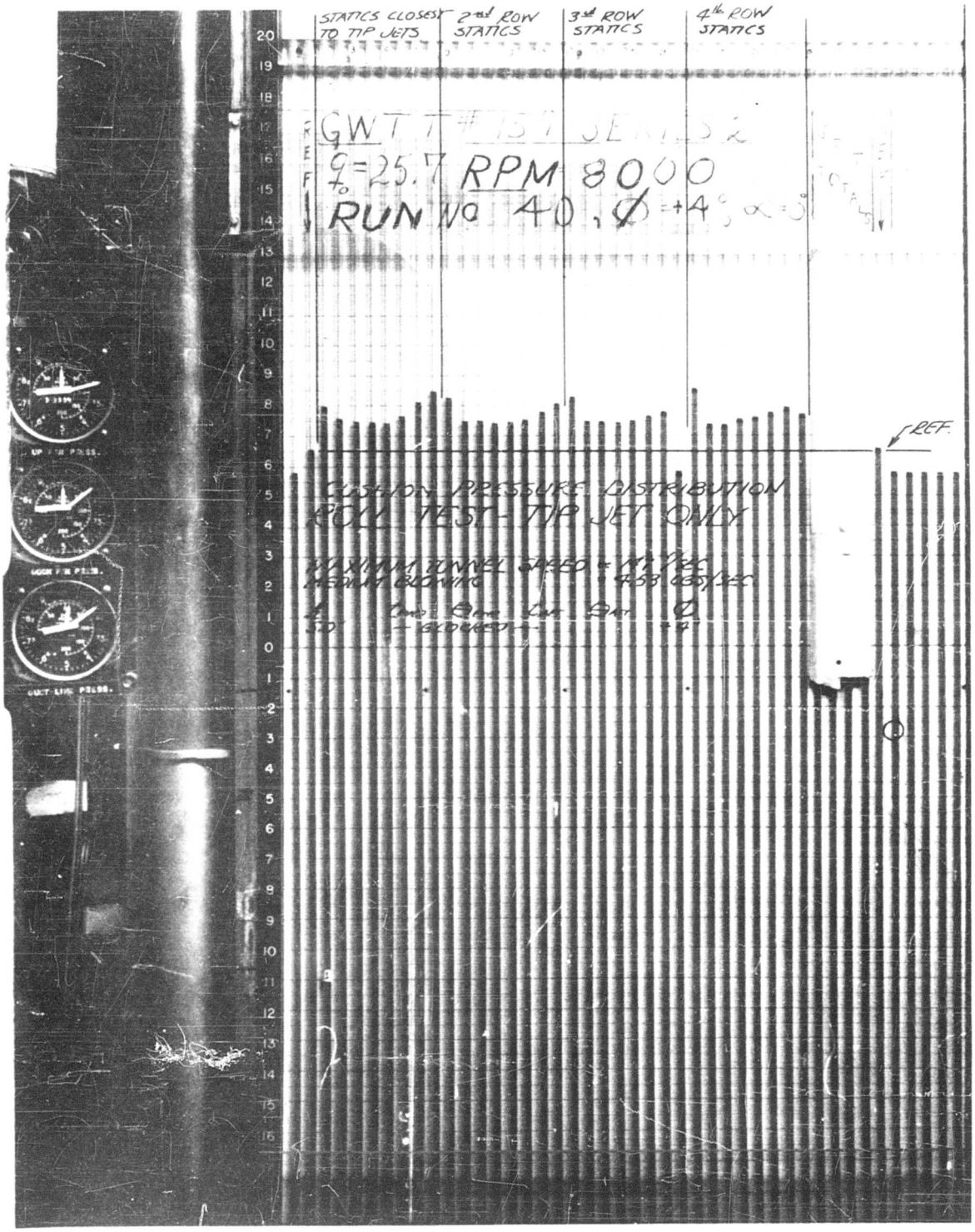

Fig. 112 Cushion Pressure Distribution During Roll Tests

4864-62

DISTRIBUTION

Ofc of Ord, ODDR & E	2
First US Army	1
Fourth US Army	1
Sixth US Army	1
USACGSC	1
USAARMBD	1
USAAVNBD	1
USATMC(FTZAT), ATO	1
USAPRDC	1
DCSLOG	1
Rsch Anal Corp	1
ARO, Durham	2
Ofc of Maint Engr, ODDR & E, OSD	1
NATC	1
ARO, OCRD	1
CRD, Earth Scn Div	1
USAERDL	2
USAOTAC, Center Line	2
OrdBd	1
QMBd	1
QMRECOMD	1
QMFEA	1
QMFSA	1
SigBd	1
CofT	8
USATCDG	1
USATB	1
USATMC	20
USATSCH	4
USATRECOM	32
USATTCA	1
USATTCP	1
OUSARMA	1
USATRECOM LO, USARDG (EUR)	1
USAEWES	3
C Co, 721st Trans Bn (Ry Opr)	1
B Co, 721st Trans Bn (Ry Opr)	2
USATDS	2
USARPAC	1
USARHAW	2

ALFSEE	1
USACOMZEUR	3
APGC(PGAPI)	1
Air Univ Lib	1
ASD(ASRMPT)	1
CNO	1
CNR	3
BUWEPS, DN	4
ACRD(OW), DN	1
USNCEL	1
USNSRDF	1
BUY&D, DN	1
USNPGSCH	1
BUSHP, DN	1
USNOTS	1
Dav Tay Mod Bas	1
MCLFDC	1
MCEC	1
USCG	1
USASGCA	1
Canadian LO, USATSCH	3
BRAS, DAQMG(Mov & Tn)	4
USASG, UK	1
NAFEC	3
Langley Rsch Cen, NASA	2
MSC, NASA	1
NASA, Wash., D.C.	6
Ames Rsch Cen, NASA	2
Lewis Rsch Cen, NASA	1
Sci & Tech Info Fac	1
USGPO	1
ASTIA	10
USAMRDC	1
USAMRL	1
WRAIR	2
HUMRRO	2
CIA	1
Grumman Aircraft Engineering Corporation	10

AD_____ Accession No._____

Grumman Aircraft Engineering Corp., Bethpage, N.Y., SUPPLEMENTARY LIFT FOR AIR CUSHIONED VEHICLES. VOL.II OF III. DATA ANALYSIS - N. KIRSCHBAUM and J. HELGESEN

TCREC Technical Report 62-50, June 1962,174pp. (Contract DA 44-177-TC-708) Task 9R99-01-005-03, Unclassified Report

A three-dimensional, half-span reflection-plane, airfoil-shaped GEM model covering speeds from 0 to 100 miles per hour, was tested.

1. Air cushion vehicles - Model test results
2. Stability
3. Performance
4. Contract DA 44-177-TC-708

AD_____ Accession No._____

Grumman Aircraft Engineering Corp., Bethpage, N.Y., SUPPLEMENTARY LIFT FOR AIR CUSHIONED VEHICLES. VOL. II OF III. DATA ANALYSIS - N. KIRSCHBAUM and J. HELGESEN

TCREC Technical Report 62-50, June 1962, 174pp (Contract DA 44-177-TC-708) Task 9R99-01-005-03, Unclassified Report

A three-dimensional, half-span reflection-plane, airfoil-shaped GEM model covering speeds from 0 to 100 miles per hour, was tested.

1. Air cushion vehicles - Model test results
2. Stability
3. Performance
4. Contract DA 44-177-TC-708

AD_____ Accession No._____

Grumman Aircraft Engineering Corp., Bethpage, N.Y., SUPPLEMENTARY LIFT FOR AIR CUSHIONED VEHICLES. VOL.II OF III. DATA ANALYSIS - N. KIRSCHBAUM and J. HELGESEN

TCREC Technical Report 62-50, June 1962,174pp.(Contract DA 44-177-TC-708) Task 9R99-01-005-03, Unclassified Report

A three-dimensional, half-span reflection-plane, airfoil-shaped GEM model covering speeds from 0 to 100 miles per hour, was tested.

1. Air cushion vehicles - Model test results
2. Stability
3. Performance
4. Contract DA 44-177-TC-708

AD_____ Accession No._____

Grumman Aircraft Engineering Corp., Bethpage, N. Y., SUPPLEMENTARY LIFT FOR AIR CUSHIONED VEHICLES. VOL.II OF III. DATA ANALYSIS - N. KIRSCHBAUM and J. HELGESEN

TCREC Technical Report 62-50, June 1962,174pp.(Contract DA 44-177-TC-708) Task 9R99-01-005-03, Unclassified Report

A three-dimensional, half-span reflection-plane, airfoil-shaped GEM model covering speeds from 0 to 100 miles per hour, was tested.

1. Air cushion vehicles - Model test results
2. Stability
3. Performance
4. Contract DA 44-177-TC-708

The first test series evaluated the effects of various leading and trailing edge jet configurations on the performance of the model at zero angle of attack. The data are presented in parametric form as a function of air mass flow coefficient. The results of this study indicate that the propulsive requirements for the lift system decrease with increasing speed.

The second series of tests evaluated the stability characteristics of the cruise configurations at cruise speed (100 miles per hour). The results of these tests indicate that all cruise configurations tested could be made longitudinally stable by locating the moment reference center (cg) at the 37 percent air cushion base chord.

The first test series evaluated the effects of various leading and trailing edge jet configurations on the performance of the model at zero angle of attack. The data are presented in parametric form as a function of air mass flow coefficient. The results of this study indicate that the propulsive requirements for the lift system decrease with increasing speed.

The second series of tests evaluated the stability characteristics of the cruise configurations at cruise speed (100 miles per hour). The results of these tests indicate that all cruise configurations tested could be made longitudinally stable by locating the moment reference center (cg) at the 37 percent air cushion base chord.

The first test series evaluated the effects of various leading and trailing edge jet configurations on the performance of the model at zero angle of attack. The data are presented in parametric form as a function of air mass flow coefficient. The results of this study indicate that the propulsive requirements for the lift system decrease with increasing speed.

The second series of tests evaluated the stability characteristics of the cruise configurations at cruise speed (100 miles per hour). The results of these tests indicate that all cruise configurations tested could be made longitudinally stable by locating the moment reference center (cg) at the 37 percent air cushion base chord.

The first test series evaluated the effects of various leading and trailing edge jet configurations on the performance of the model at zero angle of attack. The data are presented in parametric form as a function of air mass flow coefficient. The results of this study indicate that the propulsive requirements for the lift system decrease with increasing speed.

The second series of tests evaluated the stability characteristics of the cruise configurations at cruise speed (100 miles per hour). The results of these tests indicate that all cruise configurations tested could be made longitudinally stable by locating the moment reference center (cg) at the 37 percent air cushion base chord.

AD_____ Accession No._____ Grumman Aircraft Engineering Corp., Bethpage, N.Y., SUPPLEMENTARY LIFT FOR AIR CUSHIONED VEHICLES. VOL.II OF III. DATA ANALYSIS - N. KIRSCHBAUM and J. HELGESEN TCREC Technical Report 62-50, June 1962,174pp. (Contract DA 44-177-TC-708) Task 9R99-01-005-03, Unclassified Report A three-dimensional, half-span reflection-plane, airfoil-shaped GEM model covering speeds from 0 to 100 miles per hour, was tested.	1. Air cushion vehicles - Model test results 2. Stability 3. Performance 4. Contract DA 44-177-TC-708	AD_____ Accession No._____ Grumman Aircraft Engineering Corp., Bethpage, N.Y., SUPPLEMENTARY LIFT FOR AIR CUSHIONED VEHICLES. VOL. II OF III. DATA ANALYSIS - N. KIRSCHBAUM and J. HELGESEN TCREC Technical Report 62-50, June 1962, 174pp (Contract DA 44-177-TC-708) Task 9R99-01-005-03, Unclassified Report A three-dimensional, half-span reflection-plane, airfoil-shaped GEM model covering speeds from 0 to 100 miles per hour, was tested.	1. Air cushion vehicles - Model test results 2. Stability 3. Performance 4. Contract DA 44-177-TC-708
AD_____ Accession No._____ Grumman Aircraft Engineering Corp., Bethpage, N.Y., SUPPLEMENTARY LIFT FOR AIR CUSHIONED VEHICLES. VOL.II OF III. DATA ANALYSIS - N. KIRSCHBAUM and J. HELGESEN TCREC Technical Report 62-50, June 1962,174pp.(Contract DA 44-177-TC-708) Task 9R99-01-005-03, Unclassified Report A three-dimensional, half-span reflection-plane, airfoil-shaped GEM model covering speeds from 0 to 100 miles per hour, was tested.	1. Air cushion vehicles - Model test results 2. Stability 3. Performance 4. Contract DA 44-177-TC-708	AD_____ Accession No._____ Grumman Aircraft Engineering Corp., Bethpage, N. Y., SUPPLEMENTARY LIFT FOR AIR CUSHIONED VEHICLES. VOL.II OF III. DATA ANALYSIS - N. KIRSCHBAUM and J. HELGESEN TCREC Technical Report 62-50, June 1962,174pp.(Contract DA 44-177-TC-708) Task 9R99-01-005-03, Unclassified Report A three-dimensional, half-span reflection-plane, airfoil-shaped GEM model covering speeds from 0 to 100 miles per hour, was tested.	1. Air cushion vehicles - Model test results 2. Stability 3. Performance 4. Contract DA 44-177-TC-708

The first test series evaluated the effects of various leading and trailing edge jet configurations on the performance of the model at zero angle of attack. The data are presented in parametric form as a function of air mass flow coefficient. The results of this study indicate that the propulsive requirements for the lift system decrease with increasing speed.

The second series of tests evaluated the stability characteristics of the cruise configurations at cruise speed (100 miles per hour). The results of these tests indicate that all cruise configurations tested could be made longitudinally stable by locating the moment reference center (cg) at the 37 percent air cushion base chord.

The first test series evaluated the effects of various leading and trailing edge jet configurations on the performance of the model at zero angle of attack. The data are presented in parametric form as a function of air mass flow coefficient. The results of this study indicate that the propulsive requirements for the lift system decrease with increasing speed.

The second series of tests evaluated the stability characteristics of the cruise configurations at cruise speed (100 miles per hour). The results of these tests indicate that all cruise configurations tested could be made longitudinally stable by locating the moment reference center (cg) at the 37 percent air cushion base chord.

The first test series evaluated the effects of various leading and trailing edge jet configurations on the performance of the model at zero angle of attack. The data are presented in parametric form as a function of air mass flow coefficient. The results of this study indicate that the propulsive requirements for the lift system decrease with increasing speed.

The second series of tests evaluated the stability characteristics of the cruise configurations at cruise speed (100 miles per hour). The results of these tests indicate that all cruise configurations tested could be made longitudinally stable by locating the moment reference center (cg) at the 37 percent air cushion base chord.

The first test series evaluated the effects of various leading and trailing edge jet configurations on the performance of the model at zero angle of attack. The data are presented in parametric form as a function of air mass flow coefficient. The results of this study indicate that the propulsive requirements for the lift system decrease with increasing speed.

The second series of tests evaluated the stability characteristics of the cruise configurations at cruise speed (100 miles per hour). The results of these tests indicate that all cruise configurations tested could be made longitudinally stable by locating the moment reference center (cg) at the 37 percent air cushion base chord.

UNCLASSIFIED